BINDING SERVICES
Tel +44 (0)29 2087 4949
Fax +44 (0)29 20371921
e-mail bindery@cardiff.ac.uk

Model for Localised Recombination in Quantum Dots

Helen J. Pask

PhD Thesis

School of Physics and Astronomy

Cardiff University

2006

ProQuest LLC
789 East Eisenhower Parkway
P.O. Box 1346
Ann Arbor, MI 48106-1346

DECLARATION

This work has not previously been accepted in substance for any degree and is not being concurrently submitted in candidature for any degree.

Signed ..... (candidate)
Date .....

STATEMENT 1

This thesis is the result of my own investigations, except where otherwise stated. Other sources are acknowledged by footnotes giving explicit references. A bibliography is appended.

Signed ..... (candidate)
Date .....

STATEMENT 2

I hereby give consent for my thesis, if accepted, to be available for photocopying and for inter-library loan, and for the title and summary to be made available to outside organisations.

Signed ..... (candidate)
Date .....

Abstract

A new generation of diode lasers is being developed using quantum dots as the gain generating medium. A detailed understanding of the carrier recombination mechanisms and optical gain generation is essential for optimisation of their performance. The aim of this work is to further understand the optical processes occurring in quantum dots. In particular, the effect of the localisation of the energy states in the dots on the recombination mechanisms and the gain/absorption is studied.

It is often assumed that the rates of nonradiative recombination via defects, radiative recombination and Auger recombination are proportional to linear, quadratic and cubic functions of the carrier number respectively. The derivation of these functional forms is possible in quantum well and bulk structures because the extended electronic states make it meaningful to talk of a global carrier population. In a quantum dot system the dependence of the recombination processes on the total number of electrons populating the dots is modified by the localisation of all the recombination processes. In this thesis a computer model has been developed in which the dots are occupied by integer numbers of electrons and holes, with electron and hole occupancies controlled by Fermi-Dirac statistics. The recombination processes have similar dependences on the electron number and there is no clear transition from one process to another as the injection level is increased. These dependences cannot be represented by simple power law functions of the carrier number. An alternative model, in which each dot is electrically neutral, has also been studied, and the two models show significant differences for the hole distribution as the injection is increased. It is found that analyses based on power law relations between recombination rates and carrier number, as used for extended state systems, cannot be applied to localised recombination in dots.

Acknowledgements

Firstly I would like to thank my PhD supervisors, Dr. Huw Summers and Prof. Peter Blood, for their time, commitment and help throughout this project. Thanks also to my friends in the Optoelectronics group and the department. In particular, I would like to thank Iain for his help with computing problems, and my good friends Lois and Dave. Special thanks go to Lois for putting up with me at home as well as at Uni!

Thanks to my good friends Kath and Jane for letting me bore them with Physics talk!

To Kris, thanks for understanding and being there for me, and giving me something to look forward to after all this hard work is over.

Finally, I would like to thank my mum and dad for their encouragement and financial support throughout my time at University, and my sister Anna and my nana for their belief in me.

Publications

- H. J. Pask, H. D. Summers and P. Blood, *Light-current characteristics of quantum dots with localized recombination*, Applied Physics Letters, **87** (8), 083109 (2005).
- H. J. Pask, H. D. Summers and P. Blood, *Localized recombination in quantum dots*, Physica Status Solidi (c), **11**, 3860 (2005).

Conference Presentations

- H. J. Pask, H. D. Summers and P. Blood, *Localised recombination in quantum dots*, SIOE, Cardiff UK, 23rd March 2005.
- H. J. Pask, H. D. Summers and P. Blood, *Localised recombination in quantum dots*, CLEO/QELS, Baltimore USA, 26th May 2005.
- H. J. Pask, H. D. Summers and P. Blood, *Localised recombination in quantum dots*, PLMCN5, Glasgow UK, 11th June 2005.

"All of physics is either impossible or trivial. It is impossible until you understand it, and then it becomes trivial."

- Ernest Rutherford

"A theory can be proved by experiment; but no path leads from experiment to the birth of a theory."

- Albert Einstein


CARDIFF UNIVERSITY
12 APR 2006
PRIFYSGOL CAERDYDD

Contents

List of Figures

List of Tables

1 Introduction and Thesis Rationale

1.1 Thesis Rationale

The work presented in this thesis has been carried out at Cardiff University, with the aim of further understanding the optical processes occurring in quantum dots. In particular, it is studied how the localisation of the energy states in the dots affects the recombination mechanisms and the gain/absorption.

A new generation of diode lasers is being developed using quantum dots as the gain generating medium. These devices have a number of attractive features including very low threshold current with low temperature sensitivity, a wide gain spectrum attractive for ultra-short pulse generation, and long wavelength emission from structures on GaAs substrates [1]. A detailed understanding of the carrier recombination mechanisms and optical gain generation within semiconductor lasers is essential for optimisation of their performance. In systems of finite dimensions with extended electronic states, carriers are free to move along the quantum wire or quantum well, or throughout the bulk crystal. This assists the carriers in achieving an internal equilibrium throughout the crystal. The extended states form a continuum in energy which is represented by a density of states function and treatments of recombination are based on the assumption that any electron in an extended state may recombine with any hole in an extended state, subject to the appropriate k-selection rules. These ideas lead to the concept of the reduced density of states and a radiative recombination rate which is proportional to the product of the electron and hole densities in the extended state system [2]. In the absence of quantum mechanical coupling, the electronic states of a quantum dot are localised in all three directions; consequently, it is only possible for electrons and holes which are located within the same dot to recombine with each other. The maximum number of available electrons and holes within a single state is then equal to the spin degeneracy and at high injection this significantly reduces the radiative recombination rate relative to the quantum well or bulk case.

Experimentally the recombination processes are often investigated by measurement of the light versus current (L-I) characteristics in the spontaneous emission regime. This is done by consideration of the functional form of the data using assumed power law dependences on carrier density for the various recombination processes [3-5]. It is assumed that the rates of

nonradiative recombination via defects, radiative recombination and Auger recombination are proportional to linear, quadratic and cubic functions of the carrier density respectively. The light-current curve is linear if radiative recombination is dominant, super-linear if nonradiative recombination is dominant and sub-linear if Auger processes dominate. The derivation of these functional forms for the recombination mechanisms is possible in quantum well and bulk structures because the extended electronic states make it meaningful to talk of a global carrier population. In a quantum dot system it is still possible to talk of the total number of electrons populating the dot states, but the behaviour of the recombination processes on this number may be modified by the localisation of all the recombination processes. Whether simple relationships can be found in quantum dot systems is not obvious from immediate inspection and will depend on the individual contributions of the many dots that make up the whole ensemble. Light-current curves measured on quantum dot LEDs show sub-linear and super-linear behaviour but, since the number of electrons cannot be measured directly, it is not known whether the power law components of such data are indicative of specific recombination processes.

The aim of this work is to compute the recombination and gain characteristics of a quantum dot system to explore the consequences of carrier localisation on the behaviour of quantum dot light emitters. A feature of the model is that the number of electrons in a given dot is a discrete integer, not a fractional probability. Real dot samples usually incorporate a quantum well, or *wetting layer*, which does have extended states and this has also been incorporated into the model. Some aspects of localisation have been included in previous calculations [6, 7]; however, the prime aim of this thesis is to use a computer model to explore the effect of localisation and discrete occupancy number on the *measurable* characteristics, such as the light output and device current, of an *ensemble* of a large number of dots. For example, in a system where radiative recombination is the only process, the light-current curve is linear, irrespective of the relation between the radiative recombination rate and the number of carriers in the system: the radiative rate *is* the current. To focus on this it is assumed that the whole system is in thermal equilibrium so that comparisons can readily be made with non-localised systems since the global occupation probabilities are specified analytically. A consequence of this work is that it can be assessed whether methods of analysis of light-current data commonly used for bulk and quantum well systems can be transferred directly to the study of quantum dot emitters.

1.2 Thesis Outline

This first chapter of the thesis gives an outline of the project and some background information. An introduction to quantum confinement is given, focusing on quantum dots. A brief introduction to lasers is also given.

Chapter 2 outlines some of the main concepts of semiconductor optoelectronics and the properties of semiconductor structures. Equations for some of the processes involved are derived, including the Einstein relations for quantum dots.

Chapter 3 gives details of the model derived in this thesis and describes how localised population statistics are used to calculate the discrete electron and hole occupancies of the dots. Equations for the electron and hole distributions are given. This model is referred to as the *non-neutral* model since each individual dot does not necessarily contain equal numbers of electrons and holes.

Chapter 4 details how the localised population statistics are used to calculate the processes occurring in the dots, including the radiative, nonradiative and Auger recombination, and the gain.

In chapter 5 an alternative model in described, in which localised population statistics are used for the electron distribution but the number of holes in each dot is set equal to the number of electrons. This is called the *neutral* model. The equations for the recombination processes and gain for these neutral dots are given.

Chapter 6 shows how the electron and hole populations evolve with increasing injection. Hole distributions for the neutral and non-neutral dots are described. It is discussed whether or not the hole distribution for the neutral dots can be described by Fermi-Dirac statistics.

Chapter 7 shows various light-current curves and describes how the recombination processes vary with electron number. Results for neutral and non-neutral dots are compared. The computed L-I curves are also compared with experimental data.

In chapter 8 spontaneous emission plots are presented. Plots of the spontaneous emission spectra at various injection levels are shown, and the spectra of the neutral and non-neutral dots are compared. It is investigated how appropriate it is to fit the spectra with Gaussian distributions.

Chapter 9 gives gain/absorption spectra for different injection levels. The differences between the neutral and non-neutral dots are discussed, along with the absorption spectra for differing linewidths. The variation of the peak gain with electron quasi-Fermi level, electron number and radiative current is studied, with comparisons made between the neutral and non-neutral cases.

Chapter 10 brings the spontaneous emission and gain chapters together and shows gain-current plots for the neutral and non-neutral dots. The distribution function P_f is plotted for both cases.

Finally, the thesis is concluded with a summary of the main concepts of the model and its conclusions, along with suggestions for future work.

An appendix is included, in which tables of the notation and abbreviations used throughout this thesis are given.

1.3 Quantum Dots

1.3.1 Introduction – Quantum Confinement

When the dimensionality of a semiconductor structure is decreased, quantum confinement effects begin to become noticeable. Quantum confinement is possible in one, two, or all three dimensions, to produce quantum wells, quantum wires or quantum dots respectively. Structures are named according to the number of dimensions in which the electrons are free to move, which itself is determined by the number of dimensions that are small: thin layers of material are called two-dimensional (2D), wires are one-dimensional (1D), and quantum dots are zero-dimensional (0D) since the electrons are confined in all three directions. (Structures in which no dimension is significantly small for observable quantum effects are called bulk structures.) The critical thickness at which quantum confinement effects become observable is that of the de-Broglie wavelength of an electron, which is given by:

$$\lambda = \frac{h}{\sqrt{3m_c kT}}$$

equation 1.1

Here, m_c is the effective mass of the electrons, k is Boltzmann's constant, and T is the temperature. For electrons in semiconductors, the effective mass of an electron is much less

than the free electron mass and the de-Broglie wavelength is of the order of tens of nanometres.

Reducing the number of dimensions of a semiconductor structure has the effect of altering the density of states, which significantly changes the optical properties of the crystal, such as the gain and recombination spectra. The density of states for structures of differing dimensions is discussed in more detail in section 2.2.3.

Quantum wells are used extensively in optoelectronic devices, particularly in laser diodes. A potential well is formed in a heterostructure, where a thin layer of narrow bandgap semiconductor material is sandwiched between two layers of wider bandgap material. Typical quantum well widths are about 5-10nm, which is sufficiently small such that the band bending is very small and the bands can be drawn as flat.

Quantum confined structures have many advantages over bulk material. The energy levels in a quantum well are quantised, with the electrons being free to move in the other two dimensions in the plane of the well. The energy levels can be calculated by solving Schrödinger's equation and this results in a step-like density of states. This quantisation leads to an increased transition energy, well above that of bulk material. For a thin well the sub-bands are separated by an energy greater than the thermal energy kT, and so there is only a small thermal occupation of higher energy bands which reduces the threshold current density. By adjusting the thickness of the well, the transition energy can be altered and this in turn alters the wavelength of the device, which allows for semiconductor lasers of different wavelengths to be produced.

Quantum dots are formed by reducing the dimensionality of a structure in all three directions. The dots have a discrete energy level structure and the classical bandstructure model can no longer be applied. The dots have a theoretical delta-function density of states. The de-Broglie wavelength is now the critical measure for quantisation effects in all three dimensions and so typical sizes of dots are around 10nm. Some of the resulting properties of perfect quantum dots are atomic-like, although a quantum dot will contain 10^4 or more atoms.

There were several advantages proposed for the use of quantum dots over quantum wells in the active region of lasers. Because the energy level separation in quantum dots is greater than the thermal energy, it was predicted that there would be an improved temperature stability in the devices [8]. Due to the discrete energy spectrum exhibited by the dots, a

narrow spectral linewidth was expected. Also, because there are fewer states available to populate than in quantum well lasers, population inversion can be more easily achieved and so lower threshold currents were predicted [9]. Finally, devices using quantum dots can incorporate materials with greater lattice mismatches than those using wells, and so a greater spectral range can be achieved.

1.3.2 Considerations for the use of Quantum Dots in Devices

If quantum dots are to be used in devices at room temperature the following considerations need to be taken into account [1]:

- The localisation potential needs to be sufficiently deep, and the quantum dot size sufficiently small, that zero-dimensional effects are observed.
- The quantum dot should ideally contain only one electron and hole energy level, more than a few kT away from the wetting layer.
- High uniformity of the quantum dots in the ensemble is needed. A large variation in size will result in an inhomogeneous broadening of the spectra.
- For efficient device performance the material should be coherent and free from defects such as dislocations.

A large size of quantum dot is undesirable for use in devices such as lasers due to the thermal occupation of higher states, and this leads to the following condition [1]:

$$kT \leq \frac{1}{3}\left(E_{ex} - E_{gr}\right)$$

equation 1.2

In the above equation, E_{gr} and E_{ex} are the energy levels for the electrons in the ground and first excited state in the dot respectively. At room temperature this gives an upper limit for the size of InAs/AlGaAs dots of about 20nm. Different conditions will apply to the hole levels due to the small electron/hole mass ratio.

1.3.3 A History of Quantum Dots in Devices

In this section a brief history of the use of quantum dots in devices is given. The main developments and advances are summarised here and full details can be found in the paper

"Quantum-Dot Heterostructure Lasers" [10]. Other accounts can be found in references [11-13].

In 1976, Dingle and Henry introduced the idea to "exploit quantum effects in heterostructure semiconductor lasers to produce wavelength tunability" and achieve "lower lasing thresholds" via "the change in the density of states which results from reducing the number of translational degrees of freedom of the carriers" [14]. The ultimate example of size quantisation in solids is a quantum dot, which provides a practical application of atomic physics to the field of semiconductor devices. The major breakthrough in the field of semiconductor diode lasers [15-17] took place with the implementation of a double heterostructure as the active region of an injection laser to achieve efficient carrier confinement [18].

In 1986, Asada *et al.* [19, 20] theoretically considered gain in quantum wire and quantum dot lasers. They concluded that for the same homogeneous broadening of about 6meV the quantum dot devices would have increased material gain compared to the quantum wire case. However, in 1988 Vahala pointed out [20] that the inhomogeneity present in the dots would have an effect on the proposed advantages of these dots in devices, and the realisation of high gain operation would dictate that "quantum box fabrication tolerances are tightly controlled".

The real breakthrough in using quantum dots in optoelectronic devices came with the development of the self-organised growth method which was capable of producing dense arrays of uniform dots with a great reduction in the number of defects compared to other growth methods [21, 22]. One of the advantages of this method is that it is cost effective and can be done without any significant changes needing to be made to the growth equipment. The presence of a wetting layer produced during the growth process was demonstrated first in 1985 for InAs grown on GaAs [23]. It was then in 1993 that photo-pumped lasing using quantum dot heterostructures was demonstrated [21, 22] both at low and room temperatures. Even these early examples of quantum dot lasers demonstrated good device characteristics at low temperature. However, the devices still remained worse than the best quantum well devices at room temperature. The reason for this was temperature-induced escape of carriers from the dots [24]. This problem was overcome by stacking vertically coupled quantum dots, making lasing at room temperatures possible [25].

There are many potential applications for quantum dot lasers. In 2001/2002, telecoms accounted for 70% of the total semiconductor laser market [26], and there is a need for cheap and reliable 1.3μm quantum dot VCSEL lasers. With continued improvement in the fabrication and development, quantum dots could soon replace quantum wells in lasers.

1.3.4 Fabrication of Quantum Dots

There are several techniques available for quantum dot growth. The most common of these is the Stranski-Krastanow growth method [27-29] which is described here. Details of other growth methods can be found in reference [30]. In the Stranski-Krastanow growth process a layer of semiconductor material, such as InGaAs, is grown on top of another layer of different semiconductor material, such as GaAs. These materials are known as the deposited and substrate materials respectively. The lattice-mismatch between these two materials needs to be small, about 2% [31], with the substrate material having the smaller lattice constant. A two-dimensional layer of uniform thickness begins to build up which is known as the wetting layer. This situation is not energetically favourable and so to reduce the strain in the lattice small islands of material appear on top of the wetting layer: these are the quantum dots. This process is said to be *self-organising* or *self-assembled* and takes the system into a more favourable energy state. Differences in the growth conditions result in a distribution in the dots in size, shape and material composition. This leads to an inhomogeneous broadening of the energy spectra, typically in the range 18-80meV. Typical dot densities are of the order $10^{10} - 10^{11}$ cm^{-2}.

1.4 Lasers

1.4.1 Introduction

The aim of this thesis is to study the recombination mechanisms that occur in quantum dots for a better understanding of quantum dot lasers. Therefore in the following sections is a brief summary and history of semiconductor lasers. A more detailed discussion of the theory of semiconductors, and in particular quantum dots, is given in the next chapter; the purpose of these sections is to provide a brief introduction to the subject. For a more detailed account refer to books by Coldren and Corzine [30], Zory [32] or Casey and Panish [33].

1.4.2 Principles of Semiconductor Lasers

The term 'laser' is an acronym for Light Amplification by the Stimulated Emission of Radiation. In general terms, a laser is an externally pumped self-sustained oscillator, which contains electrons in an excited state that emit photons when they fall from these higher states to lower energy states. The energy of the photon is dependent on the difference in energy of these lower and upper states; this difference is a property of the material system. These emitted photons are incoherent and random in phase and direction, and the process is known as *spontaneous emission* since it is randomly occurring. Another process is stimulated emission which happens when a photon stimulates an electron in an excited state to release its energy with the emission of another photon. This second induced photon has the same phase and direction as the incoming one and this is the principle of operation of a laser. To achieve lasing there must be a large density of carriers present and the rate of stimulated emission must exceed that of spontaneous emission; for this to occur population inversion is needed. This is the situation where there are more carriers in the upper state than in the lower state. For semiconductors this means that there must be a greater number of electrons in the conduction band than the valence band. Population inversion is achieved in semiconductor lasers by electrical pumping.

A semiconductor laser consists of a *p-n* junction and this is where the term *diode laser* comes from. The diode is forward biased and electrons from the *n*-doped region and holes from the *p*-doped region are injected into the undoped active region. A double heterostructure (DH) design is usually used, which confines the carriers and the light within the gain generating region.

Cladding layers confine the carriers within the active region due to their lower refractive index compared to that of the active region. The optical mode is thus confined within this region, allowing maximum interaction of the electromagnetic field with the gain-producing region. Sufficient gain must be generated to overcome the optical losses: optical feedback is provided by the cleaved facets of the semiconductor gain medium which reflect back a percentage of the light so that further amplification can take place.

1.4.3 A Brief History of Semiconductor Lasers

Since they were first demonstrated in the 1960s, semiconductor lasers have been widely used in commercial devices and have been the subject of extensive research. They have many

varied applications due to the wide range of light wavelengths they can offer: GaN lasers can produce light in the blue part of the visible spectrum whilst the far infrared can be reached with quantum cascade lasers.

A thorough review of the development of the maser and laser is given by Bertolotti [33]. Townes first demonstrated stimulated emission from an inverted population using a maser (a laser operating at microwave wavelengths) in 1954. The first development of a true laser was in 1960 by Maiman, using a solid state ruby crystal. In 1957 Watanabe *et al.* filed a patent for the semiconductor maser which was published in 1960 [34]. Then in 1961 it was proposed by Basov *et al.* that a *p-n* junction could be used to produce stimulated emission, which proved to be more successful than earlier methods used [35]. The first diode laser was produced in 1962 by Hall, emitting at 840nm and requiring a current density of around 100,000 Am^{-2} [36]. This GaAs based laser produced so much heat it could only be operated in a pulsed mode at a temperature of 77K. It was not until 1970 that the first room temperature operating device was created [37], after Kroemer suggested the double heterostructure in 1963 [18]. Mass production of LEDs began in 1972, with the first use of diode lasers in compact disk players happening in the 1980s. In 1995 this was followed by the DVD player with a laser emitting at 650nm. Recent advances involve the development of commercial lasers based on the nitride material system, emitting in blue/violet range.

1.5 Summary

In this chapter I have introduced the aims of the thesis, as well as a background to the field of quantum dots. The main advantages of the use of quantum dots over quantum wells in semiconductor lasers are given, along with a brief summary of the main developments in the field of lasers. The next chapter provides a theoretical description of quantum dots and their use in semiconductor lasers. The optical processes are discussed and the Einstein relations are given for quantum dots.

1.6 References

[1] D. Bimberg, M. Grundmann, and N. N. Ledentsov, Quantum Dot Heterostructures, John Wiley and Sons, Chichester, 1990.

[2] W. W. Chow and S. W. Koch, Semiconductor Lasers Fundamentals, Springer, Berlin, 1999.

[3] C. v. Opdorp and G. W. t. Hooft, Journal of Applied Physics 52 (1981) 3827.

[4] R. Olshansky, J. LaCourse, T. Chow, and W. Powazinik, Applied Physics Letters 50 (1987) 310.

[5] A. F. Phillips, S. J. Sweeney, A. R. Adams, and P. J. A. Thijs, IEEE Journal of Selected Topics in Quantum Electronics 5 (1991) 401.

[6] M. Grundmann and D. Bimberg, Physical Review B 55 (1997) 9740.

[7] D. G. Deppe, D. L. Huffaker, S. Csutak, Z. Zou, G. Park, and O. B. Shchekin, IEEE Journal of Quantum Electronics 35 (1999) 1238.

[8] Y. Arakawa and H. Sakaki, Applied Physics Letters 40 (1982) 939.

[9] M. Asada, Y. Miyamoto, and Y. Suematsu, IEEE Journal of Quantum Electronics 22 (1986) 1915.

[10] N. N. Ledentsov, M. Grundmann, F. Heinrichsdorff, D. Bimberg, V. M. Ustinov, A. E. Zhukov, M. V. Maximov, Z. I. Alferov, and J. A. Lott, IEEE Journal of Selected Topics in Quantum Electronics 6 (2000) 439.

[11] M. Grundmann, Physica E 5 (2000) 167.

[12] J. P. Reithmaier and A. Forchel, C. R. Physique 4 (2003) 611.

[13] D. Bimberg, N. Kirstaedter, N. N. Ledentsov, Z. I. Alferov, P. S. Kop'ev, and V. M. Ustinov, IEEE Journal of Selected Topics in Quantum Electronics 3 (1997) 196.

[14] J. P. v. d. Ziel, R. Dingle, R. C. Miller, W. Wiegmann, and J. W. A. Nordland, Applied Physics Letters 26 (1975) 463.

[15] Z. I. Alferov, in 99th Nobel Symp., 1996.

[16] Sov. Phys. Solid. Stat 8 (1967) 2480.

[17] I. Hayashi, IEEE Trans. Electron Devices ED-31 (1984)

[18] H. Kroemer, Proc IEEE 51 (1963) 1782.

[19] M. Asada, M. Miyamoto, and Y. Suematsu, IEEE Journal of Quantum Electronics QE-22 (1986) 1915.

[20] K. J. Vahala, IEEE Journal of Quantum Electronics 24 (1988) 523.

[21] N. N. Ledentsov, V. M. Ustinov, A. Y. Egorov, A. E. Zhukov, M. V. Maximov, I. G. Tabatadze, and P. S. Kop'ev, Fiz. i Tekh. Poluprovodn. 28 1484.

[22] N. N. Ledentsov, V. M. Ustinov, A. Y. Egorov, A. E. Zhukov, M. V. Maximov, I. G. Tabatadze, and P. S. Kop'ev, Semiconductors 28 (1994)

[23] L. Goldstein, F. Glas, J. Y. Marzin, M. N. Charasse, and G. Leroux, Applied Physics Letters 47 (1985) 1099.

[24] N. Kirstaedter, N. N. Ledentsov, M. Grundmann, D. Bimberg, V. M. Ustinov, S. S. Ruvimov, M. V. Maximov, P. K. Kop'ev, Z. I. Alferov, U. Richter, P. Werner, U. Gosele, and J. Heydenreich, Electron. Lett. 30 (1994) 1416.

[25] N. N. Ledentsov, J. Bohrer, D. Bimberg, S. V. Zaitsev, V. M. Ustinov, A. Y. Egorov, A. E. Zhukov, M. V. Maximov, P. K. Kop'ev, Z. I. Alferov, A. O. Kosogov, U. Gosele, and S. S. Ruvimov, in Mater. Res. Soc. Symp. Proc., Vol. 421 (R. J. Shul, S. J. Pearton, F. Ren, and C.-S. Wu, eds.), Pittsburgh PA, 1996.

[26] M. Lebby, OIDA White Paper (2006) 5.

[27] D. Leonard, M. Krishnamurthy, C. M. Reaves, S. P. Denbaars, and P. M. Petroff, Applied Physics Letters 63 (1993) 3203.

[28] C. Priester and M. Lannoo, Physical Review Letters 75 (1995) 93.

[29] P. Bhattacharya, S. Ghosh, and A. D. Stiff-Roberts, Annual Review of Materials Research 34 (2004) 1.

[30] L. A. Coldren and S. W. Corzine, Diode Lasers and Photonic Integrated Circuits, Wiley, Chichester, 1995.

[31] V. I. Trofimov, H. S. Park, and J. I. Kim, Applied Surface Science 226 (2004) 45.

[32] P. Zory, Quantum Well Lasers, Academic Press, Boston, 1993.

[33] H. C. Casey and M. B. Panish, Heterostructure Lasers, part A, Academic Press, New York, 1978.

[34] M. Bertolotti, Masers and Lasers: A Historical Approach, Adam Hilger, Bristol, 1987.

[35] Y. Watanabe and J. Nishizawa, Japan, 1960.

[36] N. G. Basov, O. N. Krokhim, and Y. Popov, JETP 19 (1961) 1879.

[37] J. R. Hook and H. E. Hall, Solid State Physics, John Wiley and Sons, Chichester, 1991.

[38] I. Hayashi and B. Panish, Journal of Applied Physics 41 (1970) 150.

2 Theoretical Background

2.1 Introduction

The theory of quantum dots can be found in various text books. A few examples of these are "Quantum Dot Heterostructures" by Bimberg [1] and "Optical Properties of Solids" by Fox [2]. The aim of this thesis is to understand how the localisation of the energy states affects the optical processes occurring in quantum dots, for their use in semiconductor lasers and LEDs. This chapter therefore starts with a brief introduction to the theory of some of the processes involved in semiconductors, beginning with the theory of the electronic properties of semiconductors, including energy level and density of states calculations. The Einstein relations are then discussed, along with some of the optical processes in semiconductors, focussing on those of quantum dots. This includes the recombination mechanisms, as well as optical gain/absorption. Finally, the broadening mechanisms are discussed.

2.2 Electronic Properties of Semiconductors

2.2.1 Introduction

Detailed descriptions of the electronic properties of semiconductors can be found in many solid state text books, such as "Solid State Physics" by Hook and Hall [3], "Semiconductor Optoelectronics" by Singh [4] and "Introduction to Solid State Physics" by Kittel [5]. Here a brief summary of the main concepts is presented.

2.2.2 Bandstructure

To understand semiconductors the periodicity of the crystal needs to be understood. Without this periodicity semiconductor problems would be almost impossible to solve due to the extremely large densities of atoms present. However, electrons moving in semiconductors are not moving through a random distribution of ions; semiconductor structures are crystalline and ordered, and the electrons move through a well defined periodic distribution. This periodicity affects the electronic properties of a semiconductor and thus its optical properties.

Methods are available to reduce the complexity of solving the electronic properties of semiconductors such as the orthogonalized plane wave method or the *k·p* perturbation method [4], which can be used to solve for the energy levels. To represent the electronic properties *bandstructure* is used, which defines the allowed electron energy states and gives the *E-k* relation.

Semiconductors comprise of energy bands: the conduction band and valence band. In a quantum confined structure the valence band splits into three separate bands due to spin-orbit coupling: the heavy-hole (HH), light-hole (LH) and split-off bands (SO). In this thesis, all calculations are performed using values for the heavy-hole band since this is the band from which most of the light is produced in quantum dots. References to the valence band therefore relate to the heavy-hole band. Details of the other bands can be found in references [6-8]. A simplified bandstructure for a direct bandgap semiconductor is shown in Figure 2.1.

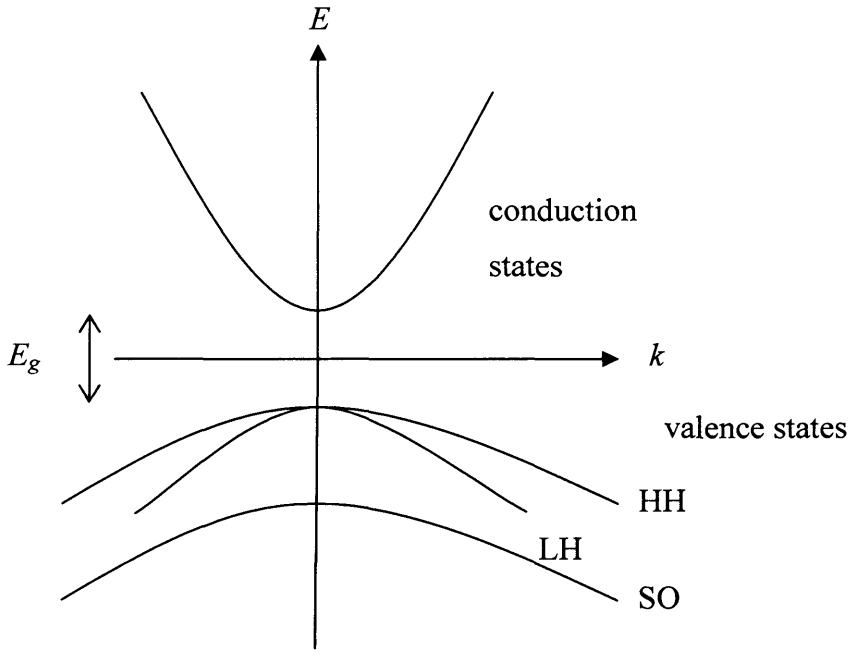

Figure 2.1 - Bandstructure for a direct bandgap semiconductor.

Direct bandgap semiconductors are ones in which the bottom of the conduction band occurs at the same value of *k* as for the bottom of the valence band, where *k* is the magnitude of the wavevector. Examples of these are GaAs and InAs, and the quantum dots modelled in this thesis are made of InAs. Semiconductors in which the bottom of the conduction band occurs at a different value of *k* to that of the valence band are known as *indirect* bandgap materials. These materials, such are Si, AlAs etc., do not make good materials for optical devices due

to their poor interaction with light. This is because of the need for momentum conservation which makes strong optical transitions in indirect semiconductors difficult.

Direct bandgap semiconductors are isotropic and the *E-k* relation is approximated to be parabolic, with constant energy surfaces that take the form of a sphere in *k*-space. The difference in energy between the minima of the conduction and valence bands is called the *bandgap* of the material, E_g. The electron energy E_c is measured from the conduction band edge and is positive into the conduction band, whilst the hole energy E_v is measured from the valence band edge and is positive into the valence band, as shown in Figure 2.1.

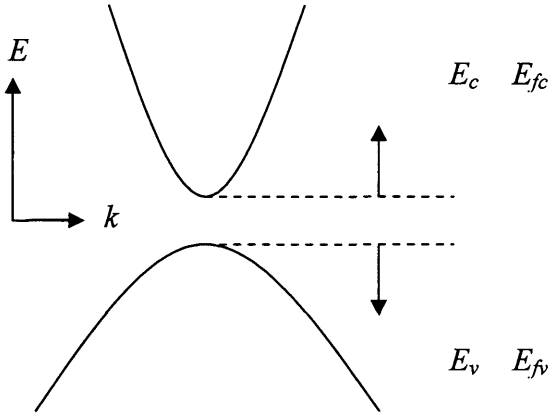

Figure 2.2 - Conduction and valence band energy measurement.

The *E-k* relation for the energy of the electrons can be written as

$$E_c(k) = \frac{\hbar^2 k^2}{2m_c}$$

equation 2.1

where m_c is the effective mass of the electrons. Similarly, for the holes in the valence band, the equation for the energies is

$$E_v(k) = \frac{\hbar^2 k^2}{2m_v}$$

equation 2.2

where m_v is the effective mass of the holes. For conservation of momentum in a transition, the photon energy $h\upsilon$ must be equal to the difference in energy of the electron and hole states:

$$h\upsilon = E_g + \frac{\hbar^2 k^2}{2m_c} + \frac{\hbar^2 k^2}{2m_v}$$

equation 2.3

A reduced electron-hole mass μ can be defined according to:

$$\frac{1}{\mu} = \frac{1}{m_c} + \frac{1}{m_v}$$

equation 2.4

From this equation 2.3 can be rewritten as:

$$h\upsilon = E_g + \frac{\hbar^2 k^2}{2\mu}$$

equation 2.5

The wavevector k is related to the momentum of an electron by:

$$p = \hbar k$$

equation 2.6

In semiconductor crystals the quantity $\hbar k$ is the equivalent of the momentum for the free space electrons, and is called the crystal momentum. It must be conserved during any transitions that occur. Since the photon has negligible momentum compared to that of the electrons and holes, radiative transitions occur between electrons and holes having the same value of wavevector.

The carrier concentration in a semiconductor is dependent on the temperature, the bandgap, the doping and the carrier mass. At a temperature of zero Kelvin the valence band is completely full with electrons and the conduction band is completely empty. As the temperature is increased to a finite value the carrier occupation numbers are controlled by the Fermi distribution function. The occupation probability of an electron or hole state with energy E is given by

$$f = \frac{1}{\exp\left(\frac{E - E_f}{kT}\right) + 1}$$

equation 2.7

where E_f is the Fermi energy. This distribution is discussed in more detail in section 2.4.2. At a temperature of zero Kelvin, the Fermi distribution function is a step function; as the temperature is raised it 'smears' out and carriers are emitted into the conduction band from the valence band.

As described in chapter 1, when one or more dimensions of a semiconductor are reduced quantum effects can become apparent, which alters the state distribution. To study the properties of electrons and holes, and obtain the energy levels, the time-independent Schrödinger equation needs to be solved:

$$\frac{\partial \psi(\mathbf{r})^2}{\partial \mathbf{r}^2} + \frac{2m_{c,v}}{\hbar^2}[E - U(\mathbf{r})]\psi(\mathbf{r}) = 0$$

equation 2.8

$U(\mathbf{r})$ is the background potential seen by the electrons and holes. The electron and hole wavefunctions in a periodic crystal satisfy Bloch's theorem, which in 3D is given by:

$$\psi_k(\mathbf{r}) = F(\mathbf{r})u_k(\mathbf{r})$$

equation 2.9

Here $F(\mathbf{r})$ is the envelope function and $u_k(\mathbf{r})$ is called the Bloch function and has the same periodicity as the crystal lattice $\boldsymbol{R}$, i.e.

$$u_k(\mathbf{r}) = u_k(\mathbf{r} + \mathbf{R})$$

equation 2.10

For a two-dimensional quantum well, in the limiting case of an infinitely deep potential, the energy levels in the confined directions are given by

$$E_n = \frac{\hbar^2}{2m_{c,v}}\left(\frac{n\pi}{L_z}\right)^2$$

equation 2.11

where L_z is the width of the well and n is a positive integer. In the limit of L_z becoming large, a continuum of states is produced and the system no longer exhibits quantum effects.

2.2.3 Density of States

A system is described as low-dimensional when one or more of its dimensions is reduced in size such that its size becomes comparable with the de-Broglie wavelength (see section 1.4.1 for more details). This alters the density of states (DOS) for the structure and thus its properties. The density of states is used in calculations of many semiconductor properties, such as absorption, and in the analysis of devices. The density of states for a two-dimensional quantum well, $\rho_{2D}(E)$, is defined as the number of available electronic states for electrons of energy E per unit energy per unit area. To derive the density of states the number of k-states that lie in an annulus of radius $\boldsymbol{k}$ to $\boldsymbol{k}$ + d$\boldsymbol{k}$ are calculated, as shown in Figure 2.3 [9].

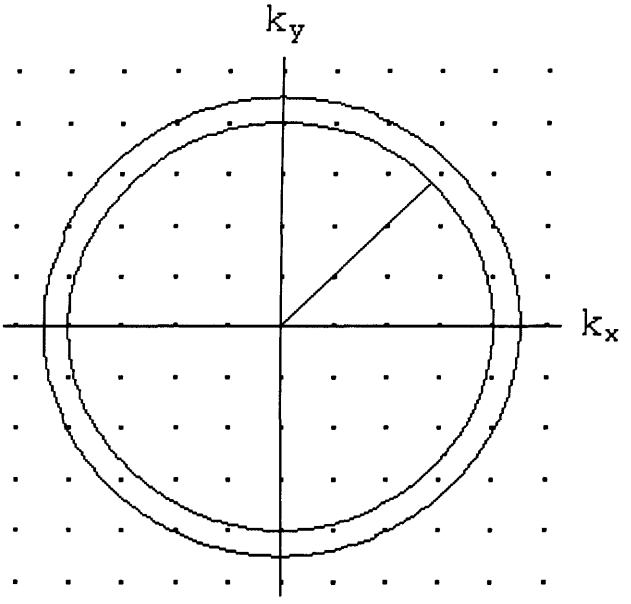

Figure 2.3 - k-space in 2D. The density of states at an energy E is the number of k-states per unit area contained within the annulus of radius k and thickness dk.

The area of the annulus is given by $2\pi|\mathbf{k}|\mathbf{dk}$, and the area that one state occupies in k-space is $(2\pi/L_z)^2$, where L_z is the width of the well. The number of states is then the area of the annulus divided by the area of one state, which gives

$$\rho(\mathbf{k})\mathrm{d}\mathbf{k} = 2\times\frac{2\pi|\mathbf{k}|\mathrm{d}\mathbf{k}}{\left(2\pi/L_z\right)^2} = \frac{L_z^{\,2}}{\pi}|\mathbf{k}|\mathrm{d}\mathbf{k}$$

equation 2.12

where the multiplication factor of two has been included to take account of the spin degenerate states. Dividing by the area L_z^2 gives the *density* of states as:

$$\rho_{2D}(\mathbf{k})\mathrm{d}\mathbf{k} = \frac{|\mathbf{k}|}{\pi}\mathrm{d}\mathbf{k}$$

equation 2.13

This equation can be re-written in terms of energy using the parabolic relation, given in equation 2.1, which rearranging gives an equation for k as:

$$|\mathbf{k}| = \left(\frac{2mE}{\hbar^2}\right)^{1/2}$$

equation 2.14

Differentiating this with respect to energy gives

$$\mathrm{d}\mathbf{k} = \left(\frac{2mE}{\hbar^2}\right)^{-1/2}\frac{m}{\hbar^2}\mathrm{d}E$$

equation 2.15

and substituting into equation 2.13 gives:

$$\rho_{2D}(E)\mathrm{d}E = \frac{|\mathbf{k}|}{\pi}\mathrm{d}\mathbf{k} = \frac{1}{\pi}\left(\frac{2mE}{\hbar^2}\right)^{1/2}\left(\frac{2mE}{\hbar^2}\right)^{-1/2}\frac{m}{\hbar^2}\mathrm{d}E = \frac{m}{\pi\hbar^2}\mathrm{d}E$$

equation 2.16

Therefore the density of states for a 2D system, for one sub-band in terms of energy, is given by

$$\rho_{2D}(E) = \frac{m}{\pi\hbar^2}$$

equation 2.17

and has dimensions of $[\mathrm{L}]^{-2}[\mathrm{E}]^{-1}$. (The density of states for a quantum well is often written, incorrectly, in units of per unit energy per unit *volume*, and an L_z appears in the denominator

of equation 2.17. The correct definition of the density of states for a quantum well is independent of the well width and has units of per unit energy per unit *area*.)

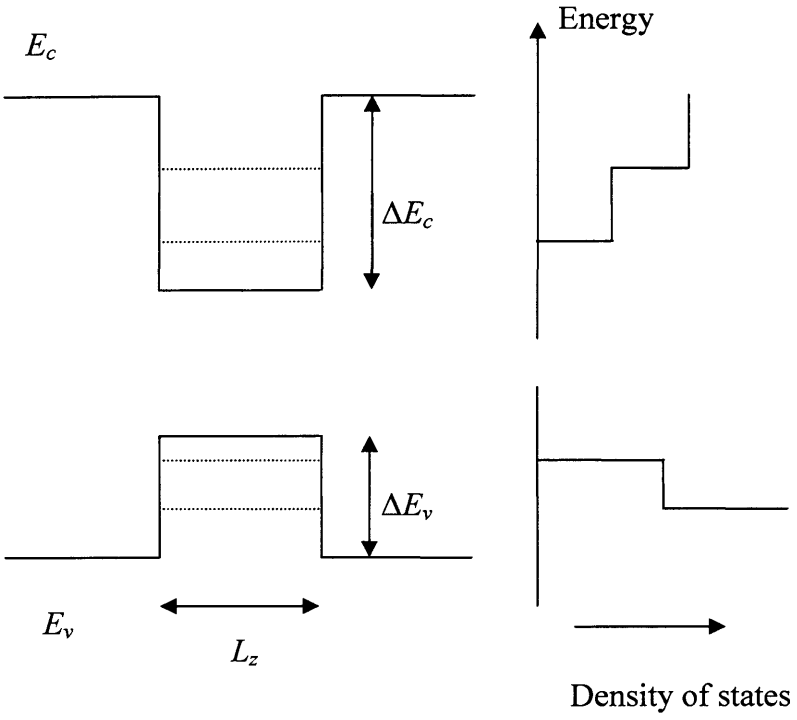

Figure 2.4 - Density of states for a two-dimensional quantum well.

Due to the quantisation effects, a quantum well exhibits a step-like density of states function. If the well is sufficiently thin then the sub-band separation is much greater than kT at room temperature, and so only a small thermal population of higher energy states will exist. This is the main reason for the improvement of semiconductor lasers using quantum wells in the active region instead of bulk. Figure 2.5 shows the difference between the density of states for a quantum well and for bulk material.

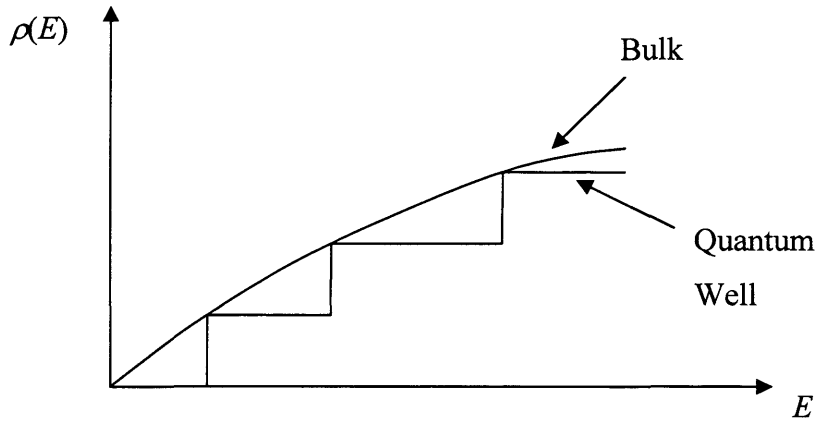

Figure 2.5 - Density of states for an infinite-barrier quantum well and for bulk material.

If all three dimensions of the structure are reduced, the result is quantum dots. The energy states are now quantised in all three directions and the dots are often said to have a theoretical delta-function density of states. However, a density of states for a zero-dimensional system has no physical meaning and it is more appropriate to refer to the *number* of states. For a quantum dot the parabolic *E-k* relation for electrons is written as

$$E = \frac{\hbar^2}{2m_c}\left(k_x^{\,2} + k_y^{\,2} + k_z^{\,2}\right)$$

equation 2.18

It has been seen from experimental investigation that quantum dots often take the shape of flat discs or pyramids [10, 11]. Throughout this thesis the shape of a quantum dot is modelled as a flat box, as shown in Figure 2.6, in which the *x-y* directions are taken to be the same

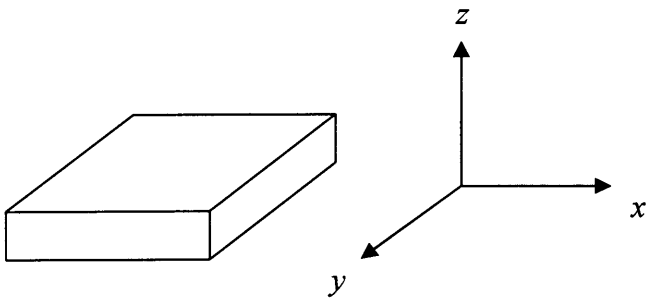

Figure 2.6 - Geometry of quantum dot.

Because of the relatively large dimensions in the x,y directions, the k_x and k_y wavevectors have a much smaller value than k_z. Therefore the energy levels in these directions are very closely spaced, and so it is the z-direction that determines the energy levels in the dot, as shown in Figure 2.7.

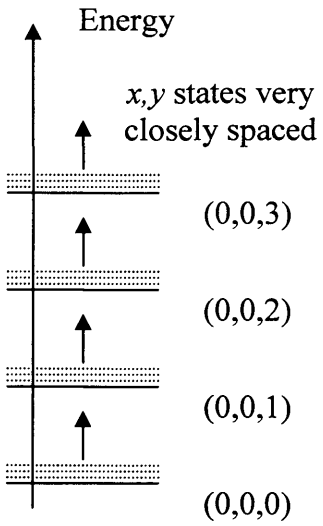

Figure 2.7 - Energy levels for a quantum dot. The states in the x,y directions are very closely spaced.

2.2.4 Atomic Levels to Bands

To understand the bandstructure of semiconductors it is useful to look at the isolated atom. The following notes are adapted from Singh [4]. The energy spectra of a typically isolated atom is made up of two regions, which are shown in Figure 2.8 [4].

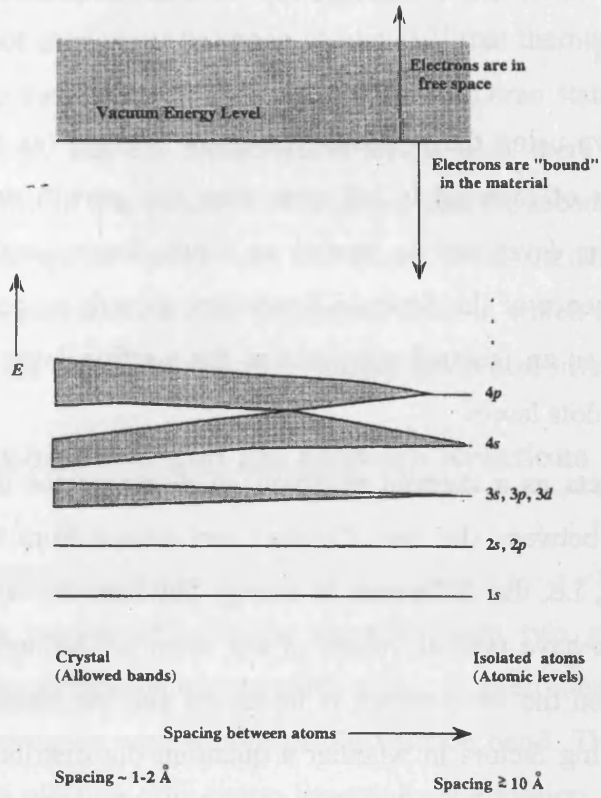

Figure 2.8 - Schematic of how allowed and forbidden bands form.

In one region are bound states in which the electron is bound to the nucleus by the Coulombic interactions; in the other region are free states in which the electron is free to move. These two regions are separated by the *vacuum energy*, and this is chosen as the zero of energy. The bound state electron energies are negative with respect to the vacuum level energy. A region of 'forbidden gap' separates each of the allowed energies, which are discrete. When a crystal is formed and the atoms are brought together an electron in a given atom begins to 'see' the nuclei of a nearby atom, i.e. the wavefunctions begin to overlap. The result is bands of allowed energy levels, as shown in Figure 2.8. These energy levels are now not continuous in energy as for the free electron case: there are now regions where there are no allowed energy values. In other words, an electron in the semiconductor cannot exist in these 'gaps'. Deep core levels are relatively unaffected and it is the outer most electrons of the atoms that form these bands because they are so loosely bound to the nucleus. Optical transitions from the conduction band to the valence band are from *s-type* states to *p-type* states.

2.3 Consequences of the Wetting Layer: Thermal or Non-Thermal Distribution

When dots are grown using the Stranski-Krastanow method (as described in the previous chapter) a thin layer of material is left over from the growth process. This thin layer is known as the *wetting layer* and is treated as a two-dimensional quantum well. It is an unavoidable consequence of the Stranski-Krastanow growth process, and therefore the dots cannot be regarded as an isolated system and the wetting layer must be included in all analysis of quantum dots lasers.

The wetting layer acts as a thermal reservoir of electrons for the dots and exchange of carriers takes place between the two. Carriers can escape from the dots due to the finite localisation energies, i.e. the difference in energy between the confined dot levels and the wetting layer, which have typical values of the order of 200meV. This process becomes more significant when the temperature is increased and the localisation energy decreased. One of the determining factors in whether a quantum dot distribution can be described by thermal statistics is the ratio of the rate of escape of carriers to the recombination rates.

If the escape time is small compared to the recombination time then a thermal equilibrium can be established between the dots and the carriers. Carriers can be emitted and recaptured into the dot ensemble before they recombine, and they can thus reallocate themselves amongst the dots. The probability of this occurring is dependent on the localisation energy: larger dots, which have higher localisation, will be more highly populated than smaller dots and this enhances the probability of escape. For this situation Fermi-Dirac statistics can be applied to the distribution, with electron and hole quasi-Fermi levels for the whole system.

On the other hand, if the recombination of carriers is happening on a faster timescale than the thermal emission of carriers then a non-equilibrium condition will occur. In this situation the population will not depend on the electron and hole energies, and dots of different sizes will have the same occupation. The dots are therefore uncoupled and are not controlled by thermal statistics; the distribution functions do not depend on the electron and hole energies and represent non-equilibrium populations. In this case it is not appropriate to apply Fermi-Dirac statistics.

If the situation is somewhere in between the two extreme cases described above, the situation is further complicated. It should also be remembered that the electron and hole

states have different localisation energies and the presence of excited states can influence the rate of thermal emission of carriers. It has been shown [12] that thermal equilibrium can be maintained down to temperatures of about 100K and Fermi-Dirac statistics can be used to describe these distributions, but for temperatures below this there is a breakdown of thermodynamic equilibrium. In this project it is assumed that the recombination occurs on a similar timescale to the escape of carriers and that Fermi-Dirac statistics *can* be applied to model the population. An alternative model for neutral dots, in which Fermi-Dirac statistics cannot be applied to both the electron and hole distributions, is also investigated.

2.4 Radiative Recombination and the Einstein Relations

2.4.1 Introduction

Generally, recombination mechanisms can be classified into two groups: radiative and nonradiative. Radiative recombination occurs when a photon is emitted when an electron in the conduction band recombines with a hole in the valence band. There are three optical processes associated with electron-hole pairs: spontaneous emission, absorption/gain, and stimulated emission. These can be described by the Einstein relations [13], which are discussed in the following section. Nonradiative recombination is the recombination of an electron-hole pair without the emission of a photon and is discussed further in section 2.6.

2.4.2 The Einstein Relations

To study the optical properties of semiconductors the transitions of electrons between the quantum mechanical energy levels are often studied. To describe these processes the Einstein relations are used [13], which describe the interaction of electrons with photons for a system in thermal equilibrium consisting of two discrete energy levels. These equations were first derived to explain the transitions between two discrete energy levels in an atom which is analogous to the quantum dot problem solved in this thesis. However, they can also be used to describe the recombination between states in a continuous energy band, such as for a quantum well [14].

Radiative recombination occurs when an electron in the conduction band recombines with a hole in the valence band producing a photon; in other words, it is a transition of an electron in the conduction band to an empty state (a hole) in the valence band. The processes associated with electron-hole pairs are spontaneous emission, absorption/gain and stimulated

emission. The transition rates are proportional to the probability of the initial state being occupied and the final state not being occupied (i.e. an empty state).

At a given temperature T the available electrons and holes in a semiconductor are distributed over a range of energies. The occupation probability, f, of a carrier with energy E is described by Fermi-Dirac statistics. f is called the Fermi function and is given by:

$$f = \frac{1}{\exp\left(\frac{E - E_f}{kT}\right) + 1}$$

equation 2.19

E_f is the Fermi level and k is Boltzmann's constant. When the system is not in thermal equilibrium, and carriers are being injected continuously, the term *quasi-Fermi level* is used. It is assumed that the electrons in the conduction band are in thermal equilibrium with each other, and correspondingly the holes in the valence band are in thermal equilibrium with each other. The *quasi-Fermi levels* of the conduction and valence bands are then referred to. The occupation probabilities of an electron in the conduction band and a hole in the valence band are calculated separately, each depending on the energy of the electron or hole, and the appropriate quasi-Fermi level.

The occupation probability of an electron in the conduction band with energy E_c, denoted by f_c, is given by

$$f_c = \frac{1}{\exp\left(\frac{E_c - E_{fc}}{kT}\right) + 1}$$

equation 2.20

and similarly, the occupation probability of a hole in the valence band with energy E_v, denoted by f_v, is given by

$$f_v = \frac{1}{\exp\left(\frac{E_v - E_{fv}}{kT}\right) + 1}$$

equation 2.21

Here, E_{fc} and E_{fv} are the conduction and valence band quasi-Fermi levels respectively. It should be noted that throughout this thesis f_v is used to represent the occupation probability

of a *hole* in the valence band and not of an electron. In the equations, E_c and E_{fc} are measured from the conduction band edge and are positive into the conduction band and in the same way, E_v and E_{fv} are measured from the valence band edge and are positive into the valence band. This is shown in Figure 2.2.

As described in section 2.2, the energy levels are given by the parabolic band approximation (equation 2.1 and equation 2.2) as:

$$E_c(k) = \frac{\hbar^2 k^2}{2m_c}$$

$$E_v(k) = \frac{\hbar^2 k^2}{2m_v}$$

For a large density of states the Fermi function is equivalent to the fraction of occupied states at energy E. When $E=E_f$ the distribution function takes a value of a half. When the energy E is a few kT below the Fermi level, the function approaches unity, and alternately when the energy is a few kT above the Fermi level it approaches zero. The Fermi function becomes a step function at T=0K, stepping from zero to unity at $E = E_f$.

The three types of possible optical transitions are described here for N_{dots} identical quantum dots having spin degenerate electron and hole energy levels. In these equations, the valence state is labelled as state *1* and has energy E_1, and the conduction state as state *2* with energy E_2. The dimensions of each of the rates are $[T]^{-1}$. The probability of an electron in a conduction state is f_c and the probability of a hole in a valence state is f_v.

- **Stimulated Emission** occurs when a photon induces an electron in a higher state *2* to fall to a lower state *1*, emitting a photon which has the same energy, phase and direction as the incident photon. The transition rate for N_{dots} identical dots is given by:

$$R_{21} = 2N_{dots}B_{21}P(h\upsilon)f_c f_v$$

equation 2.22

Here, B_{21} is the transition probability and is a measure of the strength of the interaction between the electron and photon, and has dimensions of $[E][L]^3[T]^{-1}$. B_{21} is for one transition only and so a factor of two is included in the equation to account for the two possible transitions between the spin degenerate states. $P(h\upsilon)$ is the photon density at energy $h\upsilon = E_2 - E_1$, and has dimensions of $[L]^{-3}[E]^{-1}$. $f_{v,c}$ are the

Fermi probability functions given in equation 2.21 and equation 2.20, describing the occupancy of states *1* and *2* with a hole and electron respectively. The rate is dependent on the lower level being empty (a hole) and the upper level being occupied.

- **Absorption** is when a photon is absorbed, promoting an electron from a valence state to a conduction state, with a transition rate given by:

$$R_{12} = 2N_{dots}B_{12}P(h\upsilon)(1-f_v)(1-f_c)$$

equation 2.23

Again, B_{21} is the transition probability and is for one transition, and $P(h\upsilon)$ is the photon density. The rate is dependent on the lower level being occupied and the upper level being empty.

- **Spontaneous Emission** occurs when an electron spontaneously falls from a higher state to a state of lower energy, with the emission of a photon. The incident photon in this case is called a *virtual* photon and the emitted photon has a random phase and direction and so does not contribute to the coherent optical field. The transition rate is given by:

$$R_{spon} = 2N_{dots}A_{21}f_c f_v$$

equation 2.24

Here, A_{21} is the probability of the transition occurring and again is for one transition only. Because this process is a spontaneous one it is independent of the photon density, $P(h\upsilon)$, and dependent only on the relative occupancies of the two levels. It can be thought of as stimulated emission instigated by the zero-point fluctuations of the electromagnetic field. Spontaneous emission is the major radiative mechanism in light-emitting diodes (LEDs) since optical feedback is not usually present.

Figure 2.9 shows the possible optical transitions for a simple two level system. Open circles represent empty states (holes) and filled circles represent occupied states (electrons).

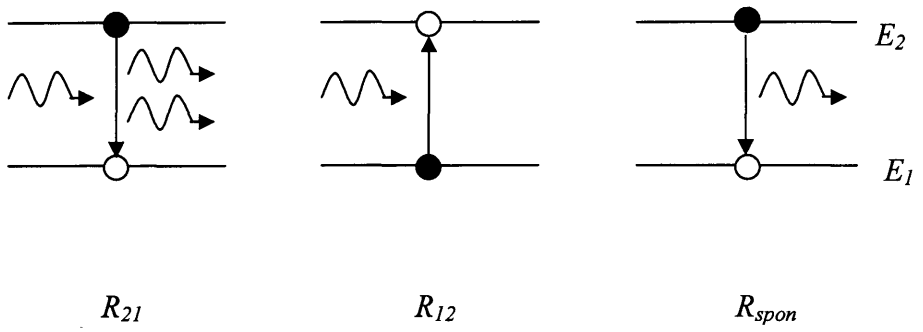

Figure 2.9 - Possible optical transitions between two levels, E_1 and E_2, of a simple system, described by the Einstein relations. Open circles represent empty states (holes) and filled circles represent occupied states (electrons).

Energy and momentum must be conserved in these transitions. Thus the energy of the emitted or absorbed photon must be equal to the energy difference between E_1 and E_2. The momentum of the photon is small, and equation 2.6 gives the relation of the momentum to the wavevector k as:

$$p = \hbar k$$

For a typical wavelength of 1000nm the wavevector k takes a value of about 10^6 m^{-1}. Typical k values of electrons and holes are of the order of 10^8 to 10^9 m^{-1}, which means the photon momentum is negligible and so the electron momentum must equal the hole momentum. This means that vertical transitions occur, between levels of similar wavevector k; this is known as the *k-selection* rule.

In thermal equilibrium the number of photons does not change and the absorption and emission are balanced, i.e. the total upward rate is equal to the total downward rate:

$$R_{12} = R_{21} + R_{spon}$$

equation 2.25

Substituting for equation 2.22, equation 2.23 and equation 2.24 into equation 2.25 and rearranging gives

$$P(h\upsilon) = \frac{f_v f_c A_{21}}{(1-f_v)(1-f_c)B_{12} - f_c f_v B_{21}}$$

equation 2.26

or using equation 2.19 and equation 2.21 for the occupation probabilities of states *2* and *1* respectively gives:

$$P(h\upsilon) = \frac{A_{21}}{B_{12}\exp\left(\frac{E_2 - E_1}{kT}\right) - B_{21}}$$

equation 2.27

From Planck's law of blackbody radiation the photon density is given by:

$$P(h\upsilon) = \left(\frac{8\pi n^3}{h^3 c^3}\right)(h\upsilon)^2 \frac{1}{\exp\left(\frac{h\upsilon}{kT}\right) - 1}$$

equation 2.28

From comparison with equation 2.27 it can be seen that for both equations to hold for all temperatures,

$$B_{12} = B_{21}$$

equation 2.29

and

$$A_{21} = \frac{8\pi n^3}{h^3 c^3}(h\upsilon)^2 B_{21}$$

equation 2.30

The constants A_{21}, B_{21} and B_{21} are known as the Einstein A and B coefficients and their relation is given above in equation 2.29 and equation 2.30.

It can be seen from equation 2.29 and equation 2.30 that there is a fundamental link between spontaneous emission and stimulated emission. This means that the system can be analysed under thermal equilibrium using just one independent constant B (or A). The reciprocal of the A coefficient is equivalent to the spontaneous lifetime for one transition and has units of reciprocal seconds:

$$\tau_{sp} = \frac{1}{A}$$

equation 2.31

In this context the reciprocal of A does not represent the band-to-band spontaneous lifetime, but is associated with the transitions between the two level system.

2.5 Spontaneous Emission and Gain

2.5.1 Introduction

In this thesis the spontaneous emission and gain are studied. The spontaneous emission is independent of the photon density $P(h\upsilon)$ in a semiconductor device and thus can provide many of the details about the physics of the device, such as information about carrier distributions and energy spectra. Spontaneous emission is related to the gain through the Einstein relations, and thus by studying the spontaneous emission a detailed picture of the optical characteristics can be built up. In the following sections the main physics of spontaneous emission and gain is summarised. The discrete energy states present in dots fundamentally changes their emission and absorption spectra, compared to those of quantum wells. Since the main focus of this thesis is quantum dots, the relations for the dots are described in most detail. The model also incorporates a quantum well wetting layer and so equations for the gain and spontaneous emission in wells are also given. Full details can be found in references [6, 8, 12].

2.5.2 Spontaneous Emission and Gain for Quantum Dots

The Einstein A and B coefficients can be related to the spontaneous emission rate and the optical cross section. As shown in the section 2.4.2 the stimulated emission and absorption rates for N_{dots} identical dots with a degeneracy of two are given in equation 2.22 and equation 2.23 respectively:

$$R_{21} = 2N_{dots}BP(h\upsilon)f_c f_v$$

$$R_{12} = 2N_{dots}BP(h\upsilon)(1-f_v)(1-f_c)$$

Here, B_{21} and B_{12} have been replaced by B, which has dimensions of $[E]^3[L]^3[T]^{-1}$, and again is for a single transition. Similarly, the spontaneous emission rate for N_{dots} identical dots is given in equation 2.24 as

$$R_{spon} = 2N_{dots} A f_c f_v$$

where A has dimensions of $[T]^{-1}$ and is for recombination between a single pair of spin states. This equation can be written in terms of the B coefficient using equation 2.30 as:

$$R_{spon} = 2N_{dots}\left(\frac{8\pi n^3}{h^3 c^3}\right)(h\upsilon)^2 B f_c f_v$$

equation 2.32

The spontaneous recombination current can be obtained by summing the spontaneous recombination over all dots and multiplying by the electronic charge:

$$J_{spon} = q\sum R_{spon}(E)$$

equation 2.33

The maximum radiative current is achieved when the dots are fully inverted, i.e. f_v=1 and f_c=1. For the ground state of an ensemble of N_{dots} identical dots with a degeneracy of two in the upper and lower states, the maximum radiative current density is given by:

$$\begin{aligned} J_{spon}^{max} &= \frac{2qN_{dots}}{area \times \tau_{spon}} \\ &= \frac{2qN_{dots}A}{area} \end{aligned}$$

equation 2.34

The factor of two is included since A refers to a single transition and there are two possible radiative transitions between the spin-degenerate dot states.

To calculate the gain it is necessary to calculate the net induced rate between the conduction and valence states of the dots:

$$\begin{aligned} R_{net} &= R_{\downarrow} - R_{\uparrow} \\ &= R_{21} - R_{12} \end{aligned}$$

equation 2.35

Substituting for the rates gives the net induced rate in dimensions of $[T]^{-1}$ as:

$$R_{net} = 2N_{dots}BP(h\upsilon)(f_c + f_v - 1)$$

equation 2.36

Optical gain is the fractional change in photon number per unit distance. The total number of photons in the cavity per unit energy is simply the photon density, equation 2.28, multiplied by the volume of the cavity, V_{cav}. The number of photons created per unit time by net stimulated processes at energy $h\upsilon$ is R_{net}. The Lorentzian broadening function $L(h\upsilon)$ also needs to be included. $L(h\upsilon)$ is known as the homogeneous broadening term and is discussed in more detail in section 2.8. It has dimensions of $[E]^{-1}$ and arises because the transitions are not delta-functions but are broadened. The optical gain therefore is the number of induced photons divided by the total number of photons in the cavity, where the factor (n/c) converts to per unit distance:

$$G(h\upsilon) = \int\left(\frac{n}{c}\right)\frac{R_{net}L(h\upsilon)}{P(h\upsilon)V_{cav}}dh\upsilon$$

equation 2.37

Substituting for R_{net}, equation 2.36, gives the gain at $h\upsilon$ for an ensemble of N_{dots} identical dots as

$$G(h\upsilon) = \int\left(\frac{n}{c}\right)\frac{2N_{dots}BL(h\upsilon)}{V_{cav}}(f_c + f_v - 1)dh\upsilon$$

equation 2.38

where the photon density has cancelled out.

Considering a waveguide of width w and length L, this is equivalent to a cavity volume V_{cav} where $V_{cav}=w_{mod}wL$. An effective mode width w_{mod} is defined which describes the coupling of the mode to the dot:

$$w_{mod} = \frac{A_{dot}^{\ 2}}{\int A^2(z)dz}$$

equation 2.39

A_{dot} is the value of the vector potential at the location of the layer of dots and is assumed to be constant over the layers. The gain for an ensemble of quantum dots can then be written as:

$$G(h\upsilon)=\frac{1}{area\times w_{mod}}\sum_i\frac{4\pi\hbar}{cn\varepsilon_0(h\upsilon)}\left(\frac{e}{2m_0}\right)^2 M^2\left[\int F_v(r)F_c(r)dr\right]^2 L(h\upsilon)N_{dots}(E_i)(f_c+f_v-1)$$

equation 2.40

where M is the momentum matrix element and F_v and F_c are the envelope functions of the holes and electrons respectively. M is obtained from the overlap integral of the initial and final states of the transition, and determines the strength of the interaction between the two wavefunctions involved. An optical cross section can be defined [15] which gives the absorption strength of the transition. Including the spin degeneracy, the expression for the optical cross section is given by:

$$\sigma_0=\frac{2\times 4\pi\hbar}{cn\varepsilon_0(h\upsilon)}\left(\frac{e}{2m_0}\right)^2 M^2\left[\int F_v(\mathbf{r})F_c(\mathbf{r})d\mathbf{r}\right]^2$$

equation 2.41

The modal absorption/gain due to N_{dots} dots is obtained by summing the contributions from all of the individual dots over the width and length of the guide ($N_{dots}wL$). So the modal absorption/gain for an ensemble of N_{dots} dots, including the inhomogeneous broadening, can be written as

$$\begin{aligned}G_{tot}(h\upsilon)&=\frac{N_{dots}}{2w_{mod}}\sum_i\sigma_0(E_i)L(h\upsilon)P(E_i)(f_c+f_v-1)\\&=\frac{1}{2w_{mod}}\sum_i\sigma_0(E_i)L(h\upsilon)N_{dots}(E_i)(f_c+f_v-1)\end{aligned}$$

equation 2.42

Here, $P(E_i)$ is the inhomogeneous broadening factor, and has been replaced in the second part of the expression with the number of dots with energy E_i, given by $N_{dots}(E_i)=N_{dots}\times P(E_i)$. Comparing equation 2.38,

$$G(h\upsilon)=\int\left(\frac{n}{c}\right)\frac{2N_{dots}BL(h\upsilon)}{V_{cav}}(f_c+f_v-1)dh\upsilon$$

with equation 2.42 gives an expression for the Einstein coefficient as:

$$B=\frac{1}{2}\left(\frac{c}{n}\right)\sigma_0$$

equation 2.43

2.5.3 Gain Relations

It was through the relations given in section 2.4.2 that Einstein first proposed the existence of stimulated emission. The process of stimulated emission allows a coherent optical field to build up in an optical cavity. Initially, when electron-hole pairs are first injected into the device, the process of absorption dominates. As more carriers are injected into a device, the quasi-Fermi levels move toward the conduction and valence band edges and the rate of spontaneous emission increases, which also increases the stimulated emission rate. When the stimulated absorption and emission rates are equal, a condition known as *transparency* is attained. Transparency occurs in dots when a particular state in the dot is half full e.g. there is one electron in the ground upper state and one hole in the ground lower state. At high currents gain saturation occurs in quantum dot lasers because the quasi-Fermi levels enter the wetting layer, which begins to become populated.

Comparing equation 2.22, stimulated emission, with equation 2.23, stimulated absorption, leads to the Bernard and Duraffourg condition [16]. This states that, when the system is in quasi-thermal equilibrium, the rate of stimulated emission will exceed that of stimulated absorption in a semiconductor when:

$$\Delta E_f > E_2 - E_1 > E_g$$

equation 2.44

In other words, for optical gain to occur in a semiconductor laser, the quasi-Fermi level separation ΔE_f must be greater than the energy of the photon, which means the minimum separation is that of the bandgap of the material, E_g. This is known as *population inversion* and an external source is needed to excite carriers into the higher state so that there are continuously more carriers in the higher state than in the lower. When the carrier density reaches a sufficient value such that the condition in equation 2.44 is satisfied optical gain occurs (for the specific transition energy). However, lasing will not occur at this point due to the absorption losses associated with the optical cavity and the mirrors. For lasing to occur, the value of the gain needs to be such that it also overcomes the losses of the cavity. This condition can be described by the following equation and is known as the threshold gain:

$$G_{th} = \alpha_i + \frac{1}{L_c} \ln R^{-1}$$

equation 2.45

Here, α_i is the internal loss of the cavity per unit length, L_c is the cavity length, and R is the reflectivity of the facet, where the reflectivity of both facets is assumed to be equal in this case. The second term on the right hand side of the equation thus represents the mirror losses. G_{th} represents the threshold *modal* gain. To get the threshold *local* (or *material*) gain the confinement factor Γ must be known; this describes the degree of coupling of the optical mode to the active region, and the two are related by:

$$G_{th} = \Gamma g_{th}$$

equation 2.46

The confinement factor is defined as the ratio of the light intensity within the gain material to the total intensity in the propagating mode. It arises because only a fraction of the power in the mode is coupled to the active gain material of the laser. The confinement factor is related to the mode width by

$$\Gamma w_{mod} = L_z$$

equation 2.47

where L_z is the thickness of the layer of dots. It is not meaningful to speak about the *local* gain of an ensemble of quantum dots, and the gain is characterised by the *modal* gain for an ensemble of dots in a specific waveguide.

It can be seen from equation 2.38 that the gain will take a maximum value when the factor ($f_c + f_v$ -1) takes a value of unity. In other words, when the conduction band is filled with electrons and the valence band is filled with holes (population inversion). Likewise, maximum absorption will be achieved when the factor ($f_c + f_v$ -1) is equal to minus one. The value of this factor is determined from the Fermi-Dirac distribution functions, for a given temperature, and is dependent on the injected current.

2.6 Nonradiative Recombination

2.6.1 Introduction

Nonradiative recombination involves the recombination of an electron-hole pair without the emission of a photon. The nonradiative processes that can be present in semiconductor lasers are nonradiative recombination via defects (often called Shockley-Read-Hall or SRH), surface recombination and Auger recombination. Surface recombination is not discussed

here but a description is given in the book by Coldren and Corzine [6]. Because of the absence of an emitted photon, nonradiative recombination is very hard to detect experimentally. One way to identify a particular nonradiative process is by measuring the variation of quantities such as carrier lifetime and internal quantum efficiency with parameters such as temperature and carrier concentration. Nonradiative recombination has the effect that it increases the threshold current in lasers and so is an undesirable effect which is ideally minimised in a laser device.

2.6.2 Nonradiative recombination via defects

In a perfect semiconductor there would be no defects present but this does not happen in reality. Defects in a semiconductor can create local disturbances in the crystal structure, which have new electronic states called *defect states* associated with them. If these new states are produced in regions of allowed bands (i.e. the conduction or valence bands) then their effects are minimal. However, if these defects appear in the forbidden bandgap region, as shown below in Figure 2.10, they will alter the optical and electronic properties of the semiconductor.

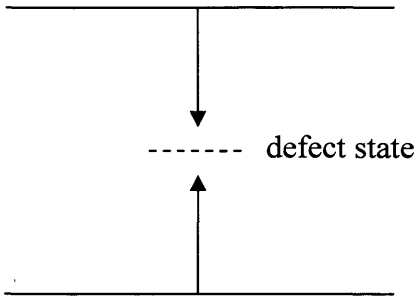

Figure 2.10 - Nonradiative recombination via defects.

The capture of electrons and holes onto the defect sites are independent events and so the overall capture rate is dependent on the slowest of these two capture processes; this is often referred to as the *rate-limiting step*. If it is taken to be electron capture then the nonradiative recombination rate, in dimensions of $[T]^{-1}$, can be written as

$$R_{nr} = \frac{n}{\tau_{nr}}$$

equation 2.48

where τ_{nr} is the nonradiative lifetime for carriers in the defect state and n is the electron number. The nonradiative rate can also be written as:

$$R_{nr} = A_{nr} n$$

equation 2.49

A_{nr} is the inverse of the nonradiative lifetime, and is given by

$$A_{nr} = \sigma v N_t$$

equation 2.50

where σ is the capture cross-section for the defects, v is the velocity of the electrons or holes, and N_t is the density of defects.

2.6.3 Auger recombination

Auger processes are essentially unimportant in semiconductors which have a bandgap greater than 1.4eV [4], such as GaAs, AlGaAs. However, in smaller bandgap materials, such as InAs, Auger recombination becomes more significant and this can have an effect on the development of long wavelength lasers. There are several processes for Auger recombination and these are explained in detail in the referenced books. For simplicity only one process is described here, which is shown schematically in Figure 2.11. An electron in a conduction state (1) recombines with a hole in a valence state (2), and the energy released in this process promotes another electron (3) to a much higher conduction state (4), which then dissipates its energy by the release of a phonon. For the case of quantum dots, this higher energy state is one in the wetting layer.

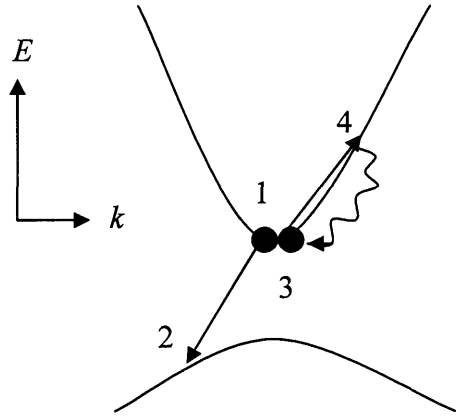

Figure 2.11 - Auger recombination.

The Auger rate for this process can be written as

$$R_{auger} = Cn^2 p$$

equation 2.51

where n and p are the electron and hole carrier densities, and C is the Auger coefficient. Auger recombination has a very strong dependence on carrier number.

2.7 Recombination in Quantum Wells

In systems with extended states such as quantum wells, all electrons in a given band can recombine with all holes in a given band, subject to k-selection. Boltzmann statistics can be approximated which leads to the result that the radiative recombination rate in a well is proportional to the product of the electron and hole densities, N and P respectively, in each band. In dimensions of $[T]^{-1}[L]^{-2}$, this is written as

$$R_{rad}^{well} = B_{wl} NP$$

equation 2.52

where B_{wl} is the radiative recombination coefficient. When the system is electrically neutral N=P and the radiative rate becomes:

$$R_{rad}^{well} = B_{wl} N^2$$

equation 2.53

In a similar way to the radiative rate in a well being approximated to be proportional to a quadratic function of the carrier density, it is assumed that the rates of nonradiative recombination via defects and Auger recombination in a quantum well are proportional to *linear* and *cubic* functions of the carrier density. The nonradiative rate for quantum wells, in dimensions of $[T]^{-1}[L]^{-2}$, can be written as

$$R_{nr}^{well} = AN = \frac{N}{\tau_{nr}^{well}}$$

equation 2.54

where A is the nonradiative recombination coefficient, and is the reciprocal of the nonradiative lifetime. (Note that this is *not* the same A as the Einstein A coefficient described in section 2.4.2.)

2.8 Broadening in Quantum Dots

2.8.1 Introduction

The theoretical density of states function for a quantum dot is a delta-function (δ-function) and so it might be expected that the absorption and emission spectra also be delta-functions. In reality the delta-function is always broadened. The result is that the radiation emitted is not perfectly monochromatic and the shape of the emission line is described by a spectral line shape function. There are two classes or broadening:

- Homogeneous broadening affects all the individual dots in the ensemble in the same way. The same emission spectrum is produced by each dot.
- Inhomogeneous broadening affects individual dots in different ways and arises due to the different sizes of dots present in the ensemble or imperfections in the sample.

A more detailed discussion of the two broadening processes is given in the following sections.

2.8.2 Homogeneous Broadening

A system will experience homogeneous broadening, which arises from the probability of a transition occurring before the system undergoes a dephasing event. This is because the energy of the electron is only well-defined after a long period of time and for some finite time there is a probability that the electron energy will not be exactly equal to that of the quantum state. This broadening is normally expressed in terms of a Lorentzian function centred on the transition energy E_n:

$$L(h\upsilon)=\frac{1}{\pi}\frac{\Lambda}{(h\upsilon-E_n)^2+\Lambda^2}$$

equation 2.55

Λ is the linewidth (Λ is equal to $\hbar\gamma$ where γ is the number of dephasing events per second), and $L(h\upsilon)$ has units of reciprocal energy and is normalised such that:

$$\int_{-\infty}^{\infty} L(h\upsilon)dh\upsilon=1$$

equation 2.56

The peak value of the function, which occurs when $h\upsilon=E_n$, decreases with increasing linewidth and is given by:

$$L(h\upsilon=E_n)=\frac{1}{\pi\Lambda}$$

equation 2.57

Typical values of homogeneous broadening in quantum dots are of the order of tens of meV [17].

2.8.3 Inhomogeneous Broadening

In a *single* quantum dot, the possible optical transitions consist of a series of homogeneously broadened delta-function lines, with the energy positions dependent on the energy of the confined levels. In a real quantum dot *ensemble*, typical surface densities are around $3\text{x}10^{10}$ cm^{-2}. This results in a typical number of dots in a laser chip of around one million, and these dots have a distribution in size, strain etc. The energy spectrum thus varies from dot to dot, and an inhomogeneous broadening of the spectra is observed.

Inhomogeneous broadening may be due to fluctuations in the radius of the quantum dot, or due to a variation in the bandgap E_g as a result of fluctuations in the composition. For the case of broadening due to bandgap fluctuations, the ground and excited states are both described by the same standard deviation. Consider the energy levels E_n (in the z-direction only) of a three-dimensional harmonic oscillator:

$$E_n = E_g + \left(n + \frac{1}{2}\right)h\upsilon \qquad n = 0,1,2,...$$

equation 2.58

A fluctuation in the standard deviation of E_g is irrespective of n, and simply shifts the entire energy spectrum up and down. Conversely, an inhomogeneous broadening due to fluctuations in the width leads to a standard deviation which is not linearly proportional to n, and this results in a non symmetrical distribution of the energy levels.

The method adopted in this thesis is to use an inhomogeneous distribution in dot *sizes*. Inhomogeneous broadening is usually modelled with a Gaussian function, which has the form:

$$g(w) = \frac{1}{\sqrt{2\pi}}\frac{1}{\sigma}\exp\left[-\frac{(w-\overline{w})^2}{2\sigma^2}\right]$$

equation 2.59

Here, $g(w)$ is the probability per unit width of a quantum dot having a width w, $\overline{w}$ is the mean width of the dots, and σ is the standard deviation. In other words $g(w)$ is the fraction of dots which have a width w for an inhomogeneous distribution centred on $\overline{w}$. A Gaussian distribution is normalised such that:

$$\int_{-\infty}^{\infty} g(w)dw = 1$$

equation 2.60

An important parameter is the full width at half maximum (FWHM), which describes the width of the spectral line (called the linewidth) and is equal to twice the standard deviation. For self-assembled dots grown by the Stranski-Krastanow method, inhomogeneous broadening is the dominant broadening mechanism [18].

2.8.4 Combined Effects of Broadening

Figure 2.12 summarises the broadening in quantum dots, for the case where the inhomogeneous broadening is larger than the homogeneous broadening.

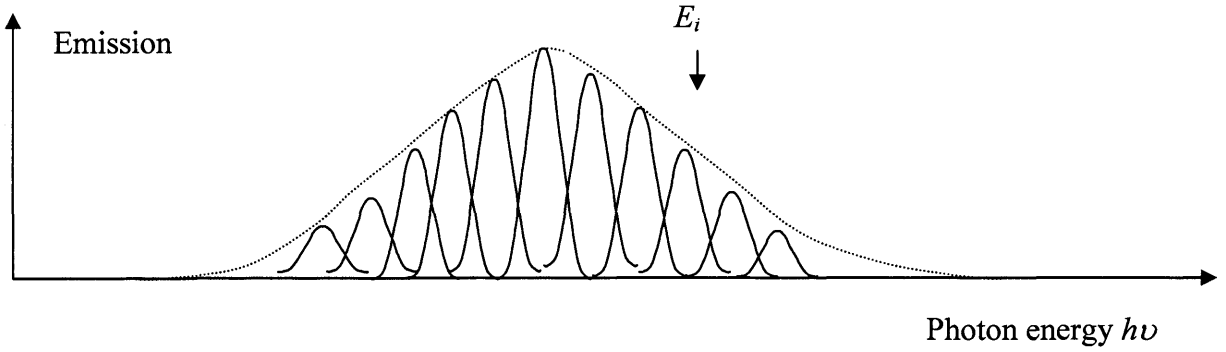

Figure 2.12 - Schematic of broadening in quantum dot lasers for the case when the inhomogeneous broadening is larger than the homogeneous broadening.

Optical transitions at each energy are broadened by the homogeneous linewidth. This means that more than one size of dot contributes to the transitions at any one photon energy, and so to calculate the gain/absorption or emission at a fixed value of photon energy it is necessary to sum over all the dots of different transition energies that make a contribution at that specific photon energy. The magnitude of the contribution that each dot makes depends on the relative magnitude of the homogeneous linewidth and the difference between the energy of the dot and the photon energy. Ordinarily, only those dots with transition energies within a few multiples of the linewidth from the photon energy of interest contribute to the gain.

2.9 Summary

In this chapter I have discussed the basis principles of semiconductors. A description of the bandstructure has been given along with equations for the density of states. This was followed by the Einstein relations, including equations for gain and spontaneous emission in dots. Finally, I discussed broadening in quantum dots. In the following chapter the model derived for calculating the localised population is described.

2.10 References

[1] D. Bimberg, M. Grundmann, and N. N. Ledentsov, Quantum Dot Heterostructures, John Wiley and Sons, Chichester, 1990.

[2] M. Fox, Optical properties of solids, Oxford University Press, Oxford, 2001.

[3] J. R. Hook and H. E. Hall, Solid State Physics, John Wiley and Sons, Chichester, 1991.

[4] J. Singh, Semiconductor Optoelectronics, McGraw-Hill, New York, 1995.

[5] C. Kittel, Introduction to Solid State Physics, Wiley, London, 1996.

[6] L. A. Coldren and S. W. Corzine, Diode Lasers and Photonic Integrated Circuits, Wiley, Chichester, 1995.

[7] H. C. Casey and M. B. Panish, Heterostructure Lasers, part A, Academic Press, New York, 1978.

[8] G. Agrawal and N. Dutta, Semiconductor Lasers, Van Nostrand Reinhold, New York, 1993.

[9] Britney Spears' Guide to Semiconductor Physics: http://britneyspears.ac/lasers.htm. Accessed December 15th 2005.

[10] D. Bimberg, N. Kirstaedter, N. N. Ledentsov, Z. I. Alferov, P. S. Kop'ev, and V. M. Ustinov, IEEE Journal of Selected Topics in Quantum Electronics 3 (1997) 196.

[11] M. Grundmann, N. N. Ledentsov, O. Stier, D. Bimberg, V. M. Ustinov, P. S. Kop'ev, and Z. I. Alferov, Applied Physics Letters 68 (1996) 979.

[12] H. D. Summers, J. D. Thomson, P. M. Smowton, P. Blood, and M. Hopkinson, Journal of Semiconductor Science and Technology 16 (2001) 140.

[13] A. Einstein, Phys Z 18 (1917) 121.

[14] D. E. McCumber, Phys. Rev. 136 (1964)

[15] S. Osborne, P. Blood, and P. Smowton, Journal of Physics: Condensed Matter 16 (2004) 3749.

[16] M. G. Bernard and G. Duraffourg, Physica Status Solidi 1 (1961) 699.

[17] P. Borri, W. Langbein, S. Schneider, U. Woggon, R. L. Sellin, D. Ouyang, and D. Bimberg, Physical Review Letters 87 (2001) 157401.

[18] M. Sugawara, K. Makai, and H. Shoji, Applied Physics Letters 71 (1997) 2791.

3 Model for Localised Population Statistics

3.1 Introduction

The aim of this work is to explore the consequences of carrier localisation on the behaviour of quantum dot light emitters. This is done by computing the recombination and gain characteristics of a quantum dot system. As with real dot samples, the model incorporates a two-dimensional wetting layer which does have extended states. The main features of the model are that the number of electrons in a given dot is a discrete integer, not a fractional probability, and that recombination is localised in each dot. It is assumed that the whole system is in thermal equilibrium; therefore comparisons can be made with non-localised systems since the global occupation probabilities are specified analytically. A thermal distribution of carriers amongst the different energy levels of the inhomogeneous dot distribution and the wetting layer is assumed, with global Fermi functions for electrons and holes; this has been shown to be appropriate for some dots systems at room temperature [1], and is discussed in more detail in section 3.5.1. The main principle of the model is the way in which the occupation probability is interpreted. It is usually taken to mean the fractional occupancy of each state. In this model, to take explicit account of the localised and discrete nature of the dot carrier populations, the occupation probability is taken to be the fraction of dot states with full occupancy. This approach maintains the paradigm of thermal equilibrium statistics whilst introducing the realistic assumption of discrete dot states with integer occupancy numbers. Consequently, for the case where both the electron and hole occupancies are controlled by their respective quasi-Fermi level, referred to as the *non-neutral* case, each dot may not necessarily contain equal numbers of electrons and holes, although the total numbers of electrons and holes in the system are equal. From these occupations a set of dot microstates are modelled, from which the spontaneous emission and gain characteristics can be calculated.

This chapter describes in detail how the electron and hole occupancies of each of the dots are calculated using Fermi-Dirac statistics. The implementation of the inhomogeneous broadening is described, along with an explanation of how the energy levels are calculated

for each size of dot. The calculation of the population of the wetting layer is also described. A full list of the notation used throughout this thesis to model the distribution is given in the appendices to the thesis.

For comparison, an alternative model, the *neutral* case in which dots are forced to contain equal numbers of electrons and holes, has also been developed. In this case, Fermi-Dirac statistics cannot be applied to both the electron and hole distributions and this model is described in chapter 5.

3.2 The System Modelled

The system modelled is an ensemble of one million quantum dots which, if taken to be equivalent to a single layer of dots of density 3×10^{10} cm^{-2}, gives the area of the sample as 3.33×10^{-7} cm^2. This is equivalent to a chip of about $6\mu m$ squared. The dots are assumed to be self-assembled and such dots, grown by the Stranski-Krastanow method [2, 3], incorporate a two-dimensional quantum well, called a wetting layer, and this is also included in the model. Figure 3.1 shows the energy diagram of the conduction band for the wetting layer and the dots.

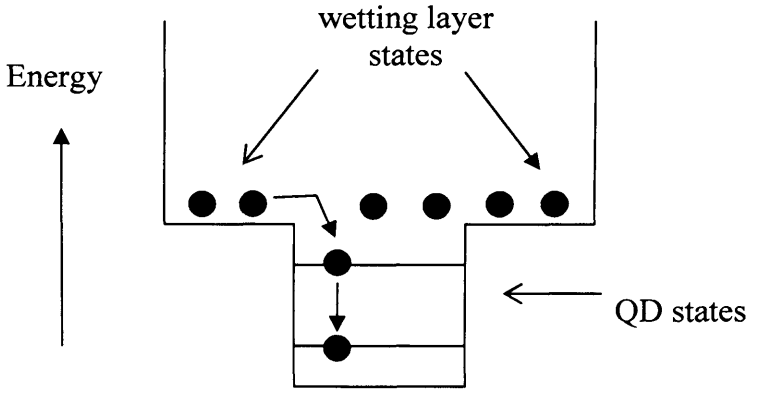

Figure 3.1 - Energy diagram of the conduction band, comprising of a wetting layer and quantum dots. Electrons can be captured into the dot states from the wetting layer.

The following sections describe the modelling of the dots and the wetting layer in more detail, including how the energy levels are calculated.

3.3 The Quantum Dots

3.3.1 Introduction

The ensemble of dots has an inhomogeneously broadened *size* distribution, and homogeneous broadening is also included. The quantum dots modelled are made of InAs with electron and hole effective masses of $0.027m_0$ and $0.34m_0$ respectively [4], where m_0 is the free electron mass. The energy levels in each size of dot are calculated using a simple harmonic oscillator (SHO) potential and this is described in detail in section 3.4. In each dot, ground and first excited states for electrons and holes are considered; the ground state can accommodate up to two electrons/holes of opposite spin, whilst the excited state can contain up to four electrons/holes, as shown in Figure 3.2. (Previous work has considered only a single electron and hole levels i.e. a ground state [5, 6].) The excited state can accommodate four electrons/holes since there are two degenerate quantum states corresponding to the first excited state due to the dot having equal dimensions in the *x,y* directions. The dots are modelled on 1μm emitting dots, and the dot material has a bandgap of 1eV with mean ground and excited state transition energies of 1.084eV and 1.249eV respectively. (However, in chapter 7 results from the model are compared with experimental data measured on 1.3μm emitting dots and for this comparison the parameters in the model are changed accordingly.)

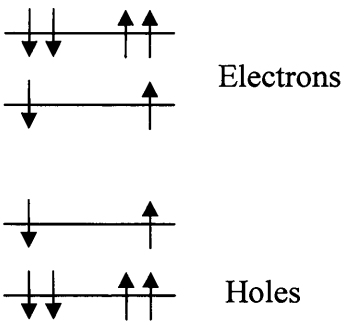

Figure 3.2 - Ground and excited state occupancies of the dots.

The electron and hole quasi-Fermi levels are defined such that the overall system, comprising of the dots plus the wetting layer, is electrically neutral. In other words, global charge neutrality is assumed over the whole system, but it is not assumed locally; i.e. it is not assumed that each individual dot is occupied by an equal number of electrons and holes. (An alternative model in which each dot *is* charge neutral is explored in chapter 5.) Table 3.1 gives the values used for the parameters throughout this thesis:

Parameter	Symbol	Value
Electron effective mass	m_c	$0.027m_0$
Hole effective mass	m_v	$0.34m_0$
Dot density	ρ_{dots}	3×10^{10} cm^{-2}
Area	$area$	3.33×10^{-7} cm^2
Number of dots	n_{QD}	1×10^6
Bandgap of dot material	E_g	1eV
Bandgap of wetting layer	$E_{g,wl}$	1.4eV
Gaussian standard deviation	σ	1.5nm
Mean width of dots	$\overline{w}$	10nm
Dot radiative lifetime	τ_{sp}	1ns
Dot nonradiative lifetime	τ_{nr}	300ps
Dot Auger lifetime	τ_{aug}	300ps
Wetting layer recombination coefficient	B_{wl}	3.5×10^{-7} s^{-1}m^2
Wetting layer nonradiative lifetime	τ_{nrwl}	300ps
Homogeneous linewidth	Λ	10meV
Mode width	w_{mod}	0.28μm
Wetting layer electron confined energy (relative to the conduction band edge)	E_{wlc}	250meV
Wetting layer hole confined energy (relative to the valence band edge)	E_{wlv}	150meV

Refractive index	n	3.5

Table 3.1 - Values used for the parameters in the model.

3.3.2 Inhomogeneous Broadening

Quantum dots grown by the Stranski-Krastanow method have a distribution in size and other properties such as composition; this broadens the energy spectra and is known as *inhomogeneous broadening*. In this thesis the inhomogeneous broadening is modelled using a Gaussian distribution in the dot *sizes* rather than directly as an energy broadening, and this gives rise to a non-symmetrical distribution of energy levels in the dots.

Real quantum dots often take the shape of flat discs or pyramids [7, 8]. In this thesis the dots are modelled as flat squares having the same size in two dimensions. This is shown in Figure 3.3. In the x and y directions the dots have dimensions of 100nm. The z-dimension (which is the smallest dimension of the dots and therefore the most sensitive to size) is subjected to an inhomogeneous broadening about a mean width of 10nm.

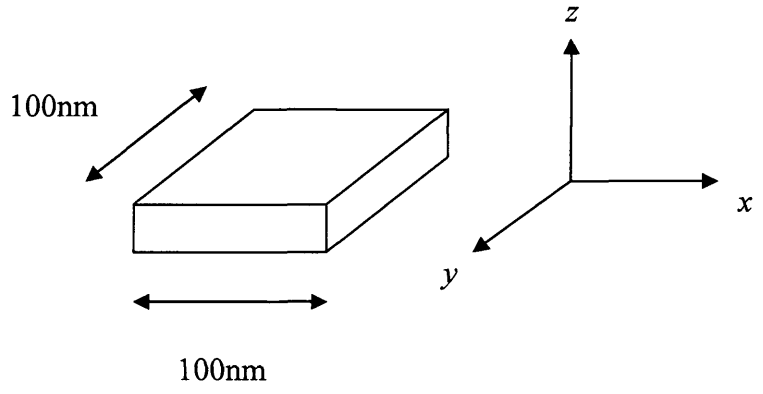

Figure 3.3 - Dimensions of the quantum dots. The dots are flat squares and the z-direction is inhomogeneously broadened.

It would be impractical to model each individual dot in the ensemble since this would involve calculating, for example, energy levels for one million dots. A finite series of discrete widths is chosen and the Gaussian function is used to calculate the numbers of dots at each width, generating groups of dots of a particular size. A Gaussian distribution has the form

$$g(w) = \frac{1}{\sqrt{2\pi}} \frac{1}{\sigma} \exp\left[-\frac{(w-\overline{w})^2}{2\sigma^2} \right]$$

equation 3.1

where $g(w)$ is the probability per unit width of a quantum dot having a width w, $\overline{w}$ is the mean width of the dots and σ is the standard deviation of the distribution. The widths are chosen at equal intervals from a minimum width w_{min} to a maximum width w_{max} centred around the mean width $\overline{w}$, and the difference between each width is Δw. If $g(w)$ is the probability per unit width of a quantum dot having a width w, then $g(w)$ multiplied by the width interval Δw gives the probability of a dot with a width in that interval. A standard Gaussian distribution is normalised such that

$$\int_{-\infty}^{\infty} g(w) dw = 1$$

equation 3.2

and extends to the range -∞ to +∞. In this thesis, because a Gaussian function is used to approximate a series of *discrete* widths, the range of widths in the distribution does not extend to ±∞, but has finite minimum and maximum values (just as in a real ensemble, there are minimum and maximum sizes of dots present, and infinitely large or small dots are unrealistic). To compensate for this the peak value of the Gaussian is modified such that the area under the truncated curve is equal to one:

$$\int_{w_{min}}^{w_{max}} P(w) dw = 1$$

equation 3.3

$P(w)$ is the redefined value of the truncated Gaussian. The integral is approximated in the model by

$$\sum_{w_{min}}^{w_{max}} P(w) \Delta w = 1$$

equation 3.4

where the limits of the summation are from the minimum width of the dots to the maximum. The integrated area of the distribution with these re-defined limits is then equal to one. So the Gaussian curve is split up into a series of rectangles of equal widths Δw, where the area

of the rectangle represents the probability of a dot having a width in the range $w \pm 1/2\ \Delta w$. Fifty-one different widths of dot are modelled, with a mean width $\overline{w}$ equal to 10nm, and standard deviation σ of 1.5nm. (An odd number of widths is chosen so that the distribution is symmetrical about the mean width.).

Multiplying $P(w)$ by the total number of dots n_{QD} gives the number of dots per unit width, $N_{QD}(w)$:

$$N_{QD}(w) = n_{QD} \times P(w)$$

equation 3.5

To calculate the distribution of carriers in the dots, the probability distribution is converted into a number of dots with a specific *discrete* width. $P(w) \times \Delta w$ is the probability of a dot having a width w ($\pm 1/2\ \Delta w$) and so to calculate how many dots there are with each discrete width, $n_{QD}(w)$, this probability is multiplied by the total number of dots n_{QD}:

$$\begin{aligned} n_{QD}(w) &= n_{QD} \times P(w) \times \Delta w \\ &\propto n_{QD} \times \frac{1}{\sqrt{2\pi}} \frac{1}{\sigma} \exp\left[-\frac{(w-\overline{w})^2}{2\sigma^2} \right] \times \Delta w \end{aligned}$$

equation 3.6

Figure 3.4 shows a plot of the number of dots with a width w. Summing these points gives the total number of dots, one million.

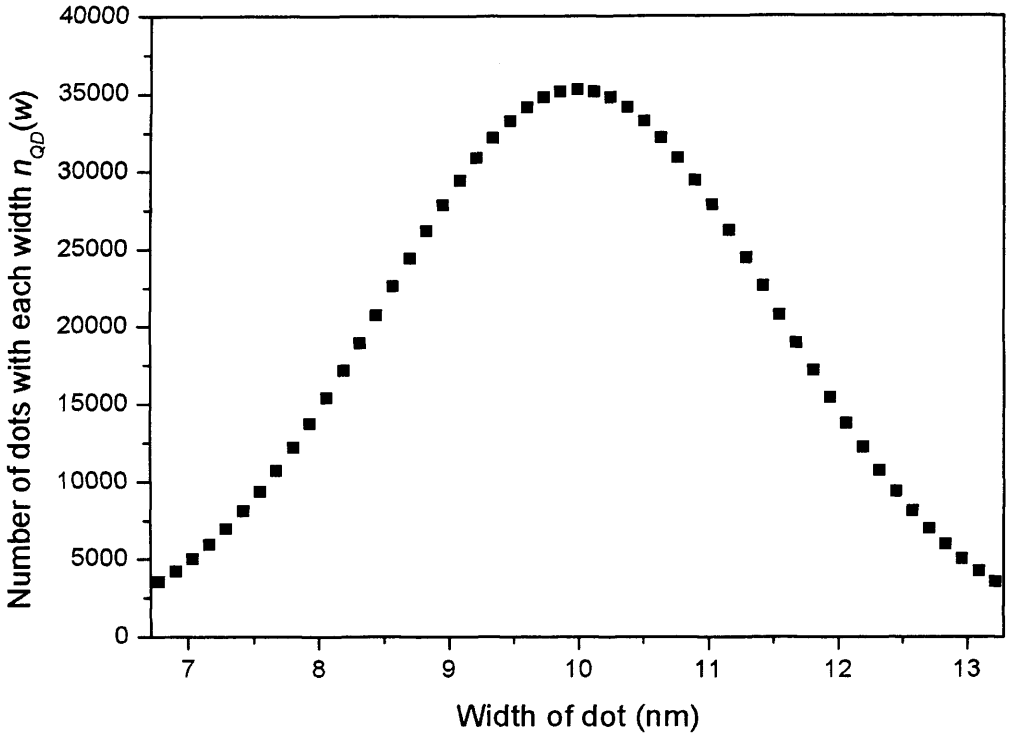

Figure 3.4 - Number of dots with a width *w* around a mean width of 10nm.

The number of dots with a width w, $n_{QD}(w)$, is converted into the number of dots with a transition energy E, $n_{QD}(E)$. To convert from a width interval to an energy interval the SHO potential equations are used, which are described in section 3.4. The energy intervals are not equal since the energy does not scale linearly with the width of the dot and each energy interval is denoted as $\Delta E(w)$ since its value is dependent on the size of the dot. The number of dots in an energy interval $\Delta E(w)$ must be equal to the number of dots in the equivalent width interval Δw, i.e.

$$\begin{aligned} n_{QD}(E) &= n_{QD}(w) \\ &= n_{QD} \times P(w) \times \Delta w \end{aligned}$$

equation 3.7

But the number of dots in an energy interval must also be equal to

$$n_{QD}(E) = n_{QD} \times p(E) \times \Delta E(w)$$

equation 3.8

where $p(E)$ is the probability per unit energy of a dot having an energy E. Rearranging these two equations gives

$$p(E) = P(w) \times \frac{\Delta w}{\Delta E(w)}$$

equation 3.9

and so the probability distribution in width can be related to the probability distribution in energy. The resulting probability distribution in energy, $p(E)$, is *not* a Gaussian distribution because the energy levels do not scale linearly with width and this gives rise to a non-symmetrical distribution of energy levels in the dots. The number of dots per unit energy interval $N_{QD}(E)$ is given by

$$\begin{aligned} N_{QD}(E) &= n_{QD} \times p(E) \\ &= n_{QD} \times P(w) \times \frac{\Delta w}{\Delta E(w)} \end{aligned}$$

equation 3.10

These equations in energy can be applied to different energy variables so that the energy distribution can be described in a number of ways, for example in terms of the ground state energy levels or the transition energy. Figure 3.5 shows the energy distribution and is a plot of the number of dots with a particular transition energy E as a function of the ground and excited state transition energies. Summing the points in each of the two curves gives the total number of dots.

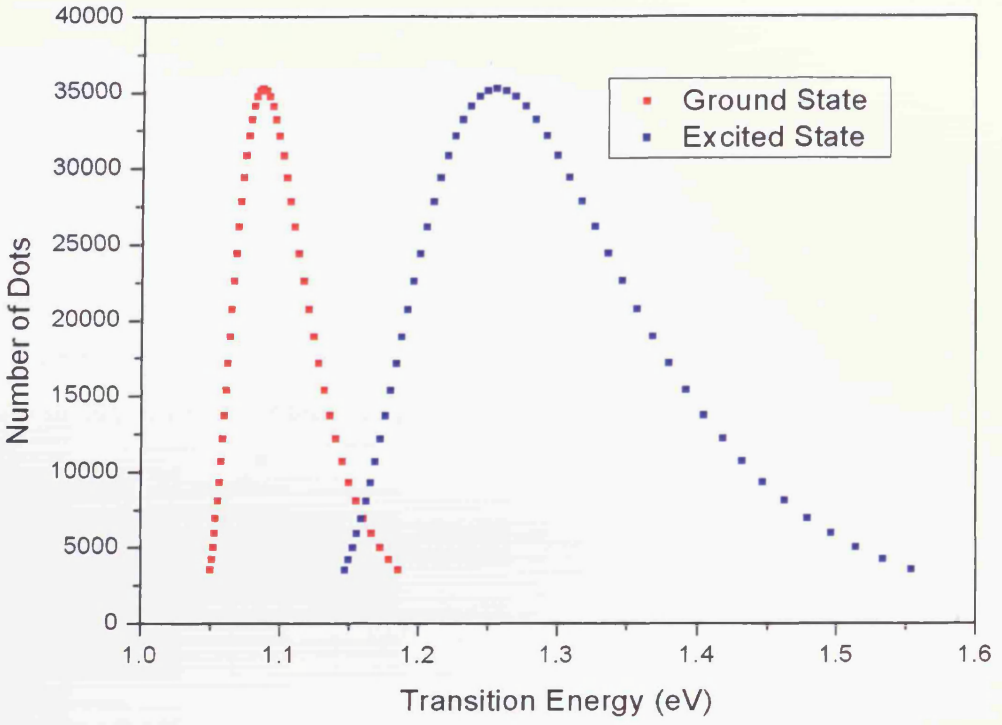

Figure 3.5 - Number of dots with each transition energy.

3.3.3 Homogeneous Broadening

The optical transitions of an ensemble of quantum dots consist of a series of broadened delta-function lines and because of this more than one size of dot contributes to transitions at any one photon energy. This is known as *homogeneous broadening*. To calculate the absorption or emission at a fixed value of photon energy it is necessary to sum over all the dots of different transition energies that make a contribution at that specific photon energy. The way in which the homogeneous broadening is implemented to calculate the broadened gain and emission spectra is described in chapter 4.

3.4 Energy Level Calculations

To calculate the distributions of electrons and holes in the dots it is necessary to know the state distribution. In this thesis the method used to calculate the energy levels of the dots is to consider the dots to be in an infinite simple harmonic oscillator (SHO) potential well [9, 10]. The form of the confinement potential is

$$V(\mathbf{r}) = \frac{1}{2} C\mathbf{r}^2$$

equation 3.11

which has associated with it a classical oscillator frequency for the electrons of

$$\upsilon = \frac{1}{2\pi}\sqrt{\frac{C}{m_c}}$$

equation 3.12

In the above equations $\mathbf{r}(x,y,z)$ is the electron position vector, m_c is the effective mass of the electrons and C is a measure of the strength of the potential. The time-independent Schrödinger equation is solved to find the confined energy states. Schrödinger's equation for the electrons with the harmonic oscillator confinement potential $V = \frac{1}{2} C\mathbf{r}^2$ is

$$\frac{\partial \psi(\mathbf{r})^2}{\partial \mathbf{r}^2} + \frac{2m_c}{\hbar^2}\left(E - \frac{1}{2} C\mathbf{r}^2\right)\psi(\mathbf{r}) = 0$$

equation 3.13

where E is the confined energy. The normalised wavefunctions corresponding to the lowest two energy states are:

$$\psi_0 = \frac{1}{\pi^{1/4} a^{1/2}} \exp\left(-\frac{\mathbf{r}^2}{2a^2}\right)$$

equation 3.14

$$\psi_1 = \frac{2^{1/2}}{\pi^{1/4} a^{3/2}} \mathbf{r} \exp\left(-\frac{\mathbf{r}^2}{2a^2}\right)$$

equation 3.15

where $a = \frac{\hbar^{1/2}}{(Cm_c)^{1/4}}$.

Figure 3.6 shows the first two normalised harmonic oscillator wavefunctions.

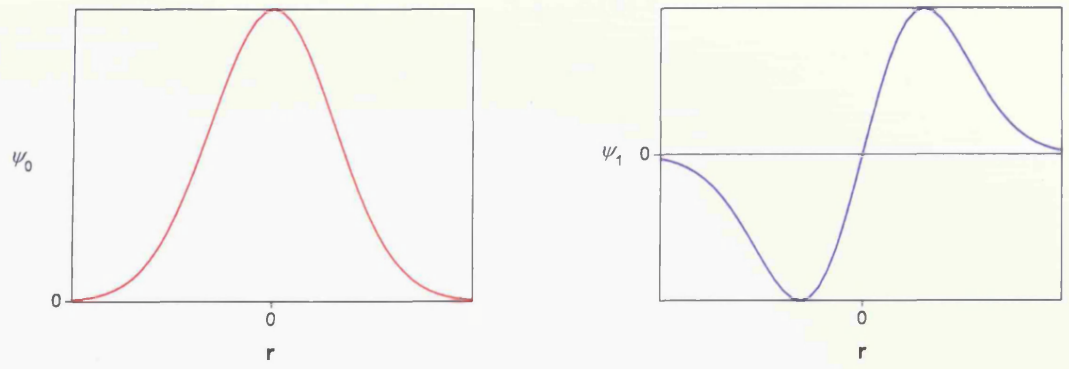

Figure 3.6 - First two normalised simple harmonic oscillator wavefunctions.

An infinite potential is assumed. The real potential is finite and so the value of C in equation 3.11 is set such that the value of the normalised wavefunction ψ_0 at full width half maximum is equal to the width of the quantum dot, i.e. $\psi_0 = 0.5\,\psi_{max}$ when $\mathbf{r} = \pm w/2$. The width of the dot thus determines the value of C, and therefore the energy levels of the dot.

Solving Schrödinger's equation gives the energy eigenvalues of the system, E_n. These are quantised for a harmonic oscillator and are given by

$$E_n = (n + 1/2)h\upsilon \qquad n = 0,1,2,3,...$$

equation 3.16

where υ is the electron frequency given by equation 3.12. Similar equations hold for the holes, with a hole effective mass m_v.

The energy levels given in equation 3.16 are now applied to the quantum dots. In the model the dots have ground and first excited states, which can accommodate two and four electrons/holes respectively. The electrons and holes have different energy levels due to their different effective masses. As described in section 3.3.2, the dots are assumed to be flat squares having the same size in the x and y dimensions, and the z-dimension is inhomogeneously broadened. In general, the energy levels in one direction for the ground and first excited states of the quantum dots, E_{gr} and E_{ex} respectively, are given by

$$E_{gr} = \frac{1}{2}h\upsilon$$

equation 3.17

$$E_{ex} = \frac{3}{2}h\upsilon$$

equation 3.18

where υ is given by equation 3.12 using the appropriate mass for electrons or holes. These equations are applied to all three dimensions of the dots.

Due to the comparatively large dimensions in the *x,y*-directions, the energy levels in the *x,y*-directions are very closely spaced relative to the *z*-direction, with only about 2meV difference in the ground and first excited state electron energies. The first excited state of the system is taken to be the E_{001} state. The equations for the energies of the ground and first excited states are thus given by

$$\begin{aligned} E_{gr} &= \frac{1}{2}h\upsilon_x + \frac{1}{2}h\upsilon_y + \frac{1}{2}h\upsilon_z \\ &= h\upsilon_{x,y} + \frac{1}{2}h\upsilon_z \end{aligned}$$

equation 3.19

$$\begin{aligned} E_{ex} &= \frac{1}{2}h\upsilon_x + \frac{1}{2}h\upsilon_y + \frac{3}{2}h\upsilon_z \\ &= h\upsilon_{x,y} + \frac{3}{2}h\upsilon_z \end{aligned}$$

equation 3.20

where $\upsilon_{x,y}$ is the frequency of oscillation in the *x,y*-directions and υ_z is the frequency in the *z*-direction. These energy levels apply to both the electron and hole states, $E^c_{gr,ex}$ and $E^v_{gr,ex}$, respectively and substituting in for υ gives:

$$E^c_{gr} = \frac{h}{2\pi}\sqrt{\frac{C^c_{x,y}}{m_c}} + \frac{h}{4\pi}\sqrt{\frac{C^c_z}{m_c}}$$

equation 3.21

$$E^c_{ex} = \frac{h}{2\pi}\sqrt{\frac{C^c_{x,y}}{m_c}} + \frac{3h}{4\pi}\sqrt{\frac{C^c_z}{m_c}}$$

equation 3.22

$$E_{gr}^{v} = \frac{h}{2\pi}\sqrt{\frac{C_{x,y}^{v}}{m_v}} + \frac{h}{4\pi}\sqrt{\frac{C_z^{v}}{m_v}}$$

equation 3.23

$$E_{ex}^{v} = \frac{h}{2\pi}\sqrt{\frac{C_{x,y}^{v}}{m_v}} + \frac{3h}{4\pi}\sqrt{\frac{C_z^{v}}{m_v}}$$

equation 3.24

These equations give analytical solutions for the energy levels of the dots, depending on the effective masses of the electrons and holes. The value of C is dependent on the size of the dot which results in different energy levels in dots of different sizes. The ground and excited state mean electron energies are 80meV and 237meV respectively. Similarly, the ground and excited state mean hole energies are 7meV and 19meV respectively. The hole energy levels are much smaller than those of the electrons due to the different effective masses. These energy levels are used to calculate the occupancies of the dots using the quasi-Fermi levels and this is described in the following section.

3.5 Applying Fermi-Dirac Statistics

3.5.1 Fermi-Dirac Statistics

To calculate the distributions of electrons and holes in the system Fermi-Dirac statistics are used, which are detailed in chapter 2. It is assumed that the dots and the wetting layer are in thermal equilibrium, specified by electron and hole quasi-Fermi levels. The quasi-Fermi levels are defined such that the whole system, comprising of the dots and the wetting layer, is electrically neutral. The occupation probability of an electron or hole state is given by the Fermi function $f_{c,v}$. This function is usually understood to be equal to the fractional occupancy of each state. However, to take into account the discrete nature of the states, here it is taken to be the *fraction of dot states with full occupancy*, and so each state is occupied by integer numbers of electrons and holes. The fraction of occupied states for electrons is given by

$$f_c = \frac{1}{\exp\left(\frac{E_c - E_{fc}}{kT}\right) + 1}$$

equation 3.25

for an electron energy E_c, and electron quasi-Fermi level E_{fc}. In this equation k is Boltzmann's constant and T is the temperature. Similarly the fraction of occupied hole states is given

$$f_v = \frac{1}{\exp\left(\frac{E_v - E_{fv}}{kT}\right)+1}$$

equation 3.26

for a hole energy E_v and hole quasi-Fermi level E_{fv}. The notation f_v represents the fraction of occupied hole states in the valence band and not electron states, as is often the case. In the model $f_{c,gr}$ and $f_{v,gr}$ are used to represent the fraction of occupied ground states for electrons and holes respectively, whilst $f_{c,ex}$ and $f_{v,ex}$ represent the fraction of occupied excited states. The electron energies and electron quasi-Fermi level are measured from the conduction band edge and are positive into the conduction band and, similarly, the hole energies and hole quasi-Fermi level are measured from the valence band edge and are positive into the valence band.

3.5.2 Nomenclature

In this thesis the dot states are occupied by integer numbers of electrons and holes, and the recombination rates for each dot depend on these occupancies. The numbers of electrons and holes in *each* dot needs to be known which involves tracking a large number of dot states. The following notation is used to represent the different dot states.

The convention adopted throughout this thesis is that a lower case n is used to represent the *number of dots* with a particular *electron* distribution. Similarly a lower case p is used to represent the number of dots with a certain *hole* distribution.

A set of dot microstates, n_i^j, are modelled for the electrons, where n is the number of dots with i electrons in the ground state and j in the excited state for a particular size of dot. The variable i has allowed values of 0, 1 and 2, whilst j has allowed values of 0, 1, 2, 3 and 4. For example, n_2^0 represents the number of dots that have two electrons in the ground state and no electrons in the excited state. A similar quantity is computed for the holes, p_l^m, where l is the number of holes in the ground state and m is the number in the excited state. No assumption

is made on the spin of the carriers at this point; the probability of different spins is included in the radiative rates.

Figure 3.7 shows some examples of different electron and hole distributions in a quantum dot and the corresponding notation used to describe them. A filled circle represents an electron whilst an empty circle represents a hole.

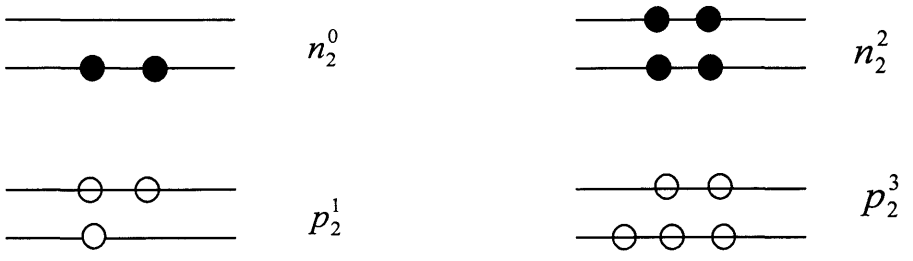

Figure 3.7 - Examples of distributions of electrons and holes in a quantum dot. The distribution on the left is denoted by n_2^0 for the electrons and p_2^1 for the holes. The distribution on the right is denoted by n_2^2 and p_2^3.

The *probability* of a dot having an electron distribution *i,j* is denoted by $prob_{i,j}$, and similarly the probability of a dot having a hole distribution *l,m* is $prob_{l,m}$. The overall probability of a dot having an electron distribution *i,j and* a hole distribution *l,m* is denoted by $prob_{i,j,l,m}$.

Each of the million dots in the model is not treated individually; rather, each group of dots with the same width is treated collectively. The distribution is worked out for one dot of that size, and this is then summed over all the dots of the same size. The total distribution is found by summing the distributions over the different widths.

3.5.3 Electron Distribution

The electron distribution is calculated using the electron Fermi function f_c for a particular value of electron quasi-Fermi level E_{fc}. The fraction of occupied states is f_c whilst alternately the fraction of unoccupied states (i.e. a hole in the conduction band) is $(1-f_c)$. For the ground state, the probability of occupation by *i* electrons is

$$\frac{2!}{i!(2-i)!} f_{c,gr}{}^{i} \left(1 - f_{c,gr}\right)^{2-i}$$

equation 3.27

where the first term is the number of ways that two empty states can be filled with i electrons, and the other terms give the fraction of occupied states. Similarly, the probability of the excited state being occupied with j electrons is

$$\frac{4!}{j!(4-j)!} f_{c,ex}{}^{j} \left(1 - f_{c,ex}\right)^{4-j}$$

equation 3.28

where in this case four empty states are being filled with j electrons. To get the probability of the complete electron distribution i,j these two equations are multiplied:

$$prob_{i,j} = \frac{2!}{i!(2-i)!} f_{c,gr}{}^{i} \left(1 - f_{c,gr}\right)^{2-i} \times \frac{4!}{j!(4-j)!} f_{c,ex}{}^{j} \left(1 - f_{c,ex}\right)^{4-j}$$

equation 3.29

For example, the probability of a dot having one electron in the ground state and one in the excited state is:

$$prob_{1,1} = 2 f_{c,gr} \left(1 - f_{c,gr}\right) \times 4 f_{c,ex} \left(1 - f_{c,ex}\right)^{3}$$

equation 3.30

Likewise, the probability of a dot having two electrons in the ground state and three in the excited state is:

$$prob_{2,3} = f_{c,gr}{}^{2} \times 4 f_{c,ex}{}^{3} \left(1 - f_{c,ex}\right)$$

equation 3.31

The sum of all the probabilities is equal to one:

$$\sum_{i,j} prob_{i,j} = 1$$

equation 3.32

The probabilities of all possible combinations of i and j are shown in the following table:

Probability of a dot having a distribution *i,j*	**Expression for probability**
$prob_{0,0}$	$\left(1 - f_{c,gr}\right)^{2} \left(1 - f_{c,ex}\right)^{4}$

$prob_{1,0}$	$2f_{c,gr}(1-f_{c,gr})(1-f_{c,ex})^4$
$prob_{2,0}$	$f_{c,gr}{}^2(1-f_{c,ex})^4$
$prob_{0,1}$	$(1-f_{c,gr})^2 4f_{c,ex}(1-f_{c,ex})^3$
$prob_{1,1}$	$2f_{c,gr}(1-f_{c,gr})4f_{c,ex}(1-f_{c,ex})^3$
$prob_{2,1}$	$f_{c,gr}{}^2 4f_{c,ex}(1-f_{c,ex})^3$
$prob_{0,2}$	$(1-f_{c,gr})^2 6f_{c,ex}{}^2(1-f_{c,ex})^2$
$prob_{1,2}$	$2f_{c,gr}(1-f_{c,gr})6f_{c,ex}{}^2(1-f_{c,ex})^2$
$prob_{2,2}$	$f_{c,gr}{}^2 6f_{c,ex}{}^2(1-f_{c,ex})^2$
$prob_{0,3}$	$(1-f_{c,gr})^2 4f_{c,ex}{}^3(1-f_{c,ex})$
$prob_{1,3}$	$2f_{c,gr}(1-f_{c,gr})4f_{c,ex}{}^3(1-f_{c,ex})$
$prob_{2,3}$	$f_{c,gr}{}^2 4f_{c,ex}{}^3(1-f_{c,ex})$
$prob_{0,4}$	$(1-f_{c,gr})^2 f_{c,ex}{}^4$
$prob_{1,4}$	$2f_{c,gr}(1-f_{c,gr})f_{c,ex}{}^4$
$prob_{2,4}$	$f_{c,gr}{}^2 f_{c,ex}{}^4$

Table 3.2 - Occupation probabilities for the electrons.

A feature of the model is that all combinations of i and j are possible. However, some will be more favourable than others. The Fermi occupation function is dependent on temperature and so at low temperatures most of the electrons are found in the ground state of the dots. For example, at a temperature of 10K the probability of the distribution n_0^2 is very unlikely

as it would be expected that the ground state be full before significant occupancy of the excited state is observed. Although this probability will increase at room temperature, at low injection the majority of the electrons will still be found in the lower state.

Now that the probabilities of each occupancy have been calculated, the *number* of dots with occupancy *i,j* can be computed. To get the number of dots for each distribution *i,j* the probability of the distribution, $prob_{i,j}$, is multiplied by the number of dots, n_{QD}:

$$\begin{aligned} n_i^j &= n_{QD} \times prob_{i,j} \\ &= n_{QD} \times \frac{2!}{i!(2-i)!} f_{c,gr}{}^{i} \left(1-f_{c,gr}\right)^{2-i} \times \frac{4!}{j!(4-j)!} f_{c,ex}{}^{j} \left(1-f_{c,ex}\right)^{4-j} \end{aligned}$$

equation 3.33

Because the number of quantum dots is large (one million), the numbers of dots with each occupancy *i,j* are integer numbers.

The full set of equations for the number of dots with each occupation is shown in the following table:

Number of dots with an electron distribution *i,j*: n_i^j	**Expression**
n_0^0	$n_{QD}\left(1-f_{c,gr}\right)^2\left(1-f_{c,ex}\right)^4$
n_1^0	$n_{QD}2f_{c,gr}\left(1-f_{c,gr}\right)\left(1-f_{c,ex}\right)^4$
n_2^0	$n_{QD}f_{c,gr}{}^2\left(1-f_{c,ex}\right)^4$
n_0^1	$n_{QD}\left(1-f_{c,gr}\right)^2 6f_{c,ex}\left(1-f_{c,ex}\right)^3$
n_1^1	$n_{QD}2f_{c,gr}\left(1-f_{c,gr}\right)6f_{c,ex}\left(1-f_{c,ex}\right)^3$
n_2^1	$n_{QD}f_{c,gr}{}^2 6f_{c,ex}\left(1-f_{c,ex}\right)^3$
n_0^2	$n_{QD}\left(1-f_{c,gr}\right)^2 4f_{c,ex}{}^2\left(1-f_{c,ex}\right)^2$

n_1^2	$n_{QD} 2 f_{c,gr} (1 - f_{c,gr}) 4 f_{c,ex}{}^2 (1 - f_{c,ex})^2$
n_2^2	$n_{QD} f_{c,gr}{}^2 4 f_{c,ex}{}^2 (1 - f_{c,ex})^2$
n_0^3	$n_{QD} (1 - f_{c,gr})^2 6 f_{c,ex}{}^3 (1 - f_{c,ex})$
n_1^3	$n_{QD} 2 f_{c,gr} (1 - f_{c,gr}) 6 f_{c,ex}{}^3 (1 - f_{c,ex})$
n_2^3	$n_{QD} f_{c,gr}{}^2 6 f_{c,ex}{}^3 (1 - f_{c,ex})$
n_0^4	$n_{QD} (1 - f_{c,gr})^2 f_{c,ex}{}^4$
n_1^4	$n_{QD} 2 f_{c,gr} (1 - f_{c,gr}) f_{c,ex}{}^4$
n_2^4	$n_{QD} f_{c,gr}{}^2 f_{c,ex}{}^4$

Table 3.3 - Number of dots with an electron distribution *i,j*.

The total number of dots from all the different combinations is equal to the total number of dots n_{QD}:

$$\sum_{i,j} n_i^j = n_{QD}$$

equation 3.34

These equations are the general equations that describe the number of dots with occupancy *i,j*, for a particular value of the electron quasi-Fermi level. In the quantum dot ensemble there are one million dots and these dots are of varying sizes due to the growth method, known as inhomogeneous broadening. As well as the quasi-Fermi level, the Fermi function is also dependent on the energy of the state, which itself depends on the size of the dot. Small dots have energy level separations greater than those of larger dots. Thus dots of different sizes have different values of Fermi function and therefore different occupancies, for fixed values of the quasi-Fermi level and temperature. Thus dots of different sizes need to be represented separately so that the occupations of the whole ensemble can be tracked. To do this arrays are used to represent dots of different sizes. As described in section 3.3.2, the one million

dots are split into groups comprising of dots of the same size, and this is done using a Gaussian function. In each group of dots of the same size, all the dots have the same occupation *i,j* since they have the same energy levels and hence the same value of the Fermi function. The symbol $n_i^j(w)$ is used to represent the number of dots of size *w* with occupation numbers *i,j*. The number of dots of a particular size *w*, determined by the Gaussian function, is $n_{QD}(w)$, and is given by equation 3.6. Applying this notation, the equation for the occupancy of dots of size *w* becomes

$$n_i^j(w) = n_{QD}(w) \times \frac{2!}{i!(2-i)!}\left[f_{c,gr}(w)\right]^i\left[1-f_{c,gr}(w)\right]^{2-i} \times \frac{4!}{j!(4-j)!}\left[f_{c,ex}(w)\right]^j\left[1-f_{c,ex}(w)\right]^{4-j}$$

equation 3.35

where *f(w)* is the Fermi function for dots of width *w*.

Including all the dots of different sizes in the summations gives the following equations

$$\sum_{i,j} n_i^j(w) = n_{QD}(w)$$

equation 3.36

$$\sum_{w} n_{QD}(w) = n_{QD}$$

equation 3.37

where n_{QD} is the total number of quantum dots. The total number of electrons in the ground state, $N_{gr}(w)$, for dots of size *w*, is

$$\begin{aligned} N_{gr}(w) = {} & n_1^0(w) + n_1^1(w) + n_1^2(w) + n_1^3(w) + n_1^4(w) \\ & + 2n_2^0(w) + 2n_2^1(w) + 2n_2^2(w) + 2n_2^3(w) + 2n_2^4(w) \end{aligned}$$

equation 3.38

Similarly, the total number of electrons in the excited state, $N_{ex}(w)$, for a dots of size *w*, is

$$\begin{aligned} N_{ex}(w) = {} & n_0^1(w) + n_1^1(w) + n_2^1(w) + 2n_0^2(w) + 2n_1^2(w) + 2n_2^2(w) \\ & + 3n_0^3(w) + 3n_1^3(w) + 3n_2^3(w) + 4n_0^4(w) + 4n_1^4(w) + 4n_2^4(w) \end{aligned}$$

equation 3.39

Substituting in the equations for $n_i^j(w)$ gives the common equations which are often used to describe systems with extended states:

$$N_{gr}(w) = 2n_{QD}(w) f_{c,gr}(w)$$

equation 3.40

$$N_{ex}(w) = 4n_{QD}(w) f_{c,ex}(w)$$

equation 3.41

These equations show that the model is consistent with other models used to describe the occupation statistics of a system, and that this approach maintains the paradigm of thermal equilibrium statistics whilst introducing the realistic assumption of discrete dot states with integer occupancy numbers.

The total numbers of electrons in the ground and excited states, N_{grtot} and N_{extot} respectively, are found by summing over all the different widths:

$$\begin{aligned} N_{grtot} &= \sum_{w} N_{gr}(w) \\ &= \sum_{w} \begin{aligned} &n_1^0(w) + n_1^1(w) + n_1^2(w) + n_1^3(w) + n_1^4(w) \\ &+ 2n_2^0(w) + 2n_2^1(w) + 2n_2^2(w) + 2n_2^3(w) + 2n_2^4(w) \end{aligned} \end{aligned}$$

equation 3.42

$$\begin{aligned} N_{extot} &= \sum_{w} N_{ex}(w) \\ &= \sum_{w} \begin{aligned} &n_0^1(w) + n_1^1(w) + n_2^1(w) + 2n_0^2(w) + 2n_1^2(w) + 2n_2^2(w) \\ &+ 3n_0^3(w) + 3n_1^3(w) + 3n_2^3(w) + 4n_0^4(w) + 4n_1^4(w) + 4n_2^4(w) \end{aligned} \end{aligned}$$

equation 3.43

3.5.4 Hole Distribution

The hole distribution is calculated in the same way as the electron distribution, using the *hole* quasi-Fermi level. To calculate the hole occupancies for the ground state the ground state hole Fermi function, $f_{v,gr}$, is used and similarly for the excited state, $f_{v,ex}$. The probability of a dot having l holes in the ground state and m holes in the excited state is given by

$$prob_{l,m} = \frac{2!}{l!(2-l)!} f_{v,gr}{}^{l} \left(1 - f_{v,gr}\right)^{2-l} \times \frac{4!}{m!(4-m)!} f_{v,ex}{}^{m} \left(1 - f_{v,ex}\right)^{4-m}$$

equation 3.44

and the number of dots with l holes in the ground state and m holes in the excited state is p_l^m, given by:

$$p_l^m = n_{QD} \times prob_{l,m}$$
$$= n_{QD} \times \frac{2!}{l!(2-l)!} f_{v,gr}{}^{l} \left(1 - f_{v,gr}\right)^{2-l} \times \frac{4!}{m!(4-m)!} f_{v,ex}{}^{m} \left(1 - f_{v,ex}\right)^{4-m}$$

equation 3.45

Again, the sum of all the hole probabilities is equal to one:

$$\sum_{l,m} prob_{l,m} = 1$$

equation 3.46

The equations for the number of dots with a hole distribution l,m are shown in the following table:

Number of dots with a hole distribution *l,m*: p_l^m	**Expression**
p_0^0	$n_{QD}\left(1 - f_{v,gr}\right)^2 \left(1 - f_{v,ex}\right)^4$
p_1^0	$n_{QD} 2 f_{v,gr} \left(1 - f_{v,gr}\right) \left(1 - f_{v,ex}\right)^4$
p_2^0	$n_{QD} f_{v,gr}{}^2 \left(1 - f_{v,ex}\right)^4$
p_0^1	$n_{QD}\left(1 - f_{v,gr}\right)^2 6 f_{v,ex} \left(1 - f_{v,ex}\right)^3$
p_1^1	$n_{QD} 2 f_{v,gr} \left(1 - f_{v,gr}\right) 6 f_{v,ex} \left(1 - f_{v,ex}\right)^3$
p_2^1	$n_{QD} f_{v,gr}{}^2 6 f_{v,ex} \left(1 - f_{v,ex}\right)^3$
p_0^2	$n_{QD}\left(1 - f_{v,gr}\right)^2 4 f_{v,ex}{}^2 \left(1 - f_{v,ex}\right)^2$
p_1^2	$n_{QD} 2 f_{v,gr} \left(1 - f_{v,gr}\right) 4 f_{v,ex}{}^2 \left(1 - f_{v,ex}\right)^2$
p_2^2	$n_{QD} f_{v,gr}{}^2 4 f_{v,ex}{}^2 \left(1 - f_{v,ex}\right)^2$
p_0^3	$n_{QD}\left(1 - f_{v,gr}\right)^2 6 f_{v,ex}{}^3 \left(1 - f_{v,ex}\right)$

p_1^3	$n_{QD} 2 f_{v,gr} \left(1 - f_{v,gr}\right) 6 f_{v,ex}{}^3 \left(1 - f_{v,ex}\right)$
p_2^3	$n_{QD} f_{v,gr}{}^2 6 f_{v,ex}{}^3 \left(1 - f_{v,ex}\right)$
p_0^4	$n_{QD} \left(1 - f_{v,gr}\right)^2 f_{v,ex}{}^4$
p_1^4	$n_{QD} 2 f_{v,gr} \left(1 - f_{v,gr}\right) f_{v,ex}{}^4$
p_2^4	$n_{QD} f_{v,gr}{}^2 f_{v,ex}{}^4$

Table 3.4 - Number of dots with a hole distribution *l,m*.

Again, groups of dots of different sizes are represented by $p_l^m(w)$. The total number of holes in the ground and excited states for dots of size w, $P_{gr}(w)$ and $P_{ex}(w)$ respectively, are:

$$\begin{aligned} P_{gr}(w) = {} & p_1^0(w) + p_1^1(w) + p_1^2(w) + p_1^3(w) + p_1^4(w) \\ & + 2p_2^0(w) + 2p_2^1(w) + 2p_2^2(w) + 2p_2^3(w) + 2p_2^4(w) \end{aligned}$$

equation 3.47

$$\begin{aligned} P_{ex}(w) = {} & p_0^1(w) + p_1^1(w) + p_2^1(w) + 2p_0^2(w) + 2p_1^2(w) + 2p_2^2(w) \\ & + 3p_0^3(w) + 3p_1^3(w) + 3p_2^3(w) + 4p_0^4(w) + 4p_1^4(w) + 4p_2^4(w) \end{aligned}$$

equation 3.48

The total numbers of holes in the ground and excited states, P_{grtot} and P_{extot} respectively, are obtained by summing over all the different widths:

$$P_{gr} = \sum_w P_{gr}(w)$$

equation 3.49

$$P_{ex} = \sum_w P_{ex}(w)$$

equation 3.50

3.5.5 Total Distribution

Now that the hole and electron distributions have been computed, the next step is to calculate the total occupancy of each dot: the number of electrons *and* the number of holes in *each* dot

needs to be known. In other words, the number of dots that have an electron distribution *i,j and* a hole distribution *l,m* need to be calculated. Because the quasi-Fermi levels are defined such that the whole system, the dots and the wetting layer, is electrically neutral, in any particular dot the number of electrons is necessarily equal to the number of holes.

The probability of a dot having electron and hole distributions *i,j* and *l,m* is given by

$$prob_{i,j,l,m} = prob_{i,j} \times prob_{l,m}$$

equation 3.51

or substituting in equation 3.29 and equation 3.44 gives:

$$prob_{i,j,l,m} = \frac{2!}{i!(2-i)!} f_{c,gr}{}^{i}\left(1-f_{c,gr}\right)^{2-i} \times \frac{4!}{j!(4-j)!} f_{c,ex}{}^{j}\left(1-f_{c,ex}\right)^{4-j} \times \frac{2!}{l!(2-l)!} f_{v,gr}{}^{l}\left(1-f_{v,gr}\right)^{2-l} \times \frac{4!}{m!(4-m)!} f_{v,ex}{}^{m}\left(1-f_{v,ex}\right)^{4-m}$$

equation 3.52

Since the dot must have one of the distributions, it follows that:

$$\sum_{i,j,l,m} prob_{i,j,l,m} = 1$$

equation 3.53

The number of dots with distribution *i,j,l,m*, given the symbol $n_i^j p_l^m$, is obtained by multiplying equation 3.52 by the number of dots:

$$\begin{aligned} n_i^j p_l^m &= n_{QD} \times prob_{i,j,l,m} \\ &= n_{QD} \times \frac{2!}{i!(2-i)!} f_{c,gr}{}^{i}\left(1-f_{c,gr}\right)^{2-i} \times \frac{4!}{j!(4-j)!} f_{c,ex}{}^{j}\left(1-f_{c,ex}\right)^{4-j} \\ &\times \frac{2!}{l!(2-l)!} f_{v,gr}{}^{l}\left(1-f_{v,gr}\right)^{2-l} \times \frac{4!}{m!(4-m)!} f_{v,ex}{}^{m}\left(1-f_{v,ex}\right)^{4-m} \end{aligned}$$

equation 3.54

Including the size dependence in this equation gives:

$$n_i^j p_l^m(w) = n_{QD}(w) \times \frac{2!}{i!(2-i!)}\left[f_{c,gr}(w)\right]^{i}\left[1-f_{c,gr}(w)\right]^{2-i} \times \frac{4!}{j!(4-j!)}\left[f_{c,ex}(w)\right]^{j}\left[1-f_{c,ex}(w)\right]^{4-j} \times \frac{2!}{l!(2-l!)}\left[f_{v,gr}(w)\right]^{l}\left[1-f_{v,gr}(w)\right]^{2-l} \times \frac{4!}{m!(4-m!)}\left[f_{v,ex}(w)\right]^{m}\left[1-f_{v,ex}(w)\right]^{4-m}$$

equation 3.55

3.6 The Wetting Layer

The wetting layer is a thin layer of material left over from the Stranski-Krastanow growth process. In this thesis it is treated as an infinite quantum well with extended states, having a step density of states function with electron and hole occupations in equilibrium with the dot states. The wetting layer is an unavoidable consequence of the Stranski-Krastanow growth process, and as so must be included in all analysis of quantum dots lasers: the dots cannot be regarded as an isolated system.

Throughout this thesis it is assumed that a thermal equilibrium exists between the dots and the wetting layer and thus the complete system can be described using Fermi-Dirac statistics. The wetting layer effective masses are also based on InAs with values of $0.027m_0$ and $0.34m_0$ for the electrons and holes respectively. The wetting layer has a bandgap of 1.4eV.

The wetting layer is treated as a two-dimensional quantum well and so its carrier population is described in terms of a density of states per unit area given by:

$$\rho_{2D}(E) = \frac{m}{\pi\hbar^2}$$

equation 3.56

The number of electrons per sub-band per unit area, N_{wl}, is given by

$$N_{wl} = \int_{E_{wlc}}^{\infty} \rho_{2D}(E) f_{c,wl}\, dE$$

equation 3.57

where E is the energy of the sub-band, and $f_{c,wl}$ is the Fermi-Dirac distribution function for the electrons in the wetting layer. Similarly, the number of holes per sub-band per unit area, P_{wl}, is given by

$$P_{wl} = \int_{E_{wlv}}^{\infty} \rho_{2D}(E) f_{v,wl}\, dE$$

equation 3.58

where $f_{v,wl}$ is the Fermi-Dirac distribution function for the holes in the wetting layer.

For the model it is not necessary to know all the possible electronic levels in the wetting layer so Schrödinger's equation does not need to be solved. To work out the densities of electrons and holes it is only necessary to know the wetting layer confined energies, which

are denoted by E_{wlc} for the electrons and E_{wlv} for the holes. Figure 3.8 shows the energy diagram for the wetting layer confined states. Values chosen for the confinement energies of the wetting layer are based on 1100nm emitting structures: E_{wlc}=250eV and E_{wlv}=150eV, relative to the quantum dot conduction and valence band edges.

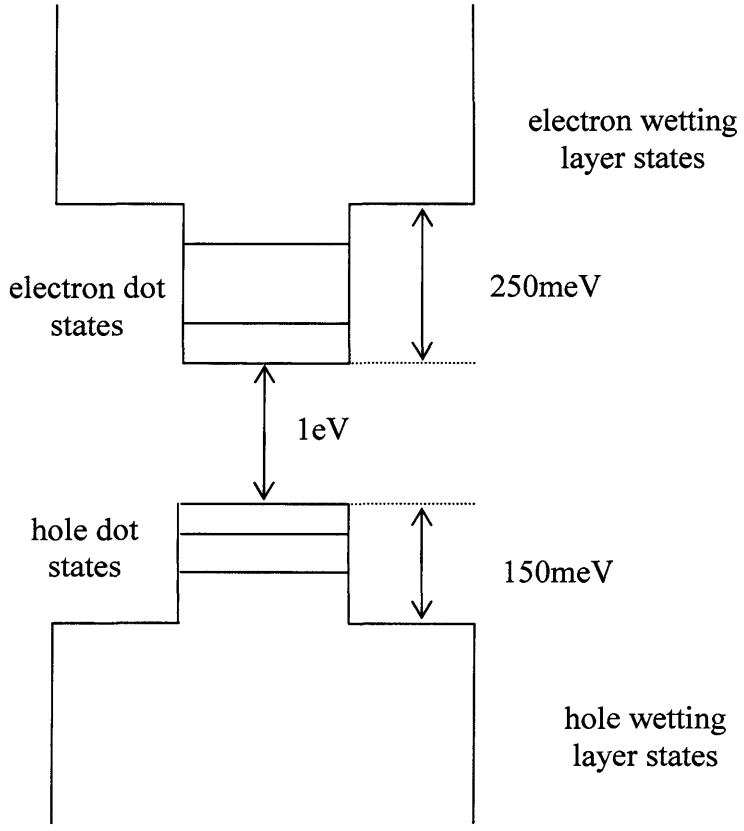

Figure 3.8 - Wetting layer confined states.

Integrating equation 3.57 analytically gives the density of electrons in the wetting layer as

$$N_{wl} = \frac{m_c}{\pi\hbar^2}(kT)\ln\left\{1+\exp\left(-\frac{E_{wlc}-E_{fc}}{kT}\right)\right\}$$

equation 3.59

where E_{fc} is the quasi-Fermi level for the electrons. Similarly, the density of holes in the wetting layer is

$$P_{wl} = \frac{m_v}{\pi\hbar^2}(kT)\ln\left\{1+\exp\left(-\frac{E_{wlv}-E_{fv}}{kT}\right)\right\}$$

equation 3.60

where E_{fv} is the quasi-Fermi level for the holes.

3.7 Implementing Computer Algorithms

To calculate the distribution of electrons and holes in the system, a computer program has been written in Fortran 90. The program first calculates the distribution of sizes in the dots using the Gaussian function. Next, the energy levels of the dots are calculated, which are dependent on the size of the dot. A value of electron quasi-Fermi level E_{fc} is inputted and then from this the distribution of electrons in the dots is computed using the equations in Table 3.3. To work out the distribution of the holes in the dots the program sets the condition that the total number of holes in the dots and the wetting layer must equal the total number of electrons. To do this the program first calculates the distribution of electrons and holes in the wetting layer using equation 3.59 and equation 3.60 for the value of E_{fc} inputted. Initially the hole quasi-Fermi level is set equal to the electron quasi-Fermi level. The hole distribution in the dots is then computed using the equations in Table 3.4. The total number of electrons and holes in the dots and the wetting layer are then summed. This procedure is repeated with the hole quasi-Fermi level being decreased in small increments until the total number of holes becomes equal to the total number of electrons. (The hole quasi-Fermi level is decreased since the holes have energy levels which are more closely spaced than those of the electrons and so a smaller value of hole quasi-Fermi level is needed to achieve a hole population equal to that of the electrons.) Once the electron and hole populations have been calculated, the recombination processes can be computed, which are described in the next chapter. The above procedure is summarised in a flow diagram in Figure 3.9.

The model has been thoroughly checked to ensure that it is calculating quantities as expected. For example, integrating the spontaneous emission spectra gives a value equal to the summed radiative rates, as expected. This is shown in more detail in chapter 8. The distributions of the electrons and holes have also been summed manually, over the dots and the wetting layer, at various injection levels to ensure that the charge neutrality condition is obeyed. The code has also been investigated at intermediate stages, to check that lines of code give reasonable and expected outputs.

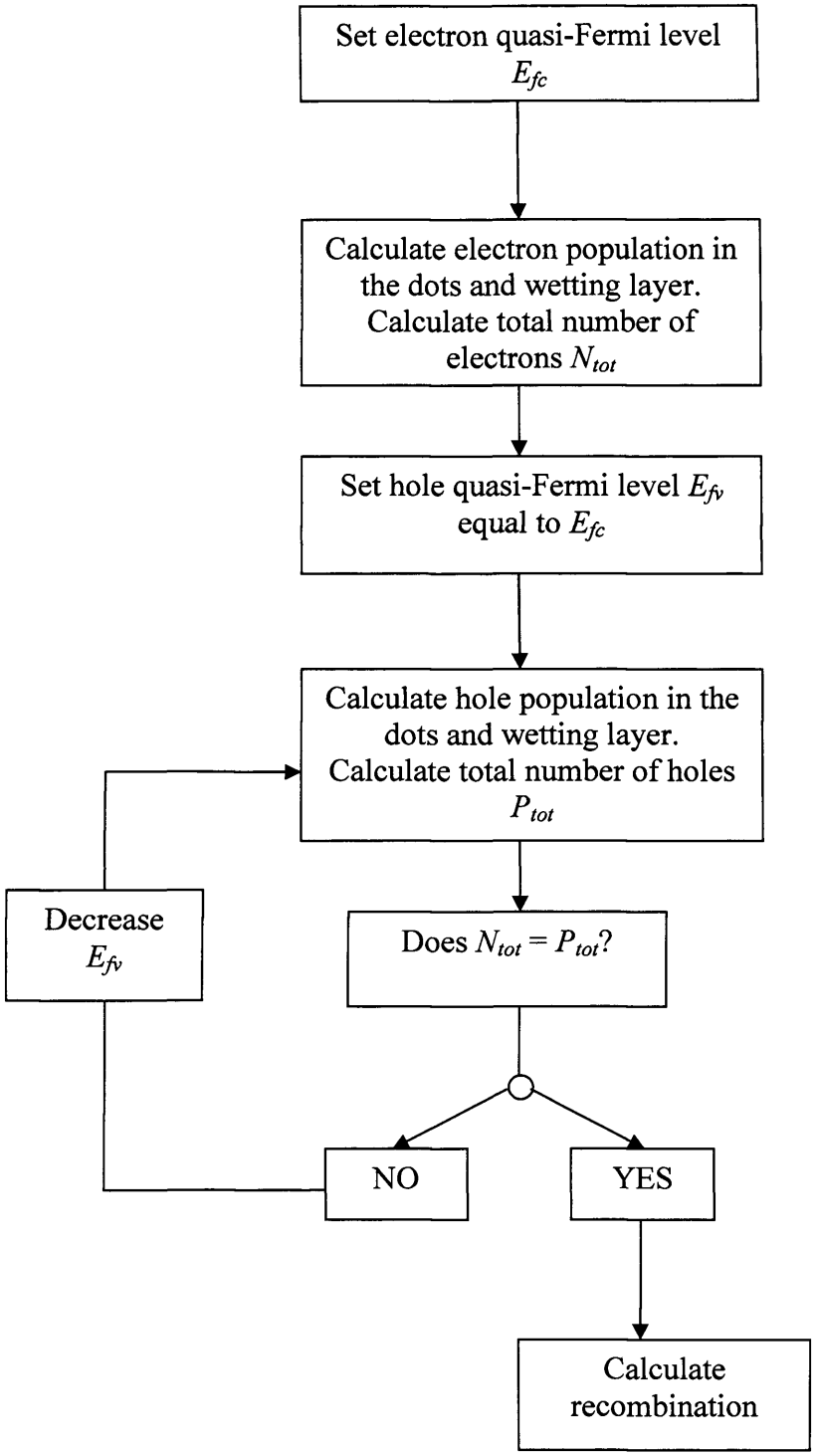

Figure 3.9 - Flow diagram showing how the computer algorithms are implemented.

3.8 Summary

In this chapter I have presented a model based on Fermi-Dirac statistics for calculating localised population statistics for an ensemble of quantum dots, for given electron and hole quasi-Fermi levels. I have described how the energy levels are calculated and how a

Gaussian distribution is used to represent the spread of different dot sizes in the ensemble. The calculation of the occupancy of the wetting layer has also been described. In the following chapter calculations of the recombination mechanisms are shown, including the spontaneous emission and gain spectra.

3.9 References

[1] H. D. Summers, J. D. Thomson, P. M. Smowton, P. Blood, and M. Hopkinson, Journal of Semiconductor Science and Technology 16 (2001) 140.

[2] D. Leonard, M. Krishnamurthy, C. M. Reaves, S. P. Denbaars, and P. M. Petroff, Applied Physics Letters 63 (1993) 3203.

[3] C. Priester and M. Lannoo, Physical Review Letters 75 (1995) 93.

[4] L. A. Coldren and S. W. Corzine, Diode Lasers and Photonic Integrated Circuits, Wiley, Chichester, 1995.

[5] H. Huang and D. G. Deppe, IEEE Journal of Quantum Electronics 37 (2001) 691.

[6] L. V. Asryan and R. A. Suris, IEEE Journal of Quantum Electronics 34 (1998) 841.

[7] M. Grundmann, N. N. Ledentsov, O. Stier, D. Bimberg, V. M. Ustinov, P. S. Kop'ev, and Z. I. Alferov, Applied Physics Letters 68 (1996) 979.

[8] D. Bimberg, N. Kirstaedter, N. N. Ledentsov, Z. I. Alferov, P. S. Kop'ev, and V. M. Ustinov, IEEE Journal of Selected Topics in Quantum Electronics 3 (1997) 196.

[9] A. A. Dikshit and J. M. Pikal, IEEE Journal of Quantum Electronics 40 (2004) 105.

[10] G. Park, O. B. Shchekin, and D. Deppe, IEEE Journal of Quantum Electronics 36 (2000) 1065.

4 Recombination Calculations

4.1 Introduction

A detailed understanding of carrier recombination mechanisms and optical gain generation within semiconductor lasers is essential for optimisation of their performance. The aim of this work is to use a computer model to explore the effect of carrier localisation and discrete occupancy number on the *measurable* characteristics, such as the recombination and gain characteristics and device current, of an *ensemble* of a large number of dots. Because the electronic states of a quantum dot are localised in all three directions it is only possible for electrons and holes which are located within the same dot to recombine with each other. The maximum number of available electrons and holes within a single state is equal to the spin degeneracy and at high injection this significantly reduces the radiative recombination rate in dots relative to the quantum well or bulk case.

In the previous chapter the method used for calculating the localised population statistics for an ensemble of dots is described, as well as the distribution of carriers in the wetting layer. This chapter explains how the recombination processes in the system (radiative, nonradiative via defects and Auger) are calculated. Other models often assume excitonic recombination in the dots and thus a radiative recombination rate that is dependent on only one type of carrier [1, 2]. Here, the radiative rate is dependent on both the electron and hole occupancies in each dot. This has been done previously [3], but this work differs to the work presented here in that recombination is not calculated in individual dots and the dots do not have integer occupancies.

In this chapter it is also described how the homogeneous broadening function is implemented to calculate the spontaneous emission and gain spectra. Finally, equations for the current flowing in the systems are derived.

4.2 Radiative Recombination: Total Spontaneous Emission Rate

The optical processes associated with electron-hole pairs are spontaneous emission, absorption/gain and stimulated emission. These processes can be described by the Einstein relations, which are discussed in detail in chapter 2 and are summarised in

Figure 4.1. Open circles represent empty states (holes) and filled circles represent occupied states (electrons).

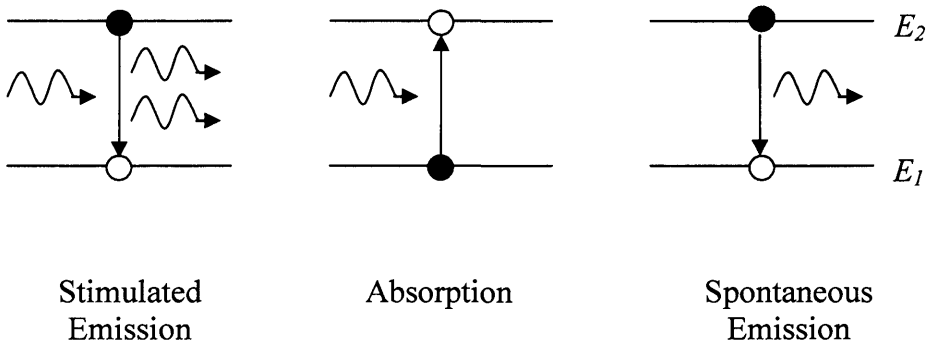

Figure 4.1 - Possible optical transitions between two levels, E_1 and E_2, of a simple system, described by the Einstein relations. Open circles represent empty states (holes) and filled circles represent occupied states (electrons).

The rates are proportional to the probability of occupancy of the states, which are given by Fermi-Dirac statistics. The Einstein relations give the equation for the rate of spontaneous emission for the ground state of an ensemble of N_{dots} identical dots as:

$$R_{spon} = 2N_{dots} A f_c f_v$$

equation 4.1

Here, A is the probability of the transition occurring and is known as the Einstein A coefficient. The Fermi functions f_c and f_v give the probability of occupancy for the conduction and valence states with electrons and holes respectively. The rate has dimensions of $[T]^{-1}$, and the Einstein A coefficient can be written in terms of a spontaneous lifetime τ_{sp} for a single transition as:

$$A = \frac{1}{\tau_{sp}}$$

equation 4.2

In the model it is assumed that ground state electrons can only recombine with ground state holes, and similarly for excited states, and that ground and excited states have the same spontaneous lifetime. It is also assumed that electrons can only recombine with holes of the same spin. This is because experimentally only TE polarised light is observed and this originates from transitions between carriers of the same spin.

Using the notation introduced in the previous chapter, the radiative rate for the ground state of one dot, in dimensions of $[T]^{-1}$, can be written as

$$R_{rad}^{gr}(dot) = 2A\left(\frac{i}{2}\right)\left(\frac{l}{2}\right)$$
$$= 2\frac{1}{\tau_{sp}}\left(\frac{i}{2}\right)\left(\frac{l}{2}\right)$$

equation 4.3

where i is the number of electrons in the ground state of the dot, and similarly l is the number of holes in the ground state. The factor of two is included to take account of the two possible transitions between electrons and holes of the same spin in the fully occupied ground state, as shown in Figure 4.2. It can be seen that when the ground state is fully occupied the rate is equal to $2A$.

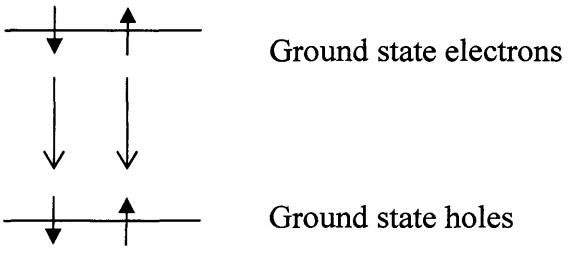

Figure 4.2 - Possible radiative transitions for the ground state of one dot containing two electrons and two holes of opposite spin. Electrons can only recombine with holes of the same spin.

The radiative rate for the excited state of one dot, where j is the number of electrons in the excited state and m is the number of holes, is given by:

$$R_{rad}^{ex}(dot) = 8A\left(\frac{j}{4}\right)\left(\frac{m}{4}\right)$$
$$= 8\frac{1}{\tau_{sp}}\left(\frac{j}{4}\right)\left(\frac{m}{4}\right)$$

equation 4.4

There is now a multiplication factor of eight because when the excited state is fully occupied there are eight possible transitions between the four electrons and four holes,

as shown in Figure 4.3. For fully occupied dots, this gives an excited state radiative rate that is four times as big as that for the ground state.

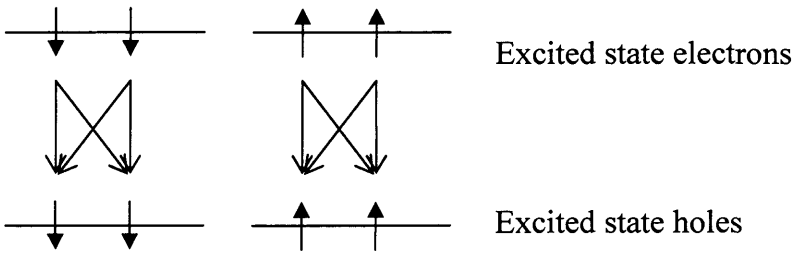

Figure 4.3 - Possible radiative transitions for the excited state of one dot containing four electrons and four holes. Electrons can only recombine with holes of the same spin.

The radiative rate must be calculated for all the different distributions of electrons and holes in the ground and excited states. As explained in chapter 3, the number of dots with a ground state electron and hole occupancy i,l is calculated by multiplying the probability of having i electrons and l holes by the number of dots. So for a particular combination of i,l the total ground state radiative rate for an ensemble of n_{QD} dots is given by

$$R_{rad}^{gr}(i,l) = n_{QD} \times \frac{1}{area} \times \sum_{j,m} prob_{i,j} \times prob_{l,m} \times 2\frac{1}{\tau_{sp}}\left(\frac{i}{2}\right)\left(\frac{l}{2}\right)$$

equation 4.5

where the area has now been included in the calculation to give the rate in dimensions of $[T]^{-1}[L]^{-2}$. The sum over j and m is included because, although the ground state radiative rate does not depend on the excited state occupation, all excited state combinations for the ground state occupation i,l need to be included. So for example, the total ground state radiative rate for dots with two electrons and one hole in the ground state is given by:

$$R_{rad}^{gr}(2,1) = n_{QD} \times \frac{1}{area} \times \sum_{j,m} prob_{2,j} \times prob_{1,m} \times 2\frac{1}{\tau_{sp}}\left(\frac{2}{2}\right)\left(\frac{1}{2}\right)$$
$$= n_{QD} \times \frac{1}{area \times \tau_{sp}} \times \left[prob_{2,0} + prob_{2,1} + prob_{2,2} + prob_{2,3} + prob_{2,4}\right]$$
$$\times \left[prob_{1,0} + prob_{1,1} + prob_{1,2} + prob_{1,3} + prob_{1,4}\right]$$

equation 4.6

The total radiative rate for the ground state of all the n_{QD} dots is obtained by summing over all the possible combinations of *i,j,l,m*, and is given by:

$$R_{rad}^{gr} = n_{QD} \times \frac{1}{area} \times \sum_{i,j,l,m} prob_{i,j} \times prob_{l,m} \times 2\frac{1}{\tau_{sp}}\left(\frac{i}{2}\right)\left(\frac{l}{2}\right)$$

equation 4.7

Dots of different sizes are now accounted for, and the rates are converted into rates per unit transition energy by dividing by the energy intervals $\Delta E(w)$, which are dependent on the size of the dot. The energy intervals are calculated by converting the widths to energies as described in chapter 3. The total ground and excited state radiative rates for all dots of size *w*, in dimensions of $[T]^{-1}[L]^{-2}[E]^{-1}$, are respectively given by:

$$R_{rad}^{gr}(w) = \frac{n_{QD}(w)}{\Delta E(w) \times area} \times \sum_{i,j,l,m} prob_{i,j}(w) \times prob_{l,m}(w) \times 2\frac{1}{\tau_{sp}}\left(\frac{i}{2}\right)\left(\frac{l}{2}\right)$$

equation 4.8

$$R_{rad}^{ex}(w) = \frac{n_{QD}(w)}{\Delta E(w) \times area} \times \sum_{i,j,l,m} prob_{i,j}(w) \times prob_{l,m}(w) \times 8\frac{1}{\tau_{sp}}\left(\frac{j}{4}\right)\left(\frac{m}{4}\right)$$

equation 4.9

The total radiative rate for the ground states of *all* the n_{QD} dots is given by summing over all the different sizes of dots and in dimensions of $[T]^{-1}[L]^{-2}[E]^{-1}$ is given by:

$$R_{rad}^{gr}(total) = \sum_{w} \frac{n_{QD}(w)}{\Delta E(w) \times area} \times \sum_{i,j,l,m} prob_{i,j}(w) \times prob_{l,m}(w) \times 2\frac{1}{\tau_{sp}}\left(\frac{i}{2}\right)\left(\frac{l}{2}\right)$$

equation 4.10

Similarly, the total radiative rate for the excited states of *all* the dots of different sizes is:

$$R_{rad}^{ex}(total) = \sum_{w} \frac{n_{QD}(w)}{\Delta E(w) \times area} \times \sum_{i,j,l,m} prob_{i,j}(w) \times prob_{l,m}(w) \times 8 \frac{1}{\tau_{sp}} \left(\frac{j}{4}\right)\left(\frac{m}{4}\right)$$

equation 4.11

Figure 4.4 shows the ground and excited state radiative rates per unit transition energy for each group of dots of the same size, in dimensions of $[T]^{-1}[L]^{-2}[E]^{-1}$. They are plotted as a function of ground/excited state transition energy for the case of fully occupied dots. The excited state rate is larger than that of the ground state rate due to there being four times as many possible transitions per dot in the excited state.

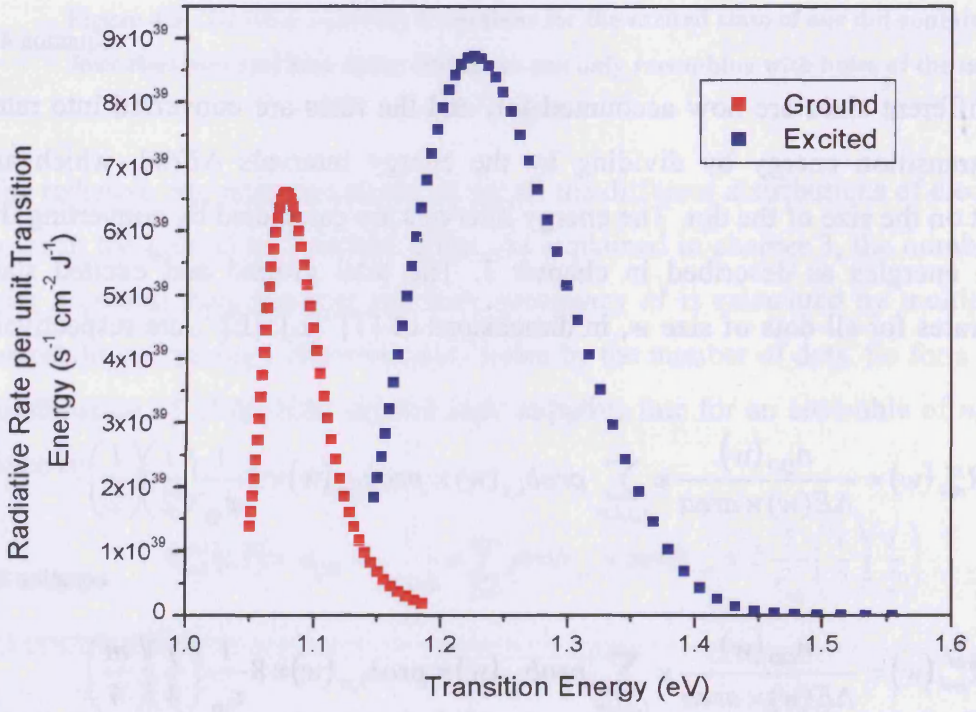

Figure 4.4 - Ground and excited state radiative rates per unit transition energy for each group of dots for the case of fully occupied dots. The excited state rate is larger than the ground state rate.

4.3 Nonradiative Recombination via Deep States

Nonradiative recombination is the recombination of an electron-hole pair without the emission of a photon and so it does not contribute to the light emission. Nonradiative recombination in semiconductor lasers can occur via defects (often called Shockley-

Read-Hall recombination or SRH) and Auger recombination. In this section nonradiative recombination via defects is discussed; Auger recombination is described in section 4.4.

Nonradiative recombination via deep states is treated locally in each dot. The capture of electrons and holes onto the defect sites are independent events and so the overall capture rate is dependent on the slowest of these two capture processes. This is often referred to as the *rate-limiting step.* Here, the rate limiting step is assumed to be *electron* capture onto the defect state, and it is also assumed that both electron and hole states can be refilled on a timescale which is faster than the recombination time. The worst case scenario is assumed, where there is a defect present in every dot. The nonradiative rate in each dot is proportional to the number of electrons *provided* there is a hole present in the *same* dot to enable the recombination process to be completed, i.e. $l>0$ for the ground state and $m>0$ for the excited state. Ground (excited) state electrons can only recombine nonradiatively with ground (excited) state holes.

The nonradiative rates of a single dot, in dimensions of $[T]^{-1}$, for the ground and excited states respectively are

$$R_{nr}^{gr}(dot) = \frac{i}{\tau_{nr}} \qquad l > 0$$

equation 4.12

$$R_{nr}^{ex}(dot) = \frac{j}{\tau_{nr}} \qquad m > 0$$

equation 4.13

where i is the number of electrons in the ground state and j is the number of electrons in the excited state. The nonradiative lifetime, τ_{nr}, is assumed to be the same for both states and has a value of 300ps.

The total nonradiative rates for the ground and excited states of dots of size w are calculated by multiplying equation 4.12 and equation 4.13 by the number of dots with the corresponding occupation (equal to the probability that a dot has an electron occupation i,j and a hole occupation l,m, multiplied by the number of dots), on the condition that there is at least one hole present in the dot. The total rates over *all* the dots are calculated by summing over all the different sizes of dots. Including the area

in the calculation, the total nonradiative rates for the ground and excited states, in dimensions of $[T]^{-1}[L]^{-2}$, are therefore given by:

$$R_{nr}^{gr}(total) = \sum_{w} n_{QD}(w) \sum_{i,j,l>0,m} \frac{i \times prob_{i,j}(w) \times prob_{l,m}(w)}{\tau_{nr} \times area}$$

equation 4.14

$$R_{nr}^{ex}(total) = \sum_{w} n_{QD}(w) \sum_{i,j,l,m>0} \frac{j \times prob_{i,j}(w) \times prob_{l,m}(w)}{\tau_{nr} \times area}$$

equation 4.15

Figure 4.5 is a plot of the total nonradiative rates for the ground and excited states, as a function of the total current in the dots and the wetting layer.

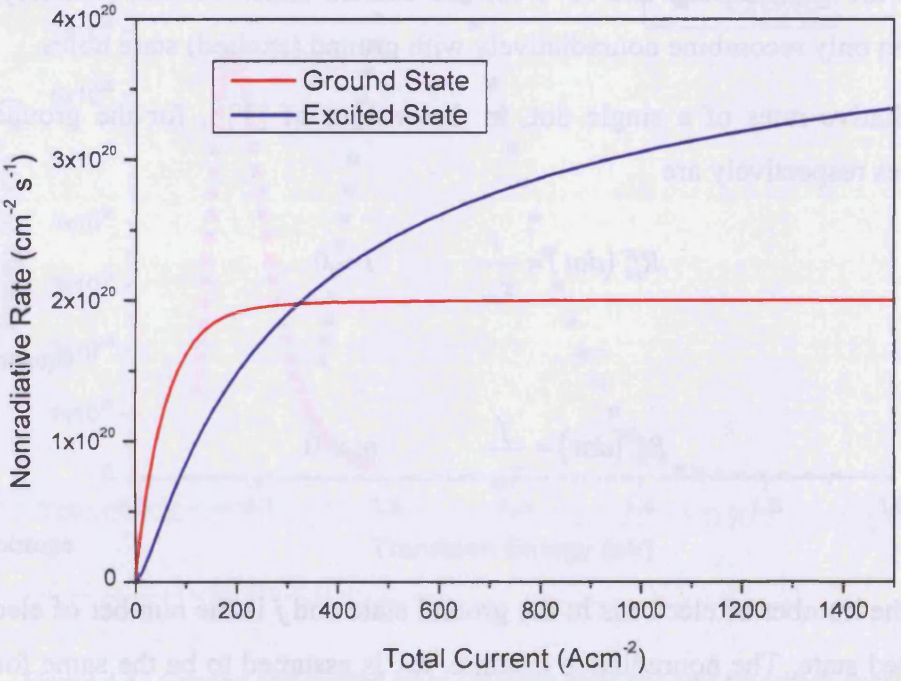

Figure 4.5 - Total nonradiative rates for the ground (red line) and excited (blue line) states, as a function of the total current in the dots and the wetting layer.

The excited state rate is much larger than the ground state rate due to its increased occupancy number compared to that of the ground state as the current is increased.

4.4 Auger Recombination

Auger recombination is also a nonradiative process since the energy released in the transition is transferred to another carrier which then dissipates its energy by the release of phonons and not a photon. There are several processes for Auger recombination but, for simplicity, only one process is modelled in this thesis. This process is shown schematically in Figure 4.6. It is assumed that a conduction electron (1) recombines with a valence hole (2). The energy released in this process promotes another electron (3) to the wetting layer (4), which then dissipates its energy by the release of a phonon.

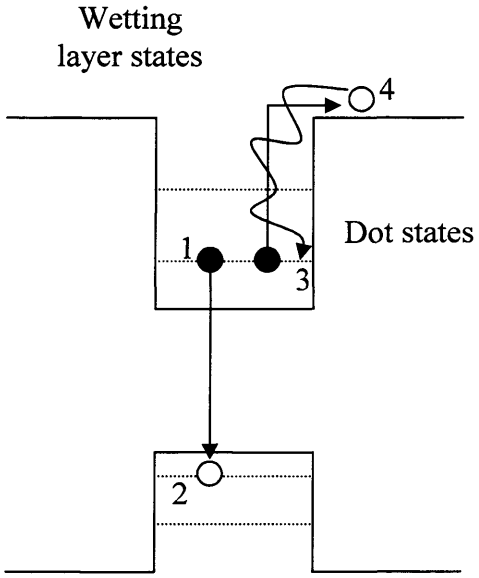

Figure 4.6 - Auger recombination in a quantum dot.

Auger recombination is also treated locally in the model. It is assumed that ground state electrons can only recombine via Auger recombination with ground state holes, and similarly for the excited state, and that for the process to be completed there must be at least two electrons and at least one hole present in the same dot. It is also assumed that there is always an empty state available in the wetting layer to complete the process. For consistency with the radiative and nonradiative via defects recombination rates, the Auger recombination is characterised using an Auger lifetime for a single dot τ_{aug}. It is assumed that this is the same for ground and excited states and equal to 300ps.

First considering the ground state only, for the Auger process to take place there needs to be two electrons (i.e. a full electron ground state) and at least one hole in the same dot; if there are two holes in the same dot the transition rate is doubled since there are two ways that the process can be completed. The Auger rate is therefore proportional to the number of holes in the dot on the condition that there are two ground state electrons in the dot i.e. i=2. The Auger rate for the ground state of a single dot is written as

$$R_{aug}^{gr}(dot) = \frac{l}{\tau_{aug}} \qquad i = 2$$

equation 4.16

The excited state is more complicated because it can contain up to four electrons and four holes, and the probability of Auger recombination occurring will depend on the number of ways of having the combination of two electrons and one hole. For example, when the electron and hole states are full there will be 24 different ways of the Auger process occurring. If the excited state contains j electrons the number of ways of having two electrons is

$$\frac{j!}{2!(j-2)!}$$

and the probability of Auger recombination occurring is proportional to this number. The probability of Auger recombination is also proportional to the number of holes on the condition that $j \geq 2$, and so the Auger rate for the excited state of one dot is given by:

$$R_{aug}^{ex}(dot) = \frac{1}{\tau_{aug}} \frac{j!}{2!(j-2)!} \times m \qquad j \geq 2$$

equation 4.17

To calculate the total Auger rates, equation 4.16 and equation 4.17 are multiplied by the number of dots with the corresponding occupation, on condition that there are two electrons present in the dot. The total Auger rates for the ground and excited states, in dimensions of $[T]^{-1}[L]^{-2}$, are therefore given by:

$$R_{aug}^{gr}(total) = \sum_{w} n_{QD}(w) \sum_{i=2,j,l,m} l \times \frac{prob_{i,j}(w) \times prob_{l,m}(w)}{\tau_{aug} \times area}$$

equation 4.18

$$R_{aug}^{ex}(total) = \sum_{w} n_{QD}(w) \sum_{i,j \geq 2,l,m} \frac{j!}{2!(j-2)!} \times m \times \frac{prob_{i,j}(w) \times prob_{l,m}(w)}{\tau_{aug} \times area}$$

equation 4.19

Figure 4.7 is a plot of the Auger rates for the ground and excited states, as a function of the total current.

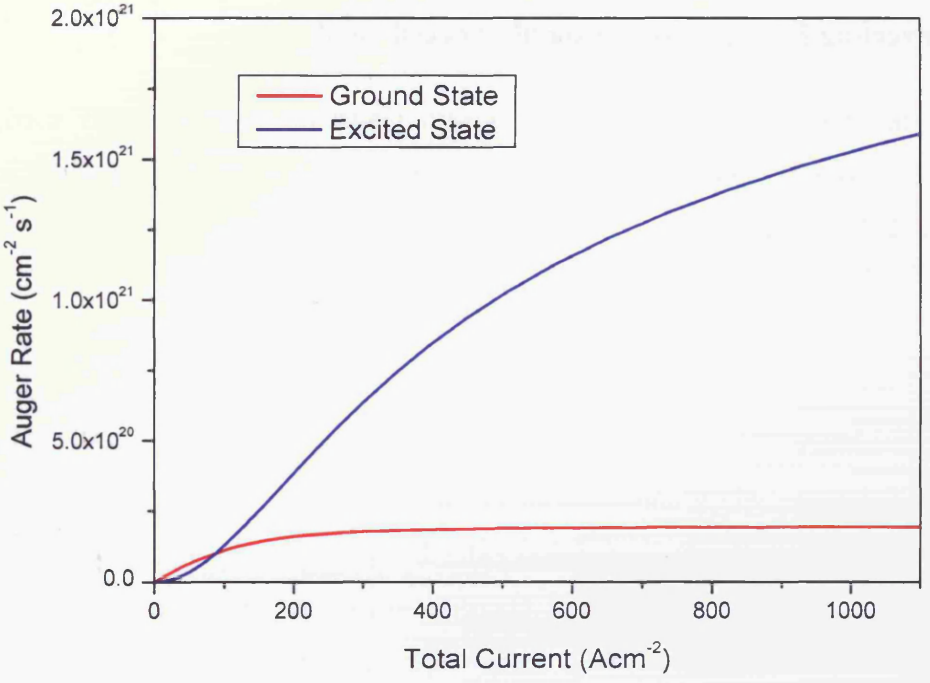

Figure 4.7 - Auger rates for the ground (red line) and excited (blue line) states, as a function of the total current in the dots and the wetting layer.

Again, the excited state rate is much larger than the ground state rate due to the higher degeneracy in the excited state.

4.5 Inhomogeneous Broadening: Converting Energies to an Equally Spaced Grid

4.5.1 Introduction

Section 4.2 describes how the total radiative rates for all the dots are calculated. Using equation 4.8 and equation 4.9 the radiative rates per unit energy in dimensions of $[T]^{-1}[L]^{-2}[E]^{-1}$ are calculated for a particular group of dots with the same width w (and consequently the same energy). The following sections describe how the rates per unit energy calculated for each group of dots are redistributed over smaller energy intervals.

4.5.2 Converting Energies to an Equally Spaced Grid

To model the ensemble of one million dots a Gaussian distribution is used, as described in chapter 3. The probability per unit width of a dot having a width w, in dimensions of $[L]^{-1}$, is given by

$$g(w) = \frac{1}{(2\pi)^{1/2}} \frac{1}{\sigma} \exp\left[-\frac{(w-\overline{w})^2}{2\sigma^2} \right]$$

equation 4.20

where $\overline{w}$ is the mean width and σ is the standard deviation of the distribution. The range of a standard Gaussian distribution extends to infinity. In the model equation 4.20 is modified, creating a truncated Gaussian function, to calculate a series of equally spaced discrete widths. This is described in detail in chapter 3. These discrete widths are subsequently converted into energies using the SHO potential. However, because these energies do not scale linearly with the dot width, the result is a non-symmetrical distribution in energy, as shown in Figure 4.8.

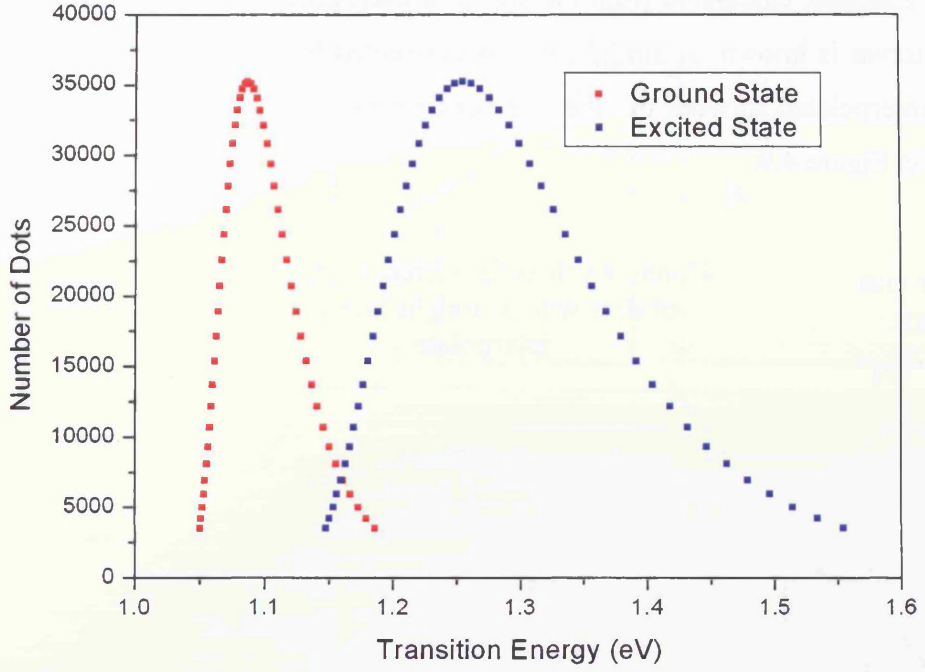

Figure 4.8 - Number of dots with ground and excited state transition energies. The distribution in energy is asymmetrical.

A series of radiative rates per unit energy are calculated, which, for the ground and excited states respectively, are given in equation 4.8 and equation 4.9 as:

$$R_{rad}^{gr}(w) = \frac{n_{QD}(w)}{area \times \Delta E(w)} \times \sum_{i,j,l,m} prob_{i,j}(w) \times prob_{l,m}(w) \times 2 \frac{1}{\tau_{sp}} \left(\frac{i}{2}\right)\left(\frac{l}{2}\right)$$

$$R_{rad}^{ex}(w) = \frac{n_{QD}(w)}{area \times \Delta E(w)} \times \sum_{i,j,l,m} prob_{i,j}(w) \times prob_{l,m}(w) \times 8 \frac{1}{\tau_{sp}} \left(\frac{j}{4}\right)\left(\frac{m}{4}\right)$$

These equations give the radiative rates per unit energy in dimensions of $[T]^{-1}[L]^{-2}[E]^{-1}$ for a particular group of dots with the same width w. The energy intervals are not equal since the energy does not scale linearly with the width of the dot and so each energy interval is denoted as $\Delta E(w)$ since its value is dependent on the size of the dot.

To calculate the spontaneous emission and gain spectra the first step is to split the rates per unit energy into smaller energy intervals. To do this a grid with equally spaced energy intervals is created, for both the ground state and the excited state transition energies. The minimum value of each of the two grids is the minimum energy of the dots, and similarly for the maximum value, as shown below. To divide

the rates into smaller energy intervals interpolation is used. At each of the discrete transition energies, calculated from the width of each group of dots, the rate per unit energy interval is known. A straight line is connected between these points and the rates are interpolated to work out the rate per unit energy at intervals along this line, as shown in Figure 4.9.

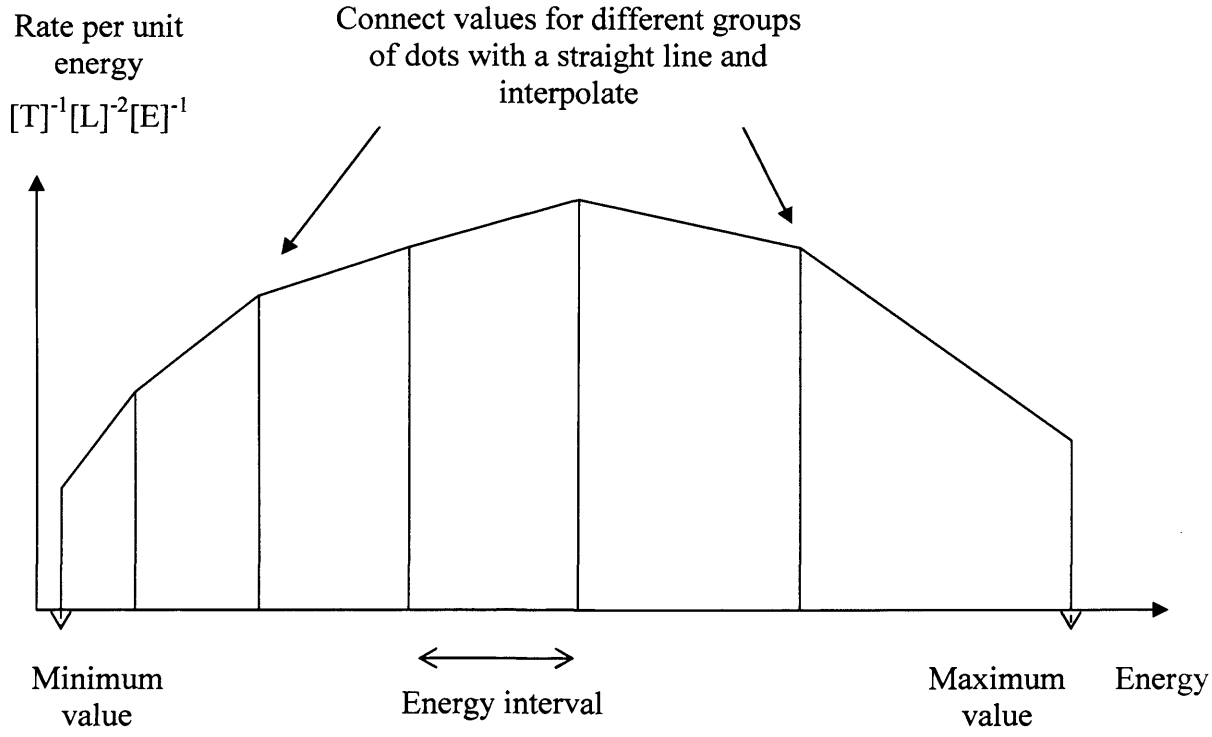

Figure 4.9 - To calculate the rates per unit energy at intermediate energy values the rates are connected with straight lines and interpolated.

The interpolation is done using the method of similar triangles, which is shown in the following figure:

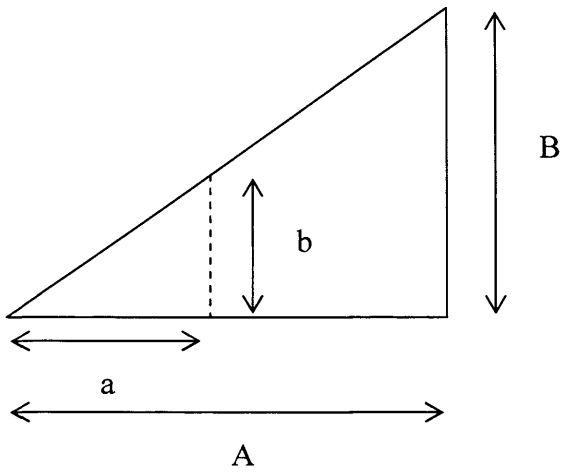

Figure 4.10 - Method of similar triangles.

Using the symbols shown in Figure 4.10, simple trigonometry shows that:

$$\frac{B}{A} = \frac{b}{a} \rightarrow b = \frac{aB}{A}$$

equation 4.21

Applying this method to the radiative rates is done as follows:

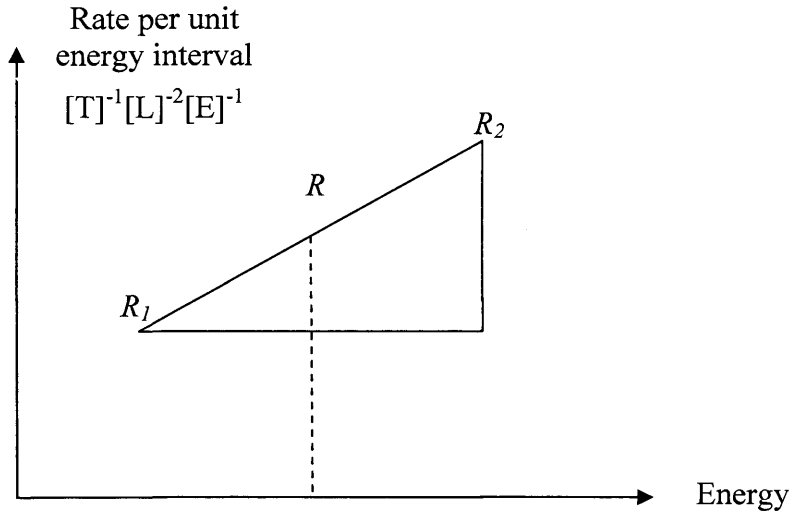

Figure 4.11 - Applying method of similar triangles to the rates.

If R_1 and R_2 are rates per unit energy at energies corresponding to the widths of the dots, then the rate per unit energy R is given by

$$R = R_1 + \frac{\Delta E(R, R_1) \times (R_2 - R_1)}{\Delta E(R_2, R_1)}$$

equation 4.22

where $\Delta E(R,R_1)$ is the difference in energy between R and R_1, and similarly $\Delta E(R_2,R_1)$ is the difference in energy between R_2 and R_1. Many values of different Rs are calculated at different equally spaced energies along the grid. The minimum and maximum energies are equal to the minimum and maximum energies of the dots since it is not possible to interpolate beyond these. The result is series of rates per unit transition energy at equally spaced intervals along the energy grid. These rates have dimensions of $[T]^{-1}[L]^{-2}[E]^{-1}$ and the energy interval is now equal to the difference in energy between the points on the new grid. Figure 4.12 shows the interpolated rates per unit energy for the ground state as a function of the transition energy. For comparison the original values are also shown.

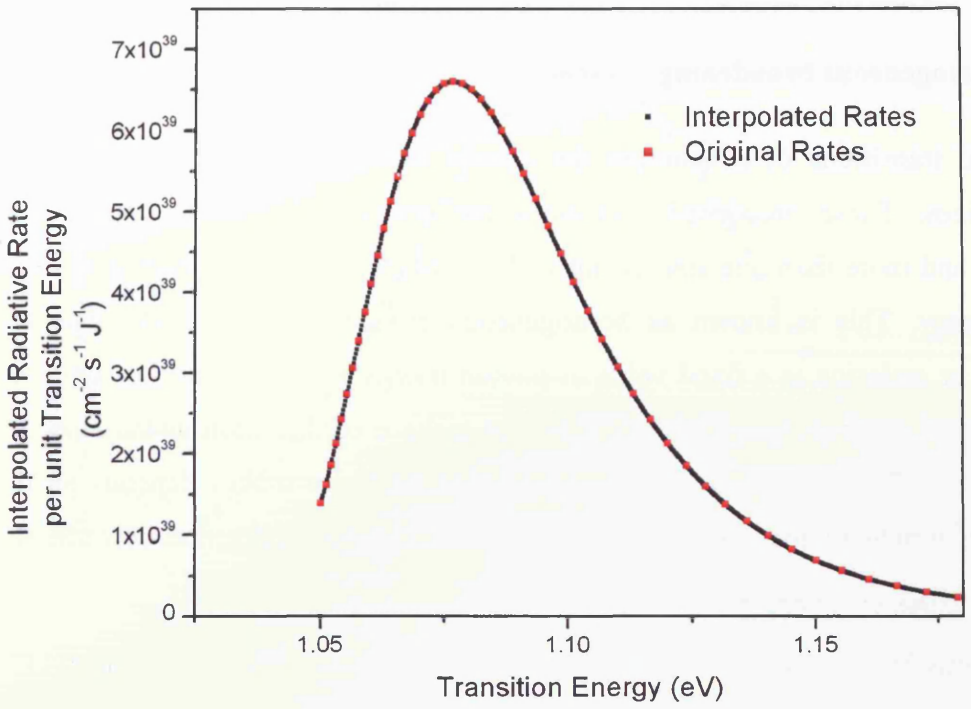

Figure 4.12 - Interpolated radiative rates per unit transition energy for the ground state, plotted for the situation when the dots are fully occupied. For comparison the original values are also shown.

Now that the rates per unit energy have been converted into points on an equally spaced energy grid, the next stage is to include the homogeneous broadening function, which is described in the next section

4.6 Implementing the Homogeneous Broadening: Spontaneous Emission

4.6.1 Introduction

Using the equations derived in section 4.2 the total radiative rates for the dots can be calculated. If total radiative rates are calculated, and not spectra, it is not necessary to include the homogeneous broadening function since the energy of each transition does not need to be known. However, the spectra of the emission as a function of energy are also studied in this thesis, and so the homogeneous linewidth must be included in

the calculations. The following sections describe how the homogeneous broadening function is implemented in the calculations for the radiative rates.

4.6.2 Homogeneous broadening

The optical transitions of a quantum dot consist of a series of broadened delta-function lines. These broadened transitions are centred on the energies of the transitions and more than one size of dot will contribute to the transition at any one photon energy. This is known as homogeneous broadening. So to calculate the absorption or emission at a fixed value of photon energy it is necessary to sum over all the dots of different transition energies that make a contribution at that specific photon energy. The magnitude of the contribution each dot makes depends on the relative magnitude of the homogeneous linewidth and the difference between the transition energy of the dot and the photon energy.

Homogeneous broadening is expressed using the Lorentzian function centred on the transition energy of the dot E_n:

$$L(h\upsilon) = \frac{1}{\pi} \frac{\Lambda}{(h\upsilon - E_n)^2 + \Lambda^2}$$

equation 4.23

Λ is the linewidth and a value of 10meV is used throughout this thesis [4]. $L(h\upsilon)$ has dimensions of $[E]^{-1}$.

So at any transition energy, more than one dot makes a contribution to the radiative rate due to the homogeneous linewidth. Equally spaced photon energies are chosen along the axis. At each value of photon energy the contribution that each dot makes at this energy to the rate is calculated. This photon energy grid can run from any minimum and maximum values; however, at energies that exceed the minimum and maximum transition energies of the dot ensemble the contributions calculated will become less accurate. The model has a cut off point for the transition energies as a truncated Gaussian is used to give the distribution of sizes in the dots (and thus energy) and this does not extend to infinity as for a real Gaussian distribution. This is shown in Figure 4.13. This means that at photon energies outside the inhomogeneous distribution there will be fewer dots contributing to the rate.

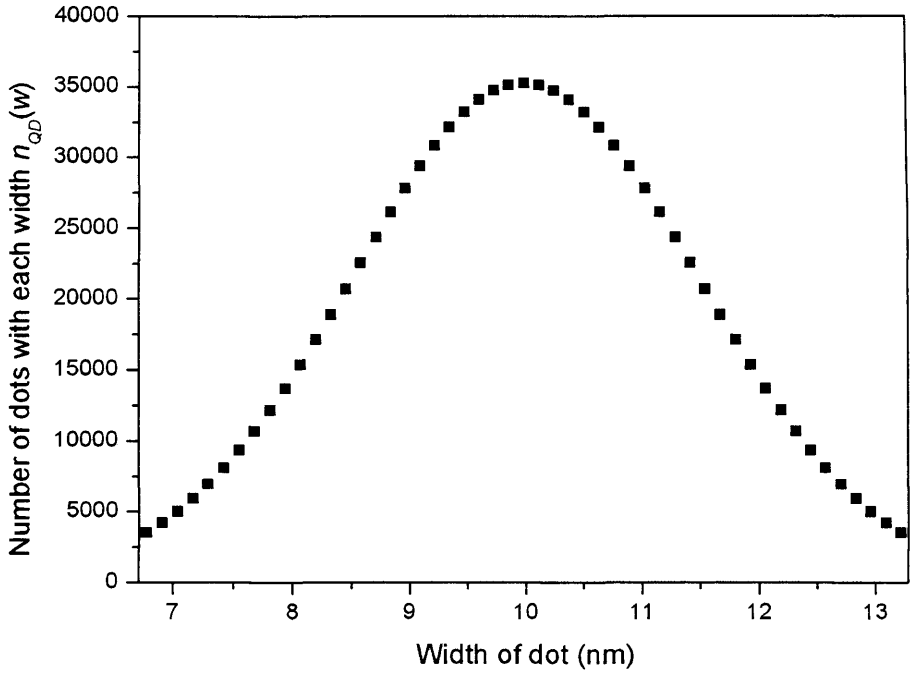

Figure 4.13 - Truncated Gaussian distribution; the range of sizes of the dots (and therefore the transition energies) does not extend to infinity as for a real Gaussian distribution.

At a particular photon energy $h\upsilon$, the contribution that a rate per unit energy at transition energy E_n will make to the rate at $h\upsilon$, in dimensions of $[T]^{-1}[L]^{-2}[E]^{-2}$, is:

$$R(E_n)\times\frac{1}{\pi}\frac{\Lambda}{(h\upsilon-E_n)^2+\Lambda^2}$$

equation 4.24

Here, $R(E_n)$ is the rate per unit energy in dimensions of $[T]^{-1}[L]^{-2}[E]^{-1}$ at transition energy E_n. So the total rate per unit energy at photon energy $h\upsilon$ is found by integrating over the energies of all the dots. In the model this is done using a summation over all the transition energies: the rates per unit energy are multiplied by the appropriate energy interval, ΔE_n, and summed:

$$\sum_n R(E_n) \times \Delta E_n \times \frac{1}{\pi} \frac{\Lambda}{(h\upsilon - E_n)^2 + \Lambda^2}$$

equation 4.25

Figure 4.14 is a plot of the homogeneously broadened ground state spontaneous emission spectrum, when all the dot states are fully occupied.

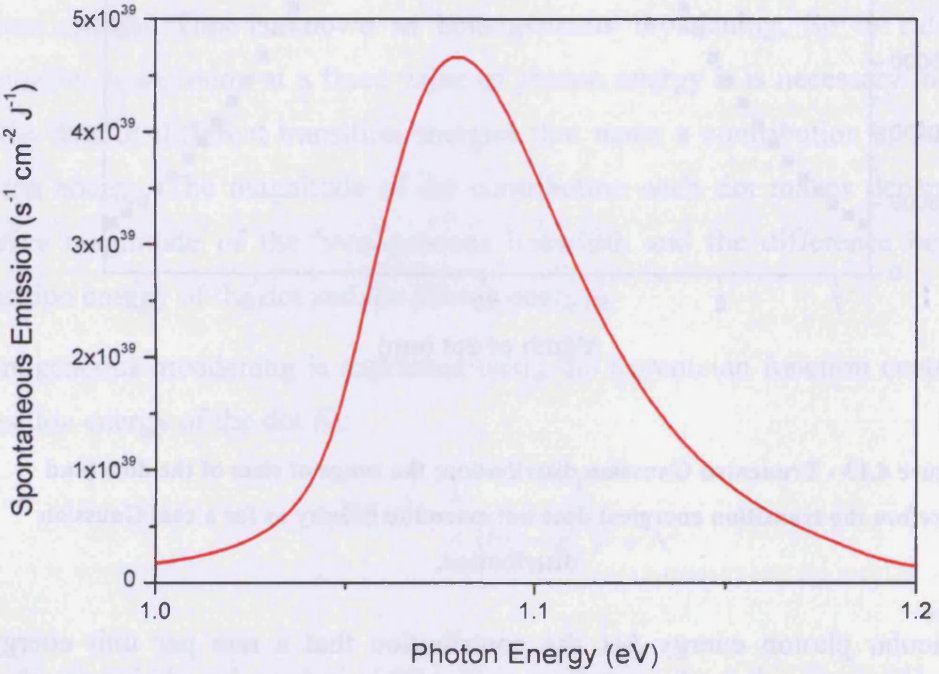

Figure 4.14 - Ground state homogeneously broadened spontaneous emission spectrum when all the dots are fully occupied.

Integrating this curve gives the total radiative rate in dimensions of $[T]^{-1}[L]^{-2}$.

4.7 Modal Gain

4.7.1 Introduction and Gain Equations

The modal gain can be related to the spontaneous emission through the Einstein relations. The Einstein *A* and *B* coefficients can be related to the spontaneous emission rate of a dot, and so can also be used to calculate the gain. Optical gain is the fractional change in photon number per unit distance, and so to calculate the gain it is

necessary to calculate the net induced rate per unit area between the conduction and valence band states of the dots.

Chapter 2 gives the equation for the net induced rate for an ensemble of N_{dots} identical dots with a degeneracy of two in the upper and lower states as:

$$R_{net} = 2N_{dots}BP(h\upsilon)(f_v + f_c - 1)$$

equation 4.26

B is the Einstein coefficient and has dimensions of $[T]^{-1}[L]^3[E]$, $P(h\upsilon)$ is the photon density in the mode and has dimensions of $[L]^{-3}[E]^{-1}$, and f_v and f_c are the Fermi functions giving the probability of occupancy for a hole (in a valence state) and an electron (in a conduction state) respectively. So applying equation 4.26 and using the notation adopted in this thesis, the net induced rate due to the ground state of a single dot, in dimensions of $[T]^{-1}$, is given by:

$$R_{net}^{gr}(dot) = BP(h\upsilon)\times 2\times\left(\frac{i}{2}+\frac{l}{2}-1\right)$$

equation 4.27

Including all dots of size w (which all have the same transition energy), and dividing by the energy interval to get the net induced rate per unit energy in dimensions of $[T]^{-1}[E]^{-1}$, the net induced rate due to the ground states of all dots of size w is given by:

$$R_{net}^{gr}(w) = n_{QD}(w)\times\frac{1}{\Delta E(w)}\times\sum_{i,j,l,m} BP(h\upsilon)\times prob_{i,j}(w)\times prob_{l,m}(w)\times 2\times\left(\frac{i}{2}+\frac{l}{2}-1\right)$$

equation 4.28

The equation for the modal gain, in dimensions of $[L]^{-1}$, is derived from the net induced rate as

$$G = \left(\frac{n}{c}\right)\frac{R_{net}}{P(h\upsilon)V_{cav}}$$

equation 4.29

where V_{cav} is the volume of the cavity and n is the refractive index of the material. Considering a waveguide of width w and length L, allows an effective mode width w_{mod} to be defined, such that $V_{cav} = w_{mod}wL$, as shown in Figure 4.15.

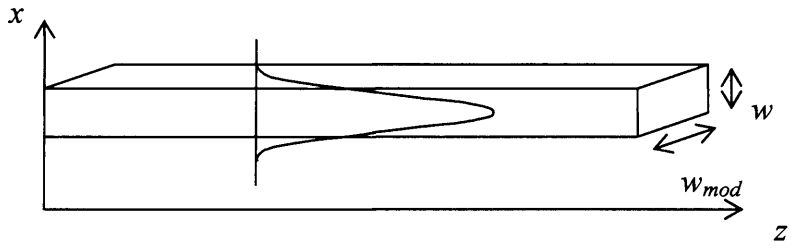

Figure 4.15 - Mode width geometry.

Using $area=wL$, the modal gain can then be rewritten as:

$$G=\left(\frac{n}{c}\right)\frac{R_{net}}{P(h\upsilon)\times area\times w_{mod}}$$

equation 4.30

So using equation 4.30 and substituting in for the net induced rate, the equation for the modal gain per unit length due to the ground state of all the dots of size w, in dimensions of $[L]^{-1}$, is:

$$G_{gr}(w)=\left(\frac{n}{c}\right)\frac{B}{area\times w_{mod}\times\Delta E(w)}\times n_{QD}(w)\times\sum_{i,j,l,m}prob_{i,j}(w)\times prob_{l,m}(w)\times 2\times\left(\frac{i}{2}+\frac{l}{2}-1\right)$$

equation 4.31

The Einstein B coefficient can be written in terms of the Einstein A coefficient, and the reciprocal of A is equal to the spontaneous lifetime τ_{sp}:

$$B_{21}=A_{21}\frac{h^3c^3}{8\pi n^3}\frac{1}{(h\upsilon)^2}=\frac{1}{\tau_{sp}}\frac{h^3c^3}{8\pi n^3}\frac{1}{(h\upsilon)^2}$$

equation 4.32

To be consistent with the recombination equations, the equation for the modal gain due to the ground state of all the dots of size w is rewritten in terms of the spontaneous lifetime τ_{sp} as:

$$G_{gr}(w)=\left(\frac{n}{c}\right)\frac{h^3c^3}{8\pi n^3}\frac{n_{QD}(w)}{(h\upsilon)^2\times\tau_{sp}\times area\times w_{mod}\times\Delta E(w)}$$
$$\times\sum_{i,j,l,m}prob_{i,j}(w)\times prob_{l,m}(w)\times 2\times\left(\frac{i}{2}+\frac{l}{2}-1\right)$$

equation 4.33

Similarly, the net induced rate due to the excited state of all the dots of size w is

$$R_{net}^{ex}(w) = n_{QD} \times \frac{1}{\Delta E(w)} \sum_{i,j,l,m} BP(h\upsilon) \times prob_{i,j}(w) \times prob_{l,m}(w) \times 8 \times \left(\frac{j}{4} + \frac{m}{4} - 1 \right)$$

equation 4.34

which gives the equation for the modal gain per unit length as:

$$G_{ex}(w) = \left(\frac{n}{c} \right) \frac{h^3 c^3}{8\pi n^3} \frac{n_{QD}(w)}{(h\upsilon)^2 \times \tau_{sp} \times area \times w_{mod} \times \Delta E(w)} \times \sum_{i,j,l,m} prob_{i,j}(w) \times prob_{l,m}(w) \times 8 \times \left(\frac{j}{4} + \frac{m}{4} - 1 \right)$$

equation 4.35

4.7.2 Implementing the Homogeneous Broadening: Gain

The implementation of the homogenous broadening for the gain spectra follows the same principle as for the spontaneous emission spectra. The modal gain has been calculated, in dimensions of $[L]^{-1}$, at fixed values of energy corresponding to the transition energies of the dots. As described in section 4.5, interpolation is used between these calculated values so as to decrease the energy intervals over which the gain is spread. Applying the method of similar triangles to the gain spectrum is done as follows:

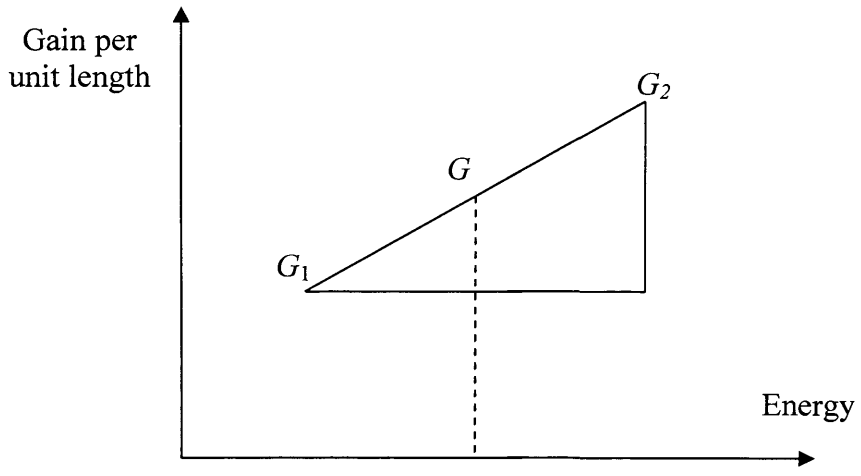

Figure 4.16 - Applying method of similar triangles to the gain.

If G_1 and G_2 are the modal gain per unit length at values of transition energy corresponding to the groups of dots, then the modal gain G is given by

$$G = G_1 + \frac{\Delta E(G,G_1)\times(G_2 - G_1)}{\Delta E(G_2,G_1)}$$

equation 4.36

where $\Delta E(G,G_1)$ is the difference in energy between the transition energies corresponding to G and G_1, and similarly $\Delta E(G_2,G_1)$ is the difference in energy between the transition energies corresponding to G_2 and G_1. Again many values of G are calculated at different equally spaced energies along the grid.

The next step in working out the gain/absorption spectra is to include the homogeneous broadening function $L(h\upsilon)$. The gain/absorption at a fixed value of photon energy is calculated by summing over all the transitions that make a contribution at that specific photon energy. Again, the magnitude of the contribution will depend on the relative magnitude of the homogeneous linewidth and the difference between the energy of the transition and the photon energy.

To work out the homogeneously broadened gain spectra equally spaced energy intervals are again chosen along the axis, and at each value of photon energy the contributions to the modal gain are calculated. So at a particular value on the energy axis of $h\upsilon$, the contribution that the modal gain at energy E_n will make to the gain at $h\upsilon$, in dimensions of $[L]^{-1}[E]^{-1}$, is

$$G(E_n)\times\frac{1}{\pi}\frac{\Lambda}{(h\upsilon - E_n)^2 + \Lambda^2}$$

equation 4.37

where $G(E_n)$ is the modal gain in dimensions of $[L]^{-1}$ at energy E_n. So the total modal gain at energy $h\upsilon$, in dimensions of $[L]^{-1}$, is given by integrating over the contributions at all energies, which is done in the model using a summation:

$$\sum_n G(E_n)\times\Delta E\times\frac{1}{\pi}\frac{\Lambda}{(h\upsilon - E_n)^2 + \Lambda^2}$$

equation 4.38

Figure 4.17 is a plot of the homogeneously broadened ground state modal gain spectrum. The blue curve is for the case where all the dots are empty, the red curve for fully occupied dots, and the black curve is for an intermediate case.

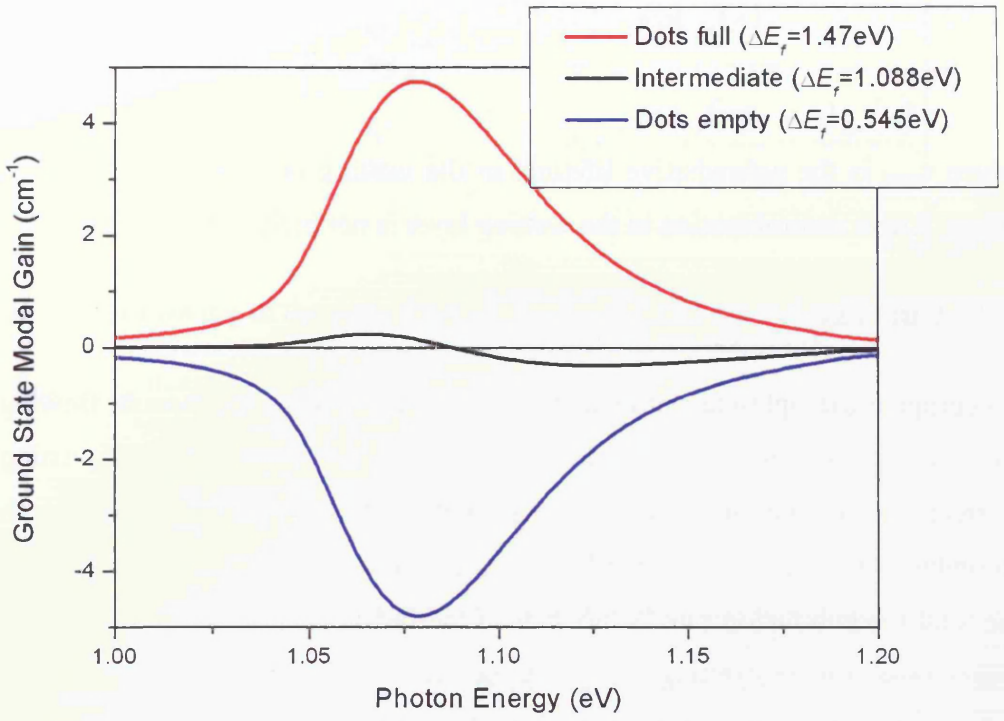

Figure 4.17 - Ground state homogeneously broadened gain spectrum. The blue curve is for the case where all the dots are empty, the red curve for fully occupied dots, and the black curve is for an intermediate case.

4.8 The Wetting Layer Recombination

The wetting layer is a two-dimensional layer left over from the growth process and is treated like a quantum well with a step-like density of states. If the distribution of carriers in the wetting layer is approximated as a Boltzmann distribution, then the radiative rate for the wetting layer, in dimensions of $[T]^{-1}[L]^{-2}$, can be written as:

$$R_{rad}^{wl} = B_{wl} N_{wl} P_{wl}$$

equation 4.39

N_{wl} and P_{wl} are the electron and hole densities in the wetting layer respectively, and B_{wl} is the recombination coefficient which takes a value of 3.5×10^{-7} $s^{-1}m^2$ [5].

The nonradiative rate in the wetting layer is proportional to the density of electrons since the rate limiting step is assumed to be electron capture onto the defect site. The nonradiative rate, in dimensions of $[T]^{-1}[L]^{-2}$, is therefore given by

$$R_{nr}^{wl} = \frac{N_{wl}}{\tau_{nrwl}}$$

equation 4.40

where τ_{nrwl} is the nonradiative lifetime in the wetting layer and is given a value of 300ps. Auger recombination in the wetting layer is not included in the model.

4.9 Current

To compute the light-current characteristics of the system the current flowing in the various systems needs to be calculated, i.e. the dot states and the wetting layer. Current is the rate of flow of charge and so to calculate the current the total recombination rate is multiplied by the electronic charge q. For the case of the dots, the total recombination rate is the sum of the radiative, nonradiative via defects and Auger rates; for the wetting layer it is the sum of the radiative and nonradiative via defects rates. It is assumed that there is no leakage current.

The current is worked out separately for the ground and excited states of the dots. In units of Am^{-2}, the equations for the total current flowing due to the ground and excited states respectively are:

$$J_{gr} = q \times \left(\sum_{w} R_{rad}^{gr}(w) \times \Delta E(w) + \sum_{w} R_{nr}^{gr}(w) + \sum_{w} R_{aug}^{gr} \right)$$

$$= q \times \sum_{w} \frac{n_{QD}(w)}{area} \times \left(\begin{array}{l} \sum_{i,j,l,m} prob_{i,j}(w) \times prob_{l,m}(w) \times 2 \frac{1}{\tau_{sp}} \left(\frac{i}{2}\right)\left(\frac{l}{2}\right) \\ + \sum_{i,j,l>0,m} \frac{i \times prob_{i,j}(w) \times prob_{l,m}(w)}{\tau_{nr}} \\ + \sum_{i=2,j,l,m} l \times \frac{prob_{i,j}(w) \times prob_{l,m}(w)}{\tau_{aug}} \end{array} \right)$$

equation 4.41

$$J_{ex} = q \times \left(\sum_{w} R_{rad}^{ex}(w) \times \Delta E(w) + \sum_{w} R_{nr}^{ex}(w) + \sum_{w} R_{aug}^{ex}(w) \right)$$

$$= q \times \sum_{w} \frac{n_{QD}(w)}{area} \times \left(\begin{array}{l} \sum_{i,j,l,m} prob_{i,j}(w) \times prob_{l,m}(w) \times 8 \frac{1}{\tau_{sp}} \left(\frac{j}{4}\right)\left(\frac{m}{4}\right) \\ + \sum_{i,j,l,m>0} \frac{j \times prob_{i,j}(w) \times prob_{l,m}(w)}{\tau_{nr}} \\ + \sum_{i,j\geq 2,l,m} \frac{j!}{2!(j-2)!} \times m \times \frac{prob_{i,j}(w) \times prob_{l,m}(w)}{\tau_{aug}} \end{array} \right)$$

equation 4.42

The total current flowing in the dots, from all the ground and excited states, is:

$$J_{dots} = J_{gr} + J_{ex}$$

$$= q \times \left(\begin{array}{l} \sum_{w} R_{rad}^{gr}(w) \times \Delta E(w) + \sum_{w} R_{nr}^{gr}(w) + \sum_{w} R_{aug}^{gr}(w) \\ + \sum_{w} R_{rad}^{ex}(w) \times \Delta E(w) + \sum_{w} R_{nr}^{ex}(w) + \sum_{w} R_{aug}^{ex}(w) \end{array} \right)$$

$$= q \times \sum_{w} \frac{n_{QD}(w)}{area} \times \left(\begin{array}{l} \sum_{i,j,l,m} prob_{i,j}(w) \times prob_{l,m}(w) \times 2 \frac{1}{\tau_{sp}} \left(\frac{i}{2}\right)\left(\frac{l}{2}\right) \\ + \sum_{i,j,l>0,m} \frac{i \times prob_{i,j}(w) \times prob_{l,m}(w)}{\tau_{nr}} \\ + \sum_{i=2,j,l,m} l \times \frac{prob_{i,j}(w) \times prob_{l,m}(w)}{\tau_{aug}} \\ + \sum_{i,j,l,m} prob_{i,j}(w) \times prob_{l,m}(w) \times 8 \frac{1}{\tau_{sp}} \left(\frac{j}{4}\right)\left(\frac{m}{4}\right) \\ + \sum_{i,j,l,m>0} \frac{j \times prob_{i,j}(w) \times prob_{l,m}(w)}{\tau_{nr}} \\ + \sum_{i,j\geq 2,l,m} \frac{j!}{2!(j-2)!} \times m \times \frac{prob_{i,j}(w) \times prob_{l,m}(w)}{\tau_{aug}} \end{array} \right)$$

equation 4.43

The current flowing in the wetting layer, J_{wl}, is given by:

$$J_{wl} = q \times \left(R_{rad}^{wl} + R_{nonrad}^{wl} \right)$$

$$= q \times \left(B_{wl} N_{wl} P_{wl} + \frac{N_{wl}}{\tau_{nrwl}} \right)$$

equation 4.44

In an experiment there is no means to eliminate the wetting layer contribution to the current (other than cooling the sample) and the current measured is the total current due to the dots and the wetting layer. The total current is calculated by adding up the contributions from the wetting layer, equation 4.44, and from the dots, equation 4.43:

$$J_{tot} = J_{wl} + J_{dots}$$

equation 4.45

4.10 Summary

In this chapter I have derived equations for the optical processes occurring in the dots using localised population statistics. First equations for the radiative, nonradiative and Auger recombination rates in the dots were described. I then explained how the homogeneous broadening is implemented to produce spontaneous emission and gain spectra. I also derived equations for the recombination in the wetting layer and the current. The next chapter describes an alternative model in which the number of holes in a dot is forced to be equal to the number of electrons, and this is called the *neutral* model.

4.11 References

[1] H. Lee, W. Yang, and P. Sercel, Physical Review B 55 (1997)

[2] S. Sanguinetti, M. Henini, M. G. Alessi, M. Capizzi, P. Frigeri, and S. Franchi, Physical Review B 60 (1999)

[3] P. Dawson, O. Rubel, D. Baranovskii, K. Pierz, P. Thomas, and E. O. Göbel, Physical Review B 72 (2005) 235301.

[4] P. Borri, W. Langbein, S. Schneider, U. Woggon, R. L. Sellin, D. Ouyang, and D. Bimberg, Physical Review Letters 87 (2001) 157401.

[5] W. W. Chow and S. W. Koch, Semiconductor Lasers Fundamentals, Springer, Berlin, 1999.

5 Localised Population Statistics for the Neutral Model

5.1 Introduction

In chapter 3 the method used for calculating the localised population statistics for an ensemble of dots in thermal equilibrium is described. A thermal distribution of carriers is assumed amongst the different energy levels of the inhomogeneous dot distribution and of the wetting layer, with global quasi-Fermi levels for both the electrons and holes. In this *non-neutral* case each dot does not necessarily contain equal numbers of electrons and holes, although the total numbers of electrons and holes are equal. In the literature, models used for quantum dots usually assume an excitonic model [1-4], in which electron-hole pairs are considered and each dot contains equal numbers of electrons and holes. For comparison, a *neutral* model has also been developed in this thesis, in which the number of holes in any dot is set equal to the number of electrons in that dot. Consequently, in this neutral model, Fermi-Dirac statistics cannot be applied to both the electron and hole distributions. The details of this neutral model are described in this chapter.

5.2 Electron and Hole distributions

The approach taken to model the dots and wetting layer for the neutral model is the same as for the non-neutral case. Again an ensemble of one million InAs dots is modelled and a two-dimensional wetting layer is included in the calculations. The energy levels are calculated using the SHO potential. Full details of the modelling can be found in chapter 3.

The distribution of electrons is calculated in exactly the same way as for the non-neutral model, as described in chapter 3. The equations for the electron distribution for a particular value of electron quasi-Fermi level are shown again for clarity in the following table. n_i^j is the number of dots with i electrons in the ground state and j electrons in the excited state and n_{QD} is the total number of dots. $f_{c,gr}$ and $f_{c,ex}$ are the fraction of occupied electron states, for the ground and excited states respectively.

Number of dots with electron distribution *i,j*: n_i^j	**Expression**
n_0^0	$n_{QD}(1-f_{c,gr})^2(1-f_{c,ex})^4$
n_1^0	$n_{QD}2f_{c,gr}(1-f_{c,gr})(1-f_{c,ex})^4$
n_2^0	$n_{QD}f_{c,gr}{}^2(1-f_{c,ex})^4$
n_0^1	$n_{QD}(1-f_{c,gr})^2 4f_{c,ex}(1-f_{c,ex})^3$
n_1^1	$n_{QD}2f_{c,gr}(1-f_{c,gr})4f_{c,ex}(1-f_{c,ex})^3$
n_2^1	$n_{QD}f_{c,gr}{}^2 4f_{c,ex}(1-f_{c,ex})^3$
n_0^2	$n_{QD}(1-f_{c,gr})^2 6f_{c,ex}{}^2(1-f_{c,ex})^2$
n_1^2	$n_{QD}2f_{c,gr}(1-f_{c,gr})6f_{c,ex}{}^2(1-f_{c,ex})^2$
n_2^2	$n_{QD}f_{c,gr}{}^2 6f_{c,ex}{}^2(1-f_{c,ex})^2$
n_0^3	$n_{QD}(1-f_{c,gr})^2 4f_{c,ex}{}^3(1-f_{c,ex})$
n_1^3	$n_{QD}2f_{c,gr}(1-f_{c,gr})4f_{c,ex}{}^3(1-f_{c,ex})$
n_2^3	$n_{QD}f_{c,gr}{}^2 4f_{c,ex}{}^3(1-f_{c,ex})$
n_0^4	$n_{QD}(1-f_{c,gr})^2 f_{c,ex}{}^4$
n_1^4	$n_{QD}2f_{c,gr}(1-f_{c,gr})f_{c,ex}{}^4$
n_2^4	$n_{QD}f_{c,gr}{}^2 f_{c,ex}{}^4$

The condition that the number of holes in any dot must equal the number of electrons in that dot is now imposed. It is assumed that the holes are distributed amongst the dot states in the same way as the electrons, i.e. if there are i electrons in the ground state there are also i holes in the ground state, and similarly for the excited state. So for any one dot the following conditions apply:

$$l = i$$

$$m = j$$

If there are n_i^j dots with i electrons in the ground state and j electrons in the excited state, then there must also be n_i^j dots with i holes in the ground state and j holes in the excited state, i.e.

$$p_i^j = n_i^j$$

equation 5.1

5.3 Fermi-Dirac Statistics

It is not possible for the electron and hole distributions to both be described by Fermi-Dirac statistics if each dot is neutral, and this can be proved as follows. Consider one dot and set the number of holes in the ground state equal to the number of electrons i.e. $i=l$. If Fermi-Dirac statistics are used then this condition can be written as:

$$\frac{1}{\exp\left(\frac{E_{gr}^c - E_{fc}}{kT}\right)+1} = \frac{1}{\exp\left(\frac{E_{gr}^v - E_{fv}}{kT}\right)+1}$$

equation 5.2

E_{gr}^c and E_{gr}^v are the ground state energy levels for the electrons and holes respectively, and E_{fc} and E_{fv} are the quasi-Fermi levels for the electrons and holes respectively. This equation reduces to:

$$E_{gr}^c - E_{fc} = E_{gr}^v - E_{fv}$$

equation 5.3

Now considering the excited states for the electrons and holes, setting the number of holes equal to the number of electrons gives $j=m$. If the excited state electron energy is written as

$E_{gr}^{c}+\delta E_c$, and the excited state hole energy as $E_{gr}^{v}+\delta E_v$, the following equation can be written

$$\frac{1}{\exp\left(\frac{E_{gr}^{c}+\delta E_c-E_{fc}}{kT}\right)+1}=\frac{1}{\exp\left(\frac{E_{gr}^{v}+\delta E_v-E_{fv}}{kT}\right)+1}$$

equation 5.4

which gives

$$E_{gr}^{c}+\delta E_c-E_{fc}=E_{gr}^{v}+\delta E_v-E_{fv}$$

equation 5.5

The two conditions in equation 5.3 and equation 5.5 can both be true only if

$$\delta E_c=\delta E_v$$

equation 5.6

However, the equations for the electron and hole energy levels in the dot are dependent on the effective masses of the electrons and holes. Therefore, because the electrons and holes have different effective masses, they have different energy levels. Thus it is not possible to satisfy the condition in equation 5.6 and the electron and hole distributions cannot both be described by Fermi-Dirac statistics. An electron quasi-Fermi level can be defined, but it is not possible therefore to define a hole quasi-Fermi level.

5.4 Recombination in Neutral Dots

5.4.1 Introduction

The condition of charge neutrality in each dot simplifies the equations for the recombination processes. The following sections give the modified recombination equations for the neutral dots.

5.4.2 Radiative Recombination

As derived in chapter 4, the radiative rate for the ground state of one dot, in dimensions of $[T]^{-1}$, is given by

$$R_{rad}(dot) = 2A\left(\frac{i}{2}\right)\left(\frac{l}{2}\right)$$
$$= 2\frac{1}{\tau_{sp}}\left(\frac{i}{2}\right)\left(\frac{l}{2}\right)$$

equation 5.7

where i is the number of electrons in the ground state, and l is the number of holes. The reciprocal of the Einstein A coefficient is the spontaneous lifetime τ_{sp} for a single transition. With charge neutrality in the dot, equation 5.7 reduces to the following equation, and it is interesting that this equation implies that recombination in neutral dots is bimolecular in *each* dot:

$$R_{rad}^{gr}(dot) = 2A\left(\frac{i}{2}\right)^2$$
$$= 2\frac{1}{\tau_{sp}}\left(\frac{i}{2}\right)^2$$

equation 5.8

Similarly, the excited state radiative rate for one dot is

$$R_{rad}^{ex}(dot) = 8A\left(\frac{j}{4}\right)\left(\frac{m}{4}\right)$$
$$= 8\frac{1}{\tau_{sp}}\left(\frac{j}{4}\right)\left(\frac{m}{4}\right)$$

equation 5.9

which for neutral dots becomes:

$$R_{rad}^{ex}(dot) = 8A\left(\frac{j}{4}\right)^2$$
$$= 8\frac{1}{\tau_{sp}}\left(\frac{j}{4}\right)^2$$

equation 5.10

The ground state radiative rate per unit energy for all dots with a distribution i,l (and $i=l$), in dimensions of $[T]^{-1}[L]^{-2}[E]^{-1}$, is

$$R_{rad}^{gr}(i,l) = n_{QD} \times \frac{1}{area \times \Delta E} \times \sum_{j,m} prob_{i,j} \times prob_{l,m} \times 2\frac{1}{\tau_{sp}}\left(\frac{i}{2}\right)\left(\frac{l}{2}\right)$$
$$= n_{QD} \times \frac{1}{area \times \Delta E} \times \sum_{j} \left[prob_{i,j}\right]^2 \times 2\frac{1}{\tau_{sp}}\left(\frac{i}{2}\right)^2$$

equation 5.11

where ΔE is the energy interval. Similarly, the excited state radiative rate per unit energy for all the dots with an electron distribution j,m is

$$R_{rad}^{ex}(j,m) = n_{QD} \times \frac{1}{area \times \Delta E} \times \sum_{i} \left[prob_{i,j}\right]^2 \times 8\frac{1}{\tau_{sp}}\left(\frac{j}{4}\right)^2$$

equation 5.12

The total ground and excited state rates for all the dots are

$$R_{rad}^{gr}(total) = \sum_{w} \frac{n_{QD}(w)}{\Delta E(w) \times area} \times \sum_{i,j,l,m} prob_{i,j}(w) \times prob_{l,m}(w) \times 2\frac{1}{\tau_{sp}}\left(\frac{i}{2}\right)\left(\frac{l}{2}\right)$$
$$= \sum_{w} \frac{n_{QD}(w)}{\Delta E(w) \times area} \times \sum_{i,j} \left[prob_{i,j}(w)\right]^2 \times 2\frac{1}{\tau_{sp}}\left(\frac{i}{2}\right)^2$$

equation 5.13

$$R_{rad}^{ex}(total) = \sum_{w} \frac{n_{QD}(w)}{\Delta E(w) \times area} \times \sum_{i,j,l,m} prob_{i,j}(w) \times prob_{l,m}(w) \times 8\frac{1}{\tau_{sp}}\left(\frac{j}{4}\right)\left(\frac{m}{4}\right)$$
$$= \sum_{w} \frac{n_{QD}(w)}{\Delta E(w) \times area} \times \sum_{i,j} \left[prob_{i,j}(w)\right]^2 \times 8\frac{1}{\tau_{sp}}\left(\frac{j}{4}\right)^2$$

equation 5.14

Figure 5.1 shows the total ground state radiative rate per unit energy as a function of the current in the dots for both the neutral dots and the non-neutral dots. It can be seen that the rate for the neutral dots is much higher at low currents than the rate for the non-neutral dots. This is because in the neutral dots there is always a hole present to complete the recombination process. At low currents for the non-neutral dots, although there may be an electron in a dot there may not necessarily be a hole.

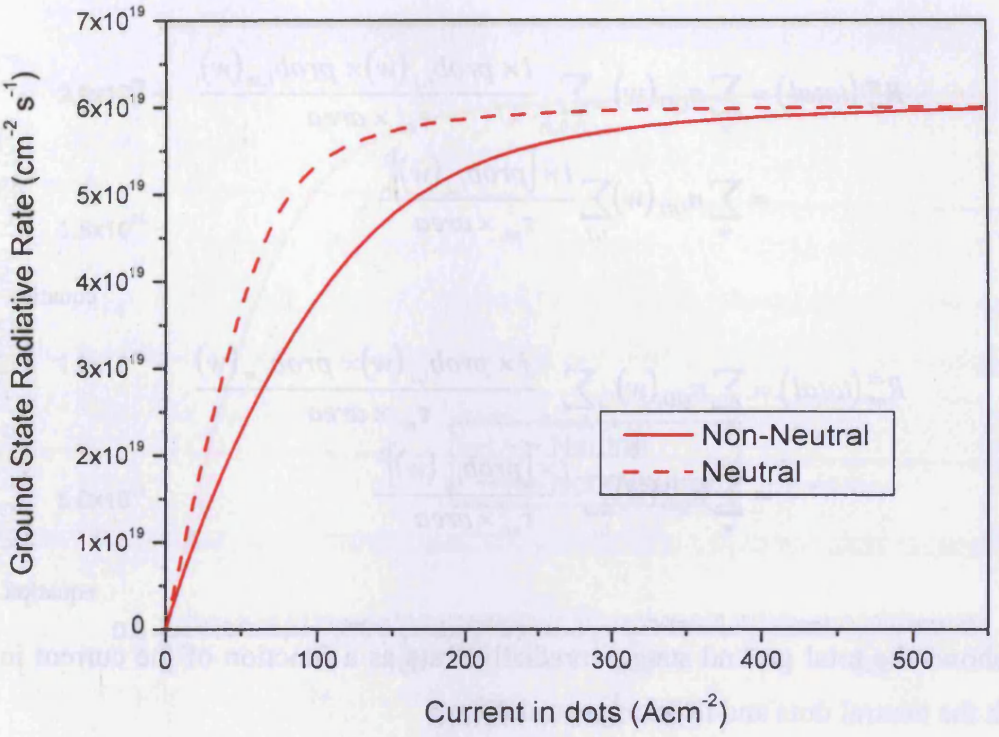

Figure 5.1 - Total ground state radiative rate for the neutral dots (dashed line) and the non-neutral dots (solid line), plotted as a function of the current in the dots.

5.4.3 Nonradiative Recombination

For nonradiative recombination in a dot an electron and hole must be present in the same dot. Thus for neutral dots, if there is an electron in the dot there will always be nonradiative recombination since there will always be a hole to complete the nonradiative process. The rate is proportional to the number of electrons as electron capture is assumed to be the slowest process. The nonradiative rates for the ground and excited states of a single dot are respectively given by:

$$R_{nr}^{gr}(dot) = \frac{i}{\tau_{nr}}$$

equation 5.15

$$R_{nr}^{ex}(dot) = \frac{j}{\tau_{nr}}$$

equation 5.16

The total nonradiative rates for the ground and excited states, in dimensions of $[T]^{-1}[L]^{-2}$, are given by:

$$R_{nr}^{gr}(total) = \sum_{w} n_{QD}(w) \sum_{i,j,l>0,m} \frac{i \times prob_{i,j}(w) \times prob_{l,m}(w)}{\tau_{nr} \times area}$$
$$= \sum_{w} n_{QD}(w) \sum_{i,j} \frac{i \times [prob_{i,j}(w)]^2}{\tau_{nr} \times area}$$

equation 5.17

$$R_{nr}^{ex}(total) = \sum_{w} n_{QD}(w) \sum_{i,j,l,m>0} \frac{j \times prob_{i,j}(w) \times prob_{l,m}(w)}{\tau_{nr} \times area}$$
$$= \sum_{w} n_{QD}(w) \sum_{i,j} \frac{j \times [prob_{i,j}(w)]^2}{\tau_{nr} \times area}$$

equation 5.18

Figure 5.2 shows the total ground state nonradiative rate as a function of the current in the dots for both the neutral dots and the non-neutral dots.

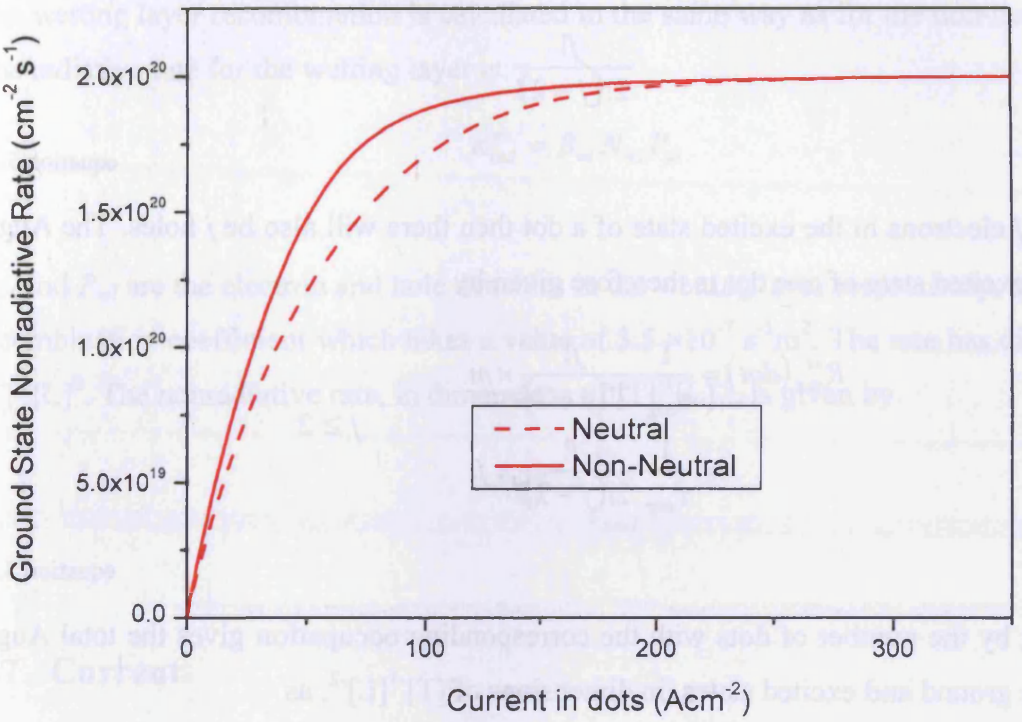

Figure 5.2 - Total ground state nonradiative rate for the neutral dots (dashed line) and the non-neutral dots (solid line), plotted as a function of the current in the dots.

5.4.4 Auger Recombination

The Auger process modelled in this thesis involves two electrons and one hole, which must be present in the same dot. For neutral dots, if there are two electrons then there will also be two holes. Considering the ground state case first, Auger recombination will only take place when the ground state is full i.e. when there are two electrons and two holes in the dot. This gives rise to two possible Auger recombination events. The Auger rate for the ground state of one dot is therefore proportional to the number of holes in the dot, on the condition that there are two electrons (and therefore two holes). The rate is given by

$$R_{aug}^{gr}(dot) = \frac{l}{\tau_{aug}} \qquad i = 2$$
$$= \frac{i}{\tau_{aug}}$$

equation 5.19

Now considering the excited state, again the number of ways of having two electrons from j is:

$$\frac{j!}{2!(j-2)!}$$

equation 5.20

If there are j electrons in the excited state of a dot then there will also be j holes. The Auger rate for the excited state of one dot is therefore given by

$$\begin{aligned} R_{aug}^{ex}(dot) &= \frac{1}{\tau_{aug}} \frac{j!}{2!(j-2)!} \times m \\ &= \frac{1}{\tau_{aug}} \frac{j!}{2!(j-2)!} \times j \end{aligned} \qquad j \geq 2$$

equation 5.21

Multiplying by the number of dots with the corresponding occupation gives the total Auger rates for the ground and excited states, in dimensions of $[T]^{-1}[L]^{-2}$, as

$$\begin{aligned} R_{aug}^{gr}(total) &= \sum_{w} n_{QD}(w) \sum_{i=2,j,l,m} l \times \frac{prob_{i,j}(w) \times prob_{l,m}(w)}{\tau_{aug} \times area} \\ &= \sum_{w} n_{QD}(w) \sum_{i=2,j} i \times \frac{[prob_{i,j}(w)]^2}{\tau_{aug} \times area} \end{aligned}$$

equation 5.22

$$\begin{aligned} R_{aug}^{ex}(total) &= \sum_{w} n_{QD}(w) \sum_{i,j\geq 2,l,m} \frac{j!}{2!(j-2)!} \times m \times \frac{prob_{i,j}(w) \times prob_{l,m}(w)}{\tau_{aug} \times area} \\ &= \sum_{w} n_{QD}(w) \sum_{i,j\geq 2} \frac{j!}{2!(j-2)!} \times j \times \frac{[prob_{i,j}(w)]^2}{\tau_{aug} \times area} \end{aligned}$$

equation 5.23

5.5 Spectra

The spectra are calculated in exactly the same way as for the non-neutral dots, as described in chapter 4, using the revised equations for the radiative recombination detailed above. When the dots are all full/empty the spontaneous emission and gain/absorption spectra are identical for both the neutral and non-neutral cases. The difference between these the two cases is simply the way that the dots are populated.

5.6 The Wetting Layer

The wetting layer recombination is calculated in the same way as for the non-neutral model. The radiative rate for the wetting layer is:

$$R_{rad}^{wl} = B_{wl} N_{wl} P_{wl}$$

equation 5.24

N_{wl} and P_{wl} are the electron and hole densities in the wetting layer respectively, and B_{wl} is the recombination coefficient which takes a value of 3.5×10^{-7} $s^{-1}m^2$. The rate has dimensions of $[T]^{-1}[L]^2$. The nonradiative rate, in dimensions of $[T]^{-1}[L]^{-2}$, is given by

$$R_{nr}^{wl} = \frac{N_{wl}}{\tau_{nrwl}}$$

equation 5.25

5.7 Current

Because there will always be a hole present in a dot if there is an electron present, the recombination rates for the same value of electron quasi-Fermi level are much greater for the neutral dots than for the non-neutral dots. Therefore, the current due to the neutral dots will also be greater for the same value of electron quasi-Fermi level.

The total current due to the ground and excited states of the dots respectively is given by

$$J_{gr} = q \times \left(\sum_{w} R_{rad}^{gr}(w) \times \Delta E(w) + \sum_{w} R_{nr}^{gr}(w) + \sum_{w} R_{aug}^{gr} \right)$$

$$= q \times \sum_{w} \frac{n_{QD}(w)}{area} \times \left(\begin{array}{l} \sum_{i,j} 2 \frac{1}{\tau_{sp}} \left(\frac{i}{2} \right)^2 \times \left[prob_{i,j}(w) \right]^2 \\ + \sum_{i,j} \frac{i \times \left[prob_{i,j}(w) \right]^2}{\tau_{nr}} \\ + \sum_{i=2,j} i \times \frac{\left[prob_{i,j}(w) \right]^2}{\tau_{aug}} \end{array} \right)$$

equation 5.26

$$J_{ex} = q \times \left(\sum_{w} R_{rad}^{ex}(w) \times \Delta E(w) + \sum_{w} R_{nr}^{ex}(w) + \sum_{w} R_{aug}^{ex}(w) \right)$$

$$= q \times \sum_{w} \frac{n_{QD}(w)}{area} \times \left(\begin{array}{l} \sum_{i,j} 8 \frac{1}{\tau_{sp}} \left(\frac{j}{4} \right)^2 \times \left[prob_{i,j}(w) \right]^2 \\ + \sum_{i,j} \frac{j \times \left[prob_{i,j}(w) \right]^2}{\tau_{nr}} \\ + \sum_{i,j \geq 2} \frac{j!}{2!(j-2)!} \times j \times \frac{\left[prob_{i,j}(w) \right]^2}{\tau_{aug}} \end{array} \right)$$

equation 5.27

The total current flowing in the dots, from all the ground and excited states, is:

$$
\begin{aligned}
J_{dots} &= J_{gr} + J_{ex} \\
&= q \times \left(\begin{array}{l} \sum_{w} R_{rad}^{gr}(w) \times \Delta E(w) + \sum_{w} R_{nr}^{gr}(w) + \sum_{w} R_{aug}^{gr}(w) \\ + \sum_{w} R_{rad}^{ex}(w) \times \Delta E(w) + \sum_{w} R_{nr}^{ex}(w) + \sum_{w} R_{aug}^{ex}(w) \end{array} \right) \\
&= q \times \sum_{w} \frac{n_{QD}(w)}{area} \times \left(\begin{array}{l} \sum_{i,j} 2 \frac{1}{\tau_{sp}} \left(\frac{i}{2} \right)^2 \times \left[prob_{i,j}(w) \right]^2 \\ + \sum_{i,j} \frac{i \times \left[prob_{i,j}(w) \right]^2}{\tau_{nr}} \\ + \sum_{i=2,j} i \times \frac{\left[prob_{i,j}(w) \right]^2}{\tau_{aug}} \\ + \sum_{i,j} 8 \frac{1}{\tau_{sp}} \left(\frac{j}{4} \right)^2 \times \left[prob_{i,j}(w) \right]^2 \\ + \sum_{i,j} \frac{j \times \left[prob_{i,j}(w) \right]^2}{\tau_{nr}} \\ + \sum_{i,j \geq 2} \frac{j!}{2!(j-2)!} \times j \times \frac{\left[prob_{i,j}(w) \right]^2}{\tau_{aug}} \end{array} \right)
\end{aligned}
$$

equation 5.28

The current flowing in the wetting layer, J_{wl}, is given by:

$$
\begin{aligned}
J_{wl} &= q \times \left(R_{rad}^{wl} + R_{nonrad}^{wl} \right) \\
&= q \times \left(B_{wl} N_{wl}^{\ 2} + \frac{N_{wl}}{\tau_{nrwl}} \right)
\end{aligned}
$$

equation 5.29

5.8 Summary

In this chapter I have described an alternative model to the one presented in chapter 3. In this model, called the *neutral* model, the dots are electrically neutral, and the number of holes in any one dot is equal to the number of electrons. I have described how this condition alters the equations for the recombination processes. I have also shown that Fermi-Dirac statistics cannot be applied to both the electron and hole distributions for this neutral case.

5.9 References

[1] M. Grundmann and D. Bimberg, Physical Review B 55 (1997) 9740.

[2] S. Sanguinetti, M. Henini, M. G. Alessi, M. Capizzi, P. Frigeri, and S. Franchi, Physical Review B 60 (1999)

[3] H. Lee, W. Yang, and P. Sercel, Physical Review B 55 (1997)

[4] D. G. Deppe, D. L. Huffaker, S. Csutak, Z. Zou, G. Park, and O. B. Schekin, IEEE Journal of Quantum Electronics 35 (1999) 1238.

6 Electron and Hole Occupancies

6.1 Introduction

One of the aims of this thesis is to study how the localisation of the states in quantum dots affects their optical properties such as the light output and gain. To get a better understanding of the processes occurring in the dots, this chapter looks at how the states in the dots are filled with increasing injection, for both the non-neutral and neutral cases. It should be noted that, due to the difference in the effective masses of the electrons and holes, the hole energies are about ten times smaller than those of the electrons. For example, the range of ground state energies for the electrons is about 120meV compared to about 10meV for the holes. The electron energies are therefore more sensitive to the quantum dot size than the hole energies [1].

6.2 Electron and Hole Distributions for Non-Neutral Dots

6.2.1 Introduction

In this section the evolution of the electron and hole distributions with increasing quasi-Fermi level separation is studied, for the non-neutral model.

6.2.2 Electron and Hole Distributions for Fully Occupied Dots

Figure 6.1 is a plot is the electron and hole distributions for the fully occupied dots i.e. a distribution of the states. The hole energies are plotted relative to the conduction band minimum. The inhomogeneity in the dots is modelled in this thesis by assuming a Gaussian distribution in the dot *widths*. The resulting distribution in *energy* is therefore *not* a Gaussian distribution, as can be seen in the plots in Figure 6.1. The ground and excited state mean electron energies are 80meV and 237meV respectively, measured from the conduction band minimum. Similarly, the ground and excited state mean hole energies are 7meV and 19meV respectively, measured from the valence band minimum. The total number of dots is one million. Each ground state can accommodate two electrons and two holes in the upper and lower states respectively, and similarly each excited state can accommodate four electrons and four holes.

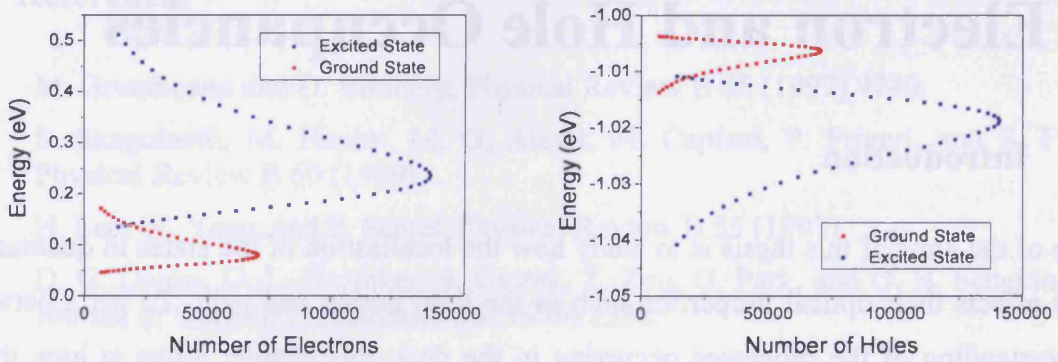

Figure 6.1 - State occupancies for the electron and hole ground (red points) and excited (blue points) states when the dots are fully occupied. The hole energies are plotted relative to the conduction band minimum (E_g=1eV). It should be noted that the hole energies are about a tenth of the magnitude of the electron energies.

6.2.3 Evolution of the Electron and Hole Distributions

The following figures show how the electron and hole distributions for the non-neutral dots evolve with increasing quasi-Fermi level separation. Figure 6.2 is plot of the electron and hole distributions for an electron quasi-Fermi level of 0.1eV and a corresponding hole quasi-Fermi level of -0.979eV, measured from the conduction band minimum. The hole quasi-Fermi level is defined by setting charge neutrality over the dots *and* the wetting layer. The fully occupied ground state for the electrons is shown for comparison (solid red line).

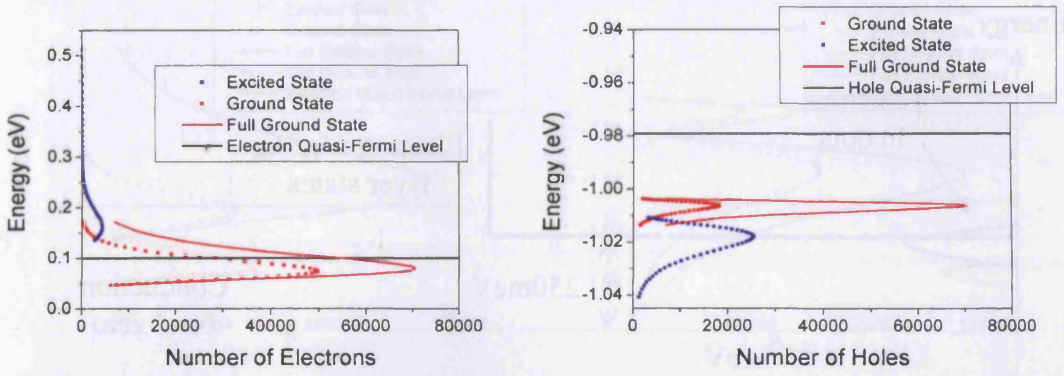

Figure 6.2 - Electron and hole distributions for the non-neutral dots. The electron and hole quasi-Fermi levels are 0.1eV and -0.979eV respectively, measured from the conduction band minimum. The fully occupied ground state for the electrons is shown for comparison (solid red line).

It can be seen that for these values of electron and hole quasi-Fermi levels, the ground state is relatively full with electrons, but there are not many electrons in the excited state. This is because the electron quasi-Fermi level is not high enough to begin significantly populating the excited state with electrons. Considering the holes, the number of holes in the ground state is less than half the number of electrons, but there are more than twice as many holes in the excited state compared with electrons. This is due to the ground and excited state hole energy levels being more closely spaced than those of the electrons. In total, there are far more electrons than holes in the dots. To explain this a schematic of the energies of the dots and the wetting layer is shown in the following figure.

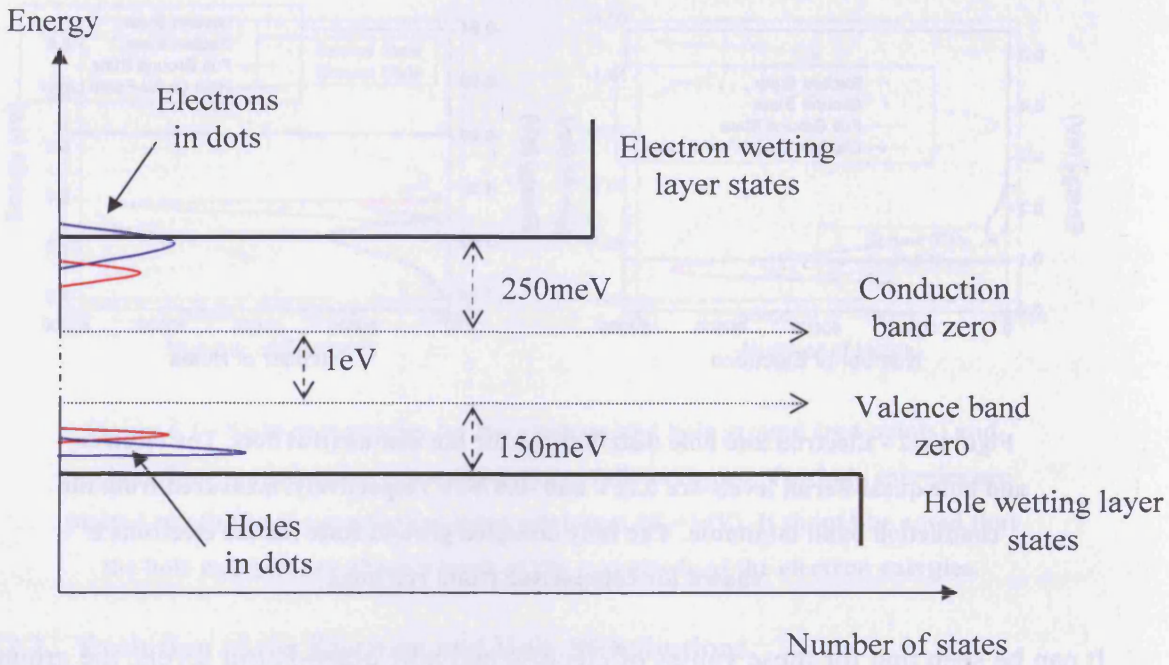

Figure 6.3 - Schematic of energies for the dots and the wetting layer.

Charge neutrality is defined over the whole system, comprising of the dots *and* the wetting layer. The value of electron quasi-Fermi level of 0.1eV is too far away from the wetting layer for high electron population there. However, the difference in energy between the quasi-Fermi level and the wetting layer energy is much smaller for the holes than for the electrons and so for the corresponding hole quasi-Fermi level of -0.979eV there is significant hole population of the wetting layer. There are 29405 electrons and 165302 holes in the wetting layer, and since overall the total number of electrons equals the total number of holes, this means that there are more electrons than holes in the dots.

Figure 6.4 shows the electron and hole distributions for the non-neutral case, for electron and corresponding hole quasi-Fermi levels of 0.2eV and -1.024eV respectively, measured from the conduction band minimum. The fully occupied ground and excited states are shown for comparison (solid lines).

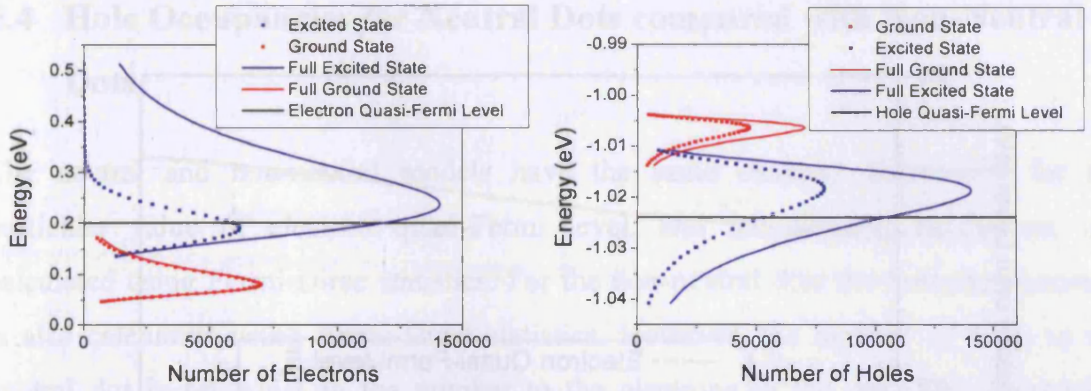

Figure 6.4 - Electron and hole distributions for the non-neutral dots. The electron and hole quasi-Fermi levels are 0.2eV and -1.024eV respectively, measured from the conduction band minimum. The fully occupied ground and excited states are shown for comparison (solid lines).

For these values of electron and hole quasi-Fermi levels, the ground state is more or less completely filled with electrons. However, only the lower energy excited states are full with electrons; the higher energy excited states have very few electrons as the value of E_{fc} is too low to populate these. There are more electrons in the ground state than there are holes. However, in the excited state there are more *holes* than electrons. Again this is because the hole energy levels are more closely spaced than those of the electrons. The value of the electron quasi-Fermi level is now high enough that the number of electrons in the wetting layer is greater than the number of holes. The number of electrons and holes in the wetting are, respectively, 1311670 and 950954. Because charge neutrality is defined over the whole system, this means that there are more holes than electrons in the dots.

As the quasi-Fermi level separation is increased further, all the ground and excited states become full, and the numbers of electrons and holes in each state become equal.

6.3 Variation of the Quasi-Fermi Levels with the Quasi-Fermi Level Separation for Non-Neutral Dots

In this section the variation of the electron and hole quasi-Fermi levels as a function of the quasi-Fermi level separation ΔE_f is studied for the non-neutral dots. Figure 6.5 is a plot of the electron (red curve) and hole (blue curve) quasi-Fermi levels as a function of the quasi-Fermi level separation for the non-neutral dots. The quasi-Fermi levels are measured with respect to the conduction band minimum (E_g=1eV).

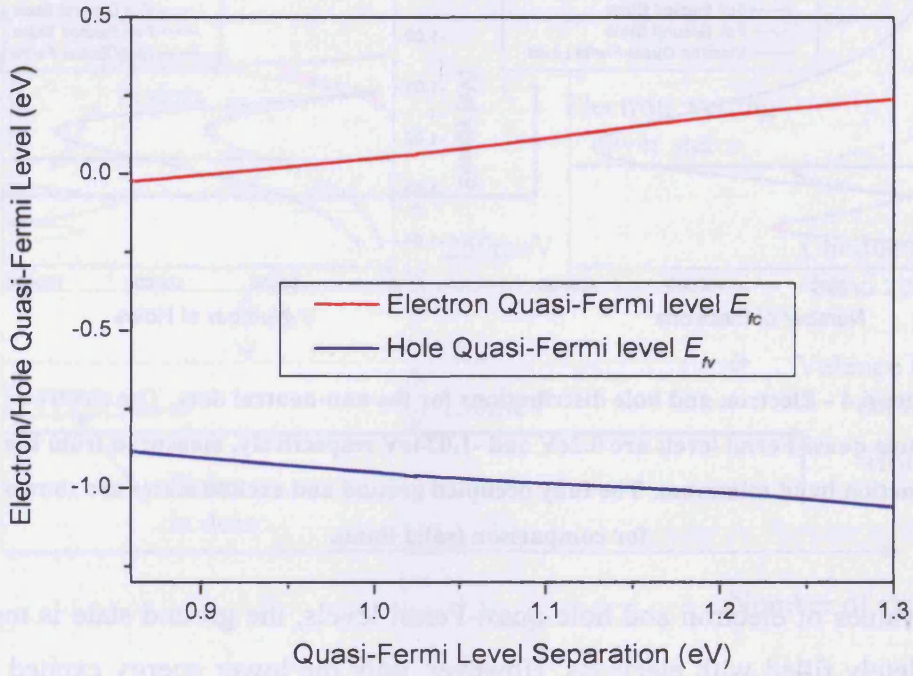

Figure 6.5 - Variation of the electron (red curve) and hole (blue curve) quasi-Fermi levels with the quasi-Fermi level separation for the non-neutral dots. The quasi-Fermi levels are measured with respect to the conduction band minimum (E_g=1eV).

It can be seen that the electron quasi-Fermi level E_{fc} shows more variation with the quasi-Fermi level separation ΔE_f than the hole quasi-Fermi level E_{fv}. The quasi-Fermi level separation is given by

$$\Delta E_f = E_{fc} + E_{fv} + E_g$$

equation 6.1

where E_g is the bandgap of the dot material. The hole quasi-Fermi level is defined for a particular electron quasi-Fermi level by setting charge neutrality over all the dots *and* the wetting layer. Because the hole levels for the dots and the wetting layer are more closely spaced than those of the electrons this means that E_{fv} does not need to increase by the same amount as E_{fc} to achieve charge neutrality.

6.4 Hole Occupancies for Neutral Dots compared with Non-Neutral Dots

The neutral and non-neutral models have the same electron distribution for a particular value of electron quasi-Fermi level, and the electron distribution is calculated using Fermi-Dirac statistics. For the non-neutral dots the hole distribution is also calculated using Fermi-Dirac statistics. However, the number of holes in a neutral dot is set equal to the number to the electrons in the dot. This approach effectively assumes that the electrons and holes have the same energy levels [2, 3]. In this section is a study of how the evolution of the hole distribution with increasing electron quasi-Fermi level differs for neutral and non-neutral dots. In each figure the hole distributions are plotted for the same value of electron quasi-Fermi level. The hole quasi-Fermi level shown is for the non-neutral case (the holes in the neutral model do not follow a Fermi-Dirac distribution). Figure 6.6 is a plot of the hole distribution for the neutral and non-neutral models, for an electron quasi-Fermi level of 0.1eV.

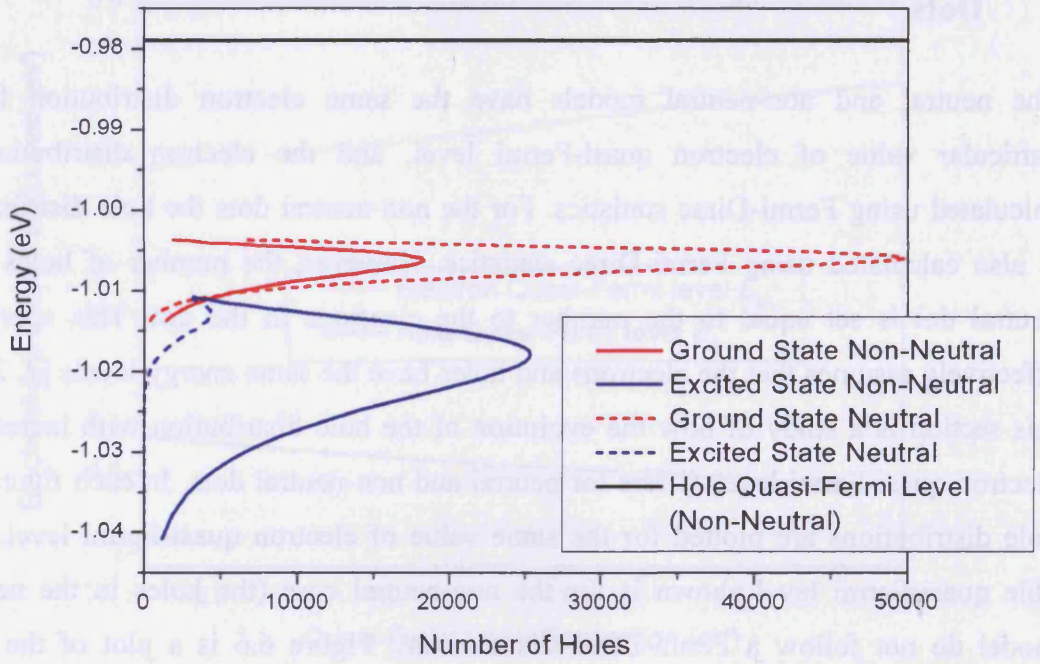

Figure 6.6 - Hole distributions for the neutral dots (dashed lines) and non-neutral dots (solid lines), plotted for the same value of electron quasi-Fermi level, 0.1eV. The hole quasi-Fermi level shown is for the non-neutral case and has a value of -0.979eV, measured from the conduction band minimum.

It can be seen that for the ground state, the neutral dots are occupied by many *more* holes than the non-neutral dots. This is because in the neutral model, for every electron in a dot, there is also a hole present in the same dot; the value of the hole quasi-Fermi level is too small to populate the non-neutral dots with as many holes. However, for the excited state there are more holes in the *non-neutral* dots than the neutral. This is because the hole energy levels are more closely spaced than those for the electrons, and so for the non-neutral dots the hole excited state begins to get occupied for relatively small values of the hole quasi-Fermi level. Because the excited state can accommodate twice as many electrons as the ground state, the excited state population of the non-neutral dots thus begins to increase quickly, and this results in more valence holes than conduction electrons in the excited state.

The following plot shows the hole distributions for the neutral and non-neutral models, for an electron quasi-Fermi level of 0.2eV.

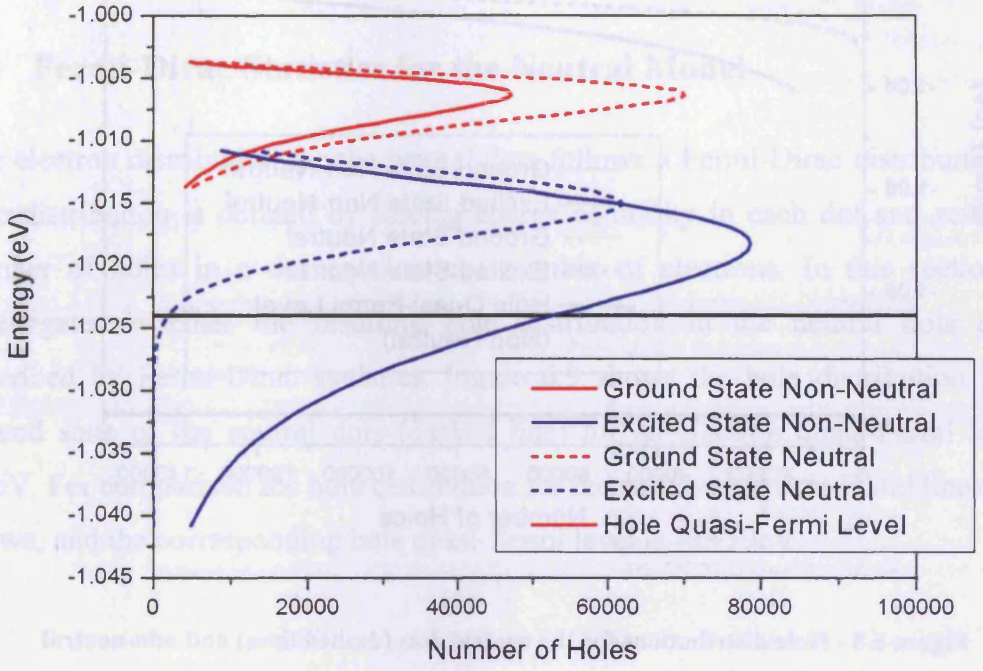

Figure 6.7 - Hole distributions for the neutral dots (dashed lines) and non-neutral dots (solid lines), plotted for the same value of electron quasi-Fermi level, 0.2eV. The hole quasi-Fermi level shown is for the non-neutral case and has a value of -1.024eV, measured from the conduction band minimum.

The situation here is similar to that in Figure 6.6. Again, there are more holes in the ground state of the neutral dots than the non-neutral dots. At lower excited state energies there are more holes in the neutral dots, but at higher excited state energies there are more holes in the *non-neutral* dots. This is because of the difference in the spacing of the energy levels for the holes compared with the electrons. At higher energies the number of electrons (and therefore the number of holes) in the neutral dots is low since the electron quasi-Fermi level is too small for higher population. Because the hole energy levels are more closely spaced, these higher energy states in the non-neutral dots get populated. Figure 6.8 shows the situation for an electron quasi-Fermi level of 0.3eV.

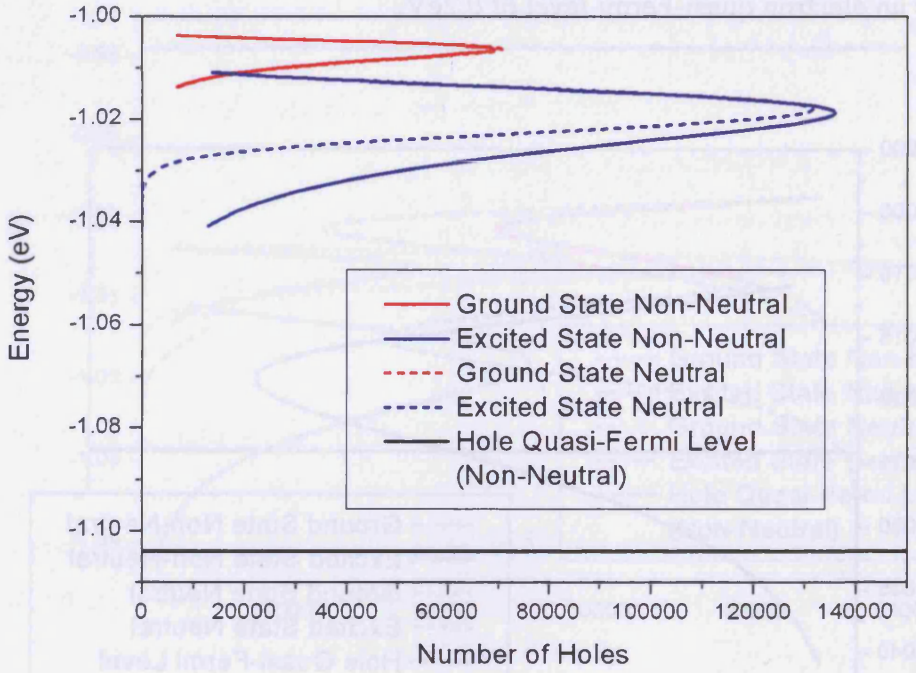

Figure 6.8 - Hole distributions for the neutral dots (dashed lines) and non-neutral dots (solid lines), plotted for the same value of electron quasi-Fermi level, 0.3eV. The hole quasi-Fermi level shown is for the non-neutral case and has a value of -1.104eV, measured from the conduction band minimum.

For this value of electron quasi-Fermi level, the ground states are more or less fully occupied and the lower energy excited states are almost full. The only differences that can be seen between the two models here is the elevated occupancy of the higher energy excited states for the non-neutral model compared with the neutral model.

As the electron quasi-Fermi level is increased further, all the states become occupied and there are no differences in the electron and hole distributions for the neutral and non-neutral dots.

6.4.1 Summary of the Differences in Neutral and Non-Neutral Hole Occupancies

In this section the evolution of the electron and hole populations with increasing electron quasi-Fermi level has been studied, for both the neutral and non-neutral dots. For the ground state, the *neutral* model shows higher occupancies of holes than the non-neutral model. The excited state is more complicated: generally, at lower energy

excited states there are more electrons for the *neutral* model but at higher excited states energies the *non-neutral* model has higher hole occupancies. These differences are due to the differences in energy between the states of the dots and the wetting layer for the electrons and holes, which is not taken into account in the neutral model

6.5 Fermi-Dirac Statistics for the Neutral Model

The electron distribution for the neutral dots follows a Fermi-Dirac distribution. The hole distribution is defined by forcing charge neutrality in each dot and setting the number of holes in a dot equal to the number of electrons. In this section it is investigated whether the resulting hole distribution in the neutral dots can be described by Fermi-Dirac statistics. Figure 6.9 shows the hole distribution for the ground state of the neutral dots (dashed line) for an electron quasi-Fermi level of 0.1eV. For comparison the hole distribution for the non-neutral dots (solid line) is also shown, and the corresponding hole quasi-Fermi level is -0.979eV.

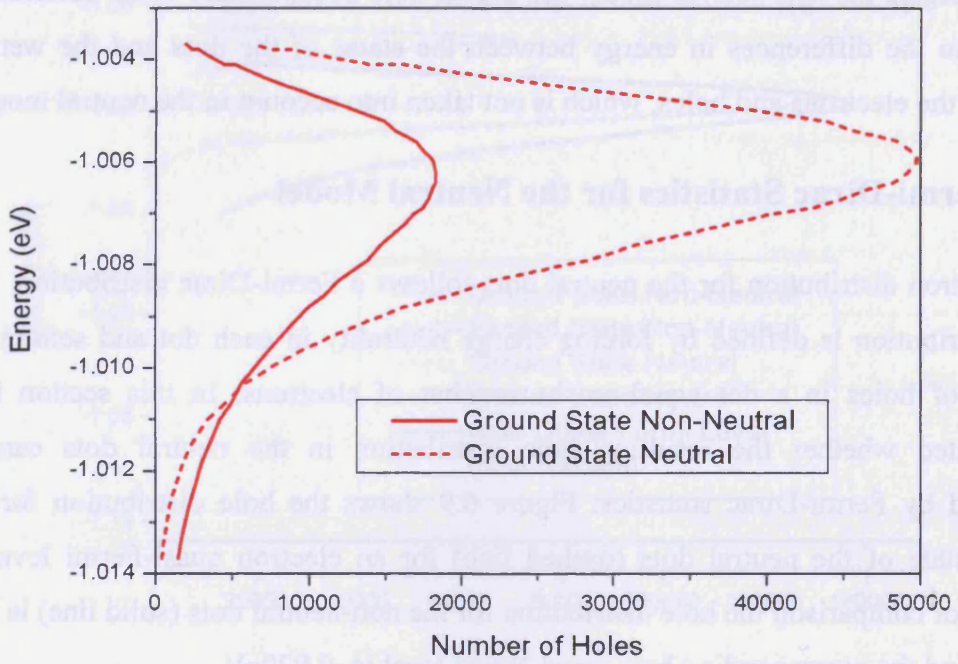

Figure 6.9 - Ground state hole distributions for neutral dots (dashed line) and non-neutral dots (solid line), plotted for E_{fc}=0.1eV.

The hole distribution for the non-neutral dots does follow a Fermi-Dirac distribution. It can be seen that to match this Fermi-Dirac distribution to the number of holes for the neutral dots, a higher value of hole quasi-Fermi level is needed. The following plot shows the fit obtained for a hole quasi-Fermi level of -1.029eV, measured from the conduction band zero.

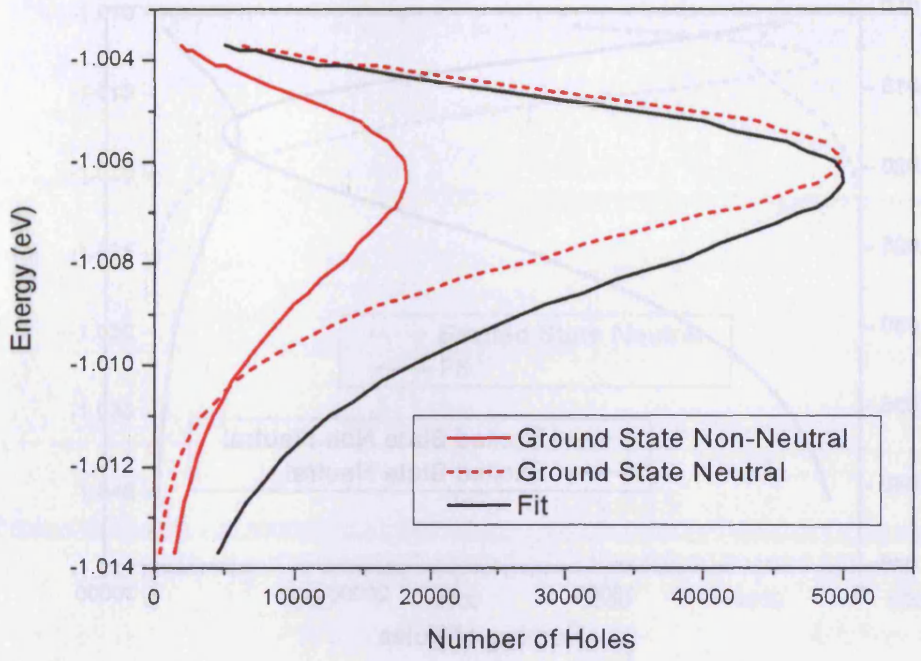

Figure 6.10 - Ground state hole distributions for neutral dots (dashed line) and non-neutral dots (solid line) for E_{fc}=0.1eV. A Fermi-Dirac distribution is plotted for E_{fv}= -1.029eV and T=300K.

It can be seen that although the values of the peaks now match, the energies at which the peaks occur are not the same. The Fermi-Dirac distribution is also a different shape to the distribution of holes in the neutral dots. The only other parameter which can be fitted is the temperature and altering the temperature does not give a match to the distribution.

Now considering the excited state, the following figure shows the excited state hole occupancy for both neutral dots (dashed line) and non-neutral dots (solid line), again plotted for an electron quasi-Fermi level of 0.1eV.

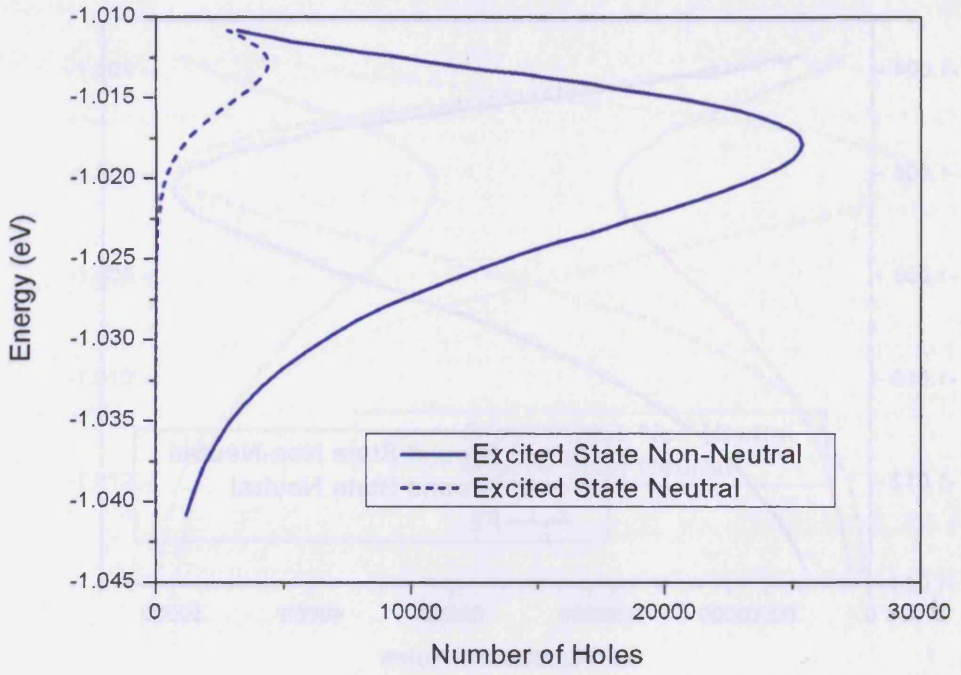

Figure 6.11 - Excited state hole distributions for neutral dots (dashed line) and non-neutral dots (solid line), plotted for E_{fc}=0.1eV.

It can be seen that to match a Fermi-Dirac distribution to the holes for the neutral dots, the energy at which the peak of the distribution occurs needs to be lowered. This is done by reducing the value of the hole quasi-Fermi level, and the distribution is shown in the following figure for E_{fv}= -0.875eV.

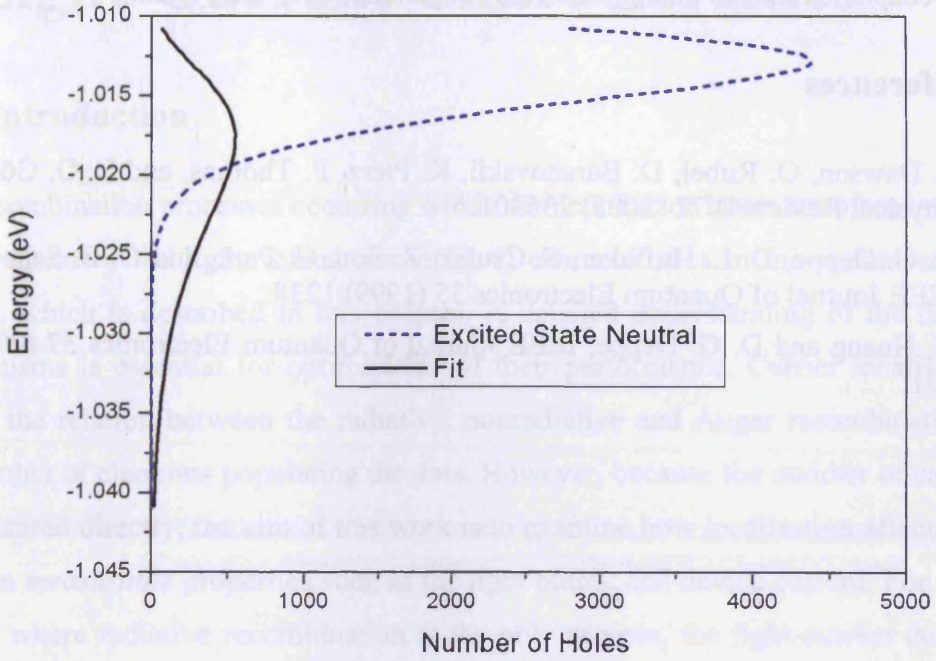

Figure 6.12 - Excited state hole distribution for neutral dots (dashed line) and non-neutral dots (solid line) for E_{fc}=0.1eV. A Fermi-Dirac distribution is plotted for E_{fv}= -0.875eV and T=300K.

Reducing the hole quasi-Fermi level does not give a match for the energies at which the peaks occur. Also, the number of holes at each energy is now too low to match the distribution, and the shape is very different to a Fermi-Dirac distribution. Therefore, in conclusion, the hole distributions for the neutral dots cannot be described by Fermi-Dirac statistics, and so it is not appropriate to define a hole quasi-Fermi level for the neutral dots.

6.6 Summary

In this chapter I have studied how the electron and hole populations evolve as the electron quasi-Fermi level is increased. I have compared the hole distributions for the neutral and non-neutral dots, and there are significant differences between the hole distributions for the two cases. These differences are due to the energy level separation of the holes being smaller than those for the electrons, which is not taken into account in the hole distribution for the neutral dots. From investigation of the hole distributions for the neutral dots I conclude that they do not follow Fermi-Dirac

statistics and therefore a hole quasi-Fermi level cannot be defined for the neutral dots.

The next chapter described the light-current characteristics of the system.

6.7 References

[1] P. Dawson, O. Rubel, D. Baranovskii, K. Pierz, P. Thomas, and E. O. Göbel, Physical Review B 72 (2005) 235301.

[2] D. G. Deppe, D. L. Huffaker, S. Csutak, Z. Zou, G. Park, and O. B. Schekin, IEEE Journal of Quantum Electronics 35 (1999) 1238.

[3] H. Huang and D. G. Deppe, IEEE Journal of Quantum Electronics 37 (2001) 691.

7 Light-Current Characteristics

7.1 Introduction

The recombination processes occurring within semiconductor lasers are often investigated by measurement of the light versus current (L-I) characteristics in the spontaneous emission regime, which is described in this chapter. A detailed understanding of the recombination mechanisms is essential for optimisation of their performance. Carrier localisation in dots affects the relation between the radiative, nonradiative and Auger recombination rates and the number of electrons populating the dots. However, because the number of carriers cannot be measured directly, the aim of this work is to examine how localisation affects the relation between *measurable* properties such as the light output and device current. For example in a system where radiative recombination is the only process, the light-current curve is linear, irrespective of the relation between the radiative recombination rate and the number of carriers in the system: the radiative rate *is* the current. One of the aims of the thesis is to determine whether radiative, nonradiative via defects and Auger recombination rates can be characterised by simple, distinctive functions of the number of carriers in the system, enabling these processes to be distinguished by their combined influence on the shape of the light-current curve. This is described in more detail in the next section.

7.2 Power Law Relations

Experimentally the recombination processes are often investigated by measurement of light versus current characteristics by consideration of the functional form of the data using assumed power law dependences on carrier number for the various recombination processes. In systems with extended electronic states carriers are free to move along the quantum wire or quantum well, or throughout the bulk crystal, and this assists the carrier systems in achieving an internal equilibrium throughout the crystal. The extended states produce a continuum in energy which is represented by a density of states function and treatments of recombination are based on the assumption that any electron in an extended state may recombine with any hole in an extended state, subject to the appropriate k-selection rules. If Boltzmann statistics are used to describe the electron and hole distributions, this leads to the

result that the radiative recombination rate is proportional to the product of the electron and hole densities, N and P respectively, in each sub-band:

$$R_{rad} = BNP$$

equation 7.1

B is the radiative recombination coefficient [1]. When the system is electrically neutral N=P and the radiative rate is written as:

$$R_{rad} = BN^2$$

equation 7.2

This bimolecular characteristic is widely used in the analysis of light emission from lasers and LEDs in extended state systems [2-4] and in the modelling of devices. It is assumed that the rates of nonradiative recombination via defects and Auger recombination are proportional to linear and cubic functions of the carrier density respectively:

$$R_{nr} = AN$$

equation 7.3

$$R_{aug} = CN^3$$

equation 7.4

The current is the sum of all the recombination processes multiplied by the electronic charge, and can therefore be written as

$$I = q\left(AN + BN^2 + CN^3\right)$$

equation 7.5

The light-current curve can then be used to distinguish radiative recombination from nonradiative recombination processes in the analysis of light emission from lasers and LEDs. In simple terms, the L-I curve is linear if radiative recombination is dominant, super-linear if nonradiative recombination is dominant, and sub-linear if Auger processes dominate, as shown in Figure 7.1.

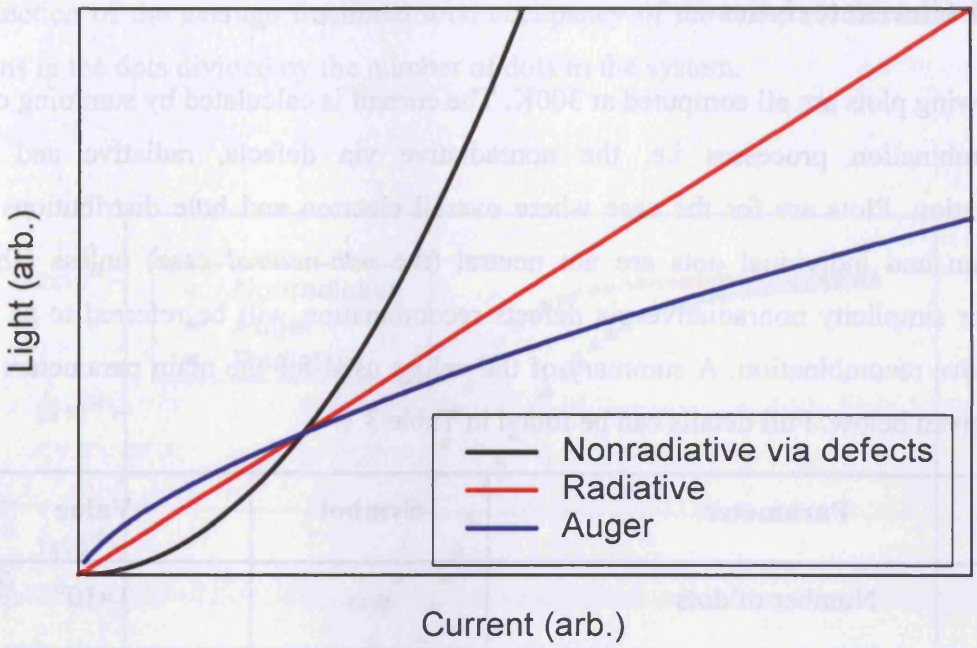

Figure 7.1 - Light-current curve shown for the cases of (i) nonradiative via defects recombination dominant (black line) (ii) radiative recombination dominant (red line) and (iii) Auger recombination dominant (blue line).

The derivation of these functional forms for the recombination mechanisms is possible in quantum well and bulk structures because the extended electronic states make it meaningful to talk of a global carrier population. In a quantum dot system it is still possible to talk of the total number of electrons populating the dot states, but the behaviour of the recombination processes on this number may be modified by localisation of all the recombination processes. In the absence of quantum mechanical coupling, the electronic states of a quantum dot are localised in all three directions; consequently, it is only possible for electrons and holes which are located within the same dot to recombine with each other. The maximum number of available electrons and holes within a single ground state is then equal to the spin degeneracy and this considerably reduces the radiative recombination rate relative to the quantum well or bulk case. Whether simple relationships can be found in quantum dot systems is not obvious from immediate inspection and depends on the individual contributions of the many dots which make up the whole ensemble. L-I curves measured on quantum dot LEDs show sub-linear and super-linear behaviours but, since the number of electrons cannot be measured directly, it is not known whether the power law components of such data are indicative of specific recombination processes.

7.3 L-I Characteristics

The following plots are all computed at 300K. The current is calculated by summing over all the recombination processes i.e. the nonradiative via defects, radiative and Auger recombination. Plots are for the case where overall electron and hole distributions are in equilibrium and individual dots are not neutral (the *non-neutral* case) unless otherwise stated. For simplicity nonradiative via defects recombination will be referred to as simply *nonradiative* recombination. A summary of the values used for the main parameters in this thesis is given below. Full details can be found in Table 3.1.

Parameter	Symbol	Value
Number of dots	n_{QD}	1×10^{6}
Bandgap of dot material	E_g	1eV
Bandgap of wetting layer	$E_{g,wl}$	1.4eV
Dot radiative lifetime	τ_{sp}	1ns
Dot nonradiative lifetime	τ_{nr}	300ps
Dot Auger lifetime	τ_{aug}	300ps
Wetting layer recombination coefficient	B_{wl}	3.5×10^{-7} $s^{-1}m^{2}$
Wetting layer nonradiative lifetime	τ_{nrwl}	300ps
Wetting layer electron confined energy (relative to the conduction band edge)	E_{wlc}	250meV
Wetting layer hole confined energy (relative to the valence band edge)	E_{wlv}	150meV

The simplest situation is the behaviour of the ground state and Figure 7.2 is a plot of the radiative, nonradiative and Auger recombination rates between the ground states of the dots

as a function of the average fractional total occupancy of the dots, i.e. the total number of electrons in the dots divided by the number of dots in the system.

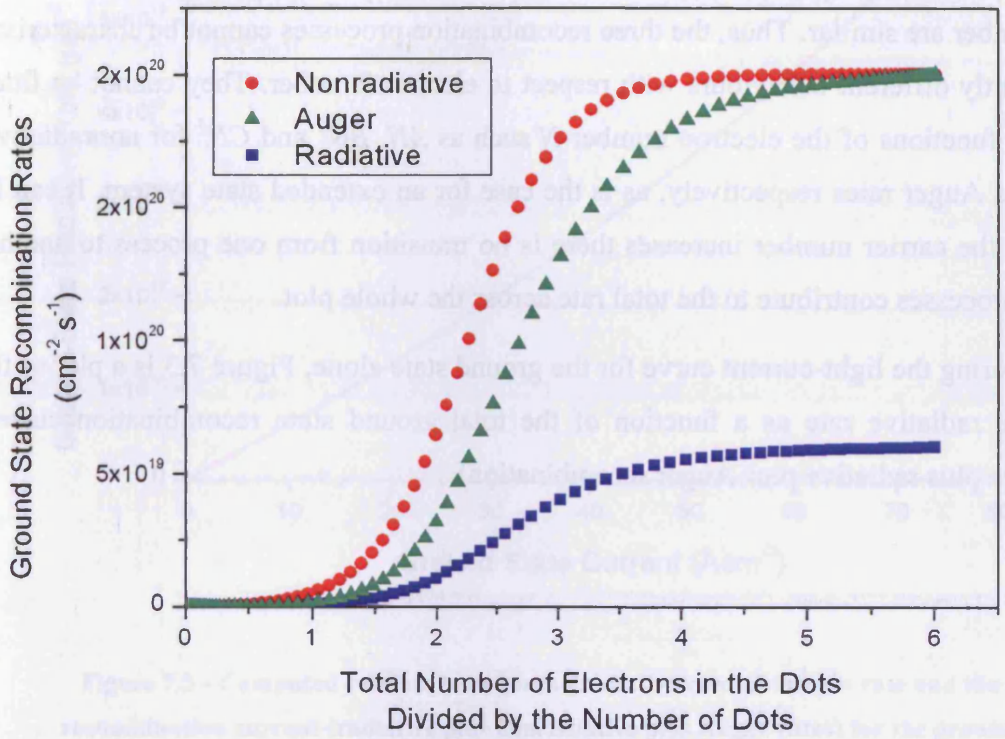

Figure 7.2 - Computed dependences of the ground state radiative, nonradiative and Auger recombination rates on the total number of electrons in the dots expressed as a fractional population relative to the number of dots, for the non-neutral dots.

The relative magnitudes of the radiative, nonradiative and Auger recombination rates are fixed by the choice of lifetimes and the detailed form of their dependences on the number of electrons is determined by the probabilities which control the numbers of dots with the appropriate occupations.

When all the dots are full it can be seen that the nonradiative and Auger rates are equal since their lifetimes are equal. For a fixed electron number the nonradiative rate is higher than the Auger rate. This is because whilst the nonradiative rate is dependent on the number of electrons in a dot (provided there is also a hole in the same dot), the Auger rate is dependent on the number of holes; for fixed values of electron and hole quasi-Fermi levels, on average there will be more electrons than holes in a dot. Also, for Auger recombination to occur in

the ground state, the state needs to contain two electrons (i.e. a full ground state) and this limits the Auger rate at low carrier numbers.

It can be seen that none of the rates can be written as a simple function of the number of electrons. Furthermore, the dependences of the radiative, nonradiative and Auger rates on electron number are similar. Thus, the three recombination processes cannot be characterised by significantly different behaviours with respect to electron number. They cannot be fitted with simple functions of the electron number N such as AN, BN^2 and CN^3 for nonradiative, radiative and Auger rates respectively, as is the case for an extended state system. It can be seen that as the carrier number increases there is no transition from one process to another and all the processes contribute to the total rate across the whole plot.

Now considering the light-current curve for the ground state alone, Figure 7.3 is a plot of the ground state radiative rate as a function of the total ground state recombination current (nonradiative plus radiative plus Auger recombination).

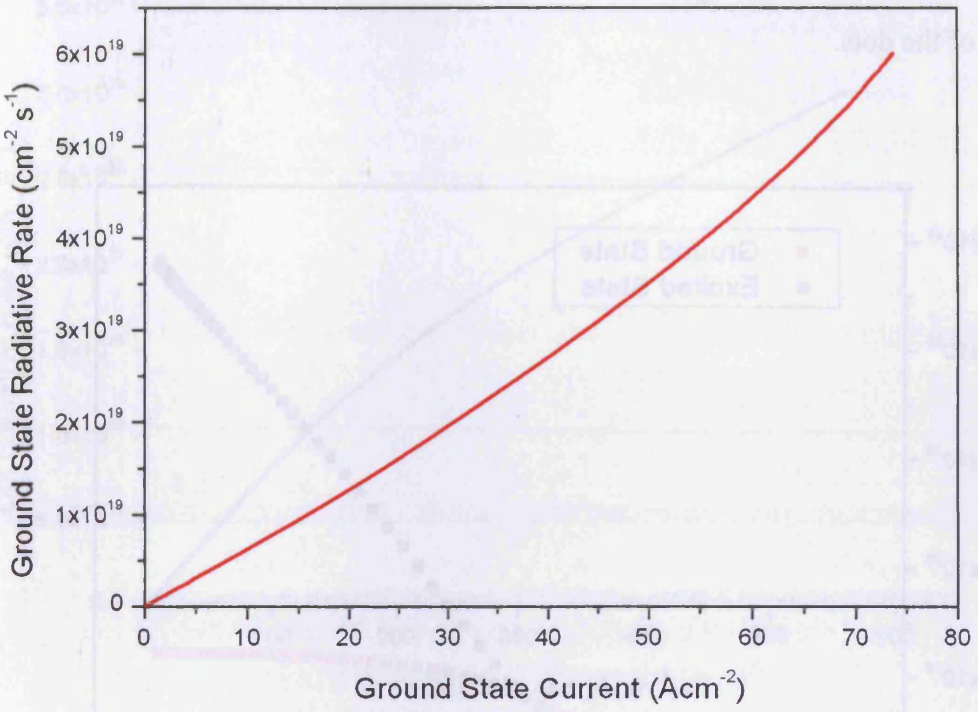

Figure 7.3 - Computed relation between the radiative recombination rate and the total recombination current (radiative plus nonradiative plus Auger rates) for the ground state alone, for the non-neutral dots.

At high injection the radiative process becomes super-linear with respect to the total rate because some of the dots have an occupancy of two for electrons and holes which enhances the radiative rate thus increasing the light output. The effect is less marked on the current due to the predominance of nonradiative processes. Figure 7.2 shows that the curvature of the light-current curve in Figure 7.3 arises from the inherent dependence of the radiative, the nonradiative *and* the Auger rates on the number of electrons. It is not a transition from nonradiative to radiative to Auger processes as the carrier number increases, as expected for an extended state system. All three processes contribute to the total rate across the whole plot and their variations with electron number are not sufficiently distinctive for them to be separated in a simple analysis of experimental measurements as represented by the data in Figure 7.2. So even for a simple ground state system, the L-I characteristics in Figure 7.3 cannot be fitted with terms of the form light = BN^2 and total recombination rate = ($AN + BN^2 + CN^3$) as is the case for a simple extended state system.

Now including the excited state contribution, Figure 7.4 shows the computed radiative recombination rates between ground and excited states as functions of the fractional occupancy of the dots.

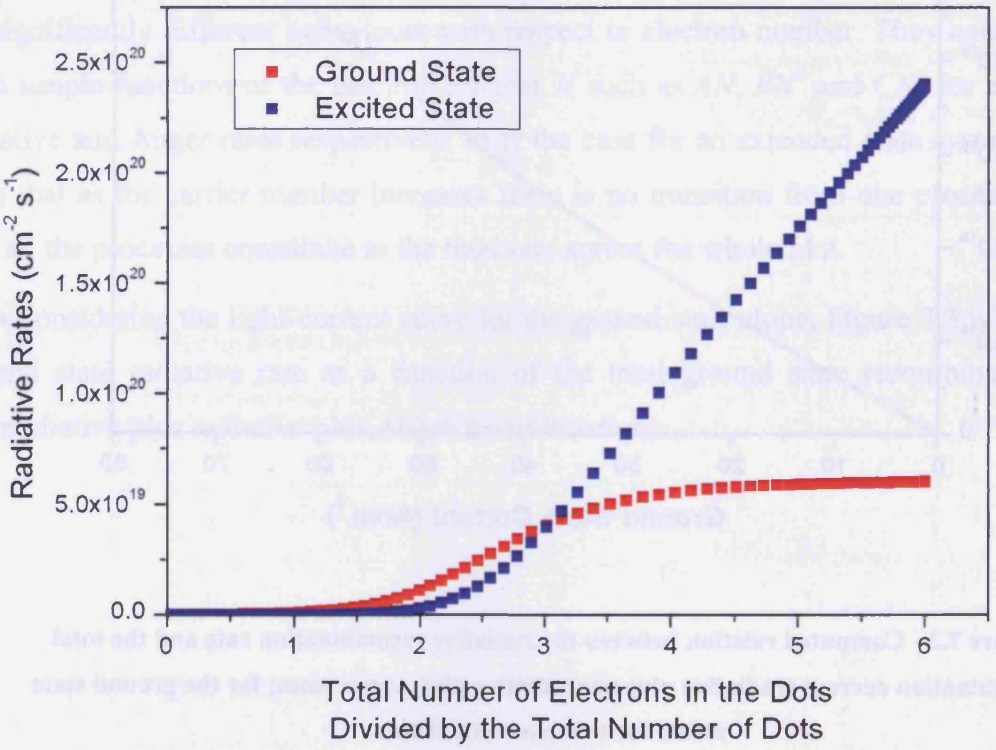

Figure 7.4 - Computed radiative recombination rates for the ground and excited states as functions of the electron number for the non-neutral dots.

At low electron number the ground state radiative rate is higher than that of the excited state. This is because initially the ground state fills up with electrons at a faster rate then the excited state. As the total number of electrons increases there are multiple numbers of electrons in the excited state of some dots; this enhances the excited state rate considerably. When the dots are full the excited state rate is four times that of the ground state rate since the excited state can accommodate twice as many electrons. Figure 7.5 shows the light-current curve for the complete dot system.

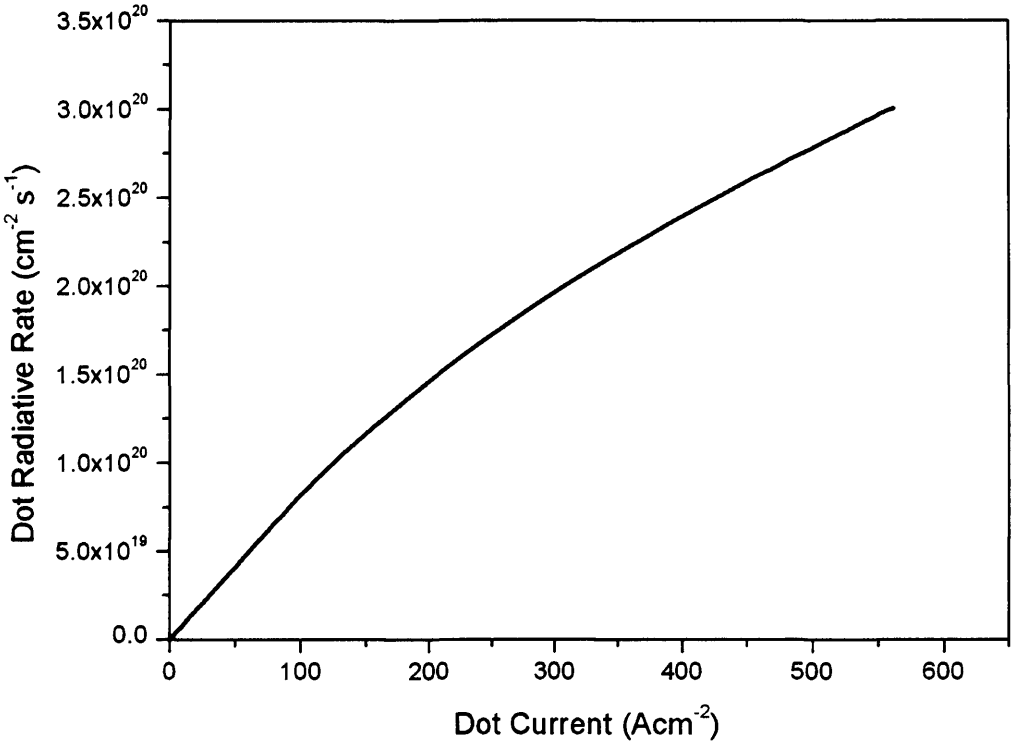

Figure 7.5 - Computed relation between the radiative recombination rate and the total recombination current (radiative plus nonradiative plus Auger rates) for the dots (ground plus excited state) for the non-neutral case.

Again it can be seen that there is no distinct transition from one process to another and the L-I curve offers little information about the processes occurring in the dots.

If the band edges in the wetting layer are made sufficiently large such that the wetting layer is not highly populated the following L-I curve is produced, Figure 7.6. The wetting layer does not contribute to the current and the combined dot emission is very similar to the L-I curve shown above in Figure 7.5. It can be seen that the light emission from the dots saturates as the dot states become full.

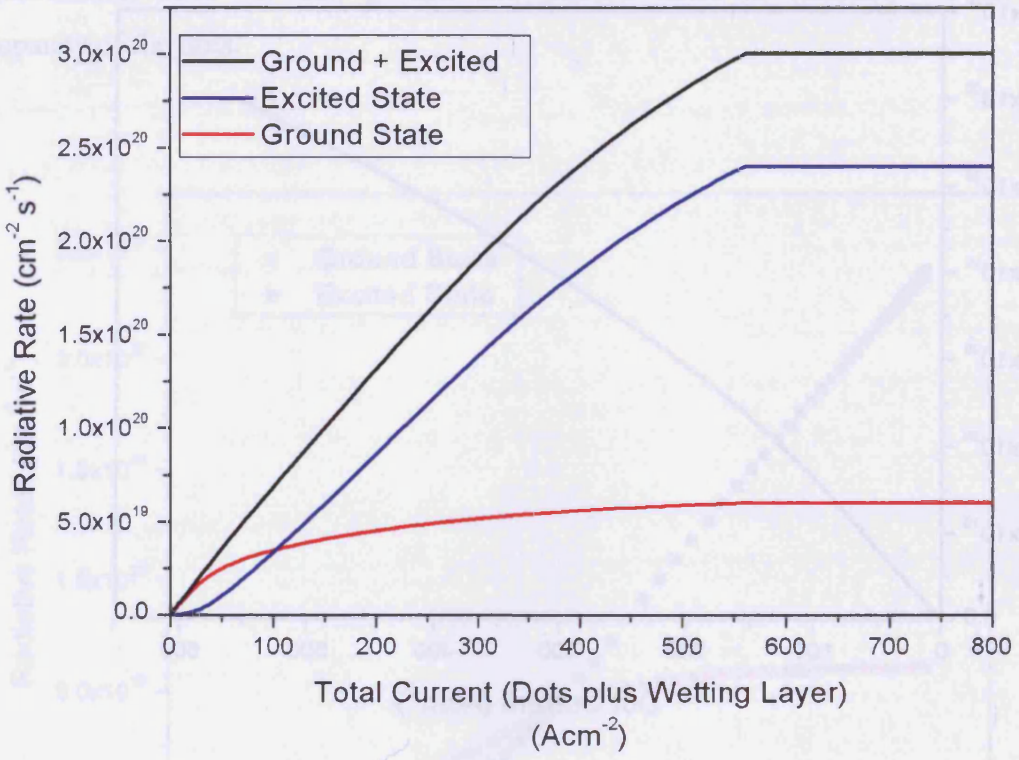

Figure 7.6 - Computed dependences of the radiative recombination rates on the total current, for the non-neutral case, where the wetting layer bandgap is made sufficiently large that the wetting layer does not contribute to the current.

The wetting layer, however, is an unavoidable consequence of the growth process for the dots and as so must be included in all calculations. Figure 7.7 shows the radiative rates for the ground and excited states of the dots and the wetting layer as a function of the average number of electrons in the dots.

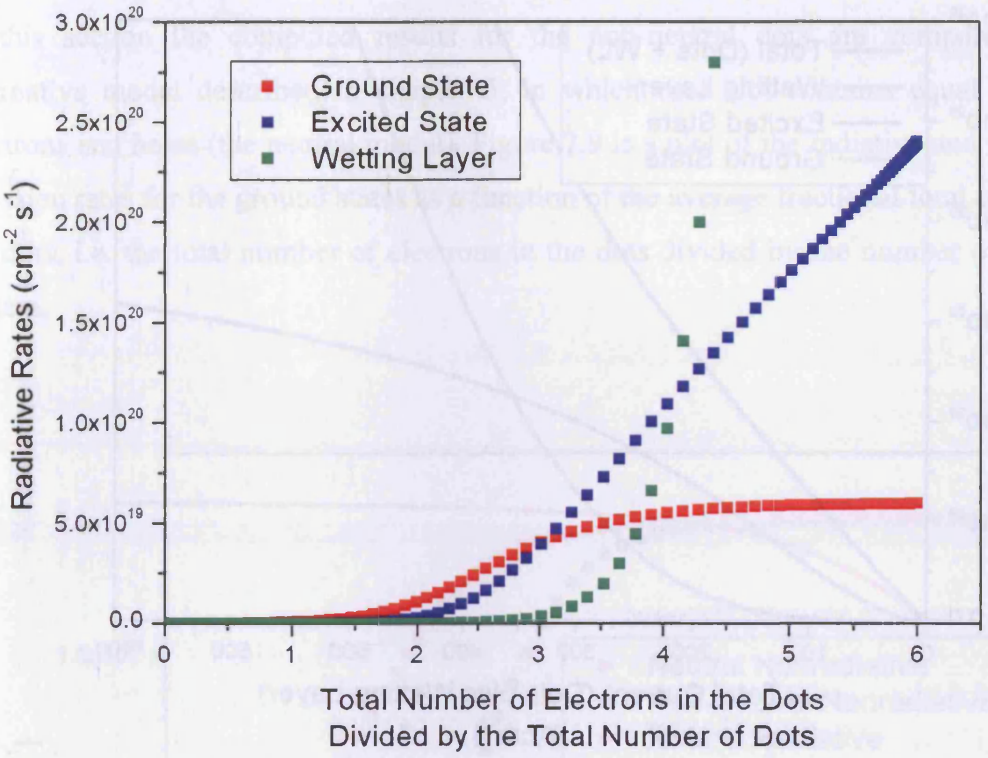

Figure 7.7 - Computed radiative recombination rates for the ground and excited states of the dots and the wetting layer as functions of the electron number, for the non-neutral dots.

It can be seen that at low electron number the wetting layer radiative rate is low compared to those of the dots. However, as the quasi-Fermi level separation is increased and the number of electrons (and holes) in the system increases, the wetting layer contribution starts to dominate. Figure 7.8 shows the computed L-I behaviour of the complete system, including the wetting layer.

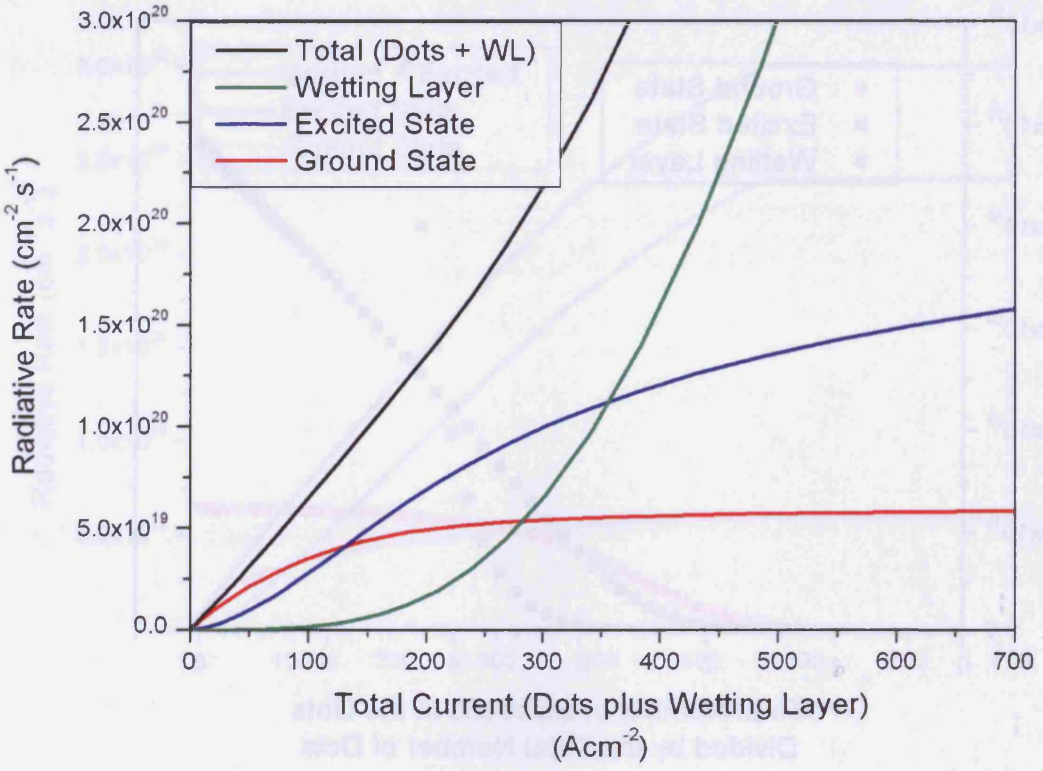

Figure 7.8 - Computed dependences of the radiative recombination rates on the total current, for the non-neutral dots, where the wetting layer is included.

The wetting layer emission dominates the total light output because the emission from the dots saturates at high current and such a plot cannot provide information about the recombination processes in the dots. The plot saturates at high current due to the rapid increase in the wetting layer current. In an experiment it is possible to resolve spectrally the light from the dots from that of the wetting layer, to produce a plot of dot emission versus total current, but there is no means of eliminating the contribution of the wetting layer to the current (other than by cooling the sample). In extended state systems a sub-linear dependence of light on current is often characteristic of Auger recombination which is proportional to N^3. In this case it arises from the combination of saturation of the emission from the dots at high occupancy and the contribution of the wetting layer to the current.

7.4 Neutral Dots compared with Non-Neutral Dots

In this section the computed results for the non-neutral dots are compared with the alternative model described in chapter 5, in which each dot contains equal numbers of electrons and holes (the neutral model). Figure 7.9 is a plot of the radiative and nonradiative emission rates for the ground states as a function of the average fractional total occupancy of the dots, i.e. the total number of electrons in the dots divided by the number of dots in the system.

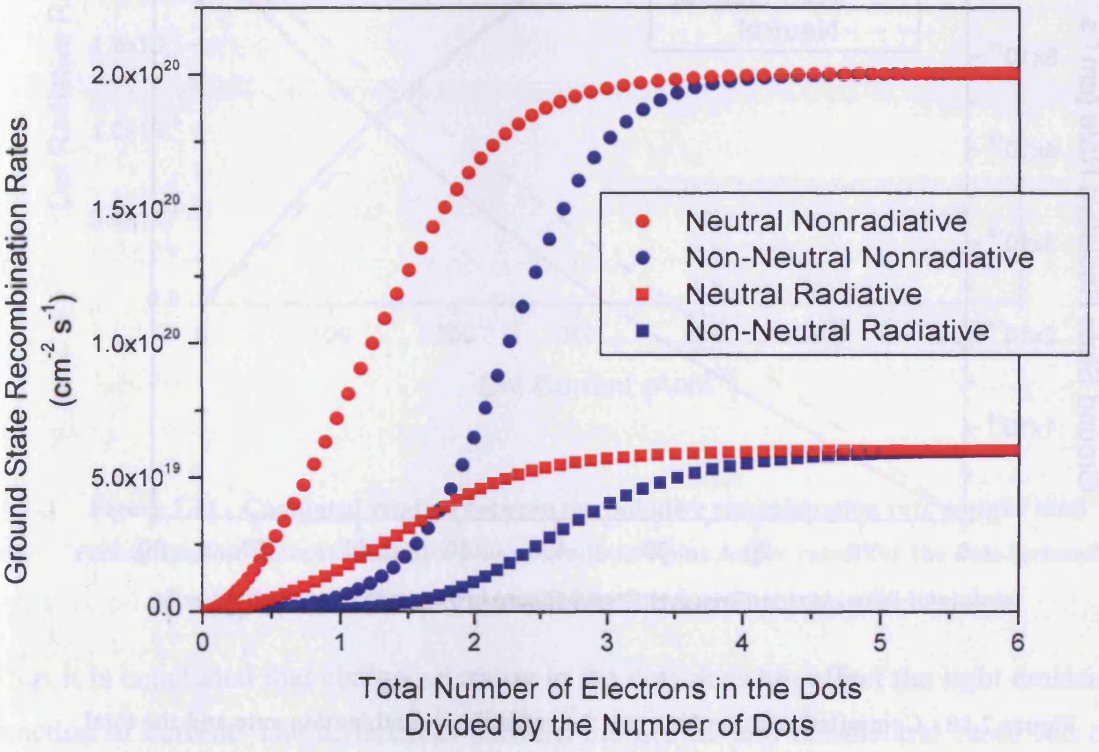

Figure 7.9 - Computed dependences of the ground state radiative and nonradiative recombination rates on the total number of electrons in the dots expressed as a fractional population relative to the number of dots, for neutral and non-neutral dots.

It can be seen that for the same total number of electrons, the neutral dots have higher radiative and nonradiative rates than those of the non-neutral dots. This is because if there is an electron present in a neutral dot there is always a hole present too, to complete the process. For non-neutral dots, a higher value of electron quasi-Fermi level is needed to achieve the same number of holes in the dots as for the neutral case. For both cases, it can be seen that the rates are not simple functions of the number of electrons. Furthermore, for each

scenario the dependence of the radiative and nonradiative rates on electron number is similar (compare blue symbols for the non-neutral dots and red symbols for the neutral dots). Thus, the two recombination processes for the neutral dots can also not be characterised by significantly different behaviours with respect to electron number. So while the dependences of the rates on electron number are very different for the non-neutral and neutral cases, the resulting ground state L-I curves shown below in Figure 7.10 are very similar.

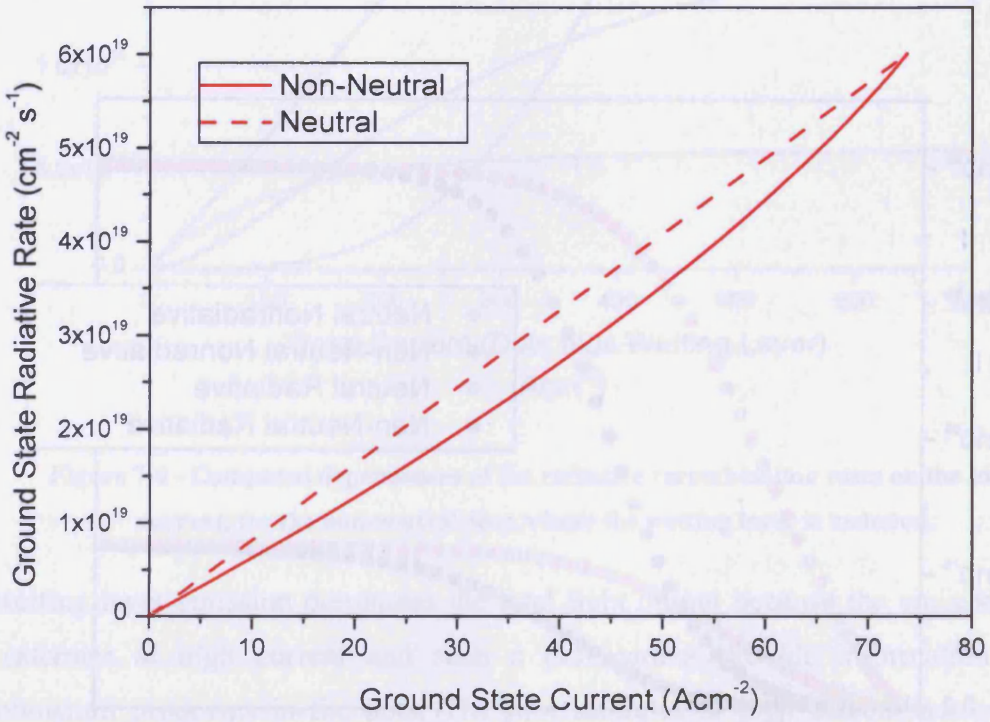

Figure 7.10 - Computed relation between the radiative recombination rate and the total recombination current (radiative plus nonradiative plus Auger rates) for the ground state alone, for neutral (dashed line) and non-neutral (solid line) dots.

The form of the curve is similar for both non-neutral and neutral dot cases. Again, for the same value of current the neutral dots have a higher radiative rate than that of the non-neutral dots because in a neutral dot there is always a hole present for every electron which enhances the rates. The light-current curve for the neutral dots is linear since the radiative process occurs even at low current because there is always a hole for every electron. When the ground and excited state rates are summed to produce an L-I curve for the complete dot system, a similar dependence to that for the ground state alone is found. The neutral and non-neutral L-I curve is shown in the following plot, and it can be seen that the curves show very

little difference for each case. The plots show sub-linear behaviour due to a high Auger recombination rate in the excited states at high current.

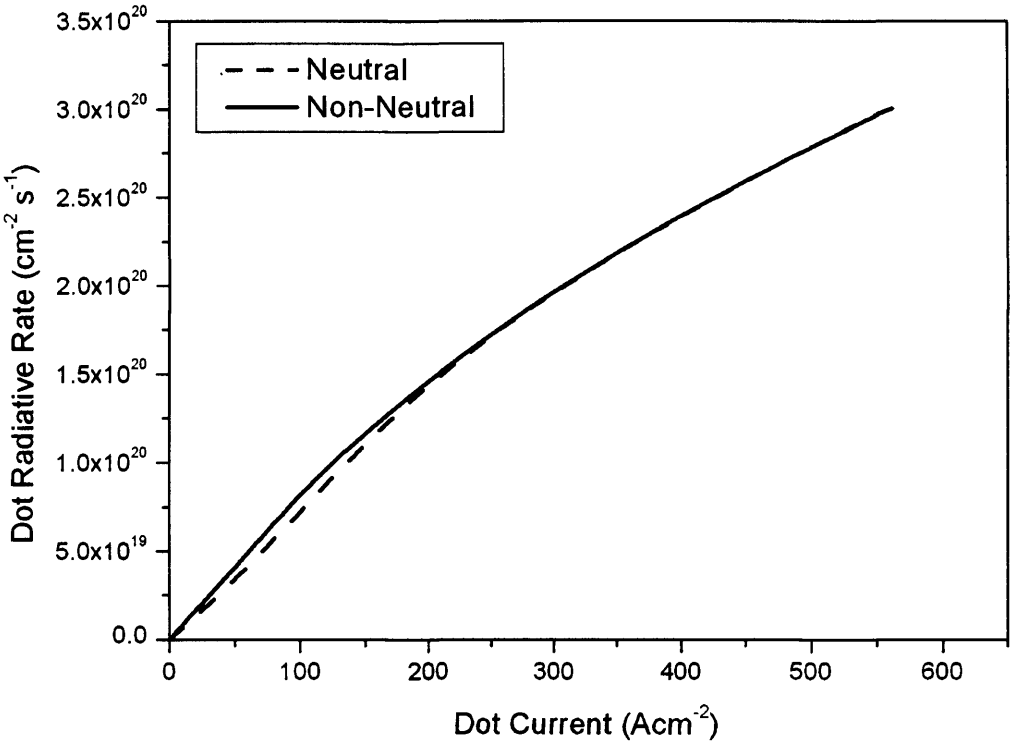

Figure 7.11 - Computed relation between the radiative recombination rate and the total recombination current (radiative plus nonradiative plus Auger rates) for the dots (ground plus excited state) for neutral (dashed line) and non-neutral (solid line) dots.

Thus it is concluded that charge neutrality in the dots does not effect the light emission as a function of current. The differences between the neutral and non-neutral cases can only be seen in the recombination rates as a function of the carrier number, and these cannot be measured experimentally.

7.5 Comparison with Experimental Results

7.5.1 Introduction

To validate the results from the model, the computed L-I curves are compared with experimental data measured by I. Sandall at Cardiff University. At the start of this project it was decided to model 1μm emitting dots since this would allow comparison with experimental data from the dot samples available. However, since this time 1.3μm emitting

dots have become available and it is therefore experimental data measured on these dots that the results from the model are compared with. To compensate for this, in this section of the thesis I have modified the input parameters to the model such that the energies of the ground and excited state in the model are comparable with those of the dot sample measured. The two-dimensional wetting layer incorporated in the model is also present in the dot sample measured. The radiative lifetime of the sample was estimated using the measured optical absorption cross section (see chapter 2). A fit to the experimental data was obtained by varying the nonradiative and Auger lifetimes in the dots, the only fitting parameters used.

7.5.2 Experimental Details

Experiments were carried out using a 1.3μm emitting quantum dot sample, which is a laser structure comprising of an $In_{0.15}Ga_{0.85}As/InAs$ dot-in-well (DWELL) structure with 50nm wide GaAs spacer layers between each DWELL. The DWELL structure is incorporated within a $GaAs\text{-}Al_{0.4}Ga_{0.6}As$ waveguide structure. Full details are given in reference [5]. The structure has five layers of dots with an estimated dot density of 4×10^{10} cm^{-2} per layer and the sample is normally doped. The measurements were done at room temperature (300K).

True spontaneous emission spectra were obtained in absolute units from analysis of the amplified spontaneous emission spectra [6] as a function of the current. By fitting the spontaneous emission spectra with Gaussian functions the total ground state spontaneous emission rate was obtained. The total radiative emission rate was also calculated from these spectra to give the total radiative current density. This was subtracted from the measured drive current density to obtain the total nonradiative current, giving the total nonradiative current versus ground state radiative current plotted in Figure 7.12.

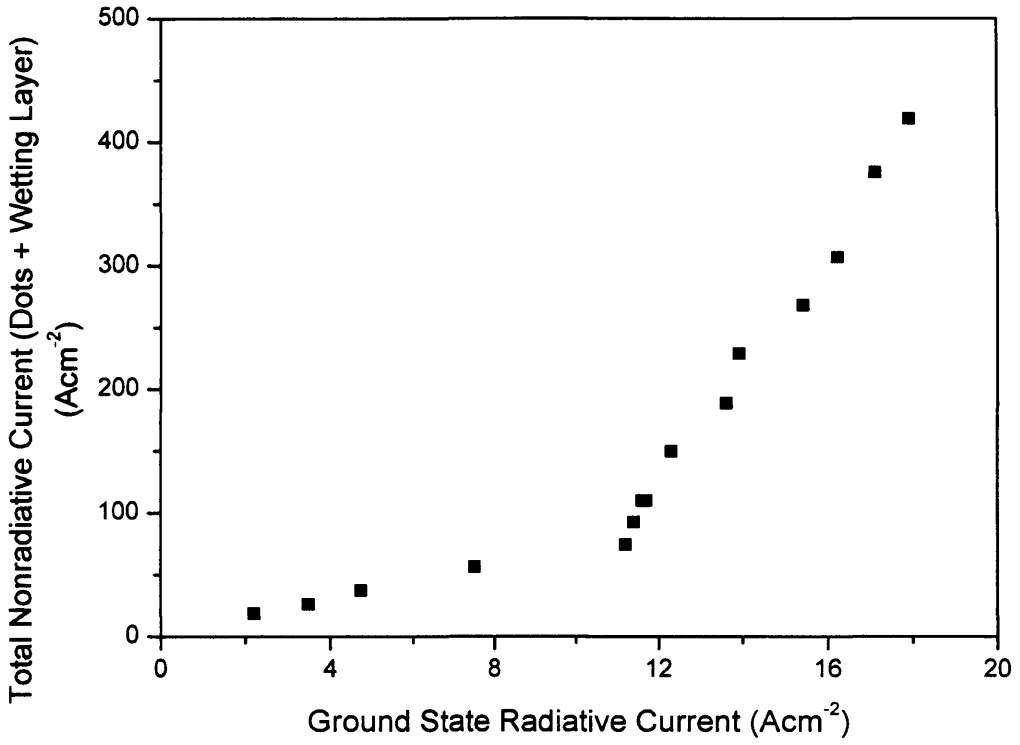

Figure 7.12 - Experimental measurements of the total nonradiative current as a function of the ground state radiative current. A radiative lifetime of 2.5ns was obtained from the measured modal absorption.

From the measured ground state optical cross section the radiative lifetime for the ground state was calculated by formulating the Einstein relations for a single dot, using the nominal dot density. This gave a value for the radiative lifetime of 2.5ns.

No assumptions about the relations between these current components and the number of carriers injected into the structure have been made. The spectra show that for currents below about 11Acm^{-2} only the ground state is populated and in this region there is a linear relation between the radiative and nonradiative currents, which would not be so if the processes were bi-molecular and mono-molecular respectively with respect to the total number of injected carriers.

7.5.3 Comparisons between Computed and Experimental Data

To fit the experimental data the only matching parameters used are the nonradiative via defects and Auger lifetimes in the dots. The standard deviation of the Gaussian curve fitted to the ground state absorption spectrum of the sample is 16meV, and the ground to excited

state separation is 65meV. To compare the model with the experimental data, the energy separations in the model were altered to match those measured for the sample. This was done by changing the standard deviation of the Gaussian to match the linewidths, and shifting the excited state energy levels so that the ground to excited state separation was comparable. The value of the radiative lifetime in the code was set at 2.5ns, the value obtained from the modal absorption of the sample. To fit the experimental data the nonradiative via defects and Auger lifetimes in the dots were varied so that the computed current matched that of the experimental data. Figure 7.13 shows the total nonradiative (via defects and Auger) current (in the dots and the wetting layer) versus the ground state radiative current. The nonradiative via defects and Auger lifetimes necessary to fit the experimental data are 2ns and 15ns respectively, using the nominal dot density.

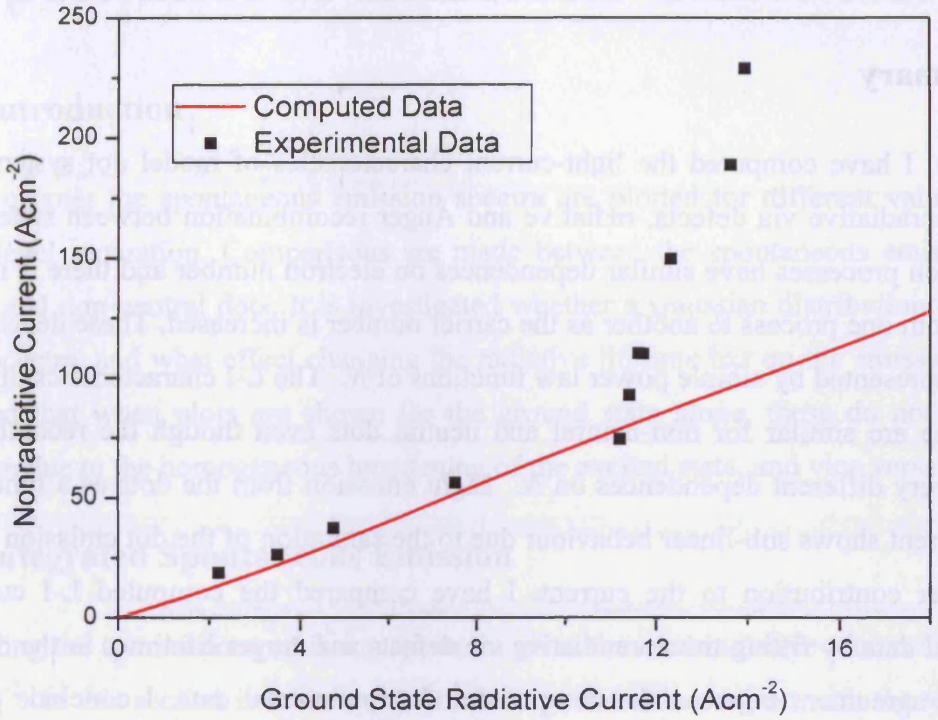

Figure 7.13 - Experimental measurements of the total nonradiative current as a function of the ground state radiative current shown as points, and computed results shown as a solid line. The calculation uses the nominal dot density and a radiative lifetime of 2.5ns obtained from the measured modal absorption. The nonradiative via defects and Auger lifetimes required to obtain this fit are 2ns and 15ns respectively.

The maximum possible ground state radiative current, when the upper state of the ground state is occupied in every dot, is 26Acm^{-2}. This is of similar magnitude to, and exceeds, the experimental values as expected. The values of the nonradiative via defects and Auger lifetimes of 2ns and 15ns respectively are physically reasonable and there is good agreement with the observed linear dependence in the region where the ground state recombination is dominant. The experimental data shows an up-turn in the total nonradiative current above a ground state radiative current of about 11Acm^{-2}. This could be due to recombination in excited states or in the wetting layer.

In summary, the model predicts a linear relation between the total nonradiative current and the ground state radiative current in the region where recombination occurs predominantly via the ground state. Good agreement is found between the model calculations and the experimental data obtained using calibrated measurements of the spontaneous emission rate.

This behaviour would not be expected for a combination of mono-molecular and bi-molecular processes with respect to the total injected carrier number.

7.6 Summary

In summary, I have computed the light-current characteristics of model dot systems with localised nonradiative via defects, radiative and Auger recombination between states. The recombination processes have similar dependences on electron number and there is no clear transition from one process to another as the carrier number is increased. These dependences cannot be represented by simple power law functions of N. The L-I characteristics of the dot system alone are similar for non-neutral and neutral dots even though the recombination rates have very different dependences on N. Light emission from the dots as a function of the total current shows sub-linear behaviour due to the saturation of the dot emission and the wetting layer contribution to the current. I have compared the computed L-I curves to experimental data by fitting the nonradiative via defects and Auger lifetimes in the dots and found good agreement between the computed and experimental data. I conclude that the analyses of L-I curves based on power law relations between recombination rates and carrier number, as used for extended state systems, cannot be applied to localised recombination in dots. The next chapter describes the spontaneous emission spectra, including a comparison between neutral and non-neutral dots.

7.7 References

[1] W. W. Chow and S. W. Koch, Semiconductor Lasers Fundamentals, Springer, Berlin, 1999.

[2] C. v. Opdorp and G. W. t. Hooft, Journal of Applied Physics 52 (1981) 3827.

[3] R. Olshansky, J. LaCourse, T. Chow, and W. Powazinik, Applied Physics Letters 50 (1987) 310.

[4] A. R. Adams and P. J. A. Thijs, IEEE Journal of Selected Topics in Quantum Electronics 5 (1999) 401.

[5] H. Y. Lui, I. R. Sellers, T. J. Badcock, D. J. Mowbray, M. S. Skolnick, K. M. Groom, and M. Hopkinson, Applied Physics Letters 85 (2004) 704.

[6] P. Blood, G. M. Lewis, P. M. Smowton, H. D. Summers, J. Thomson, and J. Lutti, IEEE Journal of Selected Topics in Quantum Electronics 9 (2003) 1275.

8 Spontaneous Emission Characteristics

8.1 Introduction

In this chapter the spontaneous emission spectra are plotted for different values of quasi-Fermi level separation. Comparisons are made between the spontaneous emission for the neutral and non-neutral dots. It is investigated whether a Gaussian distribution can be fitted to the spectra, and what effect changing the radiative lifetime has on the emission. It should be noted that when plots are shown for the ground state alone, these do not contain any emission due to the homogeneous broadening of the excited state, and vice versa.

8.2 Integrated Spontaneous Emission

Integrating the spontaneous emission spectrum gives the total radiative rate in dimensions of $[T]^{-1}[L]^{-2}$. In this section it is shown that the integrated values agree with the total summed values for the model. When the dots are fully occupied the total radiative rate for the ground state is given by

$$R_{rad}^{gr}(total) = \frac{2 \times n_{QD}}{\tau_{sp} \times area} = \frac{2 \times 10^{6}}{10^{-9} \times 3.33 \times 10^{-9}} = 6 \times 10^{23} \mathrm{s}^{-1}\mathrm{m}^{-2}$$

equation 8.1

Figure 8.1 is a plot of the ground state spontaneous emission spectrum for the fully occupied dots and integrating this curve should give a value equal to the one calculated above.

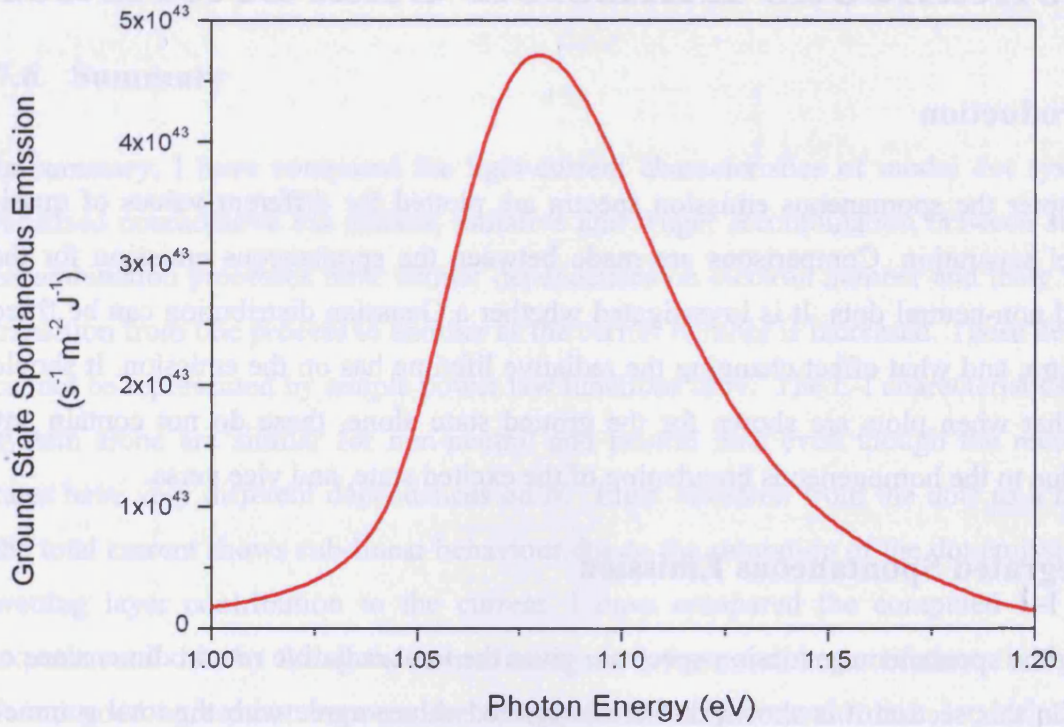

Figure 8.1 - Ground state spontaneous emission spectrum when the dots are fully occupied.

Integrating the curve shown in the above plot gives a value of 5.89×10^{23} $s^{-1}m^{-2}$ (the units have all been converted to SI units).The theoretical and actual integrated values agree within 98%. The difference in the two numbers is due to the interpolation done between the radiative rates to obtain many more data points, and also because the Lorentzian extends to energies outside those in the inhomogeneous distribution. The excited state emission spectrum is shown in the following figure, again for fully occupied dots.

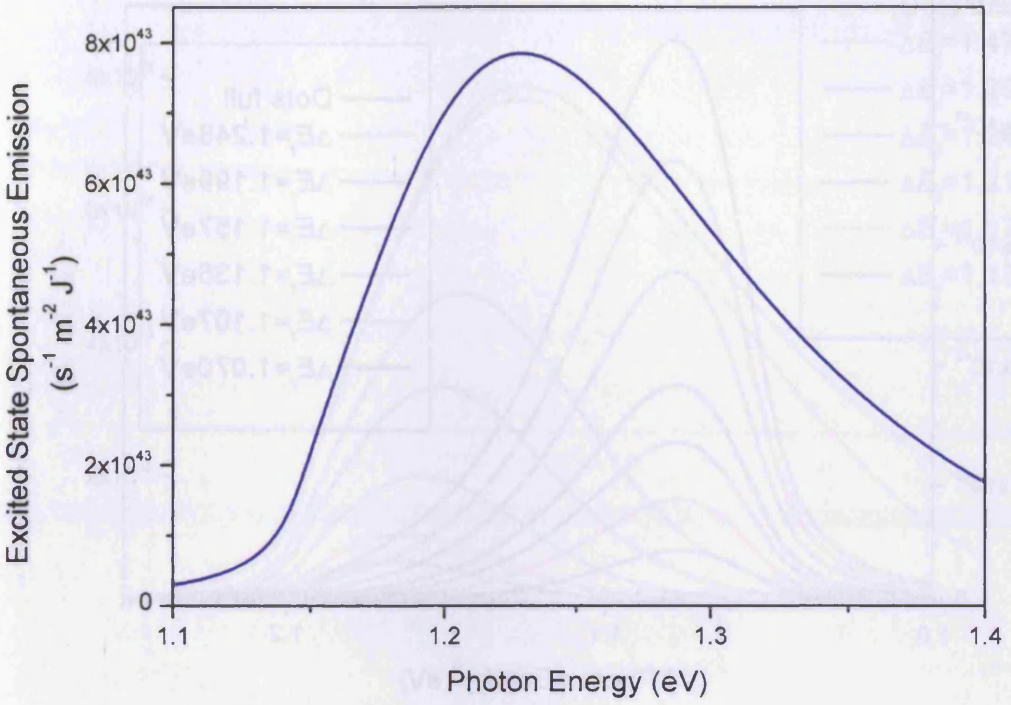

Figure 8.2 - Excited state spontaneous emission spectrum when the dots are fully occupied.

The integral for the excited state is equal to 2.28×10^{24} $s^{-1}m^{-2}$. The theoretical total radiative rate for the fully occupied excited state is:

$$R_{rad}^{ex}(total) = \frac{8 \times n_{QD}}{\tau_{sp} \times area} = \frac{8 \times 10^{6}}{10^{-9} \times 3.33 \times 10^{-9}} = 2.4 \times 10^{24}\,s^{-1}m^{-2}$$

equation 8.2

Again, the theoretical and actual integrated values for the excited state show good agreement.

8.3 Spontaneous Emission Spectra for different Quasi-Fermi Level Separations for the Non-Neutral Dots

In this section the evolution of the spontaneous emission spectra with increasing quasi-Fermi level separation is studied, for the non-neutral dots. First looking at the ground state alone, Figure 8.3 is a plot of the ground state spontaneous emission spectra for the non-neutral dots, for different values of the quasi-Fermi level separation.

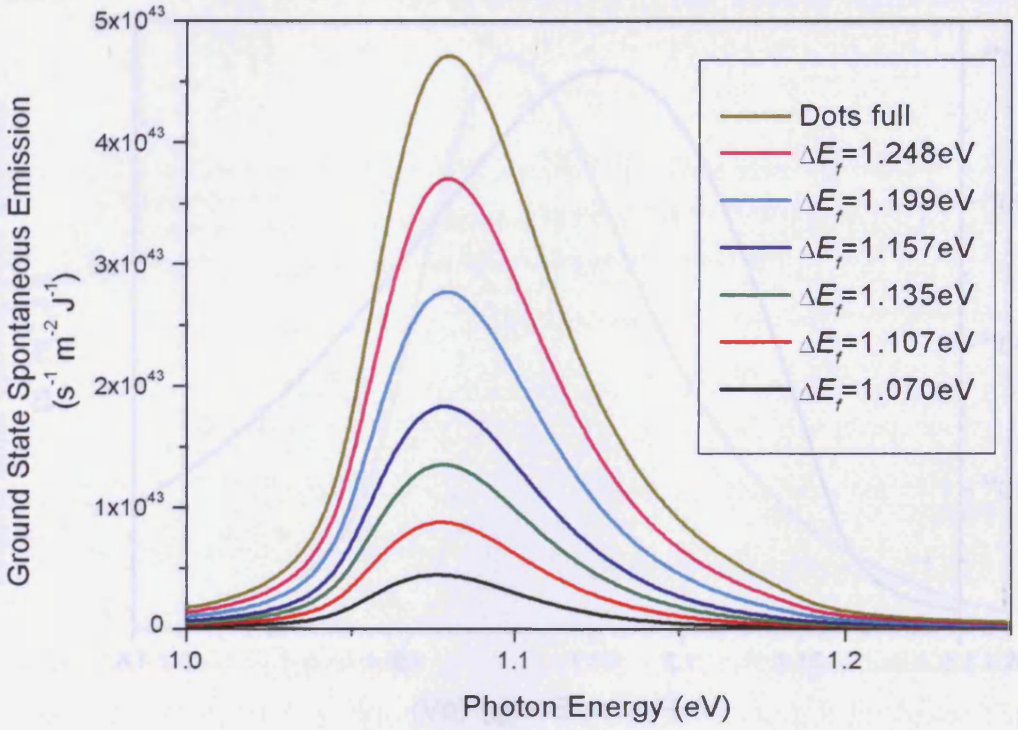

Figure 8.3 - Ground state spontaneous emission spectra for the non-neutral dots shown for different values of quasi-Fermi level separation.

As the quasi-Fermi level separation is increased the ground state spontaneous emission increases. Eventually the ground states of all the dots become full and the spontaneous emission saturates. As the quasi-Fermi level separation is increased the photon energy that corresponds to the peak emission increases slightly, from 1.076eV for ΔE_f equal to 1.070eV, to 1.079eV for the fully occupied dots.

The following figure is a plot of the excited state spontaneous emission spectra for the non-neutral dots, for different values of the quasi-Fermi level separation.

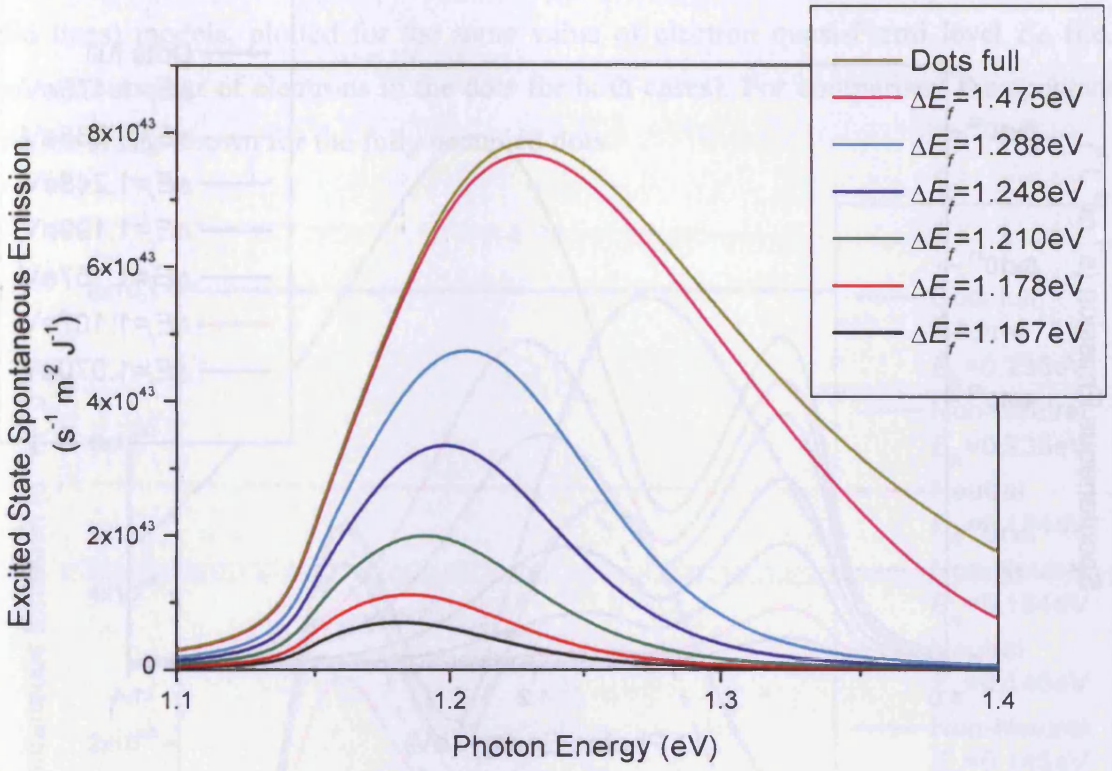

Figure 8.4 - Excited state spontaneous emission spectra for the non-neutral dots shown for different values of quasi-Fermi level separation.

Again, as the quasi-Fermi level separation is increased the excited state spontaneous emission also increases until saturation occurs when the excited state is fully occupied. For the excited state, the photon energy that corresponds to the peak emission increases from 1.181eV for ΔE_f equal to 1.157eV, to 1.229eV for the fully occupied dots.

The total spontaneous emission spectra, for both the ground and excited states, are shown in the following graph for different values of quasi-Fermi level separation.

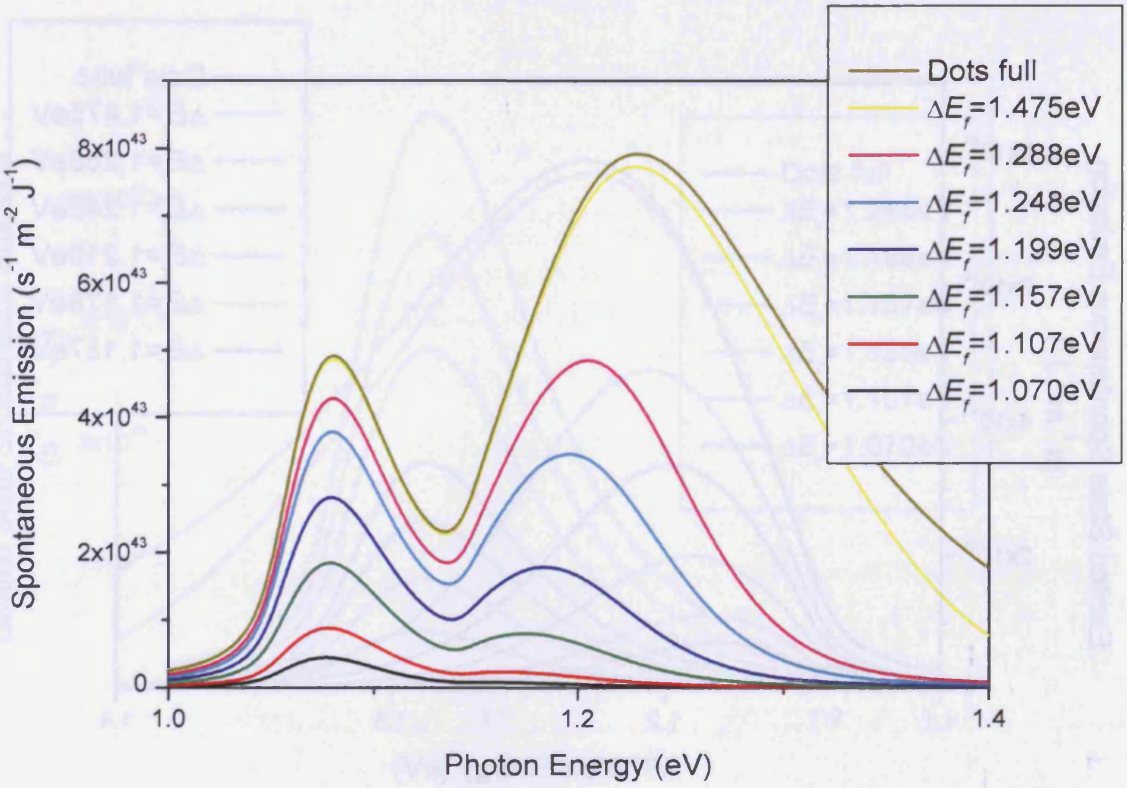

Figure 8.5 - Ground and excited state spontaneous emission spectra for the non-neutral dots shown for different values of quasi-Fermi level separation.

It can be seen that at low values of quasi-Fermi level separation, the ground state spontaneous emission exceeds that of the excited state. It is not until the ground state emission has almost reached its maximum (when ΔE_f equal to about 1.288eV) that the excited state emission dominates. There is emission from the excited state before the ground state is saturated, which has been observed experimentally [1].

8.4 Comparing the Spontaneous Emisison Spectra for Neutral and Non-Neutral Dots

Here, the spontaneous emission spectra for the non-neutral dots are compared with those for the neutral dots. The only difference in the two models is the way in which the dots are filled with holes and so when the dots are fully occupied there is no difference in the spontaneous emission spectrum for the two cases. Both models have the same electron distribution, but in the neutral model the number of holes in each dot is not controlled by Fermi-Dirac statistics (as in the non-neutral case), but is set equal to the number of electrons in the dot. Figure 8.6

is a plot of the spontaneous emission spectra for the neutral (dashed lines) and non-neutral (solid lines) models, plotted for the same value of electron quasi-Fermi level E_{fc} (i.e. the same total number of electrons in the dots for both cases). For comparison the spontaneous emission is also shown for the fully occupied dots.

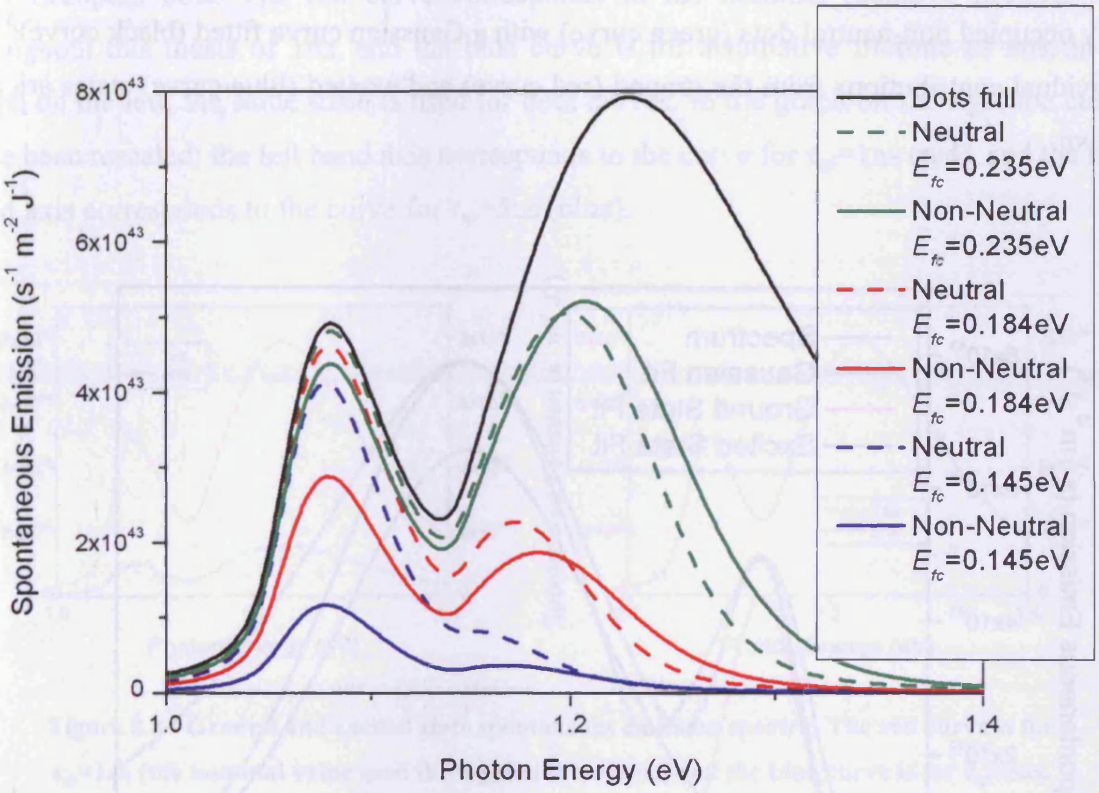

Figure 8.6 - Spontaneous emission spectra for the neutral dots (dashed lines) and non-neutral dots (solid lines), plotted for the same value of electron quasi-Fermi level.

It can be seen that for the same value of E_{fc}, the spontaneous emission due to the ground state is larger for *neutral* dots. This is because the neutral dots have more holes in the ground state than the non-neutral dots and, also, they are correlated i.e. for every electron in a neutral dot there is a hole in the *same* dot. At low excited state energies, the emission is again higher for the neutral dots due to a higher number of holes in the neutral dots. However, at higher energies the emission is bigger for *non-neutral* dots, since there become more holes in the non-neutral dots than in the neutral. This is because the hole energy levels are more closely spaced than those of the electrons, and this is taken into account in the non-neutral model where higher energy levels for holes can be populated compared with the electrons.

8.5 Fitting a Gaussian Distribution to the Emission Spectra

It is common practise to fit the spontaneous emission spectra with Gaussian functions and in this section it is investigated whether this can be done for the computed spontaneous emission spectra in the model. Figure 8.7 shows the spontaneous emission spectrum for the fully occupied non-neutral dots (green curve) with a Gaussian curve fitted (black curve). The individual contributions from the ground (red curve) and excited (blue curve) states are also shown.

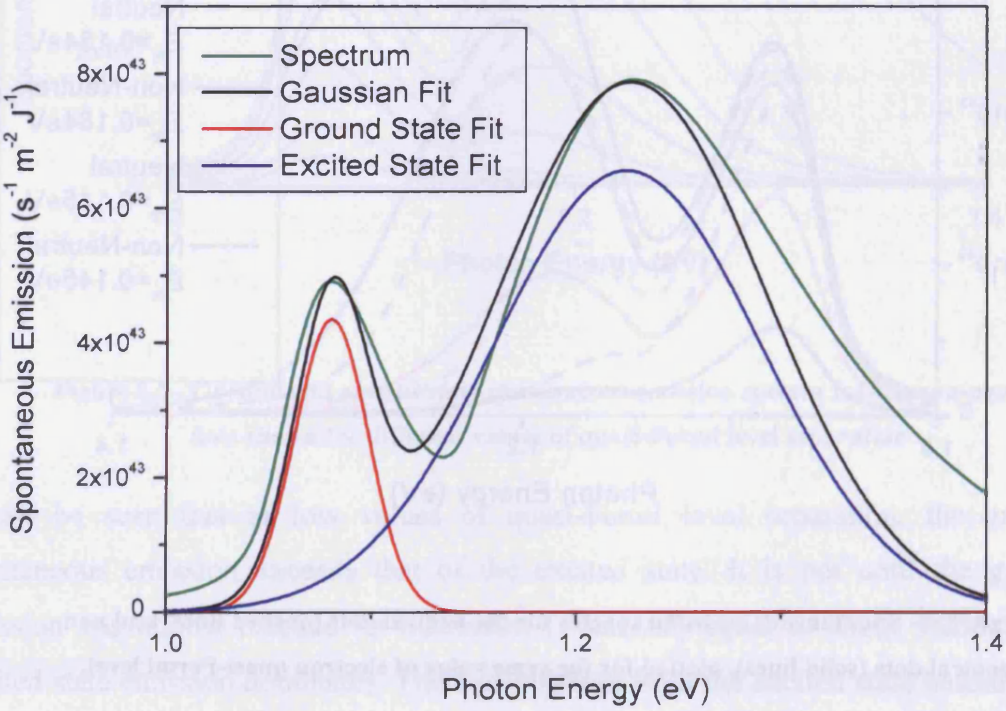

Figure 8.7 - Spontaneous emission spectrum for the fully occupied non-neutral dots (green curve). A Gaussian distribution has been fitted (black curve). The individual contributions from the ground (red curve) and excited (blue curve) states are also shown.

Values used for the standard deviation of the ground and excited states are 18meV and 65meV respectively. It can be seen that the spontaneous emission spectrum cannot be fitted with a Gaussian distribution. Whilst it is possible to fit the peaks of the emission, the tails of the emission spectrum do not follow a Gaussian distribution, particularly at high and low photon energy. This is expected since the inhomogeneous broadening is applied to the dots *sizes* and not the energies.

8.6 Spontaneous Emission Spectra for Different Radiative Lifetimes

In this section the effect that changing the radiative lifetime has on the spontaneous emission spectrum is investigated. The following plots show the spontaneous emission spectra for the fully occupied dots. The red curve corresponds to the nominal radiative lifetime used throughout this thesis of 1ns, and the blue curve is for a radiative lifetime of 5ns. In the graph on the left, the same scale is used for both curves. In the graph on the right the curves have been rescaled: the left hand axis corresponds to the curve for τ_{sp}=1ns (red), and the right hand axis corresponds to the curve for τ_{sp}=5ns (blue).

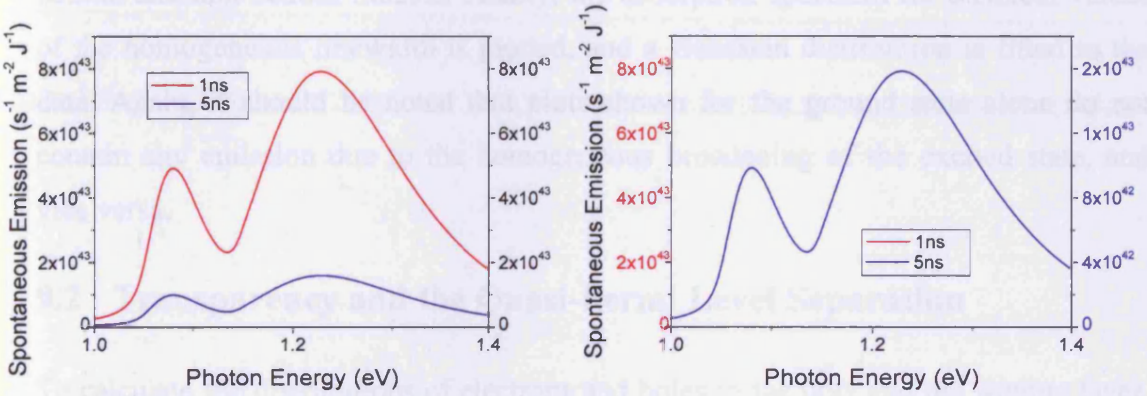

Figure 8.8 - Ground and excited state spontaneous emission spectra. The red curve is for τ_{sp}=1ns (the nominal value used throughout the thesis), and the blue curve is for τ_{sp}=5ns. The plots on the right have been rescaled and the left axis (red) is for τ_{sp}=1ns and the right axis (blue) is for τ_{sp}=5ns.

As can be seen from the plot on the left in Figure 8.8, increasing the radiative lifetime from 1ns to 5ns has the effect of *decreasing* the spontaneous emission at a particular photon energy. This is intuitive since the spontaneous emission is inversely proportional to the radiative lifetime and changing this simply scales the value at each energy. When the two curves are rescaled it can be seen that changing the radiative lifetime does not alter the shape of the emission spectrum, and this is also true at lower injection.

8.7 Summary

In this chapter I have studied the evolution of the spontaneous emission spectra for non-neutral dots as the quasi-Fermi level separation is increased. I have also compared the spectra of non-neutral dots with those of neutral dots. I have shown that a Gaussian distribution cannot be fitted to the emission spectra, and that changing the radiative lifetime

does not alter the shape of the emission. The next chapter describes the modal gain characteristics for the dots.

8.8 References

[1] M. Grundmann and D. Bimberg, Physical Review B 55 (1997) 9740.

9 Modal Gain Characteristics

9.1 Introduction

In this chapter the modal gain spectra for the quantum dot ensemble are studied, comparing the spectra for the neutral dots with those for non-neutral dots. The differences in the plots of the peak modal gain as a function of the electron quasi-Fermi level, electron number and radiative current are investigated, comparing the neutral and non-neutral models. Finally, the absorption spectrum for different values of the homogeneous linewidth is plotted, and a Gaussian distribution is fitted to the data. Again, it should be noted that plots shown for the ground state alone do not contain any emission due to the homogeneous broadening of the excited state, and vice versa.

9.2 Transparency and the Quasi-Fermi Level Separation

To calculate the distributions of electrons and holes in the dots and the wetting layer, the electron quasi-Fermi level E_{fc} is inputted. The hole quasi-Fermi level E_{fv} is then defined by setting charge neutrality over the dots *and* the wetting layer. This gives a particular value of quasi-Fermi level separation given by

$$\Delta E_f = E_{fc} + E_{fv} + E_g$$

equation 9.1

where E_g is the bandgap of the dot material (equal to 1ev).

When the photon energy is equal to the quasi-Fermi level separation, an incident photon experiences no gain or absorption and this is called the material *transparency*. This photon energy is usually equal to the intercept between the modal gain curves and $G=0cm^{-1}$. However, the inclusion of the homogeneous broadening in the gain spectra alters the photon energy at which the gain is zero, as shown in Figure 9.1.

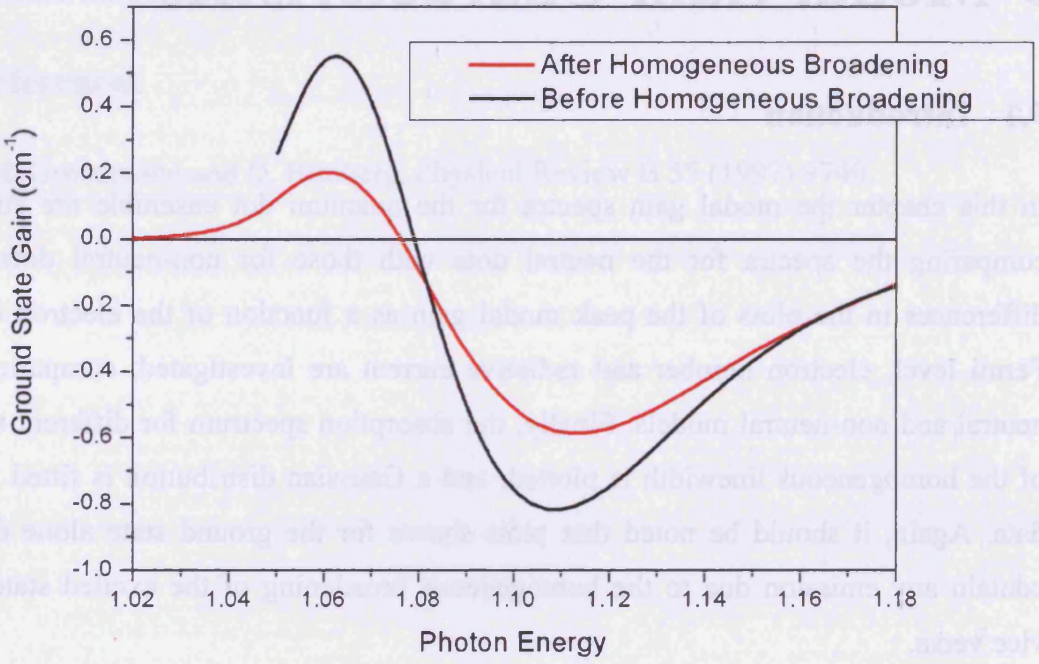

Figure 9.1 - Ground state modal gain before (black curve) and after (red curve) the inclusion of the homogeneous broadening. The photon energy at which the gain is zero changes.

Before the homogeneous broadening is included, the photon energy at which the gain is zero is equal to the quasi-Fermi level separation, which for the example shown is 1.079eV. However, the inclusion of the homogeneous broadening alters this since at the photon energy equal to the quasi-Fermi level separation, there are transitions contributing to the gain because of the homogeneous linewidth. Therefore, if homogeneous broadening is included the transparency point observed on the gain spectra cannot be equated to the quasi-Fermi level separation and is not a meaningful measurable quantity.

These effects are a well known problem and are discussed in detail in references [1, 2]. The origin of this problem is in the oversimplification in using Lorentzian functions to model the gain spectra, which do not take into account the Coulomb interaction effects. It has been shown that to reproduce gain spectra accurately it is essential to include the nondiagonal Coulomb correlation contributions to the active medium polarisation, which significantly alter the shape of the gain spectra.

9.3 Modal Gain Spectra

9.3.1 Modal Gain Spectra for Non-Neutral dots

In this section the modal gain spectra as a function of the photon energy are shown for the non-neutral dots. In the plots, the positive region on the modal gain axis indicates gain whereas the negative region indicates absorption. The following plot is the ground state modal gain as a function of photon energy for three values of quasi-Fermi level separation.

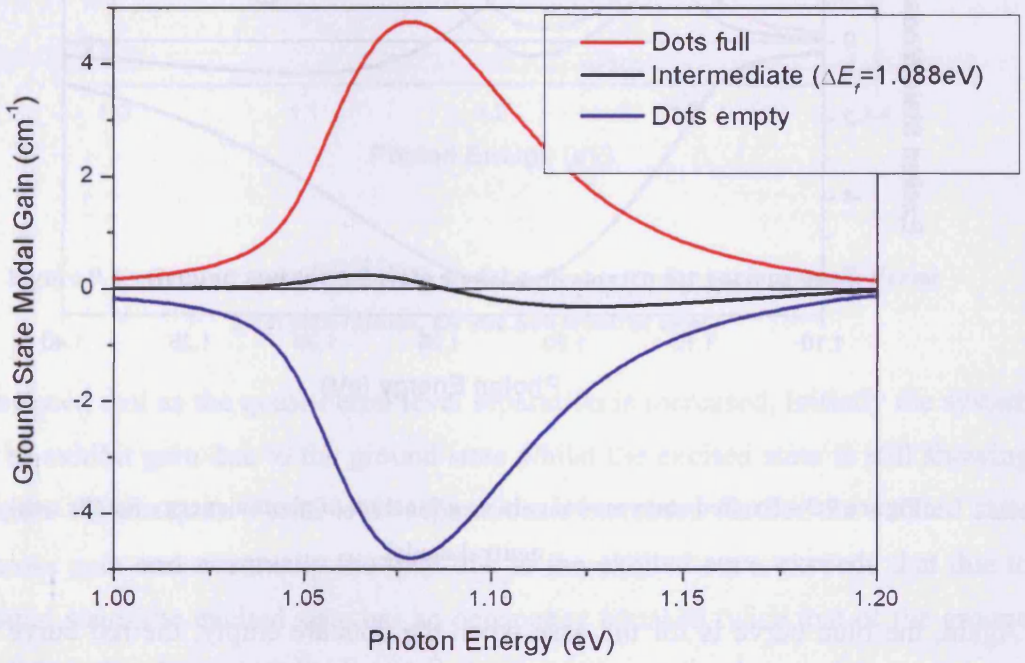

Figure 9.2 - Ground state modal gain as a function of photon energy for the non-neutral model.

The blue curve is for the case when the dots are empty, the red curve for the case of fully occupied dots, and the black curve is for an intermediate case for which the quasi-Fermi level separation is equal to 1.088eV. It can be seen that due to the spectral homogeneous broadening of the transitions, there is gain/absorption at photons energies below the bandgap; this is because there is a long tail in energy for a Lorentzian distribution. As described in section 9.2, the intercept between the modal gain curves and G=0cm^{-1} does not occur exactly when the photon energy is equal to

the quasi-Fermi level separation due to the homogeneous broadening. As the quasi-Fermi level separation is increased all the dot states become full and experience gain. The following plot, Figure 9.3, shows the excited state modal gain as a function of photon energy, for the non-neutral case.

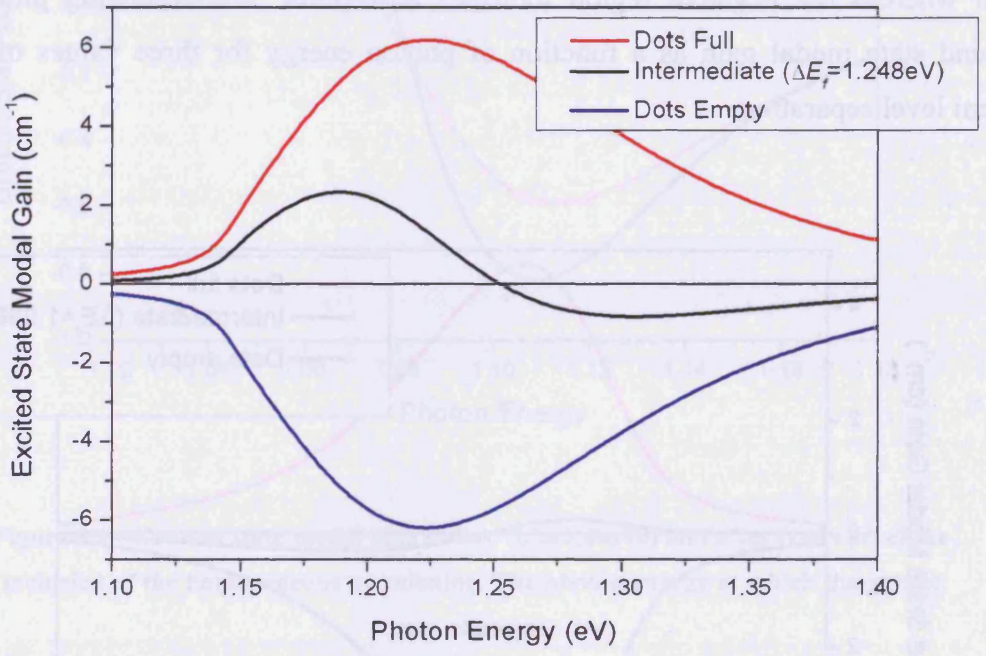

Figure 9.3 - Excited state modal gain as a function of photon energy for the non-neutral model.

Again, the blue curve is for the case when the dots are empty, the red curve for the case of fully occupied dots, and the black curve is for an intermediate case. When the dots are full (empty) there is more gain (absorption) from the excited state than the ground state as expected, since the excited state can accommodate twice as many electrons as the ground state. Figure 9.4 shows the modal gain spectra for the ground and excited states together, for various quasi-Fermi level separations (for the non-neutral case).

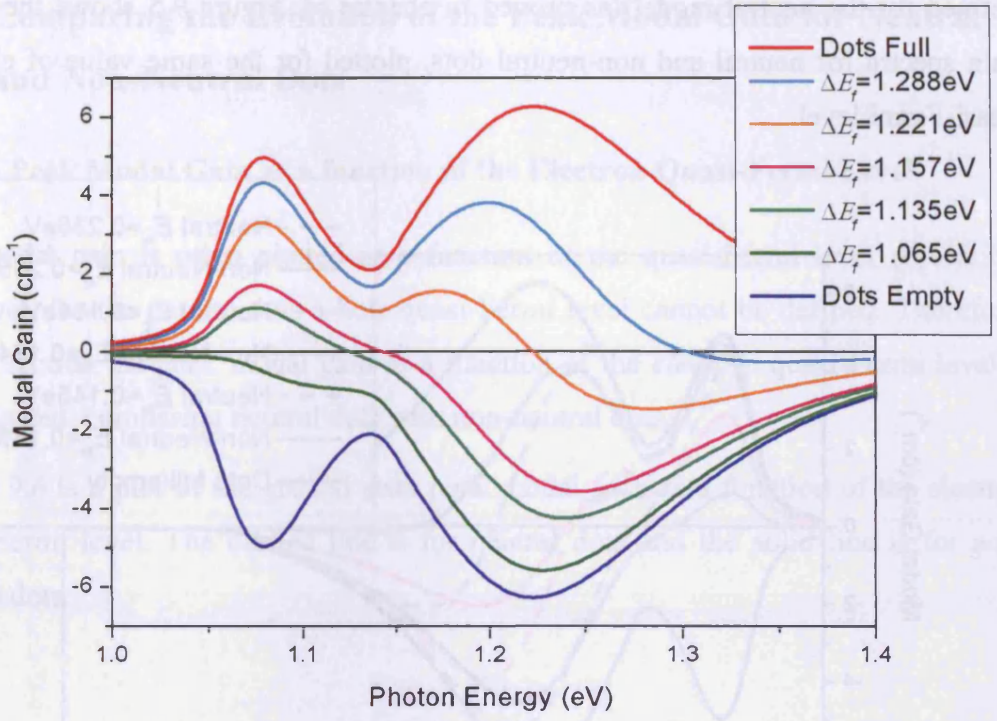

Figure 9.4 - Ground and excited state modal gain spectra for various quasi-Fermi level separations, for the non-neutral case.

It can be seen that as the quasi-Fermi level separation is increased, initially the system begins to exhibit gain due to the ground state whilst the excited state is still showing absorption. As the quasi-Fermi level separation is increased further the excited state also shows gain and eventually the gain due to the excited state exceeds that due to the ground state (the excited state has an occupancy equal to twice that of the ground state). When the dots are fully inverted the maximum gain due to the ground and excited states is about 5.0cm^{-1} and 6.3cm^{-1} respectively.

9.3.2 Modal Gain Spectra of Neutral Dots compared with Non-Neutral Dots

In this section the gain spectra for the neutral dots are compared with those for the non-neutral dots. When the dots are empty or fully occupied there are no differences between the gain spectra for the two cases: this is because the only difference in the two models is the way in which the dots are filled with holes. Both models have the same electron distribution, but in the neutral model the number of holes in each dot is not controlled by Fermi-Dirac statistics (as in the non-neutral case), but is set equal to the number of electrons in the dot. Because of this, a hole quasi-Fermi level cannot be

defined for the neutral model (as proved in chapter 6). Figure 9.5 shows the modal gain spectra for neutral and non-neutral dots, plotted for the same value of electron quasi-Fermi level.

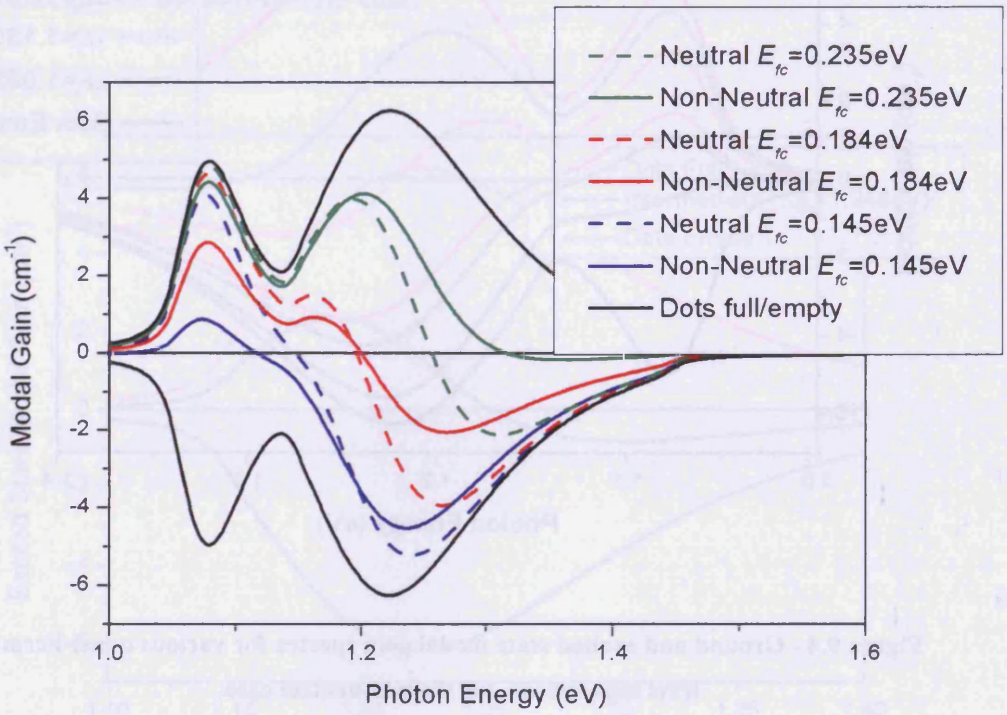

Figure 9.5 - Modal gain spectra for the neutral dots (dashed lines) and non-neutral dots (solid lines), plotted for the same value of electron quasi-Fermi level.

For comparison, the gain (absorption) for full (empty) dots is also shown (black curves), and these curves are the same for both neutral and non-neutral dots. It can be seen that for the same value of electron quasi-Fermi level, the gain due to the ground state is larger for *neutral* dots. This is because the neutral dots have more holes in the ground state than the non-neutral dots, and these are correlated such that for every electron in a neutral dot there is also a hole. Plots of the electron and hole distributions for different electron quasi-Fermi level are shown in chapter 6. At low excited state energies, the gain is again higher for the neutral dots due to a higher number of holes in the neutral dots. However, for higher energies, there become more holes in the non-neutral dots than in the neutral, and so the gain at these energies is higher for the *non-neutral dots*.

9.4 Comparing the Evolution of the Peak Modal Gain for Neutral and Non-Neutral Dots

9.4.1 Peak Modal Gain as a function of the Electron Quasi-Fermi Level

The modal gain is often plotted as a function of the quasi-Fermi level separation. However, for the neutral dots a hole quasi-Fermi level cannot be defined. Therefore, in this section the peak modal gain as a function of the *electron* quasi-Fermi level is investigated, comparing neutral dots with non-neutral dots.

Figure 9.6 is a plot of the ground state peak modal gain as a function of the electron quasi-Fermi level. The dashed line is for neutral dots and the solid line is for non-neutral dots.

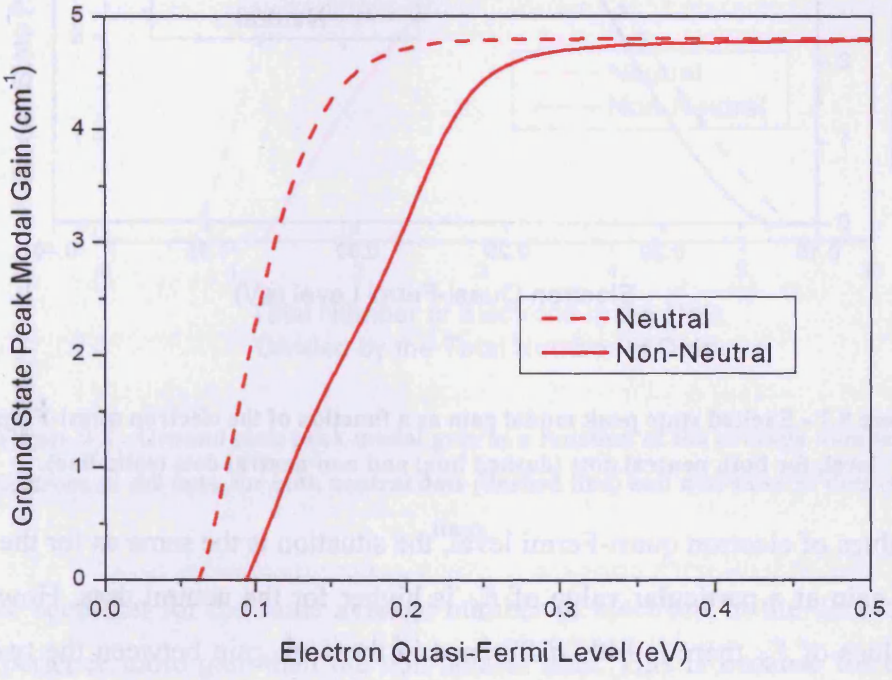

Figure 9.6 - Ground state peak modal gain as a function of the electron quasi-Fermi level, for both neutral dots (dashed line) and non-neutral dots (solid line).

It can be seen that to achieve the same value of modal gain, a higher value of electron quasi-Fermi level is needed for the non-neutral dots. This is because for the same value of electron quasi-Fermi level there are more holes in the ground state of the neutral dots than of the non-neutral dots, and this results in an increased gain. The

modal gain for both the neutral and non-neutral dots saturates at the same value, as the occupancies of the dots reach the same value.

Now considering the excited state, the following plot shows the excited state peak modal gain as a function of electron quasi-Fermi level, for neutral dots (dashed line) and non-neutral dots (solid line).

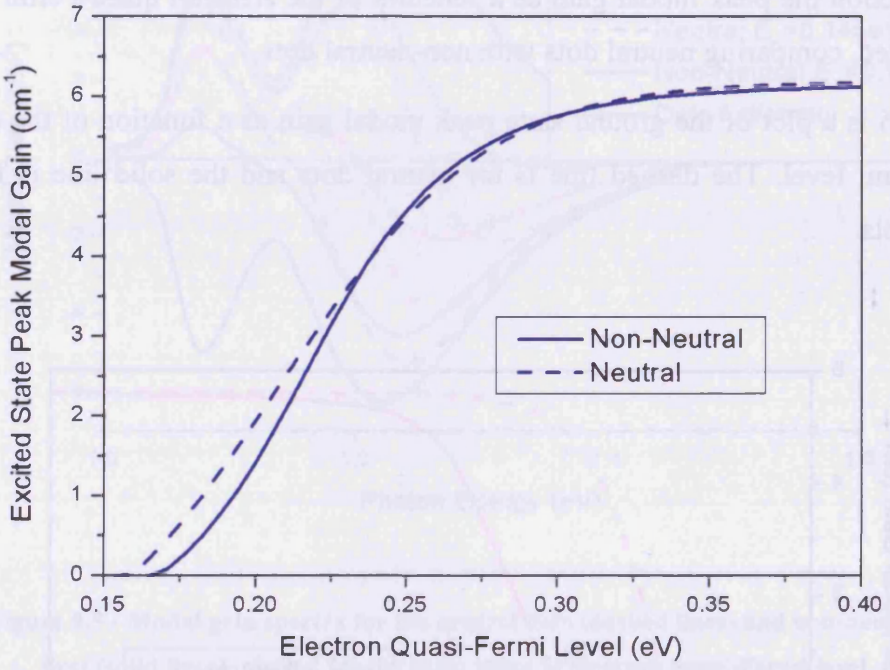

Figure 9.7 - Excited state peak modal gain as a function of the electron quasi-Fermi level, for both neutral dots (dashed line) and non-neutral dots (solid line).

At low values of electron quasi-Fermi level, the situation is the same as for the ground state: the gain at a particular value of E_{fc} is higher for the neutral dots. However, at higher values of E_{fc} there is little difference in the peak gain between the two cases. This can be explained by considering how the hole distributions differ, as described in chapter 6. For $E_{fc} \sim 0.2$eV, the distribution of holes for the neutral dots is spread over a smaller range of energies and so there is a larger contribution to the peak gain for the neutral dots. As E_{fc} increases, the difference in the hole distributions for the two cases becomes less distinct.

9.4.2 Modal Gain as a function of the Electron Number

In this section is a study of the variation of the peak modal gain with the average number of electrons in a dot i.e. the total number of electrons divided by the total number of dots. Considering the ground state only first, Figure 9.8 is a plot of the peak modal gain as a function of the average number of electrons in the dots.

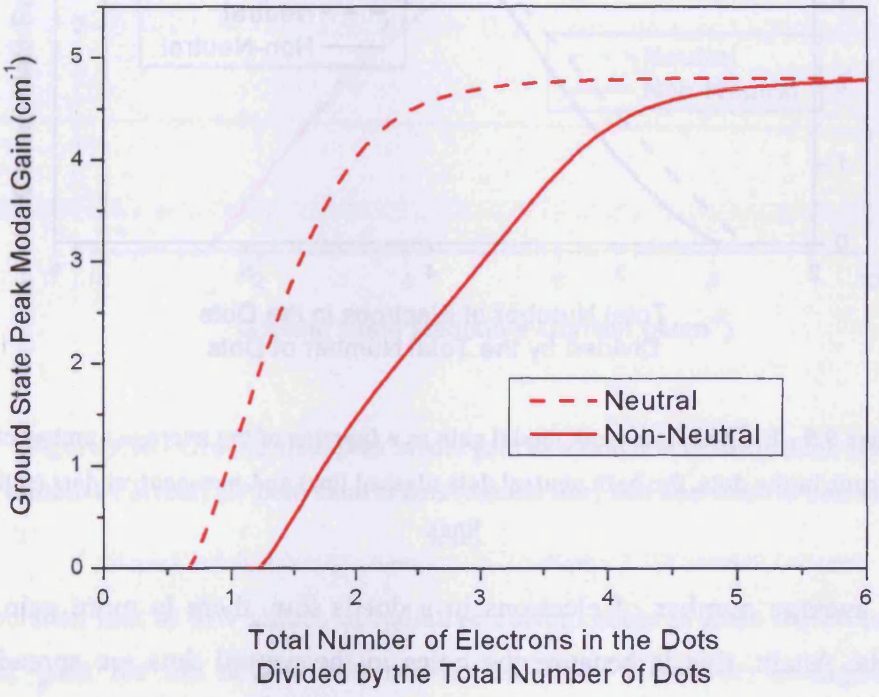

Figure 9.8 - Ground state peak modal gain as a function of the average number of electrons in the dots, for both neutral dots (dashed line) and non-neutral dots (solid line).

It can be seen that for the same average number of electrons in the dots, the neutral dots experience more gain than the non-neutral dots. This is because for the ground state in the non-neutral model, the total number of electrons in the dots is less than the total number of holes, and consequently, for every electron there is not always a hole present in the same dot. However, in the neutral model, for every electron in a dot there is also a hole and this leads to an increased gain for the neutral dots compared with the non-neutral dots.

The peak modal gain as a function of the average number of electrons in the dots is now plotted for the excited state in the following figure.

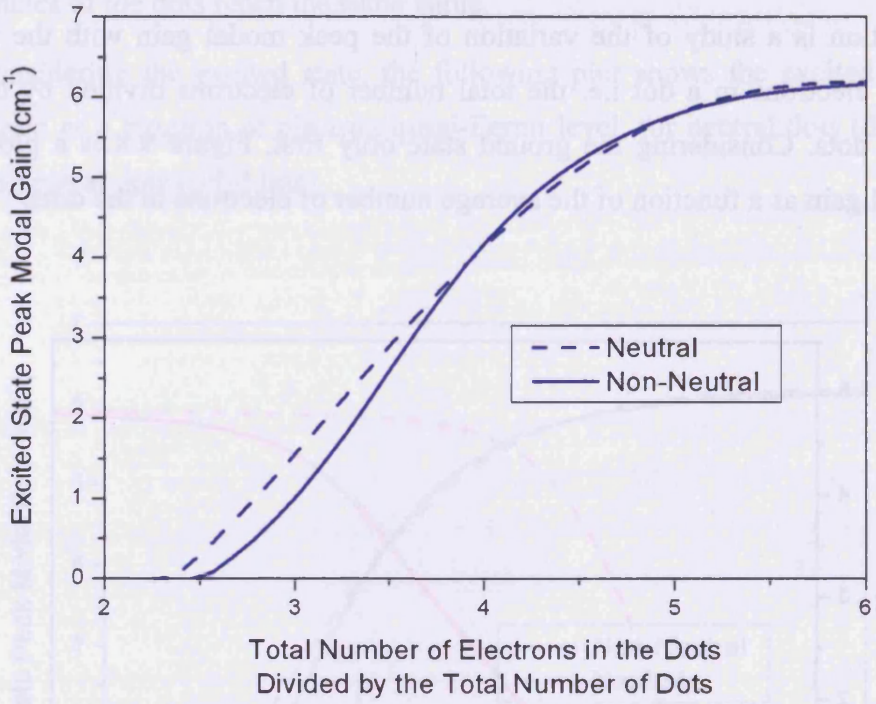

Figure 9.9 - Excited state peak modal gain as a function of the average number of electrons in the dots, for both neutral dots (dashed line) and non-neutral dots (solid line).

When the average number of electrons in a dot is low, there is more gain for the neutral dots. Again, this is because the holes in the neutral dots are spread over a smaller range of energies and so make a bigger contribution to the peak gain. As the average number of electrons increases, the hole distributions for the neutral and non-neutral dots become more similar, and there is not much difference in the peak gain between the two models.

9.4.3 Modal Gain as a function of the Radiative Current in the Dots

It is now studied how the peak modal gain varies with the radiative current in the dots. Figure 9.10 is a plot of the ground state peak modal gain as a function of the ground state radiative current in the dots, for neutral dots (dashed line) and non-neutral dots (solid line).

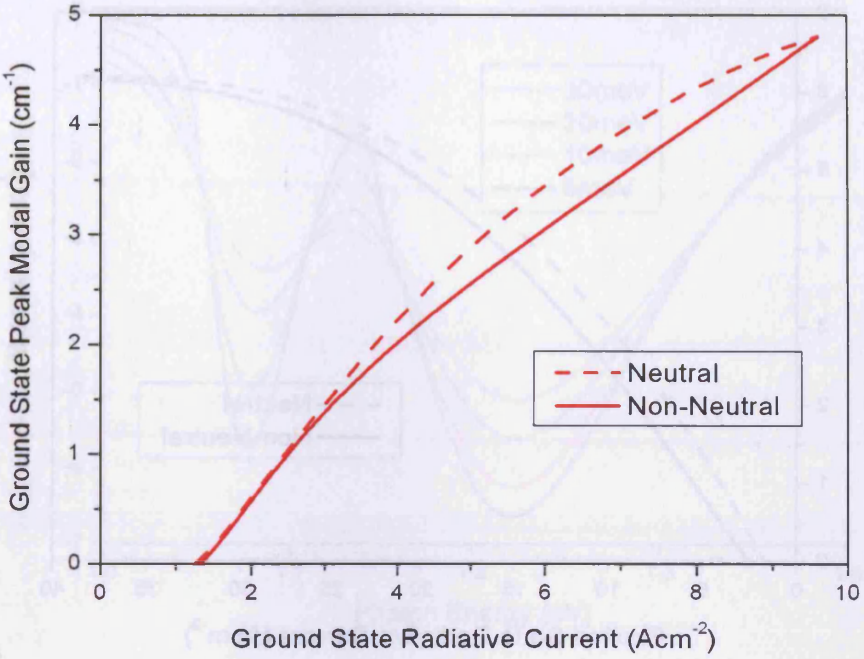

Figure 9.10 - Ground state peak modal gain as a function of the ground state radiative current, for both neutral dots (dashed line) and non-neutral dots (solid line).

It can be seen that at low values of radiative current there is little difference between the peak gain for the neutral and non-neutral dots. However, at higher radiative currents the peak gain is bigger for neutral dots, until the dots become fully occupied and the gain saturates. In these plots, both the peak gain *and* the radiative current depend on the electron *and* hole numbers. The current is simply the integrated total radiative rate and is independent of the energies of the carriers. However, the peak gain depends on the distribution of the electrons and holes amongst the available energy states. The range of energies over which the holes are spread is smaller for the neutral dots and so there are more transitions contributing to the peak gain.

The situation for the excited state is shown in the following plot of the excited state peak modal gain as a function of the excited state radiative current.

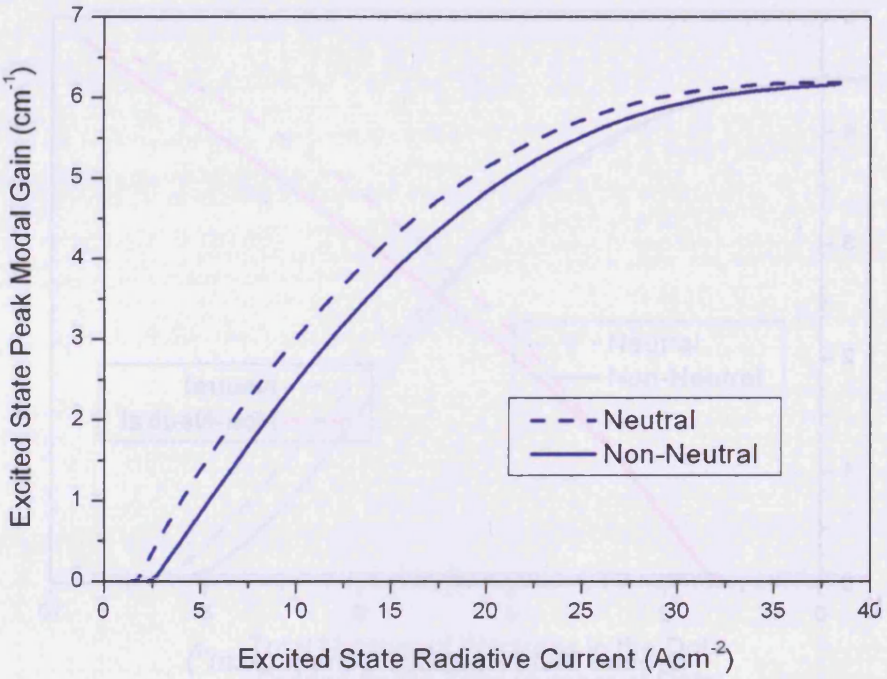

Figure 9.11 - Excited state peak modal gain as a function of the excited state radiative current, for both neutral dots (dashed line) and non-neutral dots (solid line).

The same trends can be seen as for the ground state, with the neutral dots experiencing a higher value of peak gain for the same radiative current, again due to the distribution of the holes over a smaller energy range in the neutral dots. It has been reported previously that charged dots offer, in general, higher gain at lower current [3].

9.5 Absorption Spectra with varying Homogeneous Linewidths

In this section the shape of the absorption spectrum for different homogeneous linewidths is studied, and it is investigated whether the spectra can be fitted with Gaussian distributions. Figure 9.12 is a plot of the absorption spectra for varying values of the homogeneous linewidth Λ. The standard value of the linewidth used throughout this thesis is 10meV, and the absorption spectrum for this value is shown in red.

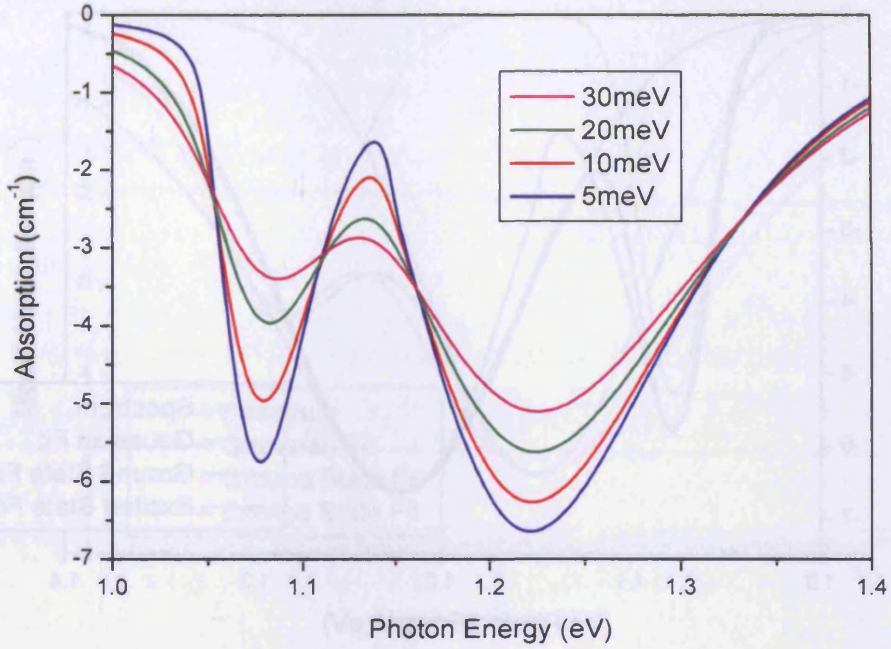

Figure 9.12 - Absorption spectrum for varying values of the homogeneous linewidth Λ. The standard value of the linewidth used throughout this thesis is 10meV (the red curve).

It can be seen that as the linewidth is increased, the ground and excited state absorption curves become less distinct, and the peak values are lower. For these curves, the high energy tail of the ground state absorption becomes merged into the excited state absorption. Also, at higher values of the linewidth, the absorption spectra extend further in photon energy. The homogeneous linewidth causes absorption below the bandgap.

The absorption spectra are now with Gaussian distributions. Figure 9.13 shows the modal absorption for the ground and excited states for the nominal value of the linewidth, 10meV. Gaussian distributions have been fitted to both the ground and excited state peaks and summed to give the best fit for the total distribution. The individual contributions are also shown for comparison.

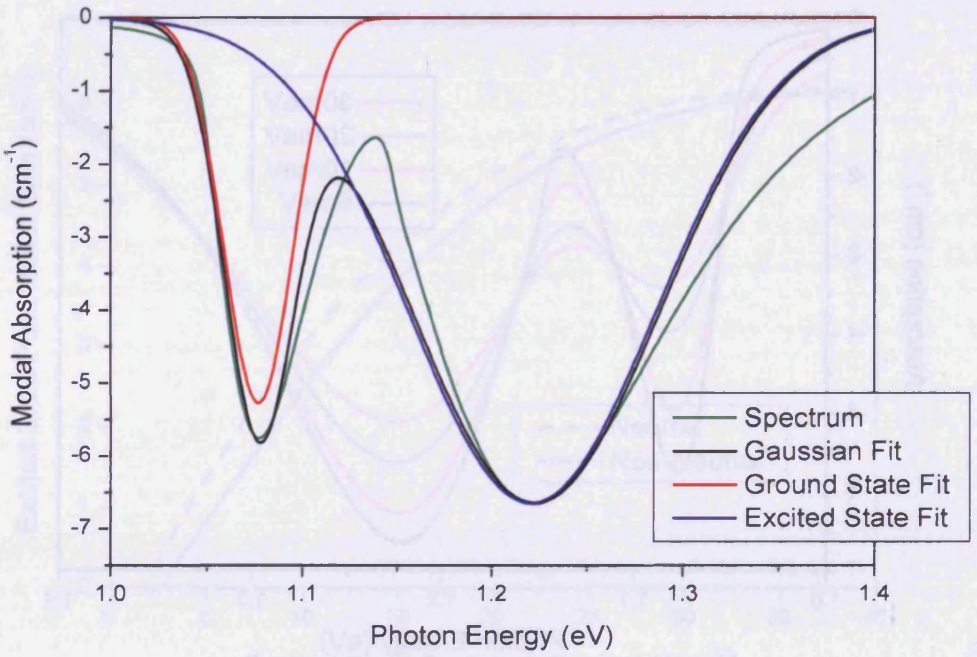

Figure 9.13 - Absorption spectrum for a homogeneous linewidth of 10meV. The plot is fitted with a Gaussian curve for the ground and excited states, using standard deviations of 18meV and 65meV respectively.

To fit the Gaussians, values used for the standard deviations are 18meV and 65meV for the ground and excited states respectively. It can be seen that the fit for the ground state peak is reasonable. The excited state fit is less good; the fit to the peak is reasonable, but away from the peak the fit does not match the absorption. The Gaussian fit is worst for the tails of both the ground and excited state curves, with the excited state showing considerable differences at higher photon energies.

The absorption spectrum for a linewidth of 30meV is now considered. Fitting a Gaussian to this spectrum is more difficult. It is not possible to fit both the absorption peaks and tails. In the following graph, Figure 9.14, a Gaussian distribution is fitted by matching the peak values of the ground and excited state absorption, using standard deviations of 38meV and 58meV respectively.

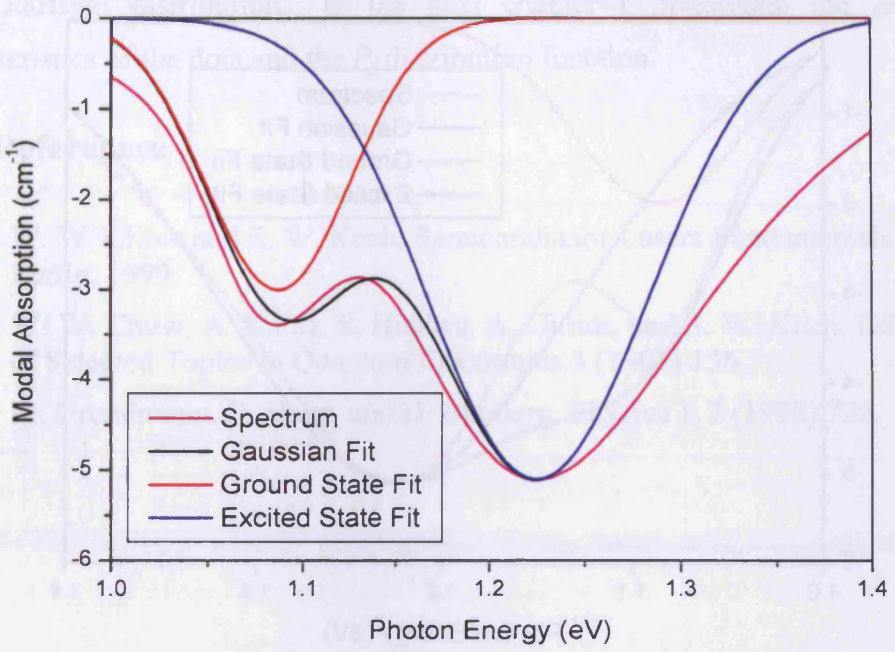

Figure 9.14 - Absorption spectrum for a homogeneous linewidth of 30meV. The plot is fitted with a Gaussian curve for the ground and excited states, using standard deviations of 38meV and 58meV respectively.

It can be seen that, whilst the peaks show a reasonable fit, the energy tails of the spectrum do not match well. In Figure 9.15 a Gaussian distribution is fitted by matching the absorption tails. For a sensible match here, the fit to the peaks is poor, and the fit to the tails at low and high energy is also poor.

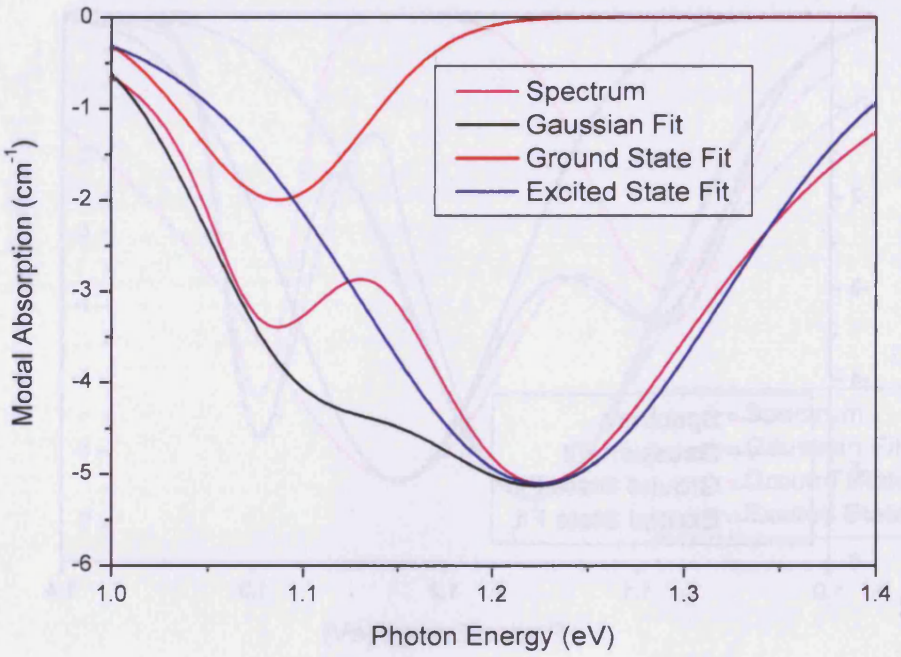

Figure 9.15 - Absorption spectrum for a homogeneous linewidth of 30meV. The plot is fitted with a Gaussian curve for the ground and excited states, using standard deviations of 45meV and 95meV respectively.

The plots shown in this section imply that the inhomogeneous broadening is changing since different values of the standard deviation are needed to fit the absorption spectra for different linewidths. But it is the *homogeneous* broadening that is changing. It is concluded that a Gaussian distribution cannot be reasonably fitted to the absorption spectra, independent of the homogeneous linewidth used. This is intuitive: the inhomogeneous broadening is implemented by using a Gaussian distribution in the *sizes* of the dots and the resulting energy distribution is not a Gaussian.

9.6 Summary

In this chapter I have studied the modal gain for both the neutral and non-neutral dots. The spectra for the neutral and non-neutral dots when the dots are empty or fully occupied are the same. However, they show big differences for intermediate occupancies due to the differences in the hole distributions for the neutral and non-neutral dots. There are also differences in the variation of the peak modal gain with parameters such as the electron quasi-Fermi level and the electron number for neutral

and non-neutral dots. I have also shown that the absorption spectra cannot be fitted with Gaussian distributions. In the next chapter I investigate the gain-current characteristics of the dots and the P_f distribution function.

9.7 References

[1] W. W. Chow and S. W. Koch, Semiconductor Lasers Fundamentals, Springer, Berlin, 1999.

[2] W. W. Chow, A. Knorr, S. Hughes, A. Girndt, and S. W. Koch, IEEE Journal of Selected Topics in Quantum Electronics 3 (1997) 136.

[3] M. Grundmann, R. Heitz, and D. Bimberg, Physica E 2 (1998) 725.

10 Gain-Current Characteristics and the Distribution Function P_f

10.1 Introduction

In this chapter the spontaneous emission and gain chapters are brought together and the gain-current characteristics are investigated. The peak gain is plotted as a function of the current, where the current is equal to the integrated spontaneous emission. Comparisons are made between the gain-current curves for the neutral and non-neutral dots. The distribution function P_f is also studied, which is derived from the gain and spontaneous emission. It is investigated whether the P_f function is appropriate for the neutral dots. Again, it should be noted that plots shown for the ground state alone do not contain any emission due to the homogeneous broadening of the excited state, and vice versa. As a reminder, a summary of the values used for the main parameters in this thesis is given below. Full details can be found in Table 3.1.

Parameter	Symbol	Value
Number of dots	n_{QD}	1×10^{6}
Bandgap of dot material	E_g	1eV
Bandgap of wetting layer	$E_{g,wl}$	1.4eV
Dot radiative lifetime	τ_{sp}	1ns
Dot nonradiative lifetime	τ_{nr}	300ps
Dot Auger lifetime	τ_{aug}	300ps
Wetting layer recombination coefficient	B_{wl}	3.5×10^{-7} $s^{-1}m^{2}$
Wetting layer nonradiative lifetime	τ_{nrwl}	300ps

Wetting layer electron confined energy (relative to the conduction band edge)	E_{wlc}	250meV
Wetting layer hole confined energy (relative to the valence band edge)	E_{wlv}	150meV

10.2 Gain-Current Characteristics

In an experiment, the peak modal gain is often measured as a function of the current. In this section the variation of the peak gain with current is studied, with comparisons made between the neutral and non-neutral cases. Figure 10.1 is a plot of the ground state peak gain as a function of the total radiative current in the dots, for the neutral dots (dashed line) and non-neutral dots (solid line).

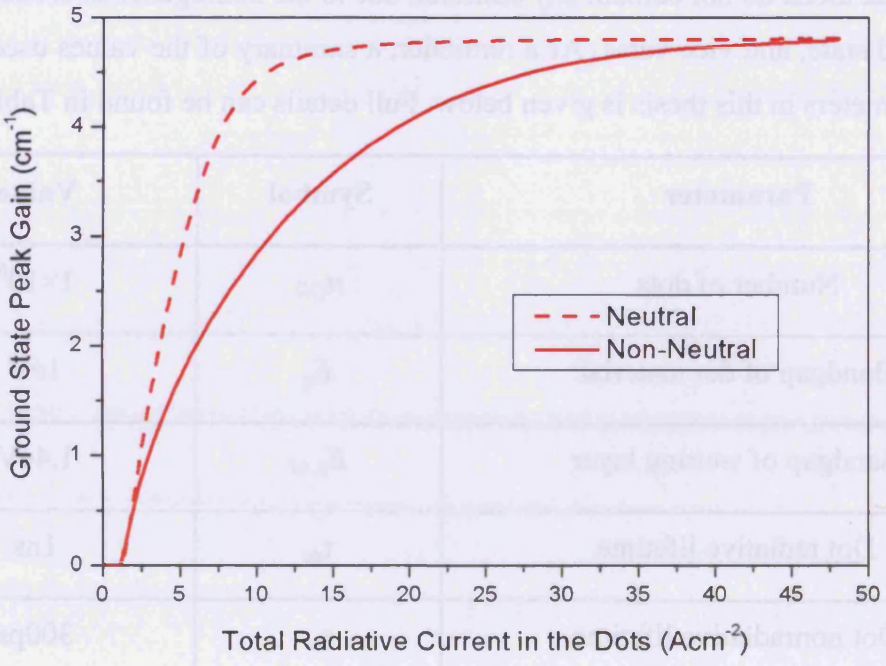

Figure 10.1 - Ground state peak gain as a function of the total radiative current in the dots, for the neutral dots (dashed line) and non-neutral dots (solid line).

It can be seen that both neutral and non-neutral dot ensembles start to exhibit gain at a similar value of the radiative current in the dots. However, as the current is increased, for the same value of current, the peak gain for the neutral dots is much higher than

the peak gain for the non-neutral dots. Both the peak gain *and* the radiative current depend on the electron *and* hole numbers. The current is simply the integrated total radiative rate and is independent of the energies of the carriers. The peak gain, however, depends on the distribution of the electrons and holes amongst the available energy states. The range of energies over which the holes are spread is smaller for the neutral dots and so there are more transitions contributing to the peak gain. An experiment in which the gain is measured as a function of the radiative current should therefore give very different results depending on the statistics of the system. Now considering the excited state, Figure 10.2 is a plot of the excited state peak gain as a function of the total radiative current in the dots, again for the neutral (dashed line) and non-neutral (solid line) cases.

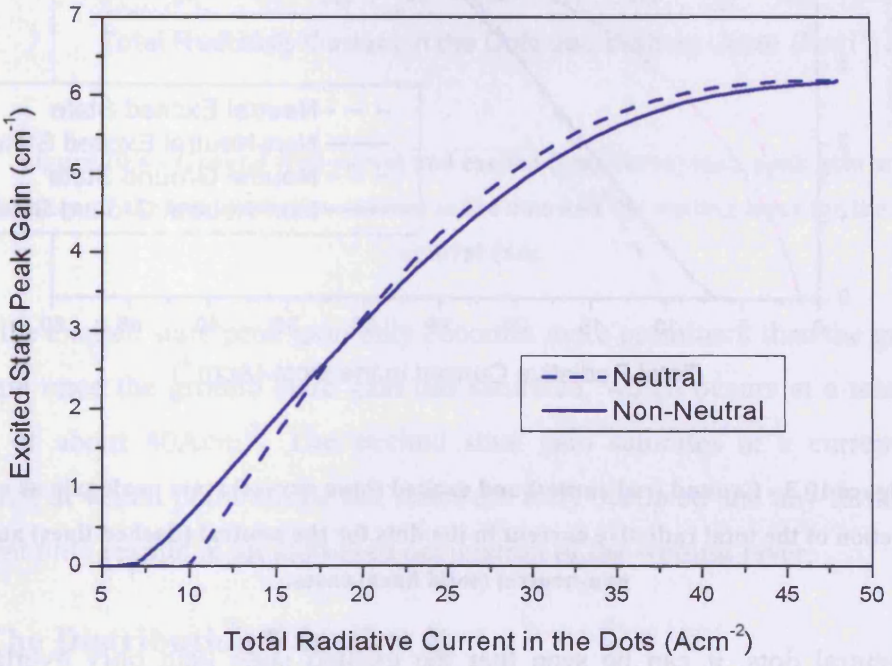

Figure 10.2 - Excited state peak gain as a function of the total radiative current in the dots, for the neutral dots (dashed line) and non-neutral dots (solid line).

For the excited state, the non-neutral dots exhibit gain at lower values of radiative current than the neutral dots. This is because the hole population in the non-neutral dots builds up at a faster rate than for the neutral dots (which contain the same number of electrons and holes). However, as the current is increased further, the neutral dots reach the maximum value of peak gain at a lower value of current than for the non-

neutral dots. The difference between the two cases is more noticeable for the ground state than for the excited state.

Considering the whole system, Figure 10.3 shows both the ground and excited state peak gain as a function of the total radiative current in the dots. Red curves show ground state gain and blue curves show excited state gain, for neutral (dashed line) and non-neutral (solid line) cases.

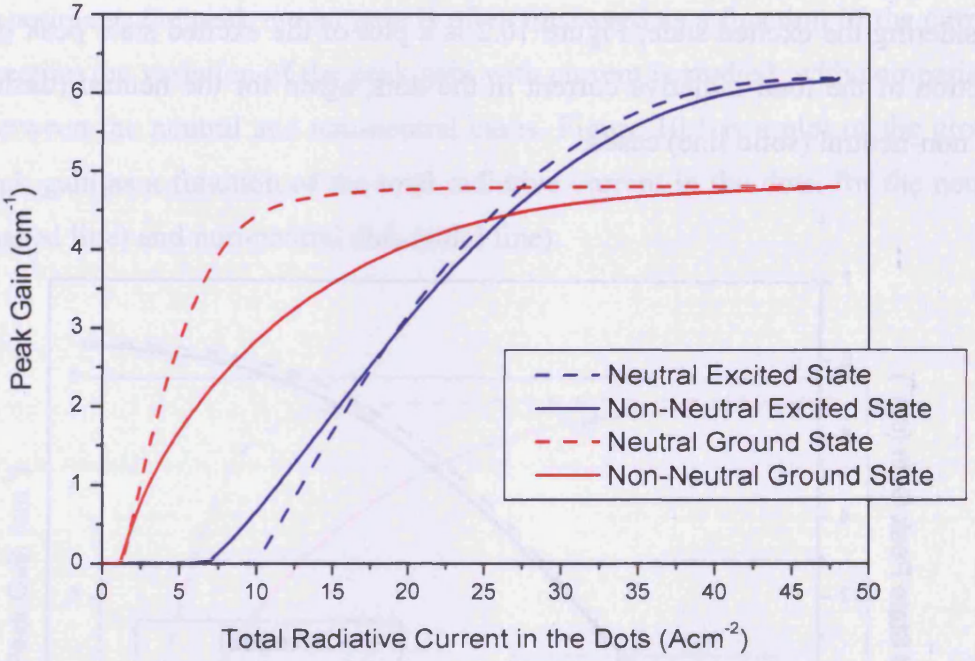

Figure 10.3 - Ground (red curves) and excited (blue curves) state peak gain as a function of the total radiative current in the dots for the neutral (dashed lines) and non-neutral (solid lines) cases.

For the neutral dots, it can be seen that the excited state gain only overtakes the ground state gain when it has reached its maximum value. However, for the non-neutral dots the excited state peak gain becomes dominant before the ground state gain has reached its maximum.

In an experiment the peak gain is often measured as a function of the total radiative current in the dots *and* the wetting layer, and this is plotted in Figure 10.4 for the non-neutral dots.

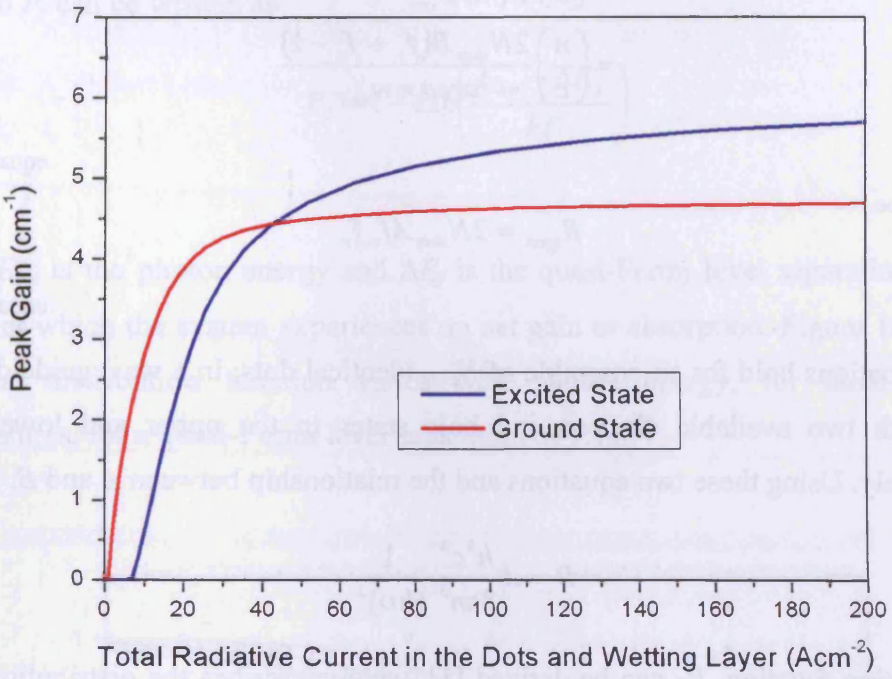

Figure 10.4 - Ground (red curve) and excited (blue curve) state peak gain as a function of the total radiative current in the dots and the wetting layer for the non-neutral case.

Again, the excited state peak gain only becomes more prominent than the ground state peak gain once the ground state gain has saturated, which occurs at a total radiative current of about 40Acm^{-2}. The excited state gain saturates at a current of about 200Acm^{-2}, at which point all the dot states are fully occupied and any further increase in current only results in an increased occupation of the wetting layer.

10.3 The Distribution Function P_f

10.3.1 Introduction

In experimental measurements, the distribution function P_f is often used as a measure of thermal equilibrium in semiconductor devices. The P_f function assumes that the distribution of carriers can be described by Fermi-Dirac statistics, and is derived from the gain and spontaneous emission calculations. Considering the ground state only, chapter 4 gives the general equations for the modal gain and radiative rate as

$$G = \left(\frac{n}{c}\right)\frac{R_{net}}{P(h\upsilon)V_{cav}} = \left(\frac{n}{c}\right)\frac{2N_{dots}B(f_v + f_c - 1)}{area \times w_{mod}}$$

equation 10.1

$$R_{spon} = 2N_{dots}Af_c f_v$$

equation 10.2

These equations hold for an ensemble of N_{dots} identical dots, in a waveguide of width w_{mod}, with two available electron and hole states in the upper and lower states respectively. Using these two equations and the relationship between A and B,

$$B = A\frac{h^3c^3}{8\pi n^3}\frac{1}{(h\upsilon)^2}$$

a distribution function, P_f, can be derived [1], which describes the distribution of the conduction electrons and valence holes

$$\frac{G}{R_{spon}} = \frac{h^3c^2}{8\pi n^2(h\upsilon)^2}\frac{1}{w_{mod}}P_f$$

equation 10.3

where:

$$P_f = \frac{(f_v + f_c - 1)}{f_c f_v}$$

equation 10.4

In terms of the gain and spontaneous emission, the distribution function P_f can thus be written as:

$$P_f = \frac{G}{R_{spon}}\frac{8\pi n^2(h\upsilon)^2}{h^3c^2}w_{mod}$$

equation 10.5

The shape of the spontaneous emission and gain is determined solely by the energy distributions of the electrons and holes. Therefore, from these the form of the carrier distributions can be determined. If the electron and hole distributions are in thermal

equilibrium, and so can be described by Fermi-Dirac statistics then the distribution function P_f can be written as

$$P_f = 1 - \exp\left(\frac{E_{h\upsilon} - \Delta E_f}{kT}\right)$$

equation 10.6

where $E_{h\upsilon}$ is the photon energy and ΔE_f is the quasi-Fermi level separation, i.e. the energy at which the system experiences no net gain or absorption. Figure 10.5 shows how the distribution function varies with photon energy, for three different temperatures, for a quasi-Fermi level separation of 1.13eV.

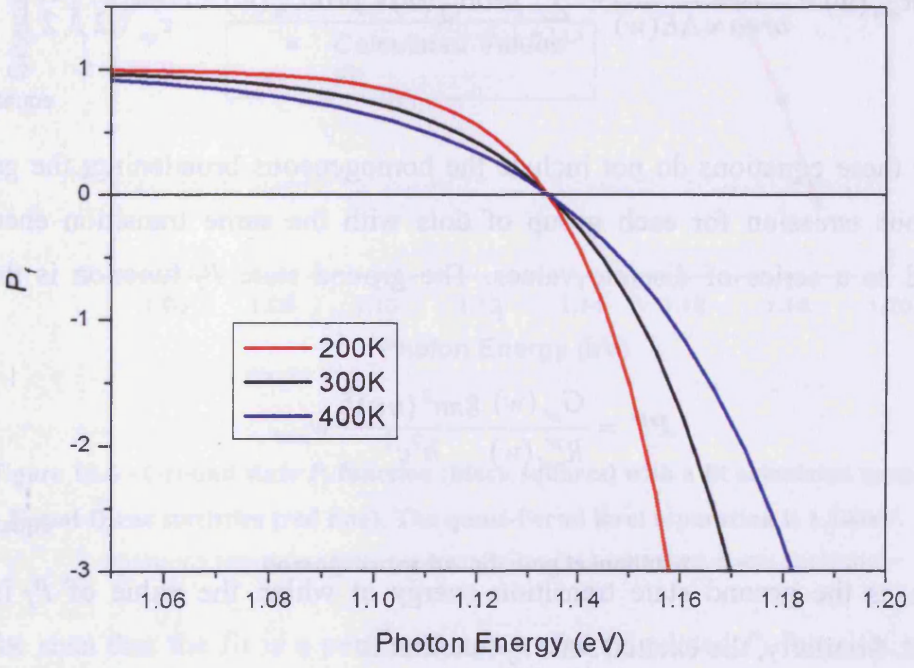

Figure 10.5 - Variation of the distribution function P_f with photon energy for three different temperatures, for ΔE_f =1.13eV.

It can be seen that at low photon energies ($E_{h\upsilon} < \Delta E_f$) the distribution function approaches a value of one. This can be explained by considering equation 10.4. At low photon energy, f_v and f_c both approach a value of one as there is a high probability that the valence and conduction states are filled with holes and electrons respectively. Thus at low photon energies P_f tends to one also. As the photon energy increases, the number of valence holes and conduction electrons decreases and so f_v and f_c both tend

toward zero. Thus, P_f tends towards infinity in the negative direction. At higher temperatures the occupancies become less sensitive to energy, and so the slope of the P_f function becomes less.

Considering the ground state only, the equations for the gain and spontaneous emission for dots of size w are:

$$G_{gr}(w) = \left(\frac{n}{c}\right)\frac{h^3c^3}{8\pi n^3}\frac{n_{QD}(w)}{E^2 \times \tau_{sp} \times area \times w_{mod} \times \Delta E(w)} \times \sum_{i,j,l,m} prob_{i,j}(w) \times prob_{l,m}(w) \times 2 \times \left(\frac{i}{2} + \frac{l}{2} - 1\right)$$

equation 10.7

$$R_{rad}^{gr}(w) = \frac{n_{QD}(w)}{area \times \Delta E(w)} \times \sum_{i,j,l,m} prob_{i,j}(w) \times prob_{l,m}(w) \times 2\frac{1}{\tau_{sp}}\left(\frac{i}{2}\right)\left(\frac{l}{2}\right)$$

equation 10.8

Note that these equations do not include the homogeneous broadening: the gain and spontaneous emission for each group of dots with the same transition energy are calculated as a series of discrete values. The ground state P_f function is therefore given by

$$P_f^{gr} = \frac{G_{gr}(w)}{R_{rad}^{gr}(w)}\frac{8\pi n^2 (h\upsilon)^2}{h^3c^2}w_{mod}$$

equation 10.9

where $h\upsilon$ is the ground state transition energy at which the value of P_f is being calculated. Similarly, the excited state P_f function is

$$P_f^{ex} = \frac{G_{ex}(w)}{R_{rad}^{ex}(w)}\frac{8\pi n^2 (h\upsilon)^2}{h^3c^2}w_{mod}$$

equation 10.10

where $h\upsilon$ is the excited state transition energy.

10.3.2 P_f for Non-Neutral Dots

Figure 10.6 shows the ground state P_f function calculated using equation 10.10 (black squares). A fit has been calculated using equation 10.6, which assumes Fermi-Dirac statistics for the electrons and holes (red line).

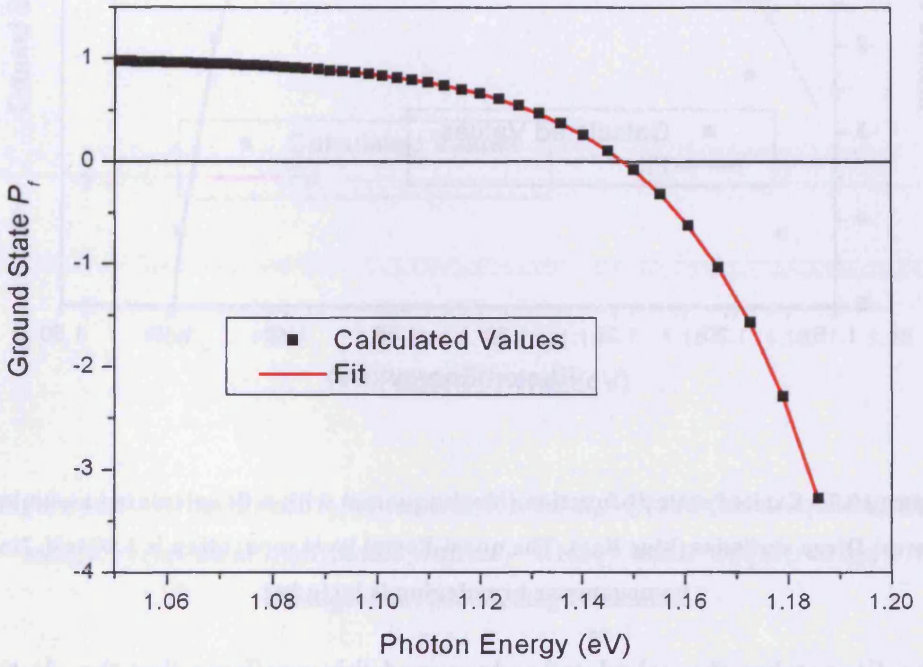

Figure 10.6 - Ground state P_f function (black squares) with a fit calculated assuming Fermi-Dirac statistics (red line). The quasi-Fermi level separation is 1.148eV. No homogeneous broadening is included.

It can be seen that the fit is a perfect match to the calculated P_f function, and this is expected since Fermi-Dirac statistics are used to calculate the distributions of electrons and holes in the model. The excited state P_f is now shown in the following figure (black squares) with a Fermi-Dirac fit (blue line).

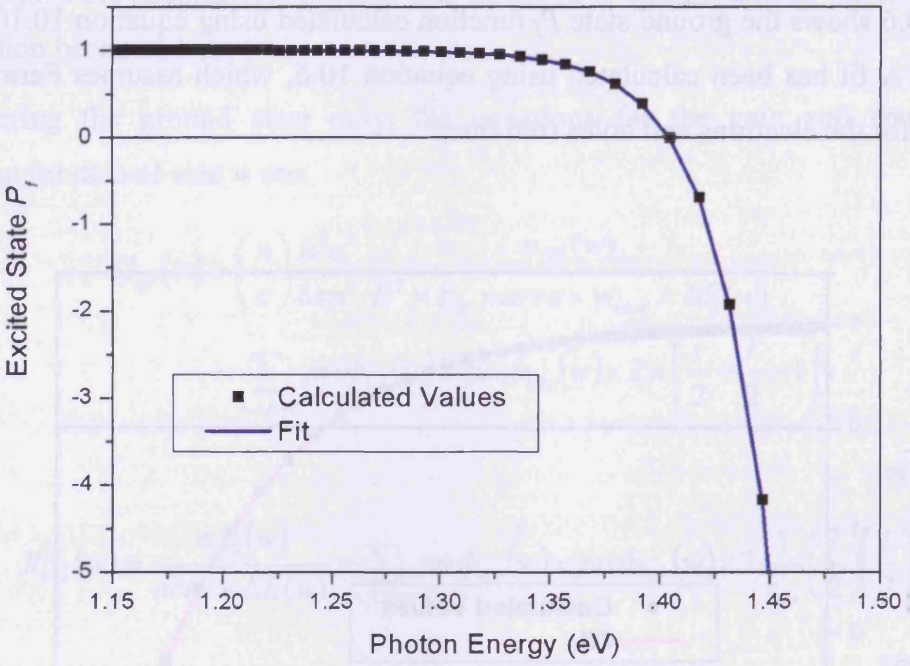

Figure 10.7 - Excited state P_f function (black squares) with a fit calculated assuming Fermi-Dirac statistics (blue line). The quasi-Fermi level separation is 1.404eV. No homogeneous broadening is included.

Again, the fit matches the calculated values, and this confirms that the electron and hole states in both the ground and excited states can be described using Fermi-Dirac statistics.

It is not possible to fit the P_f functions calculated from the homogeneously broadened gain and spontaneous emission spectra. This is because the homogeneous broadening changes the shape of the spectra (including the transparency point) and Fermi-Dirac statistics cannot be fitted. This is described in more detail in section 10.3.4.

10.3.3 P_f for Neutral Dots

In this section it is investigated whether the distribution function P_f can be fitted to the results for the neutral dots. The electron distribution follows a Fermi-Dirac distribution but the hole distribution does not. Therefore it is not possible to define the quasi-Fermi level separation for the neutral dots. The following graph shows the calculated ground state P_f function (black squares) for E_{fc}=0.15eV, calculated using equation 10.9.

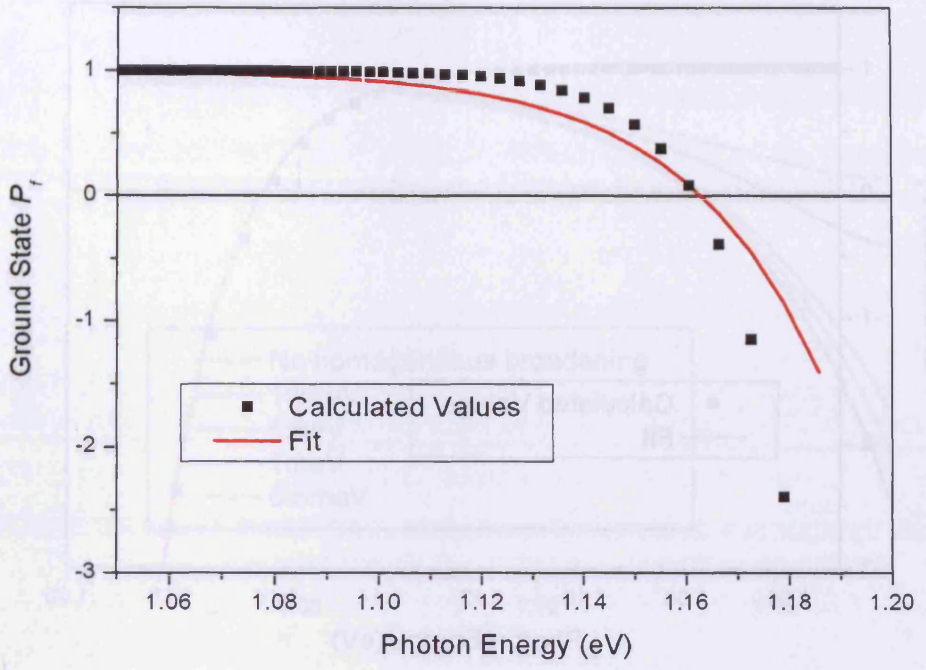

Figure 10.8 - Ground state P_f for neutral dots for E_{fc}=0.15eV (black squares), fitted using a Fermi-Dirac distribution with ΔE_f=1.163eV and T=300K (red line). No homogeneous broadening is included.

If Fermi-Dirac statistics apply then is should be possible to fit the following equation, equation 10.6, to the curve.

$$P_f = 1 - \exp\left(\frac{E_{h\upsilon} - \Delta E_f}{kT}\right)$$

A value of ΔE_f is needed, which is the energy at which the P_f is zero, which from inspection of the curve is about 1.163eV. The P_f fit for this value is shown as a red line in Figure 10.8. It can be seen that this fit does not match the calculated values. The only other parameter that can be varied is the temperature. A temperature of 155K gives a good match, as shown in the following figure.

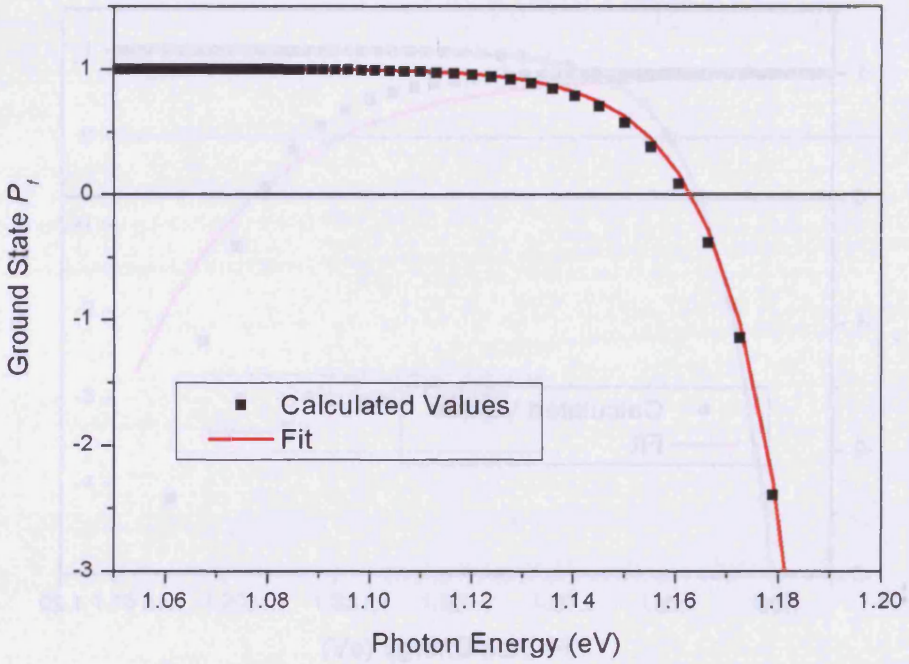

Figure 10.9 - Ground state P_f for neutral dots for E_{fc}=0.15eV (black squares), fitted using a Fermi-Dirac distribution with ΔE_f =1.163eV and T=155K (red line). No homogeneous broadening is included.

The plot implies that the neutral dots can be described using Fermi-Dirac statistics. However, this is not the case, as proved in chapter 6 where it is shown that a Fermi-Dirac distribution cannot be fitted to the hole distributions for the neutral dots. The fact that a curve can be fitted with a P_f function does therefore not explicitly imply that the system is obeying Fermi-Dirac statistics.

10.3.4 Including the Homogeneous Broadening in the Calculations of P_f

The P_f graphs shown in this chapter do not include homogeneous broadening, and the gain and spontaneous emission have been calculated at the discrete transition energies corresponding to the widths of the groups of dots. In this section it is demonstrated how the P_f function changes when the homogeneous broadening is included. The following graph shows how the ground state P_f function changes with the inclusion of the homogeneous broadening, plotted for the non-neutral dots for a quasi-Fermi level separation of 1.148eV. The black line is for the case where the homogeneous broadening is not included, as shown previously in this chapter.

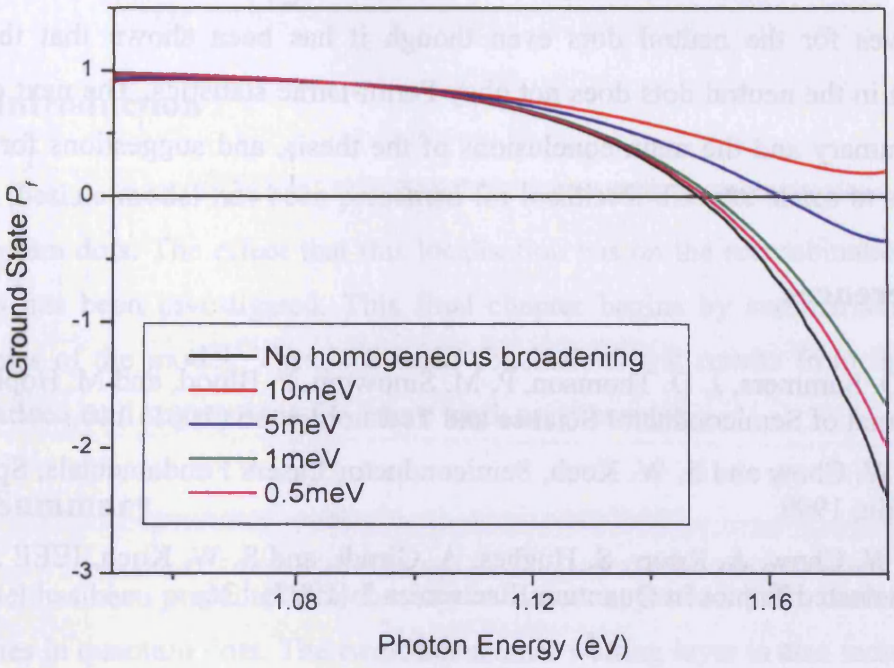

Figure 10.10 - Ground state P_f for non-neutral dots, for varying values of the homogeneous linewidth. The quasi-Fermi level separation is 1.148eV. The black curve is for the case of no homogeneous broadening.

It can be seen that as the value of the homogeneous linewidth is decreased the P_f function becomes more like the curve for no homogeneous broadening, as expected. At high values of homogeneous linewidth the transparency point becomes much larger than the quasi-Fermi level separation. The curves also show a different shape to the expected P_f function at higher photon energies. This is because when the homogeneous linewidth is large, for photon energies inside the *inhomogeneous* distribution, transitions are being included which are *outside* the inhomogeneous distribution. For further discussions on how the homogeneous broadening affects the gain spectra see reference [2, 3].

10.4 Summary

In this chapter I have investigated the gain-current relations, and compared those of neutral and non-neutral dots. There are marked differences in the two cases, and these should be observable in an experiment. I have plotted the P_f functions for both the neutral and non-neutral dots. A fit assuming a thermal distribution of carriers has been

shown for the non-neutral dots, confirming that Fermi-Dirac statistics are used to describe the electron and hole occupancies. However, a thermal fit can also be fitted to the curves for the neutral dots even though it has been shown that the hole distribution in the neutral dots does not obey Fermi-Dirac statistics. The next chapter gives a summary and the main conclusions of the thesis, and suggestions for future work.

10.5 References

[1] H. D. Summers, J. D. Thomson, P. M. Smowton, P. Blood, and M. Hopkinson, Journal of Semiconductor Science and Technology 16 (2001) 140.

[2] W. W. Chow and S. W. Koch, Semiconductor Lasers Fundamentals, Springer, Berlin, 1999.

[3] W. W. Chow, A. Knorr, S. Hughes, A. Girndt, and S. W. Koch, IEEE Journal of Selected Topics in Quantum Electronics 3 (1997) 136.

11 Summary and Discussion

11.1 Introduction

In this thesis a model has been presented for localised, discrete states in an ensemble of quantum dots. The effect that this localisation has on the recombination processes in dots has been investigated. This final chapter begins by summarising the main principles of the model. Then, the main conclusions and results from the thesis are summarised, and suggestions for future work are presented.

11.2 Summary

A model has been presented which takes into account the localised, discrete nature of the states in quantum dots. The two-dimensional wetting layer is also included, which is treated in the same way as a quantum well. The dot distribution is inhomogeneously broadened in size. A ground and first excited state are modelled, that can contain two and four electron/holes respectively.

Two types of dots have been modelled for comparison: neutral and non-neutral dots. In the model for non-neutral dots, Fermi-Dirac statistics are used, and the electron and hole populations are calculated using their respective electron and hole quasi-Fermi levels. Due to the differences in energy between the electron and hole states this means that individual dots may not contain equal numbers of electrons and holes. However, the overall numbers of electrons and holes in the dots *and* the wetting layer are equal (this is also true for the neutral model). In the model for neutral dots, Fermi-Dirac statistics are again used to calculate the electron distribution. However, the number of holes in each dot is then set equal to the number of electrons in that dot. Consequently, a hole quasi-Fermi level cannot be defined for this neutral case.

Recombination is modelled locally in each dot, and an electron can only recombine with a hole in the *same dot*. Nonradiative via defects, radiative and Auger recombination are modelled. Homogeneous broadening is included to work out the spontaneous emission and gain spectra.

11.3 Conclusions

The main conclusions drawn from this thesis are that the localisation of the states in quantum dots affects the dependence of the recombination processes on the carrier number in the dots. It is often assumed that the rates of nonradiative recombination via defects, radiative recombination and Auger recombination are proportional to linear, quadratic and cubic functions of the carrier number, and the derivation of these functional forms is possible in quantum well and bulk structures because the extended electronic states make it meaningful to talk of a global carrier population. In quantum dots, because an electron can only recombine with a hole in the same dot, the recombination processes cannot be related to the global total number of carriers, and the rates in each dot are proportional to the electron and hole numbers in *that particular dot*. Because of this, the recombination processes have similar dependences on electron number and there is no clear transition from one process to another as the injection level is increased. These dependences cannot be represented by simple power law functions of the carrier number, and so analyses of L-I curves based on power law relations between recombination rates and carrier number, as used for extended state systems, cannot be applied to localised recombination in dots.

Due to the saturation of dot emission and the wetting layer contribution to the current, the light emission from the dots as a function of the total current shows sub-linear behaviour. Comparing the neutral and non-neutral dots, the L-I characteristics of the dot system alone are similar for the two cases even though the recombination rates have very different dependences on the carrier number. The computed L-I curves have been compared to experimental data by fitting the nonradiative and Auger lifetimes in the dots, and good agreement is found between the computed and experimental data

The inhomogeneous broadening is applied to the dot *sizes* and this gives an asymmetrical distribution in energy. Therefore the gain and spontaneous emission spectra for both neutral and non-neutral dots cannot be fitted with Gaussian distributions. This has implications in that caution should be used when fitting experimental data since the form of the inhomogeneous broadening may not be known. The gain and spontaneous emission spectra for the neutral and non-neutral dots when the dots are empty or fully occupied are the same. However, they show big differences for intermediate occupancies due to the differences in the hole occupation

between the two models. These differences are due to the difference in energy levels for the electrons and holes. This is not taken into account in the neutral model and the number of holes in a dot is simply set equal to the number of electrons. From investigation of the hole distributions for the neutral dots it is concluded that they do not follow Fermi-Dirac statistics and therefore a hole quasi-Fermi level cannot be defined for neutral dots.

The main conclusions from the thesis are summarised below:

- Recombination rates in each dot are proportional to the electron and hole numbers in *that particular dot.*
- All recombination processes have a similar dependence on electron number.
- There is no clear transition from one process to another as the injection level is increased.
- Recombination processes cannot be related to the global total number of carriers.
- Analyses of L-I curves based on power law relations between recombination rates and carrier number cannot be applied to localised recombination in dots.

11.4 Future Work

Suggestions for future work can be divided into two categories: further calculations using the present model, and calculations using an improved/modified model. These are discussed in more detail in the following sections.

- **Further Calculations using the Present Model**

  The present model can be used to investigate further the properties of the quantum dot ensemble. All the calculations in this thesis have been done at room temperature. It would be interesting to investigate the emission characteristics of the dots at lower temperatures. It would also be useful to do more comparison between the computed data from the model and experimental results. This may provide some insight into whether real dot samples show behaviour similar to the neutral model or the non-neutral model, or a combination of both. Previous work has shown that neither the free carrier

nor the exciton (neutral) model can fully explain the characteristics of real quantum dot lasers [1].

Another suggestion is to use a different radiative lifetime for dots of different sizes, reflecting the different energy distributions. At present, for simplicity, the model only calculates occupancies for a small (51) number of dot sizes. Rates are then interpolated to produce a spectrum. To increase the accuracy of the calculations a wider distribution of dot energies could be calculated, using more sizes of dots.

- **Modifications to the Present Model**

  A possible option for future work would be to modify the model. Many assumptions are made in the model, and the extent to which these are reasonable could be investigated.

  Auger recombination could be investigated in more detail. At present only one process is modelled for Auger recombination, and this could be looked at in more detail. The model also assumes that there is a defect present in every dot for nonradiative recombination. A random defect could be implemented so as to make the model more realistic.

  In the current model a ground and first excited state are modelled. It may be helpful to include higher energy excited states.

  Previous work has shown that Fermi-Dirac statistics can be applied to the electron and hole distributions at room temperatures [2]. However, it would be interesting to investigate whether the use of Fermi-Dirac statistics is reasonable at lower temperatures. Another possibility for future work is to calculate the occupation statistics of the dots using different statistics to Fermi-Dirac, such as a random population model [3].

  It has been shown that the inclusion of the homogeneous broadening in the spectra changes the transparency point from that of the quasi-Fermi level separation. This could be investigated in more detail to see what implications homogeneous broadening has for quantum dots, and what effects its inclusion has on the thermal equilibrium of the system.

Finally, it would be interesting to see how excitonic states in a quantum well compare to the localised states in quantum dots, and whether they show similar properties.

11.5 References

[1] A. A. Dikshit and J. M. Pikal, IEEE Journal of Quantum Electronics 40 (2004) 105.

[2] H. D. Summers, J. D. Thomson, P. M. Smowton, P. Blood, and M. Hopkinson, Journal of Semiconductor Science and Technology 16 (2001) 140.

[3] M. Grundmann and D. Bimberg, Physical Review B 55 (1997) 9740.

Appendices

Table of Notation

The following table lists the notation used throughout this thesis, along with the corresponding dimensions. The dimensions are [E] energy, [L] length and [M] mass. Dimensionless quantities with are written as [0].

Symbol	Definition	Dimensions
$E_{gr}^{c}(w)$	Energy of the electron ground state for dots of width w	[E]
$E_{gr}^{v}(w)$	Energy of the hole ground state for dots of width w	[E]
$E_{ex}^{c}(w)$	Energy of the electron excited state for dots of width w	[E]
$E_{ex}^{v}(w)$	Energy of the hole excited state for dots of width w	[E]
E_{wlc}	Wetting layer electron confined energy (relative to the conduction band edge)	[E]
E_{wlv}	Wetting layer hole confined energy (relative to the valence band edge)	[E]
E_{fc}	Electron quasi-Fermi level	[E]
E_{fv}	Hole quasi-Fermi level	[E]
$f_{gr}^{c}(w)$	Fermi function for the electron ground state for dots of width w	[0]

$f_{gr}^{v}(w)$	Fermi function for the hole ground state for dots of width w	[0]
$f_{ex}^{c}(w)$	Fermi function for the electron excited state for dots of width w	[0]
$f_{ex}^{v}(w)$	Fermi function for the hole excited state for dots of width w	[0]
i	Number of electrons in ground state of one dot	[0]
j	Number of electrons in excited state of one dot	[0]
l	Number of holes in ground state of one dot	[0]
m	Number of holes in excited state of one dot	[0]
m_c	Effective mass of the electron	[M]
m_v	Effective mass of the hole	[M]
$n_i^j(w)$	Number of dots with i electrons in the ground state and j electrons in the excited state, for a width w	[0]
$N_{gr}(w)$	Number of electrons in the ground state for dots of width w	[0]
$N_{ex}(w)$	Number of electrons in the excited state for dots of width w	[0]
N_{wl}	Number of electrons in the wetting layer per unit area	$[L]^{-2}$
$p_l^m(w)$	Number of dots with l holes in the ground state and m holes in the excited state, for a width w	[0]

$P_{gr}(w)$	Number of holes in the ground state for dots of width w	[0]
$P_{ex}(w)$	Number of holes in the excited state for dots of width w	[0]
$prob_{i,j}$	Probability of having a dot with an electron distribution i,j	[0]
$prob_{i,j,l,m}$	Probability of having a dot with an electron distribution i,j and a hole distribution l,m	[0]
$prob_{l,m}$	Probability of having a dot with a hole distribution l,m	[0]
P_{wl}	Number of holes in the wetting layer per unit area	$[L]^{-2}$

List of Abbreviations

Abbreviation	Term
OD	Zero-dimensional
1D	One-dimensional
2D	Two-dimensional
3D	Three-dimensional
AlAs	Aluminium Arsenide
AlGaAs	Aluminium Gallium Arsenide
DOS	Density of States
DWELL	Dot-in-well structure
GaAs	Gallium Arsenide
GaN	Gallium Nitride
HH	Heavy Hole
InAs	Indium Arsenide
LED	Light Emitting Diode
LH	Light Hole
L-I	Light-Current
Si	Silicon
SHO	Simple Harmonic Oscillator
SO	Split-Off Bands

SRH	Shockley-Read-Hall
QD	Quantum Dot
QW	Quantum Well
VCSEL	Vertical Cavity Surface Emitting Laser